The use of heteropoly acids in separation and catalysis

Schrotter, Bengu Bozkaya

Award date:
2005

Awarding institution:
University of Bath

THE USE OF HETEROPOLY ACIDS IN SEPARATION AND CATALYSIS

Bengü BOZKAYA SCHROTTER

A thesis submitted for the degree of Doctor of Philosophy

Bengü Bozkaya Schrotter

University of Bath
Department of Chemical Engineering
November 2005

ProQuest LLC
789 East Eisenhower Parkway
P.O. Box 1346
Ann Arbor, MI 48106-1346

Dedicated to my son, Erin Bozkaya Schrotter

SUMMARY

The objective of this study is to investigate the applications of heteropolyacids in reaction and separation engineering.

Development of novel adsorbents for removing molecular impurities from gas streams:

Currently, the filters used for removing molecular impurities in clean room environments contain highly reactive liquid acids. These filters present a number of drawbacks: poor accessibility of active sites and significant vapour pressure. In order to overcome these drawbacks, solid super acids containing adsorbents have been developed to replace liquid acid containing adsorbents. Tungsto- and molybdo-phosphoric acids were supported onto Novacarb™, Sibunit™, SBA-15 and sol-gel derived amorphous silica. Maximum loading was attained with amorphous SiO_2. In addition, silica-acid composites containing up to 50 wt% acids were prepared and Novacarb™ was brominated to modify the surface of the carbon. SiO_2-HPA composite was characterised as the most promising material for this application.

Partial Oxidation of Hydrocarbons by Multiphase Catalytic Membrane Reactor Using Heteropolyacids:

This study was focused on the use of heteropolyacids for re-oxidising the reduced Pd^{2+} catalyst in selective hydrocarbon oxidation reaction. Currently, the process of hydrocarbon oxidation by Pd^{2+} takes place in two separate stages in order to avoid generation of potentially explosive hydrocarbon and oxygen mixtures. In this study, a catalytic reactor has been designed to carry out this reaction in one stage. Porous tubular carbon contactor is used in this reactor as a safety barrier between oxygen and hydrocarbon streams. It also offers dispersion free method of mass transfer and easy control of the flow rates/compositions of the flow streams. Inside the tubular membrane, Taylor flow regime was created to achieve high gas-liquid mass transfer.

1-butene oxidation to methyl ethyl ketone was selected as a test reaction and phosphovanadomolybdic acid (MoV-HPA) was used as co-oxidant to study the feasibility of the designed system. 1-butene concentration in the solution showed the highest impact on the reaction rate amongst all the parameters studied.

ACKNOWLEDGEMENTS

I would like to thank to Dr. Alexei Lapkin for his help throughout this PhD and to Dr. Pawel Plucinski, Professor Barry Crittenden and Dr. Tim Mays for their help for different parts of this PhD. I would also like to extend my gratitude to Dr. Serpil Awdry and Professor Stan Kolackowski for their continued support and encouragement. Thanks also go to the technical and administrative staff for their help. I am grateful to Dr. Karen Edler and Dr. Luisa Borella for their helpful discussions and cooperation during the synthesis of silica materials. This work was funded by the Engineering and Physical Sciences Research Council. A mention to MAST Carbons Ltd. and Boreskov Institute of Catalysis is also worthy.

My appreciation is given to my friends and lastly I am most indebted to my mother, Mukaddes, my father, Halil, my sisters and brother in law, Funda-Betul-Ugur, and my dearest husband Jean-Christophe for their everlasting support.

TABLE OF CONTENTS

PARTIAL OXIDATION OF HYDROCARBONS BY MULTIPHASE CATALYTIC MEMBRANE REACTOR USING HETEROPOLYACIDS

DEVELOPMENT OF NOVEL ADSORBENTS FOR REMOVING MOLECULAR IMPURITIES FROM GAS STREAMS

List of Figures

List of Tables

I.I INTRODUCTION

Clean rooms are specially constructed areas with ultra clean environment and are designed to control airborne particulates, temperature, humidity, pressure, airflow patterns, and lighting to meet the required cleanliness level in the manufacturing environment, mainly in microelectronics and pharmaceutical industries, medical engineering, hospitals, food and cosmetic industries.

Contaminants of the clean room can be classified as molecular and particulate. Molecular air pollutants have specific chemical and physical properties unique to their chemical species. Generally, molecular contaminants with a boiling point of 100 °C or greater may be removed by adsorption – condensation mechanism, whereas removal of contaminants with lower boiling points, like ammonia, requires a chemisorption mechanism in which the molecular contaminant and the reagent react to form a solid by-product on the surface of the adsorbent [Kinkead, 1997]. Currently adsorbents for removal of basic gasses contain liquid acids impregnated into porous supports. However, there are some drawbacks of using liquid acids such as, poor accessibility of the active sites and potential generation of secondary impurities, e.g. SO_2 in the case of sulphuric acid.

Adsorption of ammonia onto tungstophosphoric acid leads to the stoichiometric formation of the ammonia salt. Reaction occurs as follows:

$$H_3PW_{12}O_{40} + 3\ NH_3 \rightarrow (NH_4)_3\ PW_{12}O_{40}$$

Three molecules of ammonia at most can be chemisorbed by one molecule of heteropoly acid: analysis of stoichiometries obtained from NH_3 uptake indicates formation of 3 NH_4^+ ions per Keggin unit for W-HPA [Southward et al., 1994]. As a result, the surface area of the HPA considerably increases and that indicates the participation of the ammonia ion in the structural rearrangement of the bulk HPA, i.e. surface areas of $H_3PW_{12}O_{40}$ and $NH_4PW_{12}O_{40}$ are ca. 5 and 100 m^2/g, respectively [Soled et al., 1996]. Essayem et al. has used NH_3 TPD frontal method to deduce the maximum amount of ammonia irreversibly adsorbed by each Keggin unit [Essayem et. al., 1997]. The amount of irreversibly adsorbed ammonia was found to be equal to 4 per

Keggin unit, which is higher than the proton content of $H_3PW_{12}O_{40}$ [Essayem et. al., 1997].

Supporting heteropolyacids provides an effective way to increase the surface area of bulk acids and have been investigated using various supports in order to optimise the preparation parameters and the operating conditions. Adsorption from a solution technique is the most commonly used preparation method of supported heteropolyacids. Supports that do not strongly interact with the acid are preferred for this technique as the strongly interacting supports can hydrolyse and partially decompose the acid. However, supported acids on non-interacting supports will solubilize in polar reactants at elevated temperatures [Soled et al., 1996]. In order to overcome this problem sol-gel preparation technique was investigated. According to the literature the most common HPA composites have been prepared by entrapment of the HPAs in the silica matrix. Kukovecz et al. (2002) synthesised W-HPA – silica composites up to 80 wt. % W-HPA loading and reported that the silicate structure traps the heteropoly acid molecules and their acidic character remains intact [Kukovecz et al. 2002]. Furthermore, this method allowed controlling the synthesis variables, such as the concentration of the acid in the composite.

In order to reduce the interaction of water or other polar adsorbates with the surface of a support, placing various halogens on the surface of carbons has been studied in detail by MacDonald et al., (2000) [MacDonald et al., 2000]. Bromine was selected and Novacarb™ was brominated prior to acid adsorption in order to observe the effect of the halogenation of the surface of a support.

Regeneration of the acid supported adsorbents after their use in removing basic impurities was studied by following Shimizu et al.'s (1986) study where they produce heteropolyacids by calcining corresponding ammonium-HPA salts at a temperature of not lower than 400 °C in an inert gas, such as nitrogen, argon, carbon dioxide gas or combustion exhaust gases comprising carbon dioxide gas and steam.

Development of novel adsorbents for environmental applications using heteropolyacids is described in the first part of this thesis. The aim of this study was to investigate the feasibility of a novel sorbent suitable for removing of molecular impurities of a basic nature from gaseous streams and overcome the problems introduced by the current technology. Mesoporous supports, Novacarb™, Sibunit™, SBA-15, and sol-gel derived silica, were impregnated with tungstophosphoric acid $H_3PW_{12}O_{40}$ (W-HPA) and molybdophosphoric acid $H_3PMo_{12}O_{40}$ (Mo-HPA). Additionally, silica-heteropolyacid composites were prepared and Novacarb™ was brominated. Pure supports and prepared materials were characterised and NH_3 Temperature Programmed Desorption (TPD) technique was used to evaluate the performance of the prepared materials. Preparation and characterisation techniques and the results obtained are described in detail in the following chapters.

I.II PRIOR ART

I.II.1 HETEROPOLY ACIDS

Heteropoly compounds involve a large class of coordination type salts and free acids, which are formed by condensation of more than two different types of oxoanions [Corma, 1995 & McCormick et al., 1998]. Heteropoly acids are strong Brönsted acids, in which the solid can give or at least partially transfer a proton, which then becomes associated with surface anions [Kozhevnikov, 1995 and Corma, 1994]. They possess stronger acidic properties than the mineral acids such as sulphuric acid [Kapustin et. al, 1990]. Several applications of heteropoly acids, mainly in catalysis due to their strong acid and redox properties, have been extensively studied and reported [Izumi, 1983; Mizuno & Misono, 1998; Na et al., 1997; Kozhevnikov, 1994; Okuhara, 2003]. However, their applications in adsorption are limited

Structure of Heteropolyacids

Structure of fundamental units of heteropolyacids is called the primary structure. Secondary structure is formed when the primary units are joined to form a bulk solid. Although the synthesis of Keggin anion has been extensively reviewed, there is not much information about how the heteropoly anions are linked together to form the secondary structure [Corma, 1995; Pope, 1983; Mizuno and Misono, 1998; and Jeannin, 1998]. The primary structural unit is a heteropoly anion. Some common heteropoly anion structures were classified by Pope (1983) into five main groups: the hexametalate structure "M_6O_{19}", octahedral heteroatoms "XM_6" structures, tetrahedral heteroatoms "The Keggin structure and Isomers", tetrahedral heteroatoms " X_2M_5 and X_2M_6" structures and icosahedral heteroatoms "$XM_{12}O_{42}$" [Pope, 1983].

In the heteropolyacids of the Keggin structure "$XM_{12}O_{40}^{x-8}$", X is the central atom and can be Si^{4+}, P^{5+}, etc., x is the degree of its oxidation, and M is the metal ion and can be Mo^{6+}, W^{6+}, V^{5+}, etc. [Kozhevnikov, 1995]. The central atom is tetrahedrally coordinated to oxygens and surrounded by oxygen linked hexavalent peripheral metal atoms as shown in Figure I.II-1. Four types of oxygen atoms exist in the structure, these are terminal M=O, corner-sharing, edge-sharing M-O-M, and internal [Dias et al., 1999]. Primary structure of W-HPA is formed by a central PO_4 tetrahedron surrounded by 12 WO_6 octahedra, which are arranged in four groups of three edge-

shared octahedra W_3O_{13}. These W_3O_{13} units are linked by shared corners to each other and to the central PO_4 [Corma, 1995].

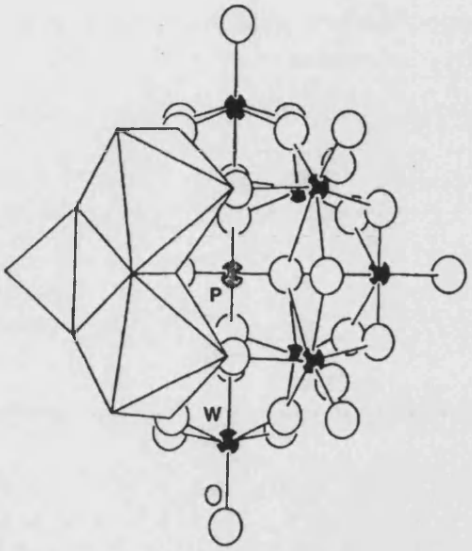

Figure I.II 1 Structure of Keggin heteropoly anion. Adopted from [Izumi, 1996]

In the solid HPAs, the protons take part in the formation of the HPA crystal structure, linking the neighbouring heteropolyanions. In this case, the more accessible terminal oxygen atoms can be protonated. The bulk proton sites in $H_3PW_{12}O_{40}$ hexahydrate are represented as diaquahydrogen ions, $H_5O_2^+$ and they link four neighbouring heteropolyanions by forming hydrogen bonds with the terminal (W=O) oxygen as shown in Figure I.II-2. The crystal structure of 12- tungstophosphoric acid shows that the Keggin anions are closed packed on a body-centred lattice with the central anion turned 90° to its neighbours. Depending on the amount of hydration water and on the countercation, several crystallographic arrangements exist.

The lattice parameter changes depending upon the number of sorbed molecules per anion, the size of these molecules and how they are bonded to the heteropoly anions. Because of the flexible nature of the secondary structure, it has been referred to as "pseudoliquid phase" [McCormick et al., 1998 and Konishi, 1982]. Solid HPAs possess extremely high proton mobility. It should be noted that proton conductivities of solids generally correlate with their acid-base catalytic activities [He et al., 1997]. Catalytic properties of the HPAs will be discussed in Part II in detail.

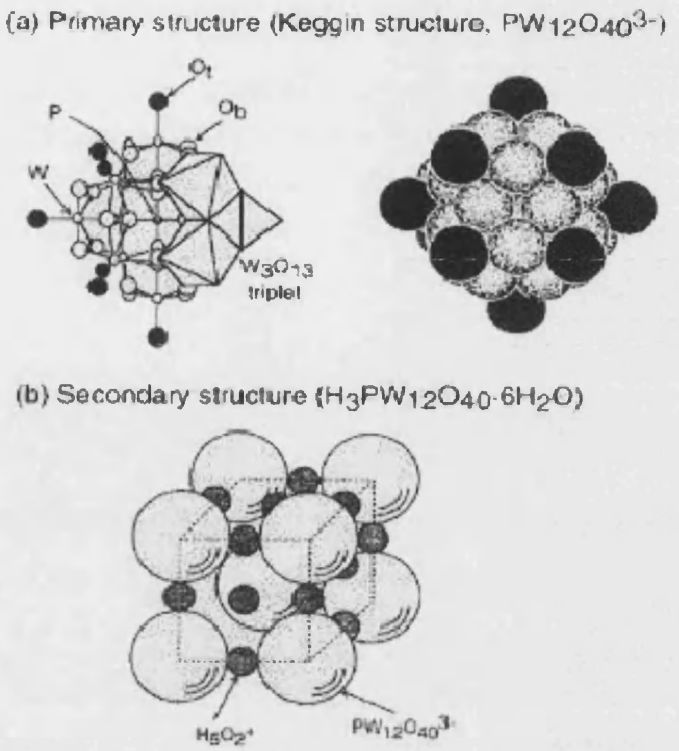

Figure I.II 2 Primary and secondary structures of heteropoly acid with the Keggin Structure $(PMo_{12}O_{40})^{3-}$ [Mizuno & Misono, 1998]

A heteropoly acid molecule may contain a different number of water molecules, physically adsorbed and crystalline water, depending on the specific treatment of the acid. For example, the acid strength of $H_3PW_{12}O_{40}.xH_2O$ depends on the number of H_2O molecules in the structure. A $H_3PW_{12}O_{40}$ molecule that contains 1-2 crystalline H_2O molecules indicates the highest acid strength ($H_0 \leq -12.77$). The acid strength of HPAs can be measured using Hammet indicators. Figure I.II-3 shows the acid strength of $H_3PW_{12}O_{40}$ as a function of the number of water molecules they contain [He et al., 1997]. Dias et al. has shown that W-HPA can be dried under vacuum for 4 hours at minimum 162°C in order to obtain anhydrous acid [Dias et al., 1999].

The radius of heteropoly anion is only 5-6 Å while the spacing between the anions is ca. 23 Å. It can easily be understood from this arrangement that in the case of the loss of some crystallisation water, porous structures with considerable surface area can be formed. It has been shown that the surface area of 12 W-HPA increases from 0.1 to 10 m^2 /g when subjected to a moderate heat treatment in a dry He stream [Corma, 1995 and Vaughan 1994].

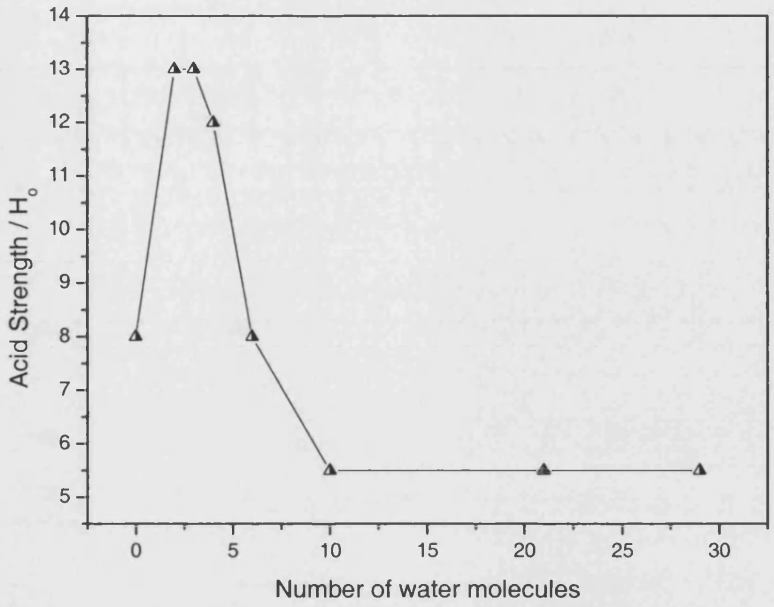

Figure I.II 3 Acid strength as a function of number of water molecules in the crystalline $H_3PW_{12}O_{40}$ [He, et. al. 1997].

Synthesis of Heteropolyacids

Heteropoly anions have been prepared from both aqueous and nonaqueous solutions. The most common preparation method so far is the acidification of aqueous solutions of simple oxoanions and the necessary heteroatoms.

$$12WO_4^{2-} + HPO_4^{2-} + 23\ H^+ \longrightarrow [PW_{12}O_{40}]^{3-} + 12\ H_2O$$

The free acids of a number of heteropoly anions are sufficiently stable to be crystallized from aqueous solution [Pope, 1983]. Unwanted side reactions and the presence of complex equilibria are possible, so caution must be taken during preparation in order to avoid hydrolytic decomposition of polyanions and nonhomogeneity of the metal cation to polyanion ratio in the solid [Corma, 1995]. Hence, in the case of a number of heteropolyanions careful control of temperature or of pH may be necessary.

Stability of Heteropolyacids

Stability of heteropoly acids depends on the nature of the central atom: the larger the central atom, the more stable the heteropoly anion structure is. In the case of the

secondary structures, water molecules connect the individual heteropoly anions through weak hydrogen bonds. Thermal stability of heteropoly compounds was studied extensively [Southward, 1995; Mizuno and Misono, 1998]. It has been shown by infrared analysis that both W-HPA and ammonium salt of tungstophosphoric acid $(NH_4)_3PW_{12}O_{40}$ (NH_4-HPS) are stable up to 400°C [Southward et al., 1994]. Thermal decomposition of Mo-HPA occurs in a wide temperature range (280-400 °C), leading to mixtures of molybdenum trioxides. Mizuno and Misono observed that the Keggin structure of Mo-HPA is completely destroyed above 450°C [Mizuno and Misono, 1998].

Applications of Heteropolyacids

Applications of heteropoly acids focus on the use of their redox properties, and high charges. HPAs are commonly used in heterogeneous and homogeneous catalysis and there have been many journal publications in this area. Examples of some of the reactions include: hydrocarbon oxidation, olefin hydration, polymerisation, epoxydation etc. HPAs have also been used in biochemistry as precipitants for proteins and analytical reagents for proteins, alkaloids and purines, e.g., for colorimetric determination of uric acid and cholesterol. Moreover, their insoluble salts have been used as ion exchange materials [Pope, 1983].

The Use of Heteropolyacids as Acid Reagents in Removing Basic Impurities

HPAs are potentially very effective in the chemisorption of basic gases. Adsorption of ammonia onto Keggin type heteropoly acids leads to the formation of stoichiometric amount of ammonia salt. Stoichiometrically, three molecules of ammonia can be chemisorbed by one molecule of heteropoly acid irreversibly. Analysis of stoichiometries obtained from NH_3 uptake indicates formation of 3 NH_4^+ ions per Keggin unit for W-HPA [Southward et. al., 1995].

$$H_3PW_{12}O_{40} + 3\ NH_3 \rightarrow (NH_4)_3\ PW_{12}O_{40}$$

As a result, surface area of the HPA considerably increases and that indicates the participation of the ammonia ion in the structural rearrangement of the bulk HPA. Furthermore, Essayem et al. has used NH_3 TPD frontal method to deduce the maximum amount of ammonia irreversibly adsorbed by each Keggin unit. The amount of

irreversibly adsorbed ammonia was found to be equal to 4 per Keggin unit, which is higher than the proton content of $H_3PW_{12}O_{40}$ [Essayem et. al., 1997].

In this project tungstophosphoric acid (W-HPA; $H_3PW_{12}O_{40}.nH_2O$) and molybdophosphoric acid (Mo-HPA; $H_3PMo_{12}O_{40}.nH_2O$) are being used as acid reagent as it has been shown that W-HPA is the strongest acid among the Keggin-type HPAs. However, it should also be noted that the acid strength of the Keggin HPA depends weakly on their composition [Kozhevnikov et. al., 1998].

Supported Heteropolyacids

Supporting heteropoly acids provides an effective way to increase the surface area of bulk acids. Adsorption from solution technique is the most commonly used preparation method of supported heteropoly acids. Supports that do not strongly interact with the acid are preferred as the strongly interacting supports can hydrolyse and partially decompose the acid. Supported acids on non-interacting supports, however, will also slightly solubilize in polar reactants at elevated temperatures [Soled et al., 1996]. Acidic or neutral substances such as SiO_2, active carbon, acidic ion-exchange resin, etc., are suitable as supports and amongst them the most often used is SiO_2. It has been observed that the basic solids, e.g. MgO, tend to decompose HPAs [Kozhevnikov et al., 1998].

Mizuno et al. (1998) reported that HPAs strongly interact with supports at low loading levels, while the bulk properties of HPAs prevail at high loading levels. On the other hand, certain active carbons can firmly entrap HPAs and show high stability. Maximum loading level of HPAs on carbons in the literature is 7-14 wt % and varied moderately with the physical properties of the carbon support, but little with the chemical treatment [Mizuno et al., 1998]. Mizuno and Misono (1998) have also reported that the acid strength of supported $H_3PW_{12}O_{40}$ decreases in the sequence of supports: SiO_2>α- Al_2O_3 > activated charcoal [Mizuno et al., 1998]. Pizzio et al. showed that when carbon is used as a support, supported acid is thermally stable up to 425°C similarly to the bulk acid [Pizzio et al., 1998].

The nature of the HPA species supported on carbons depends also on the concentration of the impregnating solutions, the solvent used and the pH of the solution, among other

variables. In this regard Kozhevnikov et al. have found that $H_3PW_{12}O_{40}$ retains its Keggin type structure when supported from concentrated aqueous solutions onto the chemically activated carbon [Kozhevnikov et al., 1998]. For low HPA contents, partial decomposition of the acid $H_3PW_{12}O_{40}$ was observed. This is probably due to depolymerization of the species $(PW_{12}O_{40})^{3-}$ into the lacunar anion $(PW_{11}O_{39})^{7-}$ in the aqueous solution used to impregnate the carbon through the following reaction:

$$(PW_{12}O_{40})^{3-} + 5\,OH^- \rightarrow (PW_{11}O_{39})^{7-} + (HWO_4)^- + 2\,H_2O$$

It was also shown that the use of ethanol-water solvent in the impregnating solutions helps to retain the original Keggin structure in the solution [Concellón et al., 1998].

Further study is necessary to be carried out to get a deeper knowledge about solute-support interaction. Moreover, the nature of the species present in the initial HPA solutions, in the solutions after the impregnation process and the species deposited on the support should be identified, as they are highly dependent on the preparation method and subsequent thermal treatment [Pizzio et al., 1997; Concellón et al., 1998].

There has been a tremendous amount of work on the preparation of supported HPAs. However, the continuous dissolution of HPAs in polar medium has remained the most severe problem for the supported HPAs. In order to overcome this problem, supporting HPAs via sol-gel method was investigated. W-HPA was trapped in the silica structure and according to the characterisation studies it has been shown that the HPA acidity is the same as of bulk acid. WHPA-silica composites were synthesized with up to 80 wt% loading [Kukovecz et al., 2002].

I.II.2 CLEAN ROOM TECHNOLOGY

Clean rooms are specially constructed areas that are designed to control airborne particulates, temperature, humidity, pressure, airflow patterns, air motion and lighting to meet the required cleanliness level in the manufacturing environment, mainly in microelectronics and pharmaceutical industries, medical engineering, hospitals, food and cosmetic industries.

The dust and particles controlled in a clean room are extremely small. Clean room contaminants can be classified as either particulate or molecular. Process-limiting molecular contaminants include: acids, bases, condensables and hydrocarbons with a boiling point greater than or equal to 150 °C. Particulate contaminants are dustlike materials and were considered as having the highest impact on device quality and performance. Hence, most of the studies on clean room equipment design have focused on removing particulate contaminants. Visible particles are generally larger than 10 μm and are removed at the stage of pre-filtering. In the case of clean room, so called submicron particles, smaller than 1 μm, are the subjects to control.

According to the United States Federal Standard the cleanliness is defined on the basis of particle diameter and the classes are named after the number of particles that are 0.5 μm or more in diameter. Some of the most commonly used standards are Federal Standard 209 Clean Room and Work Station Requirements, Controlled Environments, version history: A (1963), B (1973), C (1987), D (1988) and E (1992); British Standard 5295:1989; ISO 14644-1 Classification of Air Cleanliness (International), Australian Standard AS 1386 (1989), France AFNOR X44101 (1972) and Germany VD I.2083 (1990). Table I.II-1 compares the US FED STD 209E to the new ISO 14644-1 classifications.

Table I.II- 1 The US FED STD 209E and the new ISO 14644-1 classifications

ISO 14644-1	ISO Class	1	2	3	4	5	6	7	8	9
FED STD 209E	English			1	10	100	1000	10.000	100.000	
	Metric			M1.5	M2.5	M3.5	M4.5	M5.5	M6.5	

According to ISO standard, the classes are based on the formula

$$C_n = 10^N \times \left[\frac{0.1}{D}\right]^{2.08}$$

where, C_n is the maximum permitted number of particles per cubic meter equal to or greater than the specified particle size, rounded to a whole number; N is the ISO class number, which is 9 or less; D is the particle size in micrometers.

Table I.II- 2 ISO Airborne Particulate Cleanliness Classes

CLASS	Number of Particles per Cubic Meter					
	0.1 μm	0.2 μm	0.3 μm	0.5 μm	1 μm	5 μm
ISO 1	10	2				
ISO 2	100	24	10	4		
ISO 3	1,000	237	102	35	8	
ISO 4	10,000	2,370	1,020	352	83	
ISO 5	100,000	23,700	10,200	3,520	832	29
ISO 6	1,000,000	237,000	102,000	35,200	8,320	293
ISO 7				352,000	83,200	2,930
ISO 8				3,520,000	832,000	29,300
ISO 9				35,200,000	8,320,000	293,000

Providing clean air streams can be seen as the first step for establishing clean room environments. For this purpose, High Efficiency Particulate Air (HEPA) filters or Ultra-Low Penetration Air (ULPA) filters are used depending on the air cleanliness level required for achieving and maintaining the desired product quality. HEPA and ULPA filters have particularly high collection efficiencies for submicron particles [Schroth, 1996]. HEPA filters can remove particles larger than 0.3 μm in diameter with more than 99.97% collection efficiency. ULPA filters are now being used in the semiconductor industries and they have more than 99.999% collection efficiency for 0.1 μm particles.

It has also been realized that molecular contamination can affect the geometry and performance of electronic devices to a great extent [Kinkead, 1997]. For example, deep ultraviolet (e.g., operating at wavelengths 248 nm or 193 nm) photolithography systems can be process-limited by the presence of about 600 ppt of proton accepting contaminants such as ammonia.

The major air contamination sources particularly in semiconductor devices manufacturing sites have been classified as particulates, organic materials, metallic materials, native oxide and adsorbed molecules. Wet chemical cleaning and drying technologies have successfully achieved removal of particulates, organic and metallic materials. However, removing native oxides and adsorbed molecules is still remaining a severe problem [Ohmi, 1991].

Adsorption/condensation and chemisorption are the two common molecular contaminant removal techniques. The contaminants with a boiling point of 100° C or greater may be removed by using activated carbon alone by adsorption/condensation mechanisms, while removal of contaminants with lower boiling points such as ammonia, requires chemisorption mechanism. Therefore the design of molecular air purification equipment requires careful study of the boiling point, vapour pressure and reactivity characteristics of the molecular pollutants [Kinkead et al, 1997].

The reactivity of the reagent selected to remove the targeted molecular contaminant plays an important role in the effectiveness of the molecular filter. Unfortunately, some of the most highly reactive reagents, such as liquid acids have significant vapour pressure under normal operating conditions and, therefore, naturally generate molecular components that would affect many clean room processes. Furthermore, some reagents react with molecular contaminants and produce unstable by-products that may sublimate or have vapour pressures at normal operating temperatures (ca. 20°C) [Kinkead et al., 1997]. In this case, it will be necessary to install downstream filters to remove impurities released by the liquid strong acid reagents, which significantly increases the operating costs.

I.II.3 SUPPORT MATERIALS

Two types of synthetic carbons, Sibunit™ and Novacarb™, and two types of mesoporous silicas, SBA-15 and sol-gel derived SiO_2, have been selected as support materials for heteropoly acids. Additionally, silica-HPA composites have been prepared in order to incorporate HPAs in the silica walls to overcome their leaching from the supports' pores due to their continuous dissolution in the polar media, such

as water. Sibunit and Novacarb have been kindly supplied by Boreskov Institute of Catalysis, Novosibirsk, Russia and MAST Carbons Ltd., UK, respectively. SBA-15, sol-gel derived silica and the composites were prepared in the University of Bath Chemical Engineering Department in collaboration with the Chemistry Department.

Sibunit™

Sibunit™ is produced by the deposition of pyrocarbon on a granulated carbon black via the pyrolysis of C_1-C_4 hydrocarbons at 850-950 °C, with the consecutive burning out of the carbon black. Sibunit has higher resistance to attrition and mechanical crushing than the conventional porous carbon materials produced by the traditional methods [Fenelov et al, 1998]. Sibunit™ has been used as support material in adsorption and catalysis systems [Timofeeva, 2002 & Timofeeva 2004].

Sibunit structure formation process is shown in Figure I.II-4. First stage (Figure I.II-4 a-b) is called condensation or chemical vapour deposition (CVD) and in this stage pre-granulated carbon black is covered by a fixed amount of pyrocarbon. This amount usually ranges from 1 to 5 gr per 1 gr of the initial carbon black. Second stage (Figure I.II-4 c-d) is the activation stage and it is conducted in the flow of steam at 700-850 °C. During this stage part of the carbon is removed by gasification. Most defected parts of pyrocarbon are removed first, and then the gasification of the carbon black starts. At the end of this stage, a sponge-like structure, which consists of mesopores and macropores is obtained. Dimensions of the pores depend on the dispersion of initially formed carbon black. Granules lose their mechanical strength when the carbon black is almost completely burnt out (Figure I.II-4 e), and then they finally crash into shell-like fragments.

All structural and textural properties of Sibunit can be varied by varying the amount of the initial carbon black dispersed, temperature and the time of the activation stage in this general production scheme. For example, macropore size can be varied from 10^2 to 10^4 nm by adjusting the initial carbon black dispersion, treatment conditions and granulation. Also by using finely dispersed carbon black, varying the amount of deposited pyrocarbon and its burn off extent, mesopore size and volume can be controlled and varied in the range of 2-100 nm. Finally, in order to control the size and

volume of micropores, the quantity of pyrocarbon and its burn off extent must be controlled. The size range of the micropores varies between 0.4 and 2 nm. Finally, the specific surface area and the pore volume can be varied from 0.1 to 800 m^2 / g and 0.1 to 2.0 cm^3 / g, respectively [Fenelov et al, 1998].

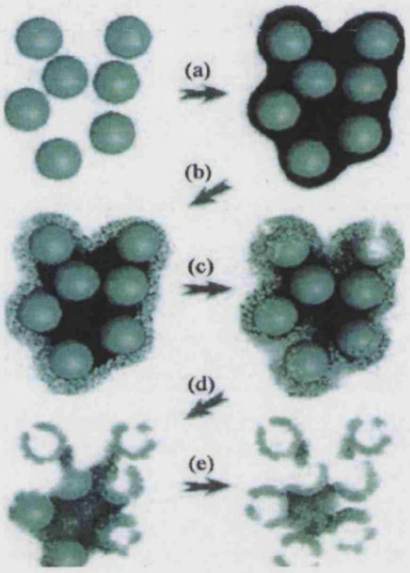

Figure I.II-4 Sibunit structure formation process [Fenelov et al., 1998].

Novacarb™

Novacarb™ is a phenolic resin derived synthetic carbon and has improved purity, strength and physical form in comparison with activated carbons, generally produced by the calcination of the various natural precursors in an inert atmosphere. Chars and pitch, produced from natural resources, can either be activated to produce a granular material or ground to a finer powder, in which case the powder is reformed into a green extrudate using the pitch from the calcination stage and then activated. Currently activated carbons are produced using a powdered char that is bound with a pitch, then re-carbonised and activated. Re-carbonisation of pitch into carbon leads to a differential shrinkage between the carbon matrix and the polymeric binder. This introduces interfacial defects and considerably weakens the carbon structure and consequently limits the production of complex carbon structures other than the simple extrudates, as more complex sructures will not withstand the mechanical stresses in the activation furnaces. Using binders could be encountered as the main problem in

the production of activated carbons. However, Novacarb™ overcomes this problem by following a binderless production process, in which all of the forming stages are carried out by using polymeric materials and these materials are carbonised and activated in the final stage.

Many polymer systems have been investigated as the precursors to synthetic carbons. The cost of the precursor and the yield of the carbon product during the carbonisation and the activation stages play an important role in the selection of precursor materials. Phenolic resins are used as a precursor to Novacarb™ production, as it has been observed that phenolic resin derived carbons have high purity and a relatively homogeneous structure combined with a controllable macro- and micropore structure [Tennison, S. R., 1998]. Polymeric resins can be produced by the polymerisation of various phenols such as, phenol, cresol, xylenols and aldehydes such as formaldehyde, acetaldehyde, glyoxal, furfural, by a sequence of three reactions: 1. aldehyde addition to phenol, 2. Chain growth or prepolymer formation and 3. Crosslinking or curing. The resin can be ground to a fine powder, typically 1-500 μm in diameter, which can then be formed into a desired shape. Novacarb™ production route is as follows:

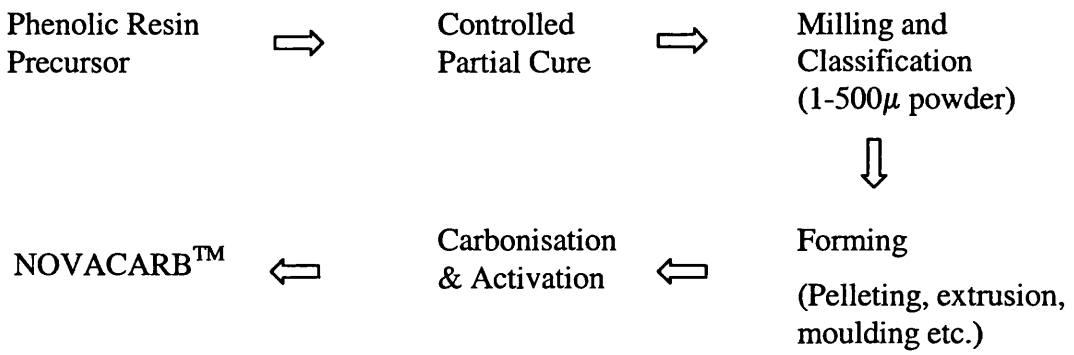

Figure I.II-5 Novacarb™ Production Route [Tennison, S. R., 1998]

SBA-15

Mesoporous silicas with narrow pore size distribution have attracted increasing attention as a novel material for separations and reactions involving large molecules. Several types of mesoporous silica have been developed since MCM-41 and FSM-16 were discovered by Mobil researchers in 1992. SBA-15 (Santa Barbara Amorphous) has recently been synthesised in an acidic medium with poly(alkylene oxide) triblock

copolymers, such as poly(ethylene oxide)-poly(propylene oxide)-poly(ethylene oxide) (PEO-PPO-PEO) [Wang et al., 2001, Washmon-Kriel et al., 2001 and Galarneau et al., 2001].

SBA-15 has well-ordered hexagonal mesoporous silica structure with uniform cylindrical pores which have pore sizes up to approximately 30 nm. They are synthesised via surfactant templating route at temperatures between 35°C and 140°C. In particular, it has been observed that poly(ethylene oxide)-poly(propylene oxide)-poly(ethylene oxide) (PEO-PPO-PEO) block-co-polymers are very good candidates as templates for the synthesis of SBA-15. Pore size and the thickness of the silica can be adjusted by varying the temperature of the reaction solution and the reaction time. Higher temperatures or longer reaction times result in larger pore sizes and thinner silica walls.

Calcination process removes the surfactant and makes the pores accessible. According to Zhao et al.'s study, calcination at 500 °C gives porous structures with pore sizes from 4.6 to 30 nm, pore volume fractions up to 0.85 and silica wall thicknesses of 3.1 to 6.4 nm [Zhao et al., 1998].

In general, micelle templated silica materials, e.g. MCM-41, MCM-48 and SBA-3, have high pore volume ca. 0.7 ml/g, surface area ca. 700 m^2/g and large pore opening ca. 2 nm. SBA-15 has a more regular structure and a thicker channel wall than MCM-41. Hence, they show much higher thermal stability. The material itself is non-acidic, as the silanol groups on the surface are non- or very weakly acidic. However if it is required, incorporation of aluminium into the framework of these mesoporous molecular sieves may create new acid sites on the surface.

SBA-15 has been used for various applications, such as, adsorption, catalysis and catalyst support, mould to template the diameter and orientation of wires of thermoelectric materials, photoredox systems for solar energy conversion, and storage and immobilisation of proteins and enzymes [Galarneau et al, 2001; Hua et al., 2001; Yiu et al, 2001; Luan et al., 2001 and Hillhouse et al., 2001].

Sol-gel derived silica

Sol-gel technology advanced over a long period of time and the patent literature reveals many industrial applications of sol-gel technology, particularly in the areas of coating and catalysts, prior to 1950. Recent improvements have enabled the sol-gel chemists to tailor ceramic materials to exhibit specific properties, leading to applications in optics, electronics and structural ceramics [Wood and Dislich, 1995]. In the late 1970s, sol-gel science and technology explosion was initiated by glass scientists in Japan, France, Germany and Italy. Over the past 25 years sol-gel science has grown rapidly in the preparation and properties of silica. Presently, research and development of sol-gel technology is very active in many countries and the leaders are the U.S.A., Japan, France and Germany [Mackenzie, 1995].

The term sol-gel was first invented in the late 1800s and it generally refers to a low temperature method using chemical precursors that can produce ceramics and glasses with better purity and homogeneity than high temperature conventional processes. Brinker and Scherer have defined sol-gel as the preparation of ceramic materials by preparation of a sol, gelation of the sol, and removal of the solvent. Sol and gel have also been defined separately as a fluid, colloidal dispersion of solid particles in a liquid phase, and a solid consisting of at least two phases wherein a solid phase forms a network that entraps and immobilizes a liquid phase, respectively. Solid particles in the colloidal precursors can be metals, metal oxides, metaloxy-hydroxides or other insoluble compounds. The aggregation or flocculation degree of the colloidal precursor can be adjusted to vary the pore size and the drying characteristics of the resulting gel.

Processing steps include the forming of the precursor mix into a desired shape, rigidifying and curing to yield a final product. The rigidifying step can involve dehydration, gelation, chemical crosslinking or freezing and the curing step can involve calcining and firing or drying or ultraviolet curing.

Advantages of this process include control of the purity of the reagents and the degree of homogeneity of mixing of the precursors, control of the phase and microstructure evolution and an opportunity for fabrication into useful, non-traditional shapes, such as,

fibers, thin films, bubbles, optical elements, patterned surfaces etc. [Wood and Dislich, 1995] and the capability to produce compositions that are not possible with the conventional methods.

Applications of sol-gel process are numerous. Particularly, it is suited for the preparation of thin films and coatings, as the use of liquid solutions at room temperature is a great advantage. Additionally if the techniques are available, just about any crystalline and non-crystalline films or coatings can be applied to many substrates. Besides, even though the preparation of relatively large monolithic samples by the sol-gel method is expensive and difficult due to the raw material prices, porosity, and large shrinkages, the formation of thin films is free from such problems. Preparation of new hybrid organic-inorganic materials is another active field of research [Mackenzie, 1995]. There are mainly three types of such materials. Type one is based on the impregnation of organics into the continuous ultra fine pores of an oxide gel, i.e. polymethylmethacrylate has been impregnated onto stabilised SiO_2 gel to give transparent nanocomposites of interesting properties. Type two is based on the entrapment of organics in an oxide gel matrix. The oxide matrix basically protects the entrapped organic. The third type of hybrids is based on reactions in solution in which the organic component forms a chemical bond with the inorganic component and the resulting compound can have interesting mechanical properties, i.e. rubbery material containing SiO_2. The field of this type of applications is extremely broad and covers divers areas, biology to electrical engineering and from catalysts to rubbery solids [Mackenzie, 1995]. The largest application areas for coatings and thin films used in electronic, optical, and electro-optic components and devices include substrates, capacitors, memory devices, infrared detectors, and waveguides. Antireflection coatings are also used for automotive and architectural applications. Powders of single- and multicomponent compositions can be made with sub-micron particle size for structural, electronic, dental, and biomedical applications. Composite powders have also been patented for use as agrochemicals or herbicides.

HPA-Sol-gel Silica / SBA-15 Composites

Adsorption from solution technique has been used by several researchers in order to support heteropoly acids onto several supports, such as carbon, silica, zirconia etc.

However, continuous dissolution of supported heteropoly acids has been observed due to the high solubility of HPAs in the polar media, such as, water. Consequently, this has become the most severe problem for the use of adsorption from solution technique for the preparation of stable supported heteropoly acid based catalysts.

In order to overcome this problem sol-gel preparation technique was investigated. According to the literature the most common HPA composites have been prepared by the entrapment of the HPAs in the silica matrix. It was reported by Kukovecz et al. (2002) that they have successfully synthesised W-HPA – silica composites up to 80 wt. % W-HPA loading and that the silicate structure traps the heteropoly acid molecules and their acidic character remains intact [Kukovecz et al. 2002]. Furthermore, this method allows controlling the synthesis variables, such as the concentration of the acid in the composite.

Molnár et al. (1999) also encapsulated W and Mo containing Keggin type heteropoly acids into silica matrix and they have studied the acidity by ammonia thermo-desorption method [Molnar et al., 1999]. They have found that the W containing composites had higher acidity than the Mo containing composites which are also in good agreement with the results reported earlier for the bulk acid samples. They have also observed that the composites had higher thermal stability than the bulk acids.

Nowińska et al. (2003) prepared a mixed system containing the Keggin units in the mesoporous silica structure by crystallisation of mesoporous material using the initial gel comprising heteropoly anions [Nowińska et al., 2003]. They have accomplished preparation of 20 wt. % HPA containing composites successfully. More importantly, they have observed that the template removal by calcination preserves mesoporous structure; however, washing of the samples with hot water for long periods resulted in the Keggin unit removal, which leads to the collapse of the mesostructure. This shows that HPAs is embedded in the silica matrix during the preparation of the composites as an important element of the structure [Nowińska et al., 2003].

Additionally, it has been reported that the HPA-carbon gel /zirconia composites have been successfully prepared via the sol-gel preparation technique [Lopez and Gomez, 1999 and Mukai et al., 2003].

HPA composites prepared by the sol-gel method have been mainly used for the heterogeneous catalysis purposes in order to replace homogeneous catalysts. In addition, Lavrenčič et al. (2001) has prepared hybrid sol-gel membranes of organically modified silicate type with embedded HPAs to study their possible applications in direct methanol fuel cells and optical switching devices due to their high proton conductivity at room temperature, ca. 0.02-0.1 S/cm, a relatively small size of the isolated Keggin ion, ca. 10Å, and their high solubility in water and in many organic solvents [Lavrenčič, 2001].

To the best of author's knowledge, there has been no work published in the literature concerning SBA-15-HPAs composite materials.

Brominated Novacarb™

Adsorption interactions are related not only to the porous structure of the carbon but also to the various heteroatoms which constitute the surface layer. The presence of these heteroatoms depends on the precursor materials used in the production process. They may also be in the form of numerous types of oxygen containing sites, ash, nitrogen or halogen containing sites. Surface properties of carbons can easily be modified by the removal or addition of oxygen groups using hydrogen reduction or aqueous nitric acid, peroxide or ammonium persulphate oxidation.

In order to reduce the interaction of water or other polar adsorbates with the surface, placing various halogens on the surface of carbons has been studied in detail by MacDonald et al., (2000) [MacDonald et al., 2000].

I.II.4 REGENERATION OF SUPPORTED HETEROPOLYACIDS

Mo-HPA was produced from its corresponding ammonium salt by Shimizu et al. (1986) [Shimizu et al., 1986]. Ammonium-HPA salt was calcined at a temperature of not lower than 400 °C in an inert gas. When the calcination of the ammonium salt was conducted in air, they have observed that the Keggin's structure in the heteropoly acid gradually decomposed and gave the crystal structure of molybdenum trioxide. Furthermore, they found that in order to obtain the heteropoly acid, it was necessary to

conduct calcination in the atmosphere where oxygen was not present. They concluded that the inert gas can be nitrogen, argon, carbon dioxide or combustion exhaust gases comprising carbon dioxide gas and steam. Finally, they found that the calcination temperature must not be lower than 400 °C since the Keggin anion structure is not broken even at around 600 °C.

During the calcination of ammonium salt in the stream of inert gas, ammonia may be volatilised and leaves a proton. At temperatures below 400 °C volatilisation of ammonia occurs very slowly. The lower the temperature the longer the calcination time is required. For the complete conversion of heteropoly salts into the free acids, at least 20 hours is necessary when calcination is carried out at 400 °C. Above 480 °C, 2 hours calcination was found sufficient for the complete conversion. In this study they have also observed that the final product showed heteropoly acid properties. It was soluble in water and the ammonium peak at 1400 cm^{-1} in the infrared spectrum representing ammonium disappeared, whereas the characteristic band of Keggin's anion was present [Shimizu et al., 1986].

Southward et al. claimed that the acid can be regenerated using thermal swing and steam reforming methods [Southward et al.,]. The first stage of this process would be to increase the temperature of the carbon supported acid onto which ammonia was adsorbed, using a hot inert purge gas (N_2), so that the weakly held ammonia that was physically adsorbed to the acid would be released from the structure at a relatively low temperature. Then, as the temperature was increased further, the salt would decompose as below:

$$(NH_4)_3PX_{12}O_{40(s)} \longrightarrow NH_{3(g)} + XO_{3(s)} + H_3PO_{4(s)}$$

This results in the evolution of the remaining ammonia gas and the production of a solid oxide and phosphoric acid. It has been suggested that these products can then be converted back to the original acid by steam treatment. Thus the entire process is:

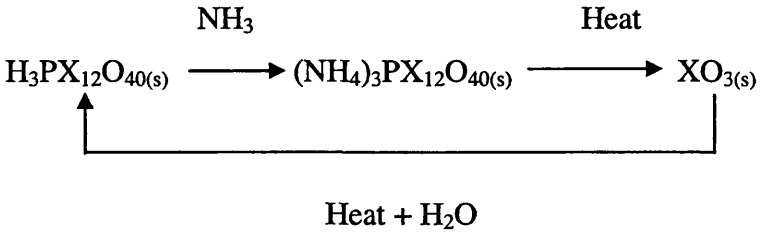

[Southward et al, 1995].

I.III EXPERIMENTAL

I.III.1 PREPARATION, HPA LOADING AND CHARACTERISATION OF THE SUPPORTS

Preparation

Sibunit™

Sibunit™ has been kindly supplied by Boreskov Institute of Catalysis. Prior to HPAs impregnation, carbon beads were washed with ethanol and water, and dried at 498 K in vacuum for 15 hours.

Novacarb™

Novacarb has been kindly supplied by MAST Carbons Ltd. Prior to immobilisation and the TPD experiments Novacarb was dried on air at 498 K for 15 hours.

SBA-15

SBA-15 was prepared following the method reported by Zhao et.al. (1998). In a typical synthesis, 2 g of Pluronic™ (BASF) (P123) co-polymer was dissolved in a mixture of 52.5 g H_2O and 12 g HCl (35.5%wt) at 313K. Once the complete dissolution of P123 was observed, 4.28 g tetraethoxy silane (TEOS) was added dropwise. The resultant mixture was stirred for 24 hours, poured in a polypropylene bottle and aged in an oven for 24 hours at 363 K.

Following aging, the mixture was filtered, washed with deionised water, dried for 48 hours under atmospheric conditions and subsequently calcined under continuous 50 ml/min O_2 flow. Calcination temperature was increased from ambient to 773 K at 1K/min and kept at 773 K for 6 hours.

Sol-gel derived silica

Sol-gel derived silica samples were prepared as described by Kukovecz et al. (2002). In a typical synthesis, 4.62 g tetraethoxy silane (TEOS, Fisher) was dissolved in a mixture of 2.753 g ethylene glycol and 2.67 g ethanol at 353 K. After stirring for 1 hour, a

mixture of 8 g ethanol, 2 g of water and catalytic amount of acetic acid were added to the system. The solution was kept stirring at 353 K until a clear transparent gel was obtained, typically 3 hours. The resulting gel was aged at ambient conditions for 24 h and dried under vacuum at 413 K for 3 hours. Finally, the samples were calcined in air at 723 K for 6 h. Calcination temperature was ramped from ambient to 723 K at 1°/min. Following the calcination the colour turned into greenish white.

SBA-15/ HPA Composites

SBA-15-HPA composites were prepared by following a very similar procedure to pure SBA-15 preparation. 2 g of P123^{TM} was dissolved in water at 313K and the calculated amount of heteropoly acid was added to this mixture. SBA-15 production required high acidity, typically pH between 0 and 1. This pH level was accomplished with the addition of HCl for SBA-15 production. However, addition of heteropoly acids lowered the pH and HCl amount was decreased accordingly. The amount of HCl in solution was adjusted to maintain pH $\approx$ 1.

It was not possible to prepare SBA-15-HPAs composites with high HPA concentrations. With the addition of HPAs in the P123 solution, formation of agglomerates occurred. Hence, the HPA concentration was lowered and 0.3970 g Mo-HPA and 0.3065 g W-HPA were used to prepare composites containing 0.5% molar W-HPA and 1% molar Mo-HPA. The amount of HCl used was 0.502 gr and 0.3034 g for the preparation of Mo-HPA and W-HPA composites, respectively. Additionally, the amount of water was increased in accordance with the reduced amount of HCl. The amount of water used was 59.93 gr and 60.05gr for W-HPA and Mo-HPA composites' production respectively. 4.28 gr TEOS was added dropwise and the resultant mixture was stirred for 24 hours.

Samples were aged in an oven at 363 K for 24 hours, filtered, washed with deionised water and dried for 48 hours under atmospheric conditions. Calcination temperature of composite samples was decreased to 723 K in order to avoid decomposition of heteropolyacids.

Sol-gel Silica/ HPA Composites

Sol-gel silica-HPA composites were prepared following the same method as sol-gel silica preparation. 4.62 g TEOS was dissolved in a mixture of 2.753 g of ethylene glycol and 2.67 g of ethanol while stirring at 353 K in a water bath. In order to obtain 20, 50 %W-HPA and Mo-HPA loading in the final silica-HPA composites, calculated amount of W-HPA and Mo-HPA were added to this solution. For 20% composites, 1.16 g W-HPA/ Mo-HPA and for 50 % composites 4.62 g W-HPA/ Mo-HPA was used. After stirring this mixture for 1 hour, a mixture of 8 g ethanol, 2 g of water and catalytic amount of acetic acid (3 drops) was added to the first solution and stirred for 3 hours at 353 K to obtain a clear, transparent solid gel state. The resulting gel was aged at ambient conditions for 24 h and dried under vacuum at 413 K for 3 hours. Finally, the samples were calcined in oxygen flow at 723 K for 6 h. During calcination, temperature was increased from ambient temperature to 723 K in 8 hours.

Brominated Novacarb^{TM}

2.5 g Novacarb^{TM} was placed in a three neck glass flask. The flask was placed in a heating mantle and the temperature was increased to 400 °C. Carbon was flushed with argon in order to remove oxygen from the flask and the connecting lines. Small amount of bromine was added dropwise for 5 hours, under continuous argon flow. The final weight of the carbon was 3.39 gr, hence the increase in weight was 35.6%.

I.III.2 IMMOBILIZATION OF HPAs ONTO SUPPORTS

HPAs were impregnated onto various supports. Preliminary adsorption studies were carried out in order to obtain conditions for maximum loading of acids. HPAs were adsorbed from solution by means of stirring support materials in HPA solution for several hours and finally removing the solution by filtering and drying.

W-HPA and Mo-HPA were obtained from Fisher and purified by re-crystallization prior to preparing the solutions. 6-50-120 g (W) / L and 110 g (Mo) / L containing solutions were prepared by dissolving 7.83-67.76-156.65 gr W-HPA and 161.765 gr Mo-HPA in a mixture of 50 v% demineralised water and 50 v% 96% ethanol (soria) solution. pH of the solutions were measured and tabulated in Table I.III-1.

Table I.III- 1 pH Values of Heteropoly Acid Solutions

Acid	Concentration	pH Values
W-HPA	6g (W)/ L	2.32
	50 g (W)/ L	1.68
	120g (W)/L	1.33
Mo-HPA	110g (Mo) /L	1.06

Sibunit, Novacarb™, pure SBA-15 and sol-gel silica, brominated Novacarb™ were used as support materials. 1 g of support was weighted and placed in a glass vial. 4 ml of ethanol-water solution containing HPAs was added to the vial and stirred at 20 °C. Contact time was varied between 24 hours and 72 hours. Three equivalent samples were prepared for each support-solution set and stirred for 24-48-72 hours in order to observe the effect of the contact time. Once the selected contact time elapsed, samples were filtered and dried at 200 °C for 2 hours in an oven in air. Supported HPA amount was determined gravimetrically by weighting the sample before and after supporting HPAs.

Quantitative Analysis of Impregnated HPAs

Apparent adsorption of a given solute depends on the concentration of solute, temperature, type of solvent and type of adsorbent. When adsorbent is mixed with a binary solution, adsorption of both solute and solvent occurs. As a result of preferential adsorption of solute, the solute concentration in the liquid falls from the initial value c_o to the final equilibrium value c. The apparent adsorption of solute, neglecting any volume change in the solution, is then $V*(c_o - c)$ gr solute adsorbed / gr adsorbent, where V is the volume of the solution. This is satisfactory for dilute solutions when the fraction of the original solvent, which may be adsorbed, is small [Gregg and Sing, 1982]. In this study, volume of the solution, which is adsorbed, is assumed to be negligible. Following the impregnation, W and Mo concentrations in the solutions can be measured by atomic absorption spectroscopy (AAS). However, due to the unavailability of AAS, gravimetric method has been used to determine the adsorbed acid amounts on the samples. Supports were weighted before and after the contact with an acid solution. The difference between the two measurements was equal to the amount of acid loaded into supports.

I.III.3 CHARACTERISATION OF THE PLAIN AND IMPREGNATED SUPPORTS

Support materials and acid impregnated samples were characterized using low temperature nitrogen adsorption, mercury porosimetry, scanning electron microscopy, Fourier Transform Infrared Spectrometry, X-Ray diffraction and pycnometry techniques.

Porous structure of the supports and impregnated samples were determined from low temperature nitrogen adsorption. Additionally, Brunauer-Emmet-Teller (BET) specific surface areas, micro- and mesopore volumes of the samples were evaluated from the data obtained. Experiments were performed at -196 °C using ASAP-2010 instrument (Micromeritics). Samples were treated under vacuum at 200 °C for 12 hours prior to the measurements.

SEM analysis has been done to observe external morphology of the support materials. SEM pictures also enabled the determination of the mean size of Novacarb particle diameters. JOEL 6310 (JOEL UK Ltd.) model scanning electron microscope was used at 15 kV. Samples were immobilised on an aluminium tray of 1.5 cm diameter and coated with gold prior to the measurements. In addition, elemental analysis was carried out using EDAX for W-HPA and Mo-HPA loaded Sibunit particles.

FTIR spectra were recorded using Bruker EQUINOX 55 FT-IR spectrometer in transmission and reflection modes between 4000-650 cm^{-1} wavenumbers, using MCT-A detector with 4 cm^{-1} resolution. ATR cell (Golden Gate™, Specac Ltd.) and transmission cell were selected for the measurements. In the ATR mode, powder samples were used. For transmission measurements, samples were prepared as pellets prior to measurements. In the preparation step, 5mg sample was mixed with 70mg of potassium bromide (KBr). KBr was used to obtain self-supporting pellets with low sample concentration. The resultant powder was then cast into a 10mm die and pressed into a disc under 8-9 bar pressure.

Structures of pure SBA-15, W-HPA/ Mo-HPA-SBA-15 composites and W-HPA/Mo-HPA impregnated SBA-15 were studied by recording powder XRD patterns using

Bruker D8 powder diffractometer with Goebels mirrors in the 0 to 10° and 0.5 to 40 ° 2θ ranges.

In order to obtain water vapour sorption of the pure supports, static adsorption experiments were carried out at 30 °C using Intelligent Gravimetric Analyser (Hiden Analytical Ltd., UK). Increase in the sample mass was recorded against relative pressure p/p_o, where p is the actual pressure of the vapour and p_o is the saturated vapour pressure at 30 °C. Experimental study also includes a comparative study of the isotherms of the sorption and desorption of water vapour by pure support materials.

I.III.4 AMMONIA ADSORPTION AND TEMPERATURE PROGRAMMED DESORPTION

Adsorption and temperature programmed desorption of NH_3 onto plain, acid impregnated and composite supports were measured using a custom-built set-up equipped with a thermal conductivity detector (TCD). Temperature programmed desorption (thermal desorption spectroscopy) is particularly useful in surface science to study desorption of gasses. In the experimental system, the reactor is inside an oven, so that the temperature can be increased linearly in time. Gas consumption by the substance is derived from the change in thermal conductivity of the gas mixture. Typical heating rates used in the TPD experiments are between 0.1 and 25 K per second. TPD gives information on: quantitative adsorbate coverage, adsorption energy, lateral interactions between the adsorbates through the coverage dependence of the adsorption energy, the preexponential factor of desorption, which in its turn reflects the desorption mechanism [Niemantsverdriet, 2000].

Experimental Set-up for NH_3 Adsorption and TPD

An experimental rig for adsorption and TPD experiments was designed and constructed. The flow diagram of the rig is shown in Figure I.III-1. Bronkhorst Hi-Tec nitrogen and ammonia mass flow controllers with max 100 ml/min and 20 ml/min flow capacities respectively were used to measure the flow rates of the gas streams. Mass flow controllers were calibrated by using both bubble-flowmeter and Gillmont Precision

Rotameter. A quartz U shaped tubular reactor with 5 and 10 mm ID was used in the system. Quartz wool was placed in the large side of the tube acting as a bed in order to hold the sample. For very fine samples, e.g. Novacarb™, it was observed that the small particles blocked the flow and caused back pressure in the system. In order to overcome this problem, quartz beads were mixed with the sample as an inert and enabled gas streams flowing through the reactor by creating small channels.

The reactor was placed in a furnace built by Isoheat, UK, operating between 20-1000 °C with a temperature controller. Reactor temperature was observed by means of a thermocouple placed in the reactor. There was also another thermocouple attached to the furnace and connected to a separate thermometer. A data card was connected to this thermometer in order to record and store the data.

In order to obtain vapour mixtures, a simple vaporizer was designed. 250 ml Pyrex flask was used as a container for water and placed in a heating mantle to set and maintain the temperature hence the vapour pressure of the water. This heating mantle was connected to a temperature controller and the temperature was measured via a thermocouple placed in the mantle. A concentric heat exchanger was connected to the outlet of the vaporiser in order to adjust the temperature and, therefore, the amount of the vapour in the gas stream.

A thermal conductivity detector (TCD) (Pre Unicam Ltd., UK) was used to analyze gas concentration. The TCD was calibrated with premixed ammonia-nitrogen calibration gasses (Scientific and Technical Gasses Ltd., UK).

The connecting tubing used was stainless steel throughout the system and connections from the mass flow controllers to the reactor were heated and insulated. Temperature of the furnace, experiment duration and the signal from the thermal conductivity detector are displayed on the computer using LabView 6. The picture of the temperature programmed desorption rig can be seen in Figure I.III.2.

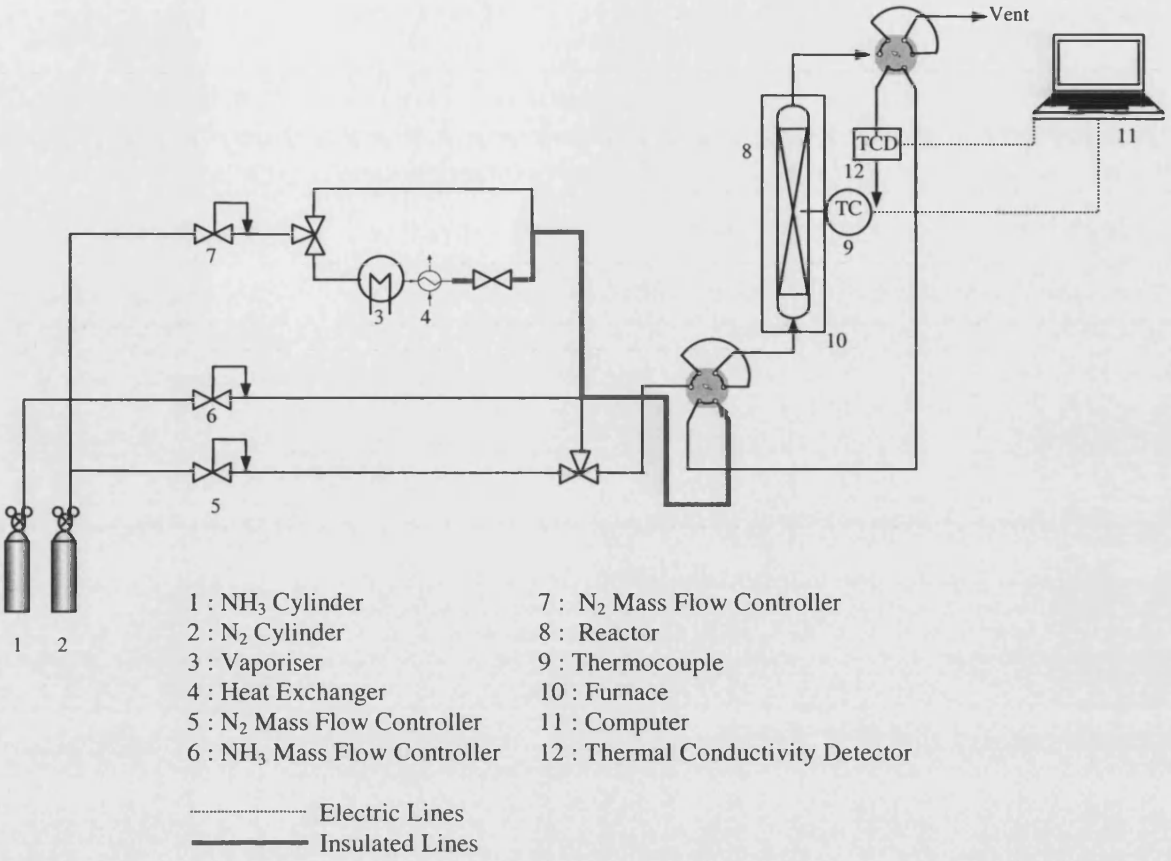

Figure I.III- 1 Temperature Programmed Desorption rig

Experimental Procedure for NH_3 Adsorption and TPD

Ammonia adsorption and temperature programmed desorption experiments were conducted and adsorption breakthrough and desorption curves were recorded using a custom-built set-up equipped with a thermal conductivity detector (TCD).

0.3 g sample was weighted, mixed with 0.3 g quartz beads and placed in the reactor. The reactor was then attached to the system tightly. Samples were pre-treated in the reactor at 20 ^{o}C in a stream of nitrogen until a stable TCD signal was observed, typically ca. 2 hours. Following the pre-treatment, nitrogen flow was switched to ammonia-nitrogen mixture. In a typical experiment 2.1 vol% ammonia in 70 ml/min nitrogen flow was used. During this process the TCD signal was observed and recorded against time. Ammonia-nitrogen mixture was flown through the reactor for 30 min. until TCD signal was back to the starting point, which indicated the end of ammonia adsorption.

The reactor and the system were flushed with nitrogen at 20 °C in order to sweep the physically adsorbed ammonia from the sample. TPD experiments were started from 20 °C at a heating rate of 5 °C/min using 70 ml/min nitrogen as a carrier gas and the TCD signal was recorded against sample temperature.

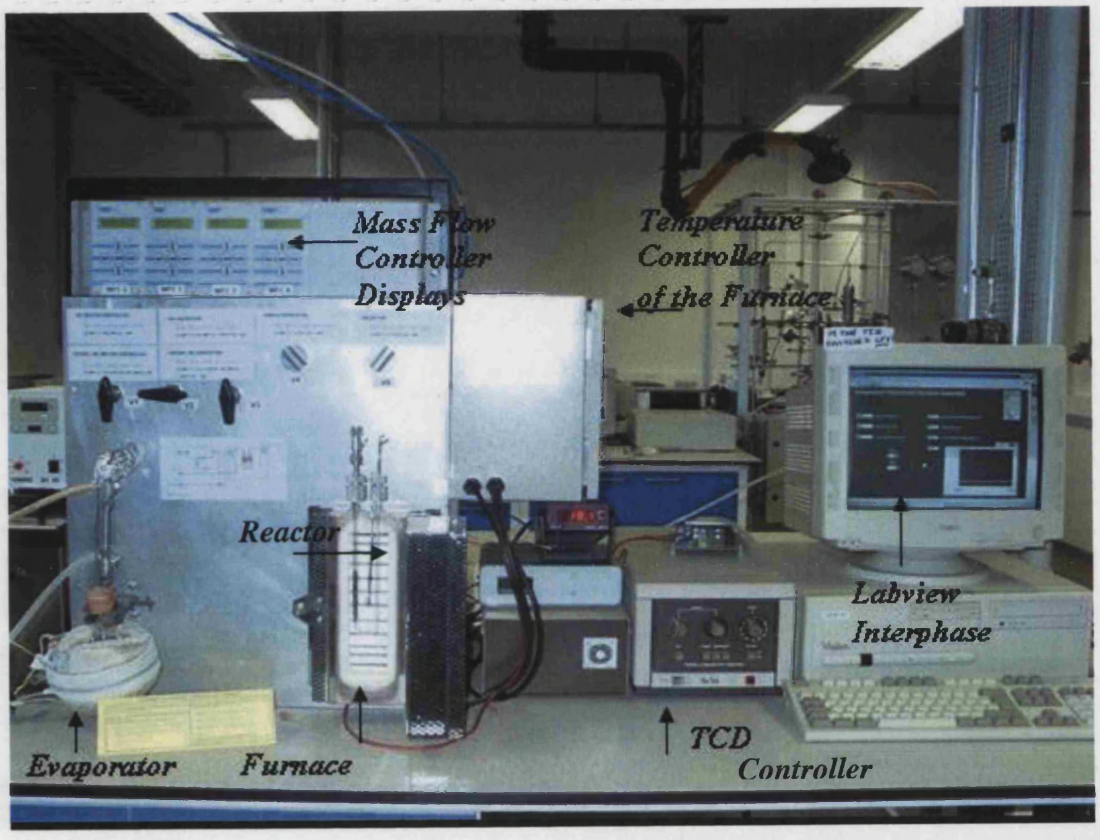

Figure I.III- 2 Temperature Programmed Desorption Rig

I.III.5 REGENERATION OF SUPPORTED HETEROPOLYACIDS

Regeneration of supported HPAs was carried out according to the study of Shimizu et al. [Shimizu et al., 1996]. Following the adsorption of ammonia onto Novacarb™ supported Mo-HPA and W-HPA at 20°C, samples were flushed with nitrogen in order to remove the physically adsorbed ammonia on the acids and the support. Then, temperature was increased to 500°C under 60 ml/min nitrogen flow and maintained at 500 °C for 2 hours. FT-IR spectra of the samples before and after the treatment were measured to observe the change in the ammonium peak.

I.IV RESULTS

I.IV.1 ACID IMPREGNATION

HPAs were impregnated onto various supports via adsorption from solution method using solutions containing 120 g (W)/L and 110 g (Mo)/L. The results obtained are tabulated in Table I.IV-1.

Table I.IV- 1 Heteropolyacid loading onto supports (%)

Sample	*W-HPA Loading (%)*	*Mo-HPA Loading (%)*
Novacarb™	24	20
Brominated Novacarb™	16	19
Sibunit	22	19
SBA-15	16	16
Sol-gel Silica	33	35

I.IV.2 CHARACTERIZATION OF THE SUPPORTS

Scanning Electron Microscopy

SEM images of Sibunit (crushed), Novacarb™, SBA-15, sol-gel silica are shown in Figures I.IV-1, I.IV-6, I.IV-3, I.IV-5, respectively. Figure I.IV.2 shows EDAX analysis of W-HPA and Mo-HPA loaded crushed Sibunit™. These results clearly show the presence of W and Mo in the Sibunit™. In addition to the carbon peak, a peak indicating gold element is also observed due to the gold coating of the sample during the sample preparation process in order to make samples conductive.

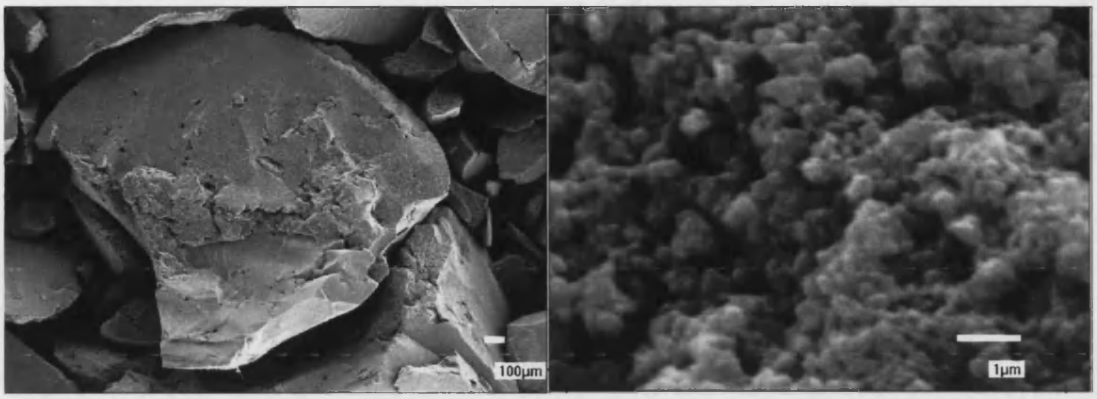

Figure I.IV- 1 Sibunit^{TM}(crushed) at magnifications 650 and 6500.

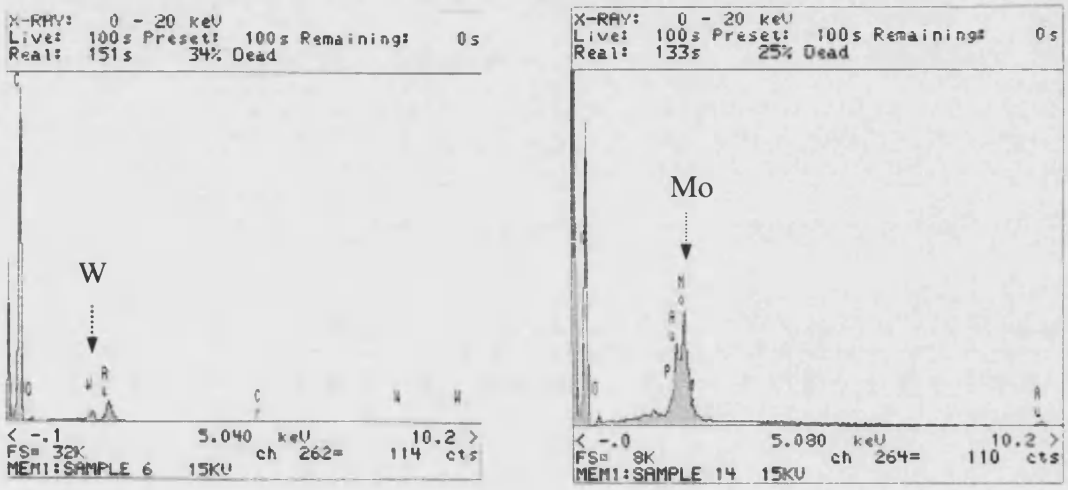

Figure I.IV- 2 EDAX analysis results for W-HPA and Mo-HPA supported Sibunit^{TM}.

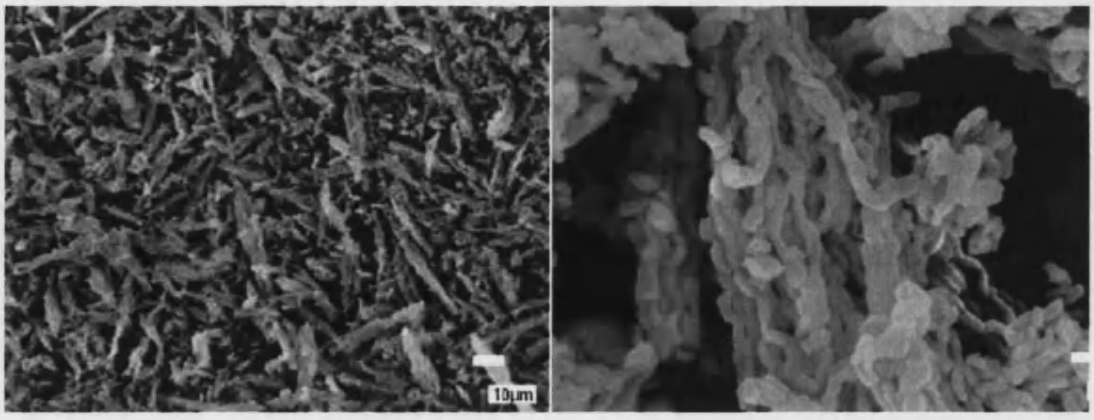

. Figure I.IV- 3 SEM images of SBA-15, before calcination at different magnifications

SEM images in Figure I.IV-3 shows SBA-15 morphology before calcination at different magnifications. It can clearly be seen that SBA-15 consists of ropelike structures approximately 1μm of size, aggregated into chain macrostructures. This structure is unique to SBA-15 and was reported earlier in literature [Zhao et al., 1998].

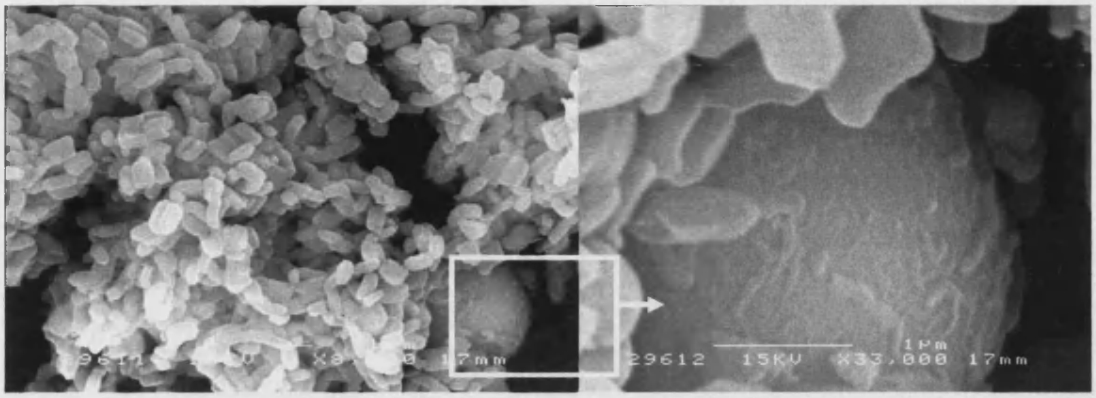

Figure I.IV- 4 SEM Image of Plain SBA-15 after calcination

Furthermore, in the calcined plain SBA-15 sample (Figure I.IV-4), a lump was observed which can most probably be identified as unstructured amorphous silica particle.

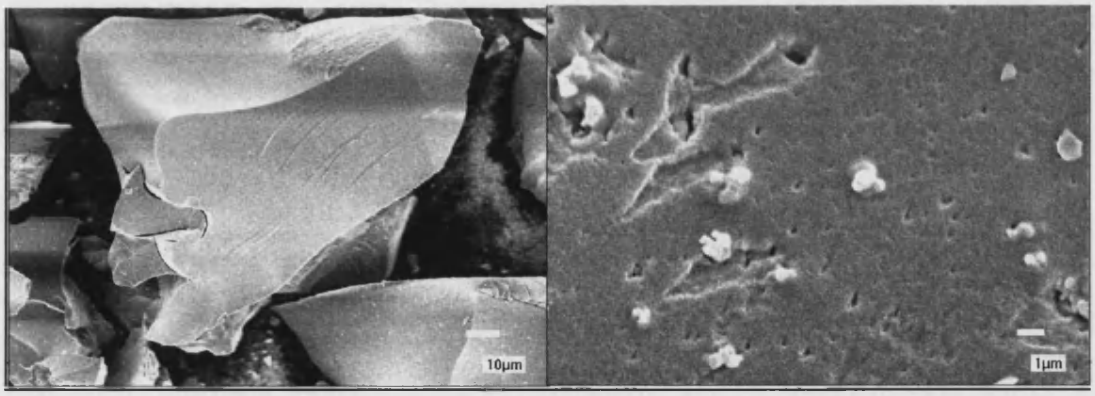

Figure I.IV- 5 SEM Images of plain Sol-Gel Silica

Amorphous silica samples prepared by sol-gel method have an irregular structure. Both powder and small particles of silica are present after the calcination. Figure I.IV-5 shows two SEM images of the sol-gel silica after calcination at 650 and 6500 magnifications. Large particles having smooth surfaces are observed. At higher

magnification some small pores of between 0.1 and 1 μm diameter can be seen on the surface.

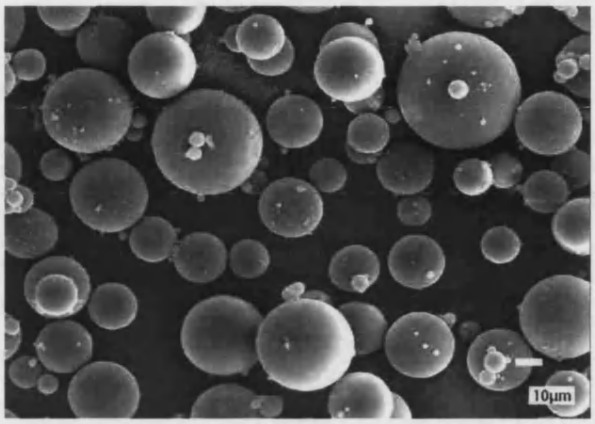

Novacarb is a very fine powder consisting of spherical particles of diameter between ca. 2 and 50 μm. Mean particle diameter was calculated as 22μm from the Figure I.IV-6 (30 particles were counted).

Figure I.IV- 6 SEM Image of Novacarb™

Low Temperature Nitrogen Adsorption

Low temperature nitrogen adsorption measurements were performed in order to obtain information about the porous structure of the samples prepared. Isotherms obtained are shown in Figure I.IV-7. All four isotherms posses a hysteresis loop. The shape of the hysteresis loops may vary. Certain shapes are associated with specific pore structures. Hysteresis loops in the isotherms obtained for Sibunit™ and Novacarb™ have particular shapes that might be associated with slit shaped pore and a pore in the form of an interstice between close-packed and equal-sized spherical particles, respectively. Certain silica gels tend to give loops as in sol-gel silica and SBA-15 isotherms and in these cases the shape of the pores is not well defined.

Additionally, if a solid contains micropores, the potential fields from neighbouring fields will overlap and the interaction energy of the solid with a gas molecule will be correspondingly enhanced. This will result in a distortion of the isotherm, especially at low relative pressures, in the direction of increased adsorption. It can be seen in Figure I.IV-7 that all samples also contain micropores due to nitrogen uptake at lower relative pressures.

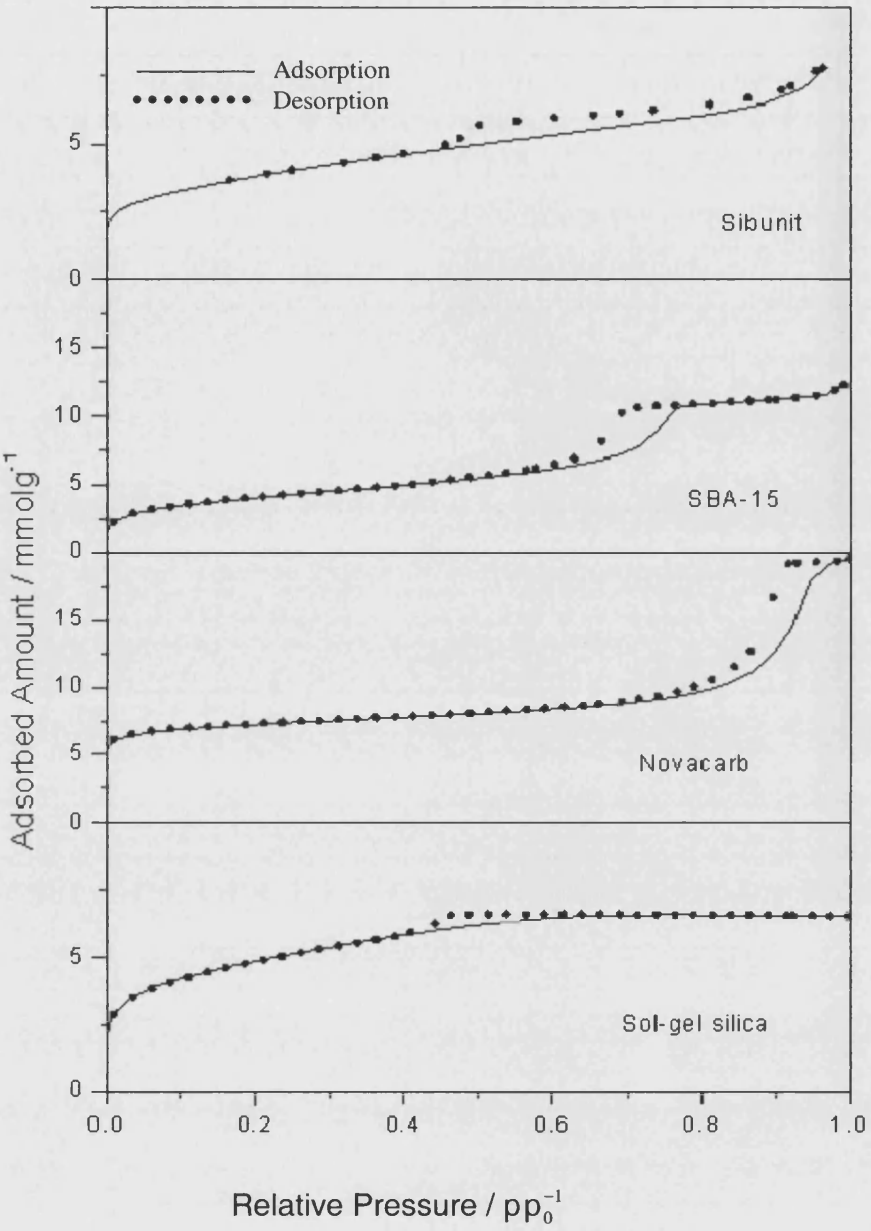

Figure I.IV- 7 Low-temperature nitrogen isotherm adsorption data measured at 77 K.

Table I.IV- 2 BET area, Micropore and Mesopore Volume of the supports

Sample	*BET (m^2/g)*	*Micropore Volume (cm^3/g)*	*Mesopore Volume (cm^3/g)*
Novacarb	522.06	0.18	0.52
Novacarb- WHPA (Impregnated)	359.37	0.12	0.35
Sibunit	286.08	0.02	0.23
Sibunit - WHPA (Impregnated)	149.09	0	0.17
SBA-15	321.10	0.01	0.38
SBA-15 - WHPA(Impregnated)	421.90	0.05	0.64
SBA-15 - MoHPA(Impregnated)	522.36	0.04	0.52
Sol-Gel Silica Plain	381.45	0.03	0.15
Sol-Gel Silica - WHPA(Impregnated)	240.10	0.03	0.10

Table I.IV-2 shows the Brunauer-Emmett-Teller (BET) area, micropore and mesopore volumes of the samples that were calculated using the 77K low temperature nitrogen adsorption method. The relative pressure range selected for BET area calculations was between 0.05 and 0.3. Mesopore volume was calculated from the desorption branch of the isotherms using BJH method and micropore volumes were calculated using t-plot method. Sibunit™ has been characterized as the support with the lowest specific surface area of the selected supports. It has previously reported with higher BET area (402 m^2/g and 0.6 cm^3/g total pore volume, all mesopores, 6.2 nm mean pore diameter) [Timofeeva et al., 2002]. Mesoporous pore volume is dominant in the structure of Sibunit™ and it has almost no micropore volume.

Novacarb was characterized as having the highest BET area, micropore and mesopore volumes amongst the support materials studied. The most significant difference between Novacarb and all other supports is that Novacarb has a relatively high micropore area as can be seen on the nitrogen adsorption isotherm that Novacarb adsorbs relatively high amounts of nitrogen at low relative pressures (see Figure I.IV-7). Reduction in the meso-pore and micro-pore volumes after impregnation indicates that the W-HPA molecules are adsorbed in both meso- and micro-pores of Novacarb. A decrease in the meso- and micropore volumes shows that micropores might also contain HPAs.

SBA-15 produced in this study has lower BET area than those reported in literature, e.g. between 600 and 1000 m^2/g [Zhao et al., 1998]. SEM study showed that SBA-15 has unstructured amorphous silica lumps, which could most probably the reason for characterising SBA-15 produced in this study with lower BET than that reported in the literature.

The Barrat–Joynmer–Halenda (BJH) method was employed for pore size measurements. Mean pore diameter for each support was calculated using the desorption branch of the isotherms. Figure I.IV-8 shows the pore size distribution of the plain supports Novacarb, Sibunit, SBA-15 and amorphous sol-gel silica.

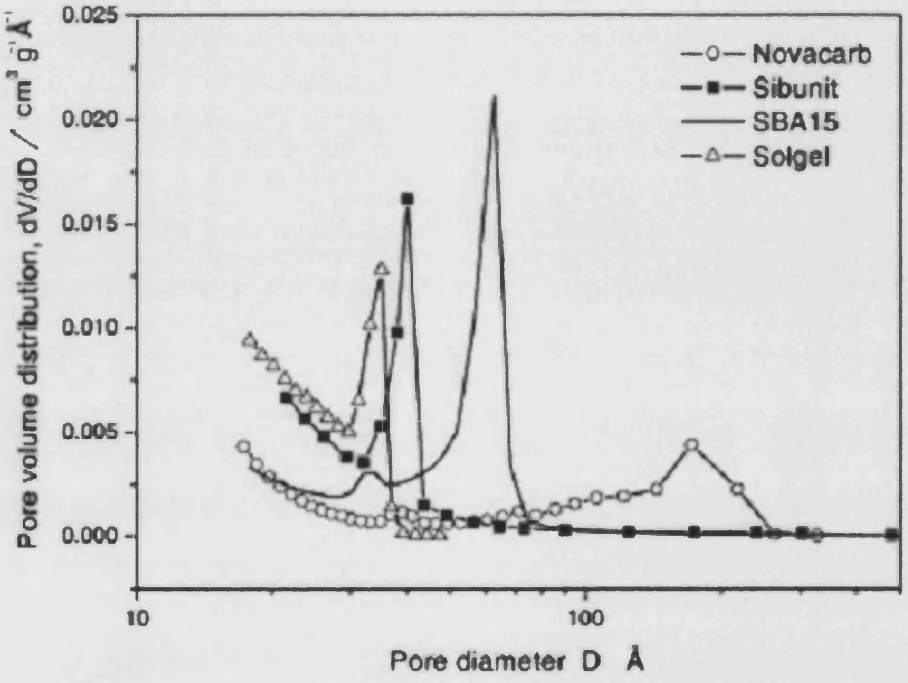

Figure I.IV- 8. Pore-size distributions calculated from nitrogen adsorption data using BJH method

Table I.IV- 3 Mean Pore diameter of the Supports

Support	*Mean Pore Diameter (Å)*
Novacarb	174
SBA-15	62
Sibunit	38
Sol-gel SiO_2	33

FT-IR Analysis

Each M_3O_{13} triad in the Keggin structure has a common oxygen vertex connected to the central heteroatom $X–O_a(M_3O_{13})$, (X :P and M:W and Mo). The other three classes of symmetric equivalent oxygens in the Keggin structure are $M - O_b - M$ connecting two M_3O_{13} units by corner sharing; $M - O_c - M$ connecting two M_3O_{13} units by edge sharing; and terminal oxygens $M = O_t$ [Concellón et al., 1998]. Measured wavenumbers and corresponding molecular vibrations of W-HPA and Mo-HPA are tabulated in Table I.IV-4 & I.IV-5 and are in good agreement with the previously published data [Concellón et al., 1998]. Keggin unit of the HPAs retains its structure when they are supported on Novacarb™ and so the characteristic peaks of the unit are clearly observed in both Novacarb supported Mo-HPA and W-HPA spectra (Figure I.IV-9 & I.IV-10). Characteristic peaks of the Keggin unit were recorded at 802-893-983-1075 cm^{-1} and 787-864-962-1062 cm^{-1} for Novacarb supported W-HPA and Mo-HPA, respectively.

Table I.IV- 4 FT-IR Bands of Keggin unit in pure and Novacarb supported W-HPA

Molecular Vibration	*Pure W-HPA (cm^{-1})*	*Novacarb™ Supported W-HPA(cm^{-1})*
ν_{as}(P-Oa)	1078	1075
ν_{as}(W=Ot)	986	983
ν_{as}(W-Ob-W)	895	893
ν_{as}(W-Oc-W)	802	802

Table I.IV- 5 FT-IR Bands of Keggin unit in pure and Novacarb supported Mo-HPA

MolecularVibration	*Pure Mo-HPA (cm^{-1})*	*Novacarb™ Supported Mo-HPA(cm^{-1})*
$\nu_{as}(P\text{-}O_a)$	1078	1062
$\nu_{as}(Mo{=}O_t)$	959	962
$\nu_{as}(Mo\text{-}O_b\text{-}Mo)$	866	864
$\nu_{as}(Mo\text{-}O_c\text{-}Mo)$	783	787

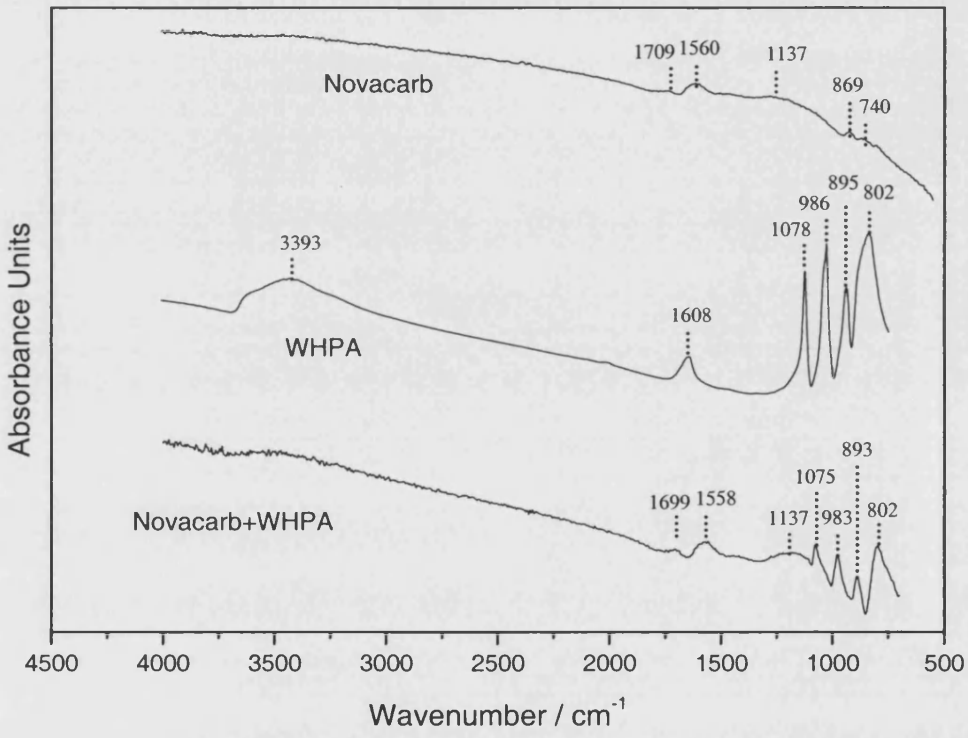

Figure I.IV-9 FT-IR Spectra of Novacarb, W-HPA and W-HPA (I) Novacarb

W-HPA and Mo-HPA spectra in Figures I.IV-9 & I.IV-10 show a strong absorption band at 3393cm^{-1} that corresponds to ν(OH) vibrations and a peak at 1608cm^{-1} is assigned to $\delta(H_2O)$ vibrations, Essayem et al. (2001) and Southward et al. (1994) have also reported the presence of these peaks. The peak at 3393 cm^{-1} essentially corresponds to water adsorbed on the sample. The later absorption at 1608$cm^{-1}$is representative of the presence of water clusters, probably the diaqua proton H_5O^+, and/or the hydroxonium ion.

Interpretation of the FT-IR bands of activated carbons could be very complicated as the characteristic bands of the activated carbons strongly depend on the type of precursor and treatment techniques used for the activated carbon production. The bands observed on Novacarb™ spectrum shown in Figure I.IV-9 are tabulated in Table I.IV-6. The peak at 1709 cm^{-1} could refer to either C=O groups of carboxylic acids or lactones. Similarly, the peak at 1560 cm^{-1} could be assigned to either C=O groups of surface quinine groups or C=C aromatic stretching band. C-O stretching in ether groups or C-OH stretching in phenolic groups might be the cause of the peak at 1137 cm^{-1}. Finally, the peaks at 740 and 869 cm^{-1} might be referred to C-H and O-H groups on the surface.

Table I.IV- 6 Characteristic Peaks of Novacarb™

Wavenumber (cm^{-1})	*Molecular Vibration*
1709 cm^{-1}	C=O
1560 cm^{-1}	ν_{as}(C=C)
1137 cm^{-1}	ν_{as}(C–O)
869 cm^{-1}	δ(C–H)
740 cm^{-1}	δ(O–H)

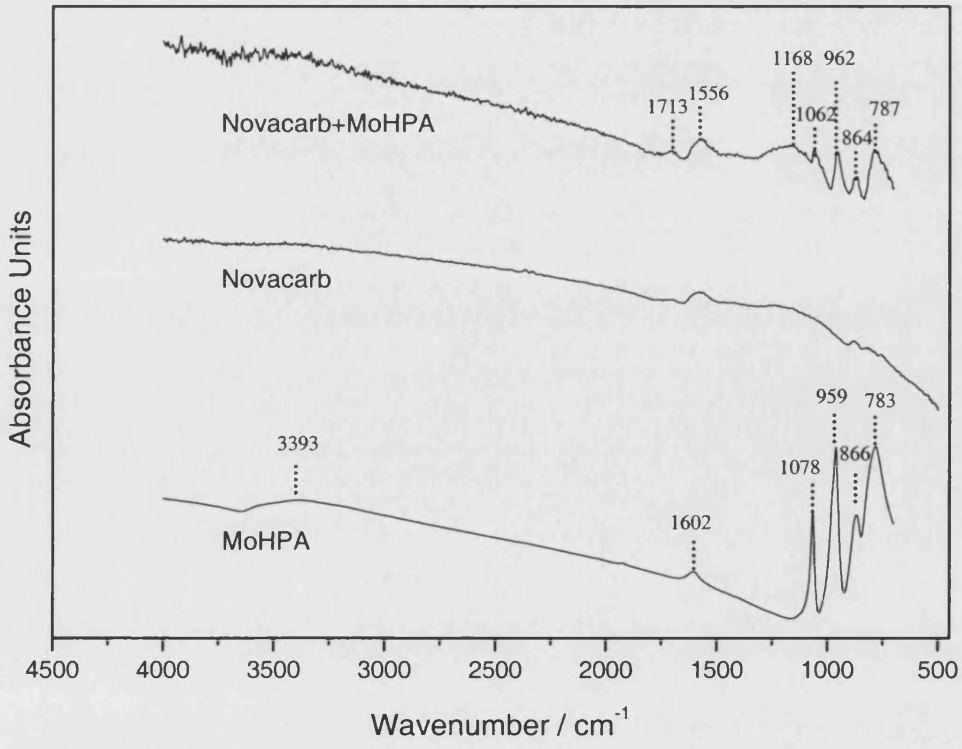

Figure I.IV- 10 FT-IR Spectra of Novacarb, pure Mo-HPA and Novacarb supported Mo-HPA

In order to obtain Sibunit bands, both MCT and DTGS detectors were employed, however, it was impossible to obtain clear spectrum. The best spectrum obtained is shown in Figure I.IV-11. The peak at 2353 is assigned as CO_2. Tremendous efforts have been put to eliminate this peak; however, its presence was very strong. The peaks at 821-904-977-1084 cm^{-1} with a slight shift could possibly be referred as the Keggin unit fingerprints on the Sibunit supported WHPA. Similar to Novacarb™, the peak at 1573 cm^{-1} is likely to show the presence of a C=C vibration. There are also two shoulders present at 997 and 1226 cm^{-1} that could possibly represent either stretching C-O bonds in ethers or carboxylic anhydrites [Figueiredo et al., 1999].

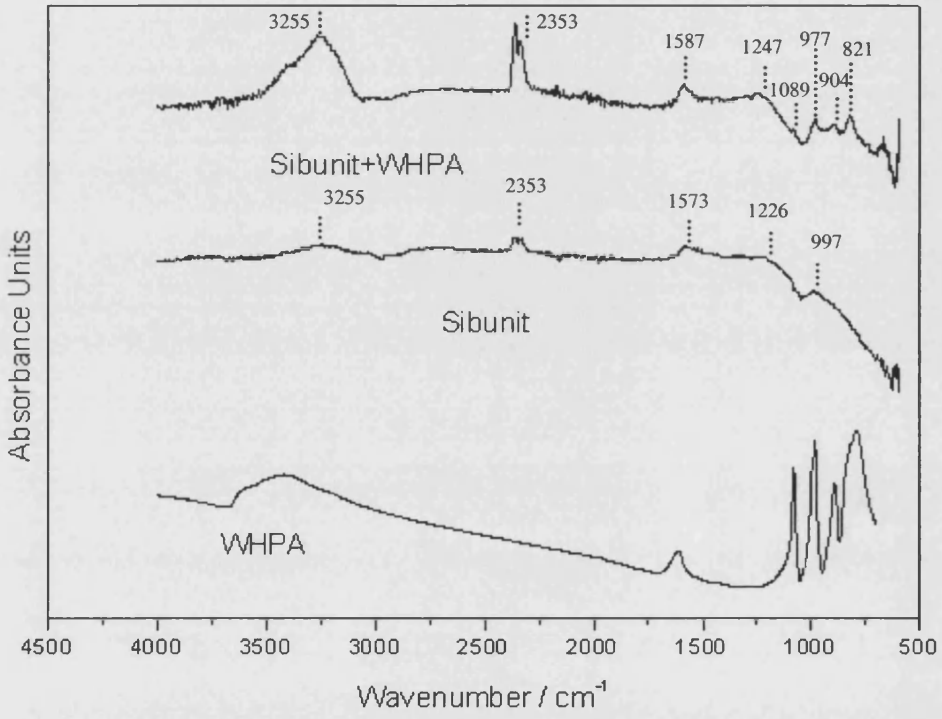

Figure I.IV- 11 FT-IR Spectra of Sibunit, pure W-HPA and Sibunit supported W-HPA

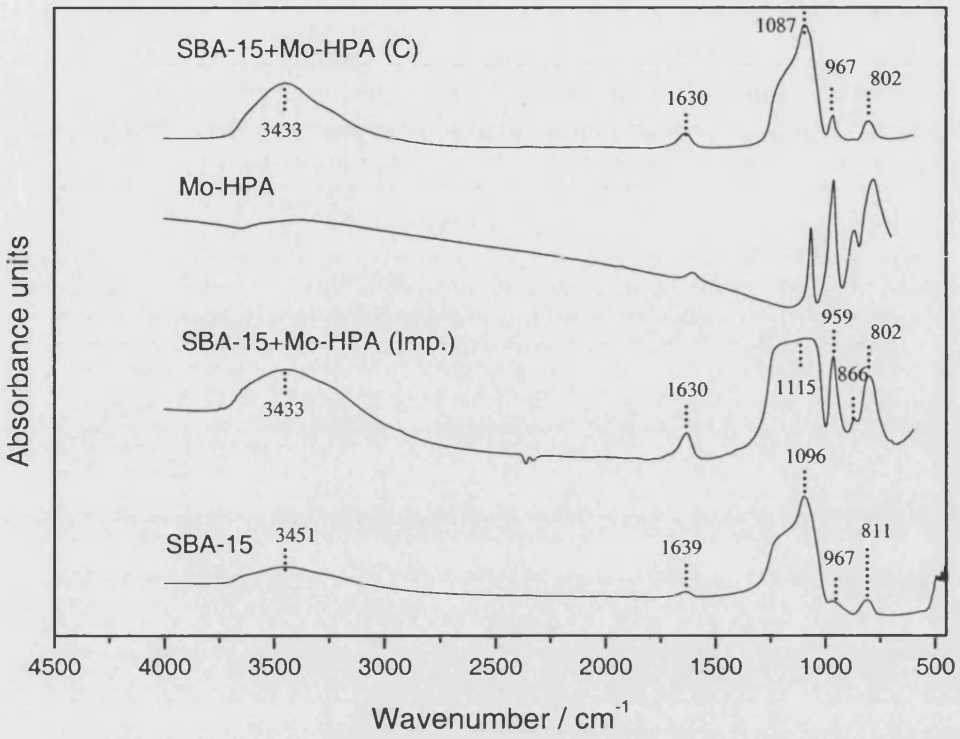

Figure I.IV- 12. FT-IR spectra of pure SBA-15 and Mo-HPA and Mo-HPA impregnated- composite SBA-15

SBA-15 and sol-gel SiO_2 show three characteristic peaks at 1096, 967 and 811 cm^{-1}. There are also two peaks at 1639 and 3451 cm^{-1}, which indicate the presence of water as clusters in an adsorbed state. Figure I.IV-12 shows the spectra of pure SBA-15 and Mo-HPA, and Mo-HPA impregnated and composite SBA-15. Mo-HPA impregnated sample shows three peaks at 959, 866 and 802 cm^{-1} that are assigned to Keggin unit fingerprints. The fourth peak is not present as the wide silica peak covers the area between 1000 and 1300 cm^{-1} giving a maximum at 1096 cm^{-1}. On the other hand, the wide Mo-HPA peaks at 959 and 866 cm^{-1}, cover the silica peaks. The Keggin unit cannot be observed on the SBA-15+Mo-HPA composite clearly due to the low heteropoly acid concentration; however, there is a relative rise in the peaks at 811 and 967 cm^{-1}, most probably caused by the heteropoly acid.

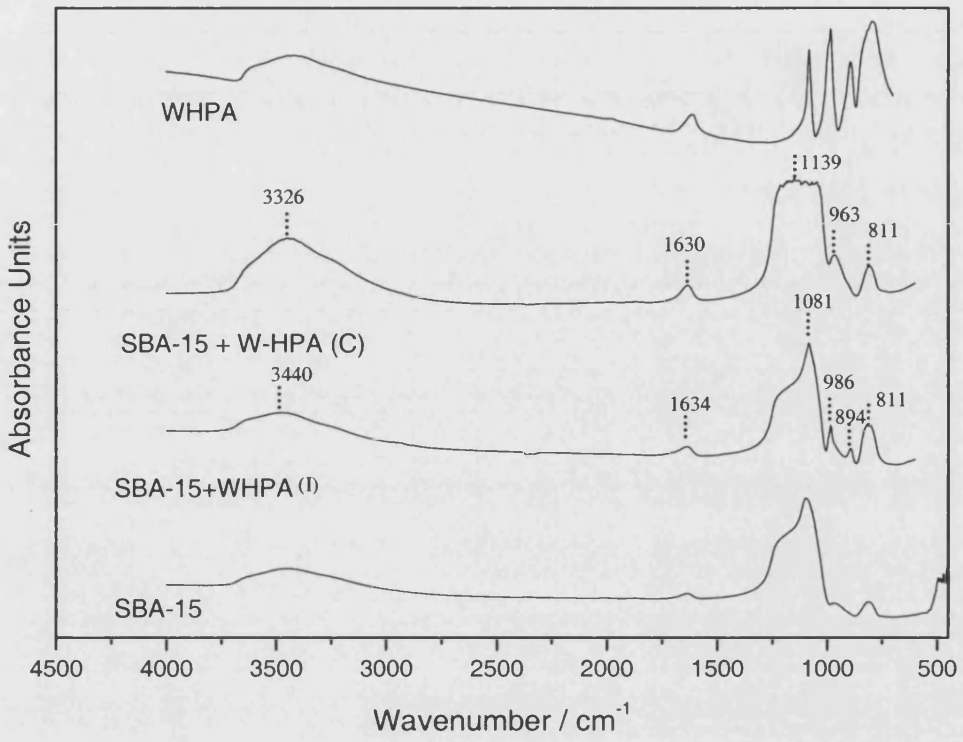

Figure I.IV- 13 FT-IR Spectra of pure W-HPA and SBA-15, W-HPA impregnated-composite SBA-15

Similarly, due to the low concentration of W-HPA, Keggin unit bands are not visible on the W-HPA-SBA-15 composite spectrum, however, the peaks at 963, 811 and 1139 cm^{-1} that indicate SBA-15 may have the contributions from Keggin unit bands. Whereas the peaks at 986 and 894 cm^{-1}, on the W-HPA impregnated SBA-15 spectrum, are more visible and are the evidence of the presence of the Keggin unit.

In the case of W-HPA composites of sol-gel SiO_2, the increase in the peak at 820 cm^{-1}, the shoulder at 894 cm^{-1} and the increase in the peak at 959 cm^{-1} could be the indications of the Keggin unit bands. W-HPA impregnated sample has a similar set of bands to the composite spectrum.

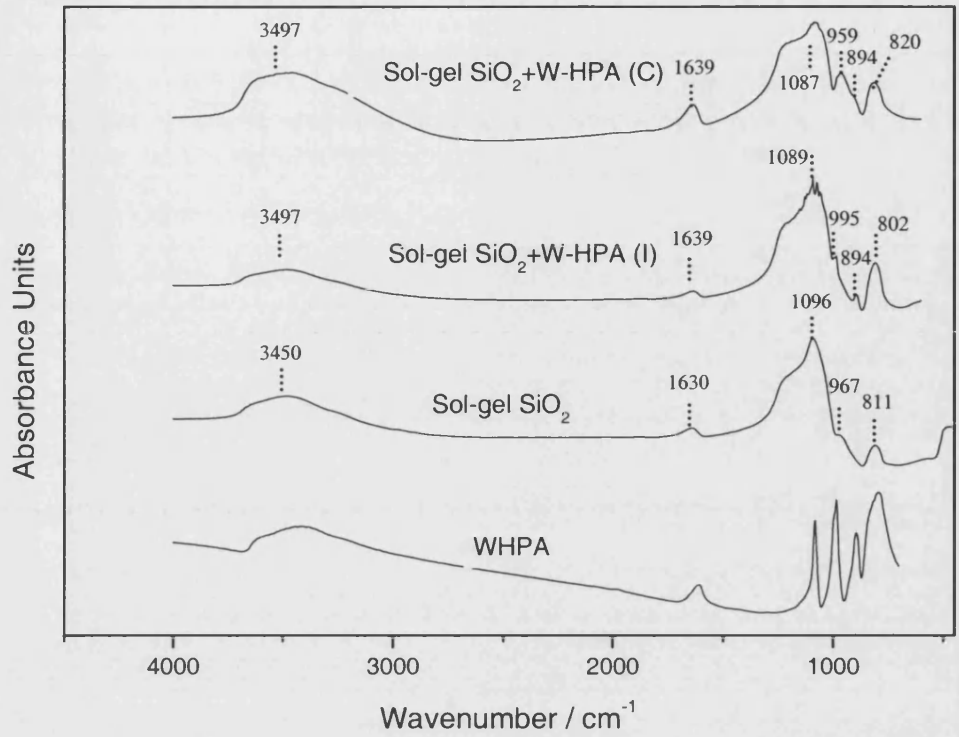

Figure I.IV- 14. FT-IR Spectra of pure sol-gel SiO_2 and W-HPA impregnated-composite sol-gel SiO_2.

The FT-IR spectra of Mo-HPA impregnated, 20 and 50w% composite sol-gel SiO_2 show clear bands of the Keggin unit as shown in Figure I.IV-15. When we have a closer look at the Mo-HPA composite sol-gel SiO_2 materials, we see the increase in the intensity of the Keggin unit fingerprints in the 50% composite, as expected.

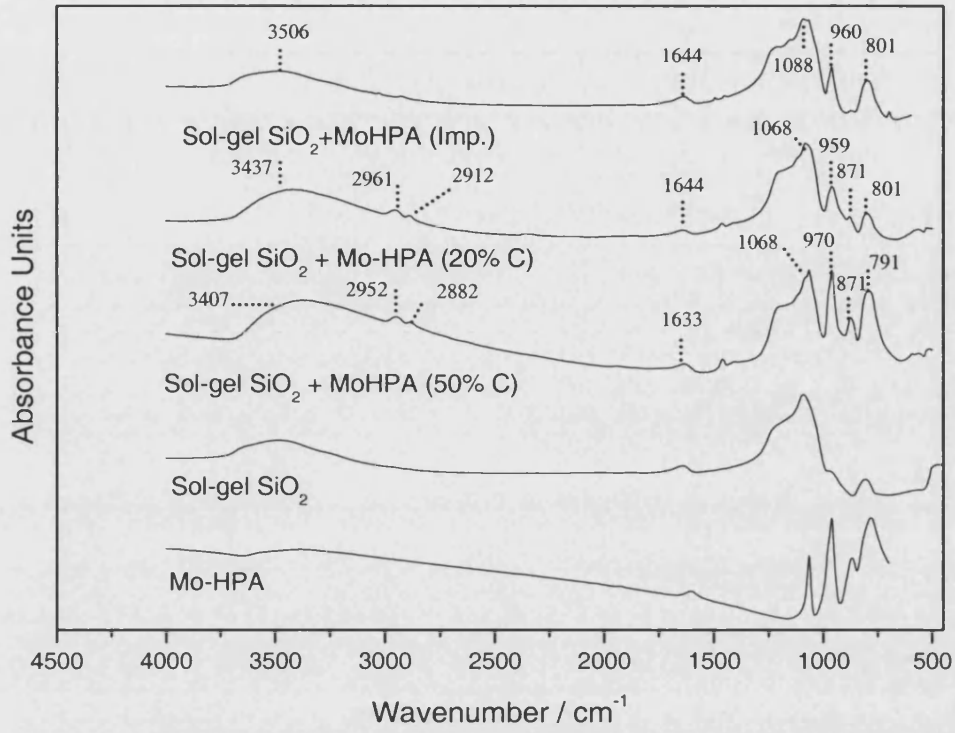

Figure I.IV- 15 FT-IR Spectra of pure sol-gel SiO_2 and Mo-HPA and Mo-HPA impregnated-20&50 wt% composite SiO_2

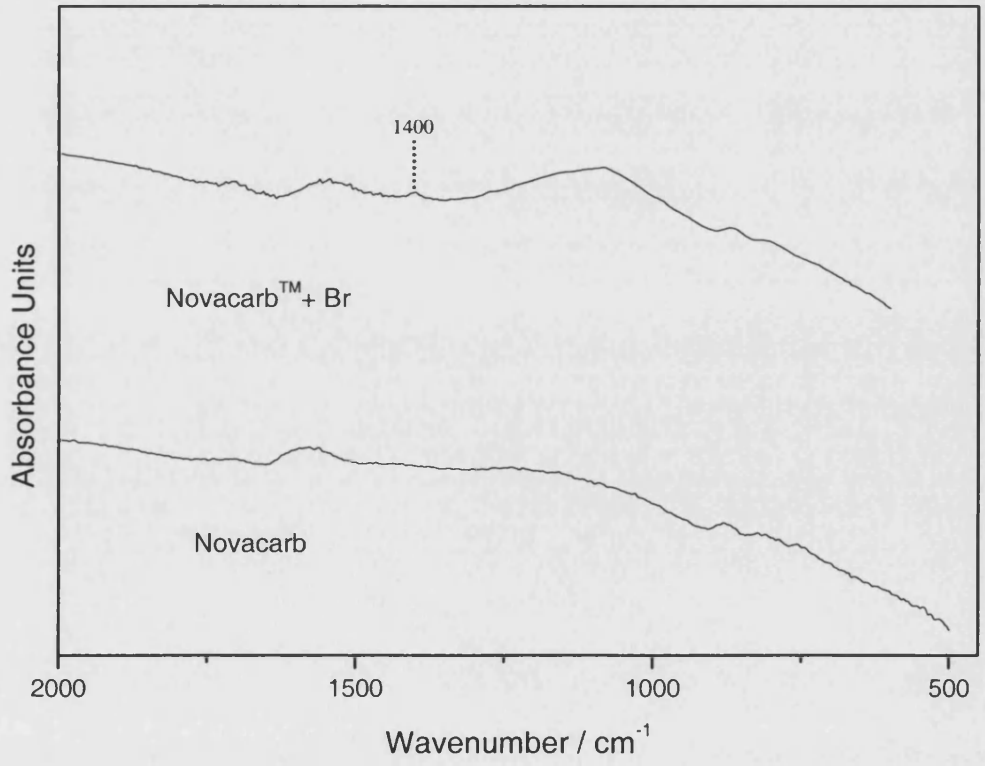

Figure I.IV- 16. FT-IR spectra of NovacarbTM and brominated NovacarbTM

The FT-IR spectrum of brominated Novacarb shows a band at 1400 cm^{-1} that is not present on the pure Novacarb™ spectrum (Figure I.IV-16). Additionally, an increase in the intensity of the peaks at 1709 and 1137 cm^{-1} is observed. The peak at 1400 cm^{-1} is probably due to symmetrical stretching of –COO–. Slight oxidation of the surface of the carbon might be the cause of the increase in the intensity of the peaks at 1709 and 1137 cm^{-1} due to the oxygen present during the bromination process. It is possible that the formation of C=O groups of carboxylic acids or lactones that shows a band between 1120 and 1370 cm^{-1} and 1665 and 1790 cm^{-1} is the reason for this increase [Figueiredo et al., 1999]. It is suggested that the peak that refers C-Br stretching appears in the range of 600–500 cm^{-1}, however due to the method used for this study, it was not possible to observe this band.

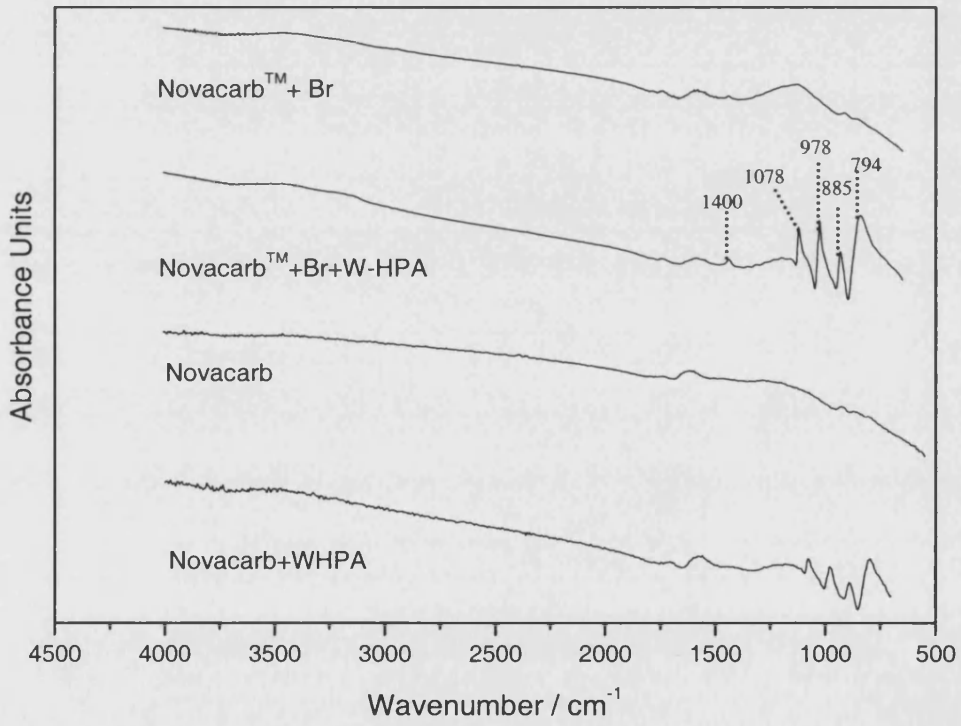

Figure I.IV- 17 Comparison of W-HPA loaded-brominated Novacarb™ to W-HPA loaded Novacarb™

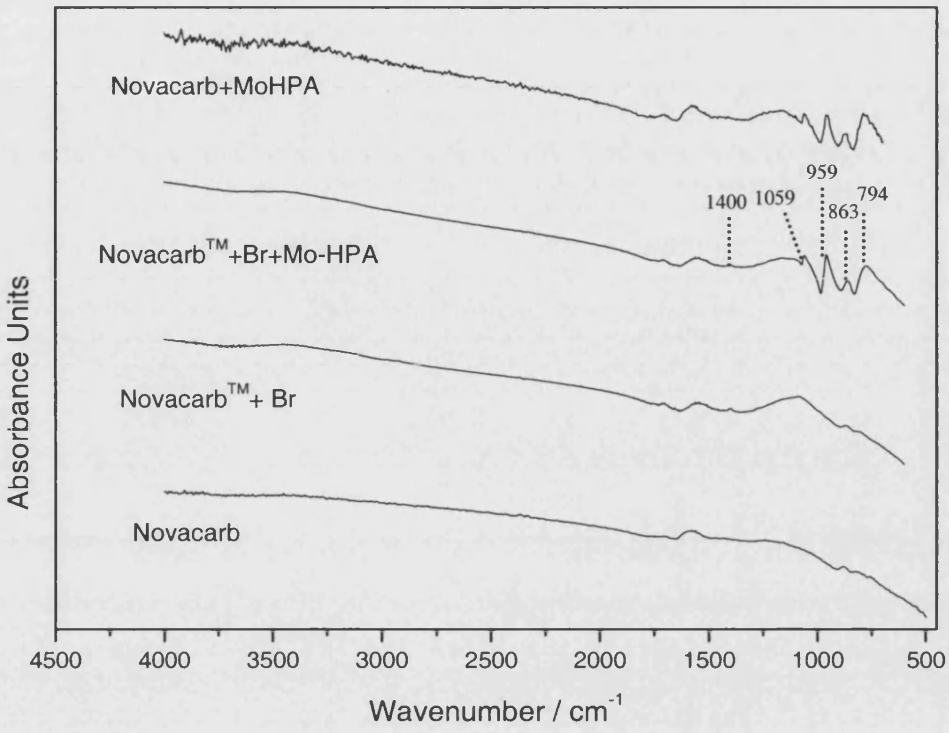

Figure I.IV- 18 Comparison of the brominated-Mo-HPA loaded NovacarbTM and Mo-HPA loaded Novacarb™

In conclusion, characteristic fingerprints of the Keggin unit of HPAs were observed during the analysis of pure, impregnated and incorporated samples. This finding clearly shows that HPAs retain their structure when they are supported onto adsorbents studied and incorporated into silica structure.

XRD

The powder XRD patterns of the SBA-15, 0.5 % W-HPA+SBA-15(composite), 1% Mo-HPA+ SBA-15(composite), W-HPA + SBA-15 (I), Mo-HPA+ SBA-15 (I) were recorded using Bruker D8 Powder Diffractometer with Goebels mirrors at room temperature. Selected 2θ range was 0.5° to 40 ° for W-HPA + SBA-15 (I) and 0 to 10° for other samples The small angle XRD pattern for all samples shows three peaks (Figure I.IV-19). These three peaks can be listed as (100), (110), (200) reflections and indicates hexagonal mesostructure. The (100) peak, which has the highest intensity, reflects a d-spacing of 94 Å.

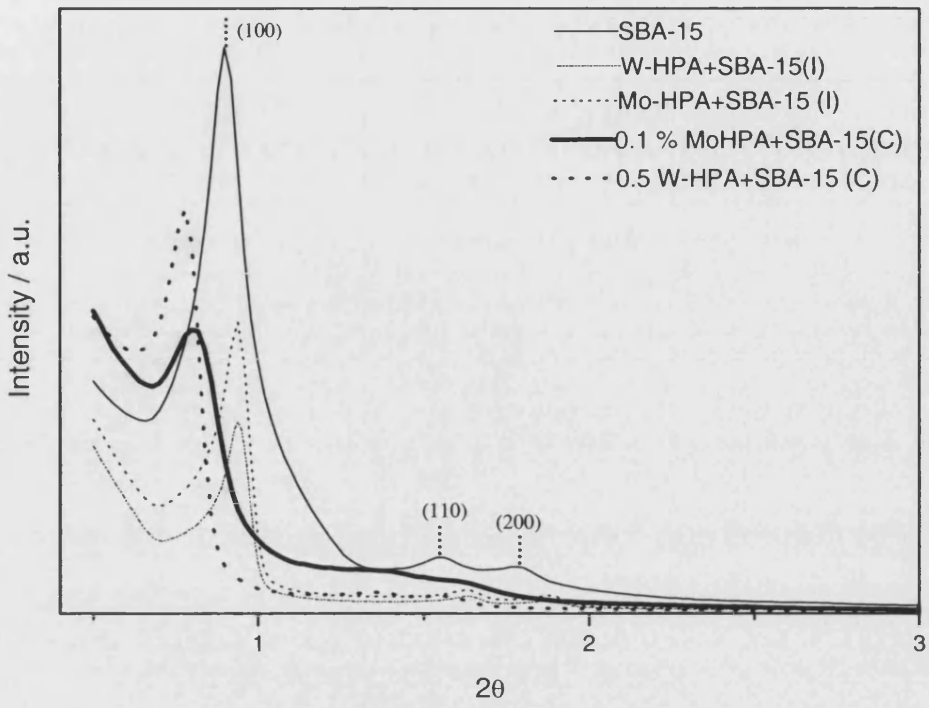

Figure I.IV- 19. Small angle XRD patterns of the W/Mo-HPA composite and impregnated SBA-15 samples

Diffraction from the (100) planes of the composite materials shifted to lower angles, from 0.9° to 0.82° and 0.78° for 0.1% Mo-HPA+SBA-15 and 0.5 %W-HPA+SBA-15, respectively. According to Bragg's Law, this decrease refers to an increase in the d-spacing most probably due to the interaction between the surfactant and the acids. Unlike composite materials, in the impregnated samples 2θ value shows a slight increase, from 0.9° to 0.94° for both samples, referring a decrease in the d-spacing. Bragg's Law equation is,

$$n\lambda = 2d\sin\theta$$

where, n is the order of scattering, θ is the angle of scattering and d is the space between the scattering entities.

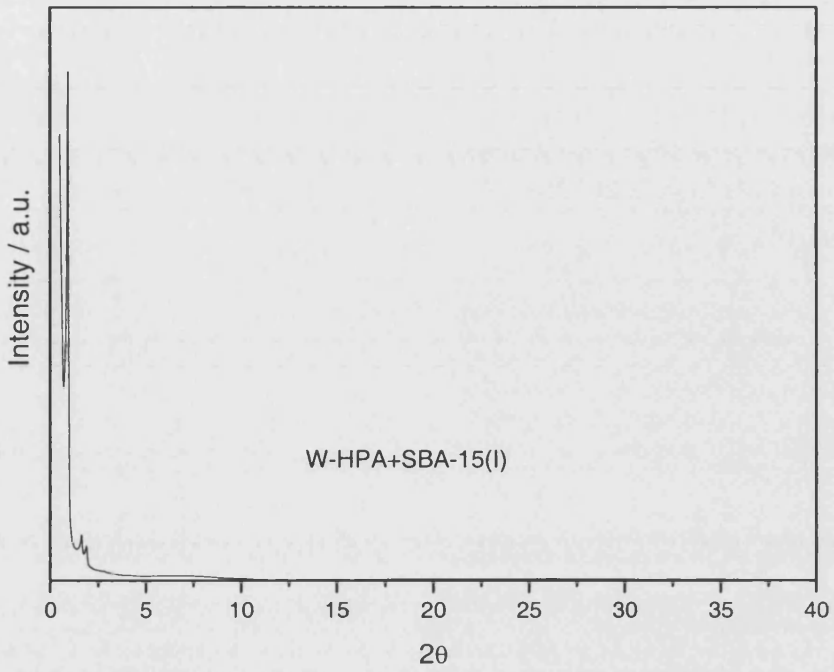

Figure I.IV- 20. XRD Pattern of W-HPA impregnated SBA-15

Although the 2θ range for W-HPA (I) sample was selected as 0.5° to 40 °, no further peaks were observed.

Water Vapour Adsorption

Carbon samples have shown relatively low uptake. It can be seen in Figure I.IV-21 that up to relative pressure of 0.4, water vapour was adsorbed by Sibunit™ only to a very low extent. Similarly, up to relative pressure of 0.3, uptake of Novacarb™ was also very small. SBA-15 had a significantly higher uptake when compared to carbon and sol-gel silica samples. At higher relative pressures, a sharp rise occurs in the sorption and the formation of hysteresis loop, that is typical for water vapour sorption, was observed. Dubinin et al. (1954) stated that the sharp rise is caused by the capillary condensation of the water vapour. In addition, it may be assumed that in the region of low equilibrium pressures, adsorption of water vapour is mainly due to the formation of hydrogen bonds between the adsorbed molecules of water and the surface oxides of the carbon and silica. Adsorbed water molecules serve as a subsidiary adsorption centres which are capable of attaching other molecules by means of hydrogen bonds.

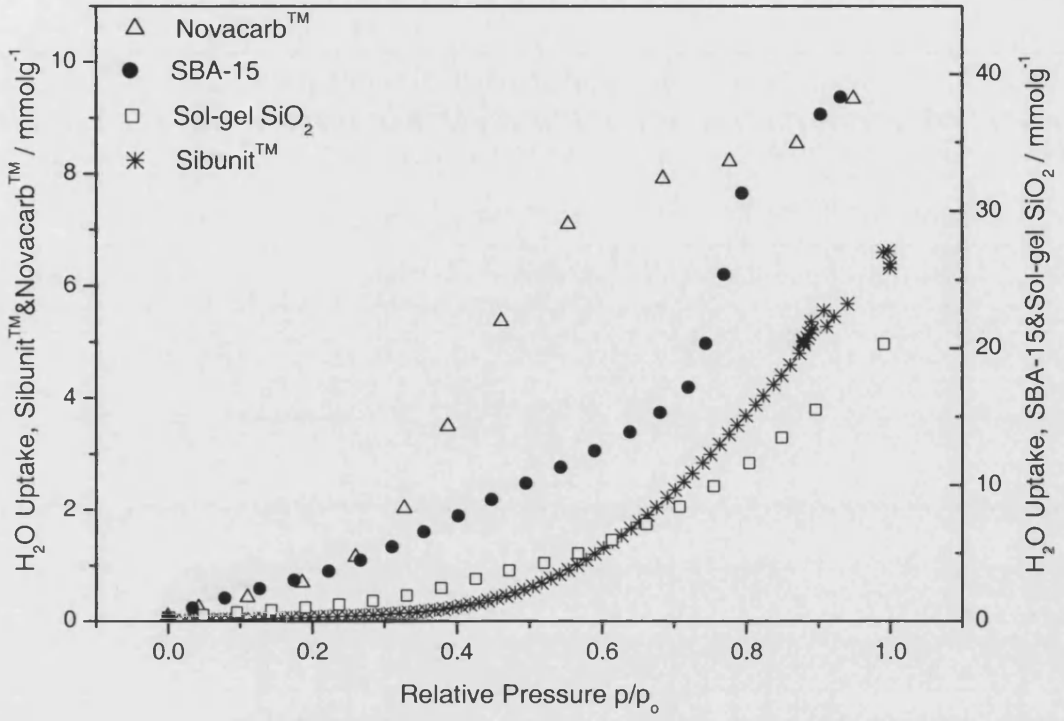

Figure I.IV- 21. Water vapour sorption branches of the adsorbants

Figure I.IV-21 shows the sorption branches of the isotherms for water vapour on pure supports and different scales were used for illustration purposes. Sibunit™ isotherm shows a different path and has a considerably lower uptake at ca. 6.62 mmol/g than the uptake on Novacarb, ca. 9.33 mmol/g. Similarly, the uptake on sol-gel SiO_2, ca. 20.30 mmol/g is lower than the uptake on SBA-15, ca. 38.39 mmol/g.

Although, there is a great difference between the total uptakes of Novacarb™ and SBA-15, their sorption branches have similarities. The regions of sharp rises are moved somewhat, most probably due to the different surface properties of carbon and silica. The points where the curves bend for SBA-15 and Novacarb™ at p/p_o=0.69 and 0.60, respectively, corresponds to the completion of the formation of a continuous uni-molecular adsorption layer. At this point, surface properties become identical for all samples as the whole surface is assumed to be covered with water molecules. Multi-molecular adsorption or capillary condensation plays the main part in the sorption of water vapour after the point where the uni-molecular adsorption layer is completed. In the case of a capillary condensation, at a relative pressure of 1, the volume of the filled pores is the main factor in determining the maximum sorption capacity. However, if the

main role is played by a multi-molecular adsorption the difference between the absolute values for the sorption capacity of various specimens of the adsorbents of a similar nature must be very small. Table I.IV-7 shows the maximum sorption capacities per unit of surface area of adsorbents.

Table I.IV- 7 Maximum Sorption Capacity of the adsorbents

Adsorbent	*Specific area* $s\ (m^2/g)$	*Maximum Sorption* a_s *(mmoles/g)*	*Maximum Sorption* $a_s = a_s/s$
Novacarb™	522.1	9.33	0.0178
Sibunit™	286.1	6.6	0.023
SBA-15	321.1	38.39	0.120
Sol-gel SiO_2	381.4	20.30	0.053

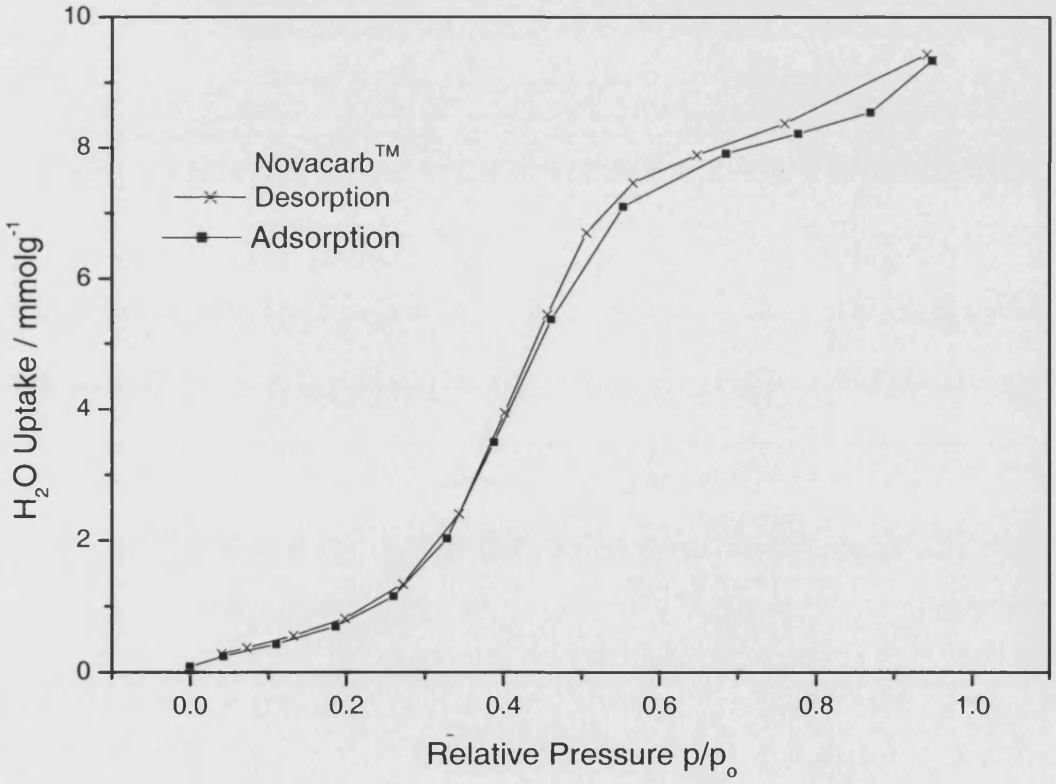

Figure I.IV- 22. Water vapour sorption and desorption on Novacarb™

Maximum sorption capacity of Novacarb™ and Sibunit™, and SBA-15 and sol-gel SiO_2 are different. This may show that after the formation of uni-molecular adsorption layer, water vapour uptake may involve both multi-molecular sorption and capillary

condensation effects. Moreover, it is necessary to take into account that the formation of multi-molecular adsorption layer on SBA-15 and Novacarb isotherms can clearly be observed whereas on sol-gel SiO_2 and Sibunit™, the bend that occurs after the completion of the first layer, is not clear.

It must also be noted that the completion of the formation of a condensed adsorption layer may not involve any noticeable bend in the sorption branch of the isotherm because of a superimposed process of capillary condensation. Additionally, the complexity of the sorption process for water vapour over the entire range of equilibrium relative pressures makes a simple approach to a quantitative analysis of the whole sorption branch of the isotherm rather unpromising. Quantitative analysis should be restricted to the region of uni-molecular adsorption that corresponds to adsorption values up to 10 mmol/g for carbon samples. This region is most characteristic for the sorption of the water vapour and includes the beginning of the isotherm, the transition to the sharp rise of the sorption branch and the substantial part of the rapidly rising curve [Dubinin et al., 1954].

Adsorption isotherms of SBA-15 and Novacarb™ in Figure I.IV-21 coincide in the p/p_o region of 0.685, where the adsorption is multi-molecular. This coincidence of the isotherms also shows a linear relation between the quantities of adsorbed water vapour on the supports at identical relative pressures. It is also necessary that the linear fit goes through the origin. Figure I.IV-23 shows that there is a linear relation between SBA-15 and Novacarb™ [Dubinin et al., 1954].

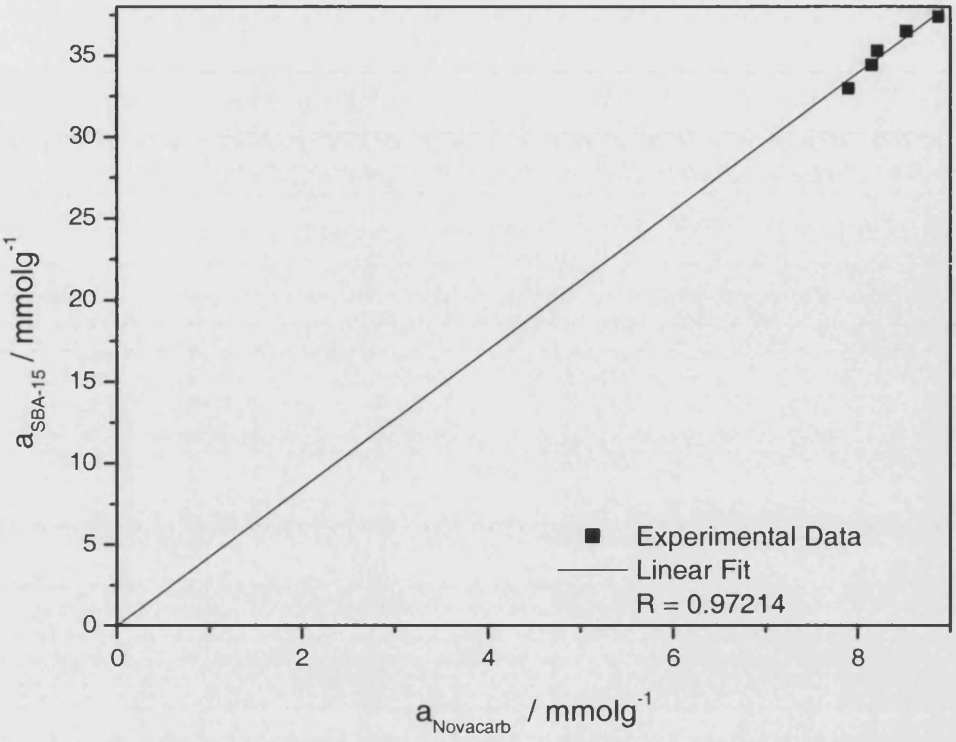

Figure I.IV- 23 Linear relation of water vapour sorption on Novacarb™ and SBA-15

On the other hand, on the sorption branch of the Sibunit™ and sol-gel SiO_2 isotherms, it is observed that the monolayer completion occurs at relative pressure of almost 1. Therefore, water vapour uptake is limited to the amount in which the Sibunit™ and sol-gel SiO_2 surfaces can uptake. Hence, lower surface area may lead to a considerably lower water vapour uptake. The nature of the surface area of any adsorbent should be carefully taken into account when a possible mechanism for water vapour sorption is considered.

Both adsorption and desorption curves of Novacarb™, Sibunit™, SBA-15 and sol-gel SiO_2 are shown Figures I.IV-22, I.IV-24, I.IV-25 and I.IV-26, respectively. It can be seen from Figures I.IV-25 and I.IV-26 that the end point of the desorption branch of sol-gel silica and SBA-15 samples are higher than zero. That is most probably due to the modification of the surface of the silica during the sample preparation. Prior to water sorption, samples were outgassed under vacuum at 200 °C for ca. 15 hours. This might cause removal of water molecules from the surface. Consequently, removed water molecules may have been replaced during the water sorption irreversibly.

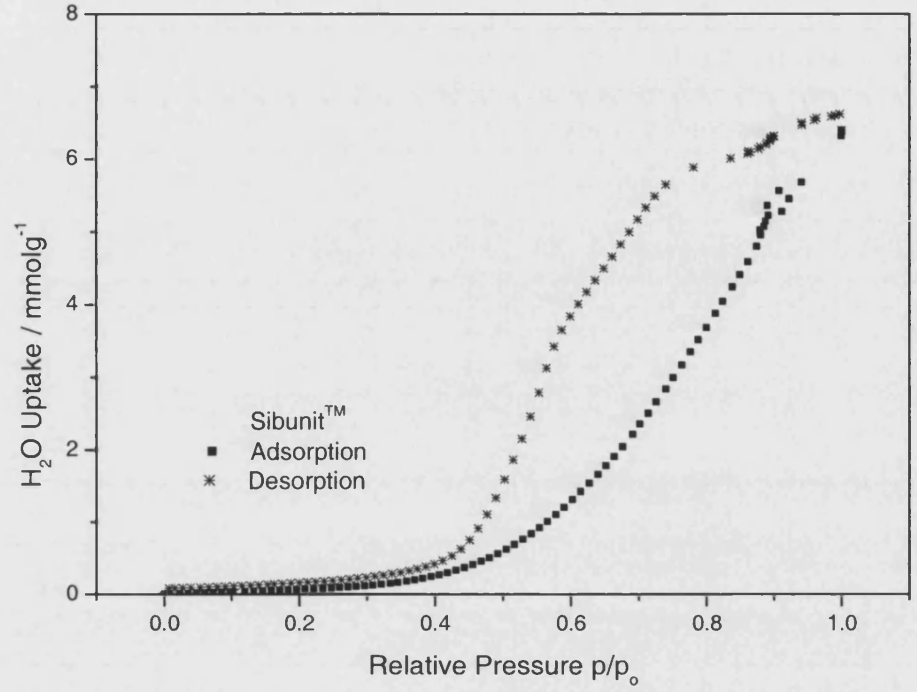

Figure I.IV- 24. Water vapour sorption and desorption on Sibunit™

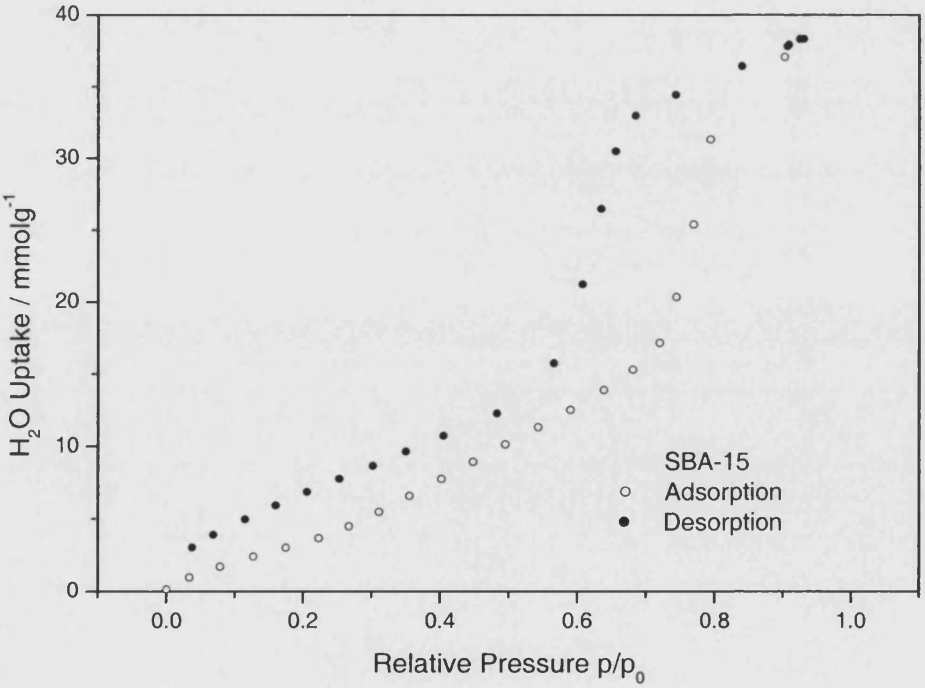

Figure I.IV- 25. Water vapour sorption and desorption on SBA-15

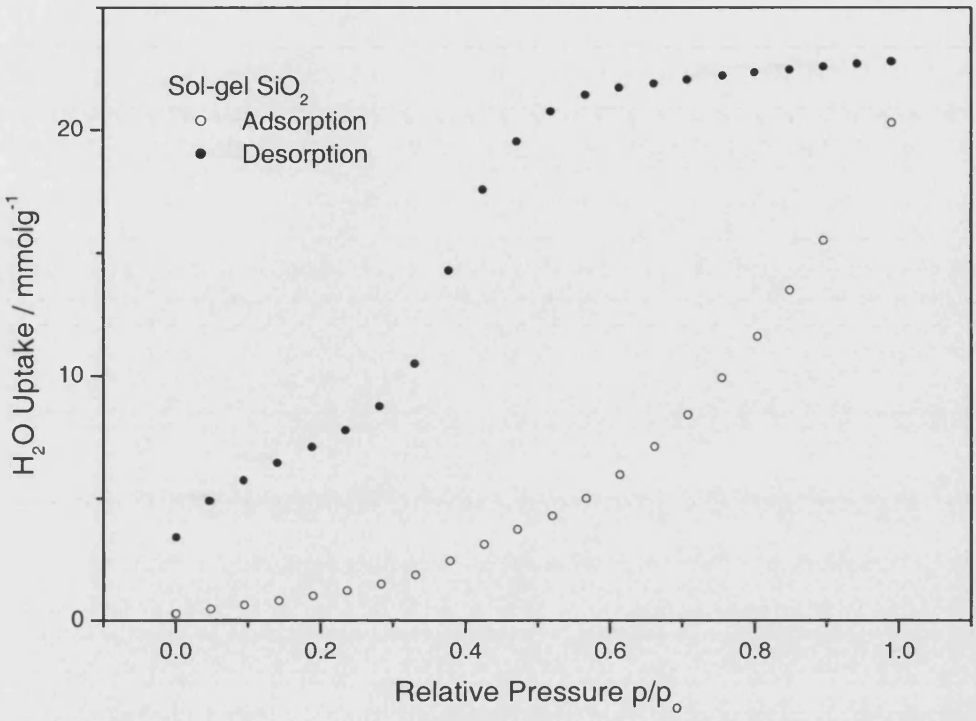

Figure I.IV- 26. Water vapour sorption and desorption on sol-gel SiO_2

I.IV.3 NH_3 UPTAKE

Equilibrium ammonia uptake of the pure and W-HPA and Mo-HPA loaded supports were measured quantitatively using the previously calibrated thermal conductivity detector. Experiments were carried out at ambient temperature, ca. 25 °C and atmospheric pressure. Calibration of the thermal conductivity detector was carried out using nitrogen/ammonia gas mixtures with various NH_3 concentrations obtained from Scientific & Technical Gasses Ltd., UK.

Adsorbed amounts were calculated from adsorption breakthrough curves. Figure I.IV-27 shows the breakthrough curve obtained on Novacarb™. Point 1 is the point where the experiment was started; NH_3 started flowing through the reactor. Immediately after that, a sharp decrease in the TCD signal was observed. The signal was low for a while indicating low NH_3 concentration in the outlet flow, hence, adsorption/chemisorption of NH_3 on the sample. Subsequently, the signal gradually increased, and eventually reached the starting point that is shown by point 2.

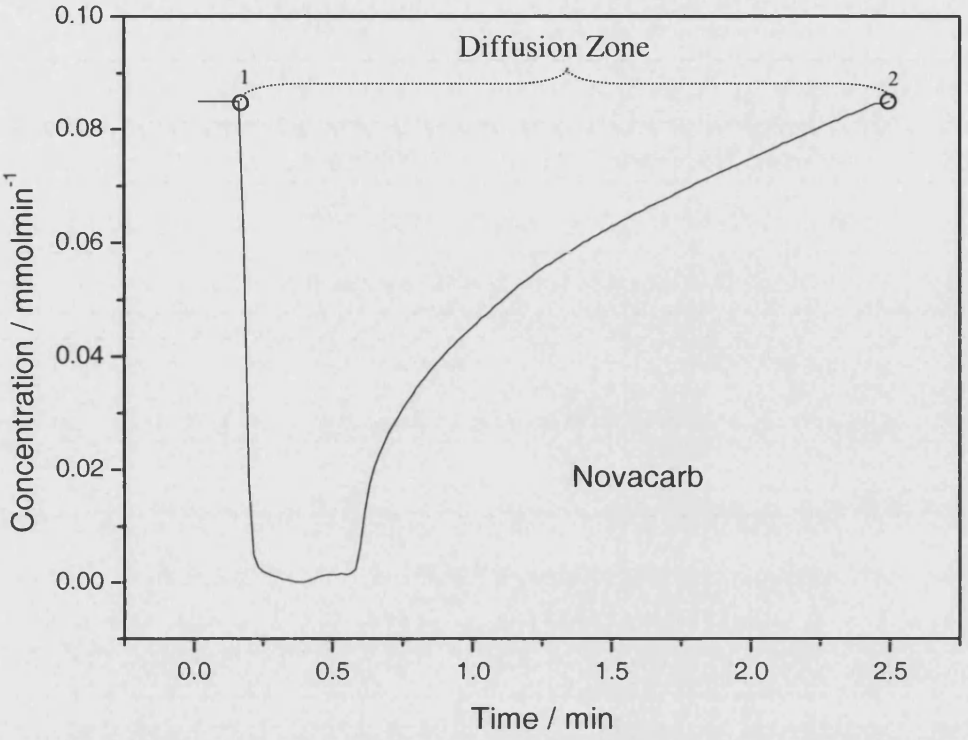

Figure I.IV- 27 Equilibrium NH_3 uptake breakthrough curve for Novacarb™

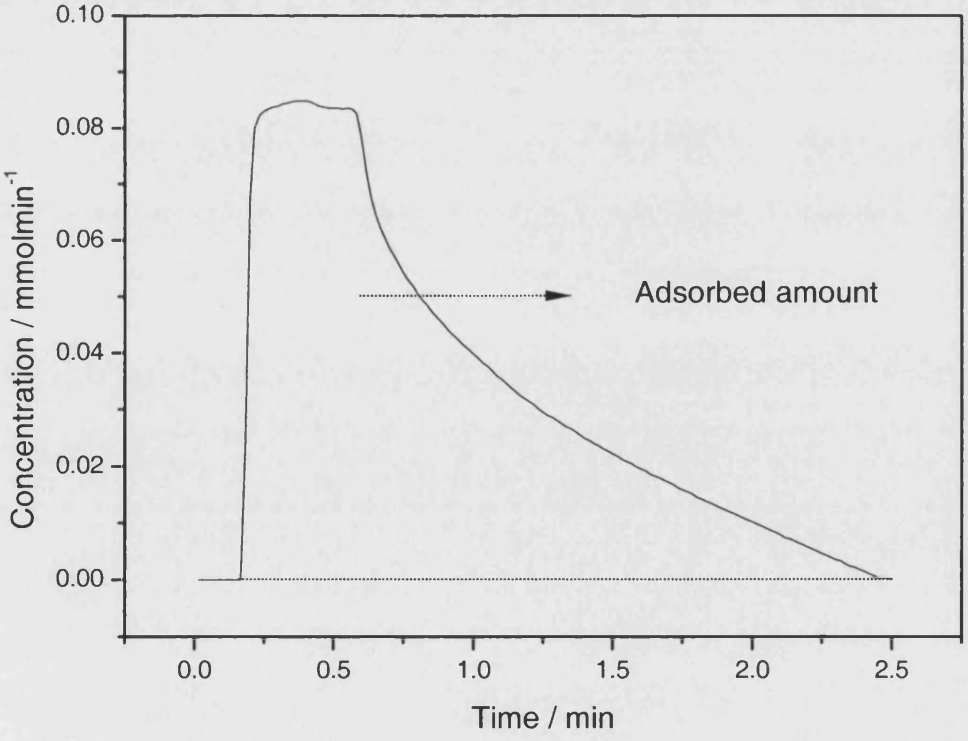

Figure I.IV- 28 Adsorbed amount of NH_3 on Novacarb™

By using Origin software, this line was subtracted from a straight line between the start and the end points of the experiment in order to obtain the area indicating the amount of NH_3 adsorbed by the sample. This area under the line was calculated by integration between the start and the end points. This value was then divided by the amount of sample used for each experiment (that is 0.3 g), in order to obtain the adsorbed amount per mass of sorbent.

The same experiment was carried out with an empty reactor loaded with quartz wool and beads, in order to observe the effect of the dead volume. The value obtained, (0.0153 mmol/run) was subtracted arithmetically from the value obtained for each sample and the actual adsorbed amounts were calculated by following this procedure for all the samples. Equilibrium uptake of each sample is shown in Table I.IV-9.

Amongst the pure supports, SBA-15 and sol-gel SiO_2 showed much higher performance in ammonia uptake than the pure carbons. This is most likely due to the acidic nature of the silica itself as the carbon samples have higher volumes than the sol-gel SiO_2 sample and SBA-15. Moreover, Novacarb™ adsorbs more NH_3 when it is compared to Sibunit™. This is most probably due to the physical characteristics of the two carbons: higher meso/micro-pore volume results in higher NH_3 uptake.

Sibunit has considerably lower ammonia uptake, due its physical structure. Lower mesopore and almost non-existent micropore volume are believed to be the main reason for lower ammonia uptake than the rest of the supports. However, the loaded acid is accessible, as the acid loaded Sibunit™ samples showed much greater performance in ammonia uptake than the pure support.

The amount of sorbed ammonia on W-HPA- SBA-15 is nearly twice that amount sorbed on pure SBA-15, which clearly shows that the acid retains its acidic properties when it is supported, and moreover this shows that the acidic sites are accessible in the pores. It was unfortunately not possible to obtain experimental data for Mo-HPA loaded SBA-15 samples due to the problems occurred during the recording of the data. Furthermore, with the SBA-15 composite containing only 0.5 molar % of W-HPA, that is equal to 6.7 weight %, it was possible to obtain high ammonia uptake. However, due to the problems which occurred during the SBA-15-HPA composite preparation; i.e.

surfactant reacting with the acid, resulting in a disordered SBA-15 structure, it was not possible to obtain composites with higher acid compositions. However, it will be worth trying to impregnate composite materials in order to increase the acid composition on the support.

20 wt% W-HPA – sol-gel SiO_2 has the highest uptake amongst pure and acid impregnated sol-gel SiO_2 samples as well as amongst all pure and acid loaded supports, showing that heteropoly acids retain their structure and acidic properties when they are incorporated into silica walls.

Bromination of Novacarb™ resulted in a much higher ammonia uptake than the pure Novacarb™ most probably due to the change in the surface chemistry of the carbon. However, the uptake of the W-HPA and Mo-HPA loaded brominated Novacarb™ is lower than that of the W-HPA and Mo-HPA loaded Novacarb™. It is suggested that the bromine interacts with the loaded acid and this results in the inactive acidic sites.

Essayem et al. (1997) studied ammonia uptake on pure W-HPA using both catharometric (thermal conductivity detector) and mass spectrometry analysis methods to analyse their data. They recorded reversibly and irreversibly adsorbed ammonia. Their results are shown in Table I.IV-8.

Table I.IV- 8. NH_3 Uptake of W-HPA (Essayem et al., 1997)

	TCD Analysis NH_3/KU^b	*MS Analysis equivalent* NH_3/KU^b
Adsorption		
Total uptake	**6.7**	**7.7**
Reversible uptake	**2.6**	**3.3**
Irreversible uptake	**4.1**	**4.4**
Desorption		
NH_3 desorbed	**-**	**1.5**
N_2 desorbed[a]	**-**	**1.2**
Total NH_3 desorbed	**-**	**2.7**

[a] Expressed as N atom

[b] Keggin Unit

They recorded total ammonia uptake as 7.7 molecules per Keggin unit. By using this data as a reference, total uptake was calculated for our system. For Novacarb™ + W-HPA:

HPA Loading = 0.24 gr
Molecular Weight of W-HPA = 2880.2 gr/mol.
0.24 gr W-HPA = 8.33×10^{-2} mmol
Since each Keggin unit can react with 7.7 molecules
$7.7 \times 8.33 \times 10^{-2} = 0.64$ mmol NH_3/ g support

According to this calculation, 0.64 mmol NH_3 should be both reversibly and irreversibly adsorbed by the loaded W-HPA. Total uptake was measured as 0.94 mmol/g. Considering the amount adsorbed by pure Novacarb™, that is 0.22 mmol/g and the error in acid adsorption measurements, measured amount is reasonable. W-HPA was reported as the strongest acid among the Keggin-type HPAs, however, it was also added that the acid strength of the Keggin HPA depends weakly on their composition [Kozhevnikov et al., 1998]. If the total ammonia uptake per Keggin unit for Mo-HPA is also assumed as 7.7, total uptake for Mo-HPA loaded supports can easily be calculated. The results obtained are tabulated in Table I.IV-9.

Considerable difference between the calculated and measured ammonia uptake of 20 % W-HPA sol-gel SiO_2 is most probably caused by the following reason. Essayem et al. (1997) have used bulk heteropoly acid for their measurements, in our study HPA was incorporated into the walls of SiO_2 and the amount adsorbed by the SiO_2 itself is high due to its acidic nature.

Table I.IV-9. Calculated and Measured NH_3 uptake according to the HPA loading

Sample	*HPA Loading*		*Equilibrium NH_3 Uptake (mmol/g)*	
	(wt%)	*mmol/g*	*Calculated*	*Measured*
Novacarb™	-	-	-	0.22
Novacarb™ + W-HPA (I)	24	0.083	0.64	0.94-0.98
Novacarb™ + Mo-HPA (I)	20	0.11	0.84	1.37
Br Novacarb™	-	-	-	0.55-0.57
Br Novacarb™ + W-HPA (I)	16	0.056	0.43	0.45
Br Novacarb™ + Mo-HPA (I)	19	0.1	0.80	1.21
Sibunit™	-	-	-	0.05
Sibunit™ + W-HPA (I)	22	0.076	0.59	0.47
Sibunit™ + Mo-HPA (I)	19	0.1	0.80	0.35
SBA-15	-	-	-	0.89
SBA-15 + W-HPA (I)	16	0.056	0.43	1.67
SBA-15 + W-HPA (C)	6.7	0.023	0..18	1.31
Sol-gel SiO_2	-	-	-	0.85
Sol-gel SiO_2 + W-HPA (I)	35	0.12	0.94	1
Sol-gel SiO_2 + Mo-HPA (I)	33	0.18	1.39	1.29
Sol-gel SiO_2 + W-HPA (C)	20	0.11	0.53	2.11

I.IV.4 REGENERATION OF W-HPA AND MO-HPA SUPPORTED NOVACARB

Regeneration of the Mo-HPA and W-HPA supported on Novacarb™ was carried out by calcination of the samples after NH_3 uptake. Samples were qualitatively analysed using FT-IR spectrometry. Ammonia uptake on W-HPA impregnated Novacarb™ gives the spectrum shown in Figure I.IV-29. The peak at 1400 cm^{-1} appears following the NH_3 chemisorption indicating the presence of NH_4^+ ion [Shimizu et al., 1986]. The Keggin anion characteristic bands, as well as the peak at 1570cm^{-1} seen before on the W-HPA impregnated Novacarb™, are still present. The peak, previously observed at 978cm^{-1},

splits into two peaks at 978cm^{-1} and 949cm^{-1} possibly due to the changes occurring upon the physical interaction of the ammonium ions with the Keggin structure.

Similarly after the NH_3 uptake, Novacarb supported Mo-HPA, the peak at 1396cm^{-1}, indicating the presence of the NH_4^+ ion, was observed. However, Mo-HPA seems to show considerable degradation on reaction with ammonia. The peak at 1035cm^{-1} (Figure I.IV.30) almost completely disappeared and has been replaced by a clear shoulder. The peaks at 935cm^{-1} and 873cm^{-1} shows a considerable loss in intensity and a shift from 961cm^{-1} and 868cm^{-1} respectively. There appears to be complete loss of the peak seen previously at 781cm^{-1}.

Table I.IV- 10. FT-IR bands of the W-HPA, after NH_3 uptake and after calcination

Novacarb™ Supported W-HPA(cm^{-1})	*After NH_3 Uptake (cm^{-1})*	*After Calcination (cm^{-1})*
1075	1077	1074
983	949-978	972
893	885	888
802	800	797

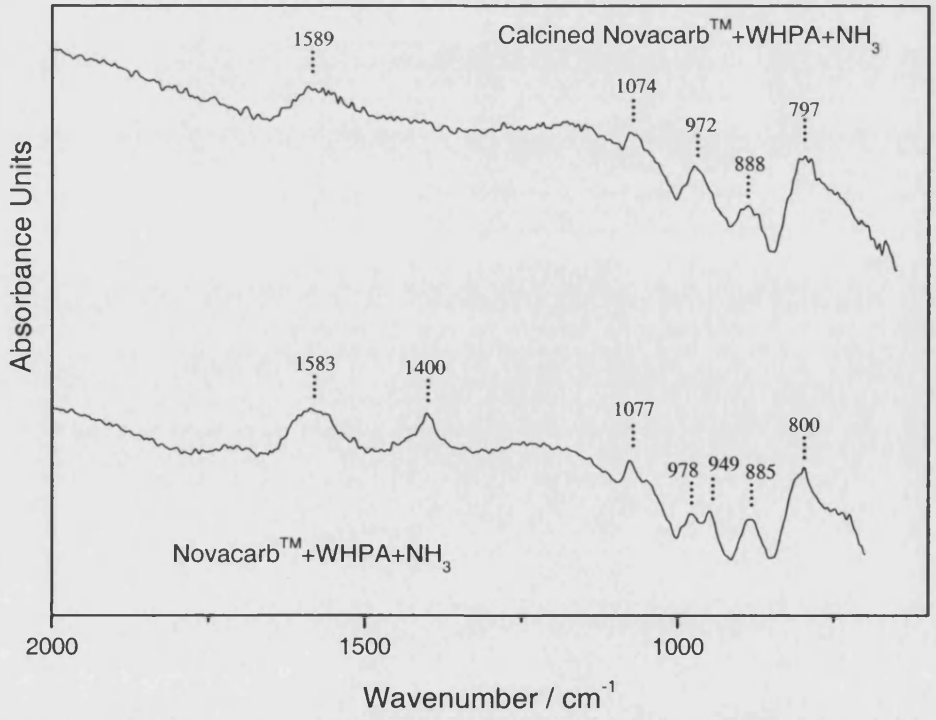

Figure I.IV- 29 FT-IR spectra of W-HPA impregnated Novacarb™ after NH_3 uptake and calcination

Following the NH_3 uptake on the W-HPA supported Novacarb, sample was calcined and the peak that was previously observed at 1400cm^{-1} indicating the presence of NH_4^+ ion has completely disappeared, hence showing complete removal of the adsorbed ammonia. Characteristic Keggin anion bands are still present at 1074 cm^{-1}, 972 cm^{-1}, 888 cm^{-1} and 797 cm^{-1} showing only a slight decrease in intensity as shown in Figure I.IV-29. There also observed that the peaks at 949 and 978 cm^{-1} that appeared after the NH_3 uptake, form a single peak after the calcination.

Ammonia adsorbed/chemisorbed Novacarb supported Mo-HPA sample was also calcined in order to obtain complete recovery of the supported acid. Removal of the peak at 1400cm^{-1} observed showing that the NH_4^+ ion was removed. The shoulder seen before shifts slightly to 1035cm^{-1} and the Keggin anion peaks previously at 961cm^{-1} and 868cm^{-1}, shift to 947cm^{-1} and 875cm^{-1}, respectively. Moreover, considerable reduction in intensity of the peaks was observed.

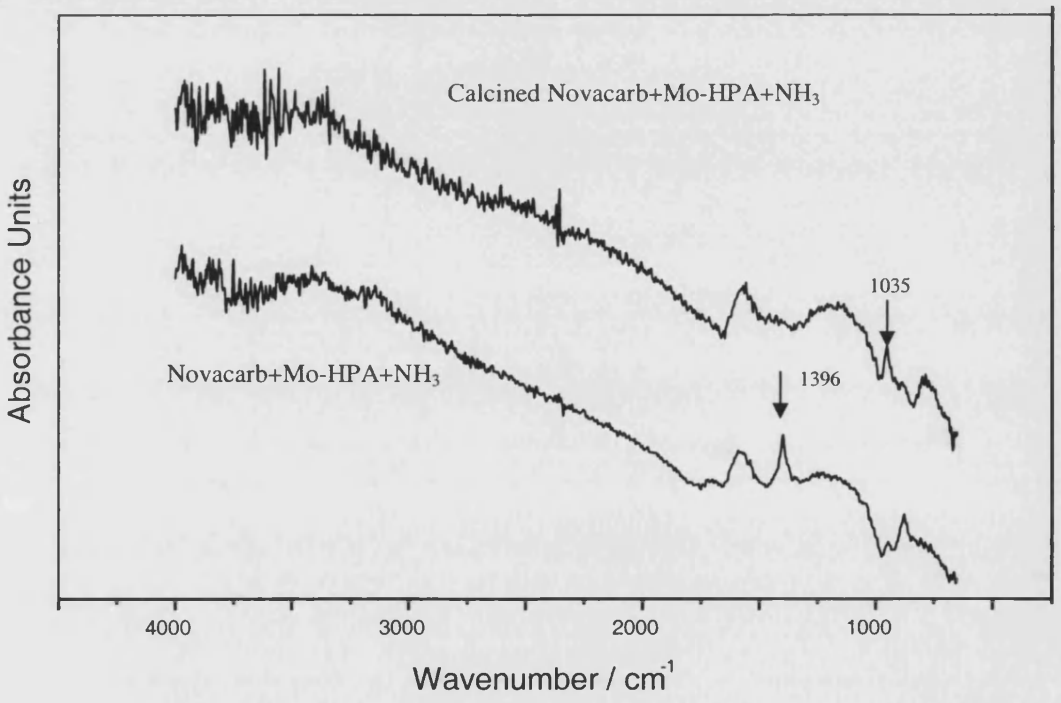

Figure I.IV- 30 FT-IR spectra of Mo-HPA impregnated Novacarb™ after NH_3 uptake and calcination

I.IV.5 TEMPERATURE PROGRAMMED DESORPTION

Temperature programmed desorption technique was applied to characterise ammonia adsorbed/chemisorbed samples. Due to the unavailability of the mass spectrometry system we were only able to characterise samples qualitatively since in addition to desorption of NH_3, other products, such as H_2, H_2O and N_2, are expected to be present in the flow coming out of the reactor [Essayem et al., 1997]. The presence of these products was confirmed by the mass spectrometry study (m/z=2 for H_2, m/z=18&17 for H_2O, m/z=28 for N_2 and m/z=15 for NH_3) carried out by Essayem et al. (1997). They claim that these three products must be formed by thermal or catalytic decomposition of NH_3 and reduction of the HPAs by NH_3 and/or H_2 release through its decomposition. Reactions which can take place parallel to the simple decomposition of the ammonium salt are,

$(NH_4)_3HPW_{12}O_{40} \rightarrow 3\ NH_3 + H_3PW_{12}O_{40}$

$NH_3 \rightarrow \frac{1}{2}\ N_2 + 3/2\ H_2$

$H_2 + HPA \rightarrow H_2O + HPA_{reduced}$

Therefore, the integration of the desorption peak obtained by the catharometric measurement is not reliable enough to obtain irreversibly and reversibly adsorbed amount of NH_3.

The total amount of desorbed NH_3 was measured as 2.7 molecules per Keggin unit by Essayem et al. (1997). They also added that this amount was lower than that given by chemical analysis. However, the amount of NH_3 desorbed either as NH_3 or N_2 is close to 3 molecules of NH_3 per Keggin unit. Therefore, part of the irreversibly adsorbed NH_3 may be strongly held on the surface or in the pores of the materials.

Figure I.IV-31 shows the TPD data obtained for pure supports following the ammonia adsorption experiments. Only one single peak was observed showing desorption of physically adsorbed ammonia. Desorption peaks of SBA-15 and sol-gel SiO_2 are greater than the carbon materials. This data also confirms the quantitative analysis of the

adsorption breakthrough curves. This single peak observed around 100 °C indicates most likely the presence of H_2O.

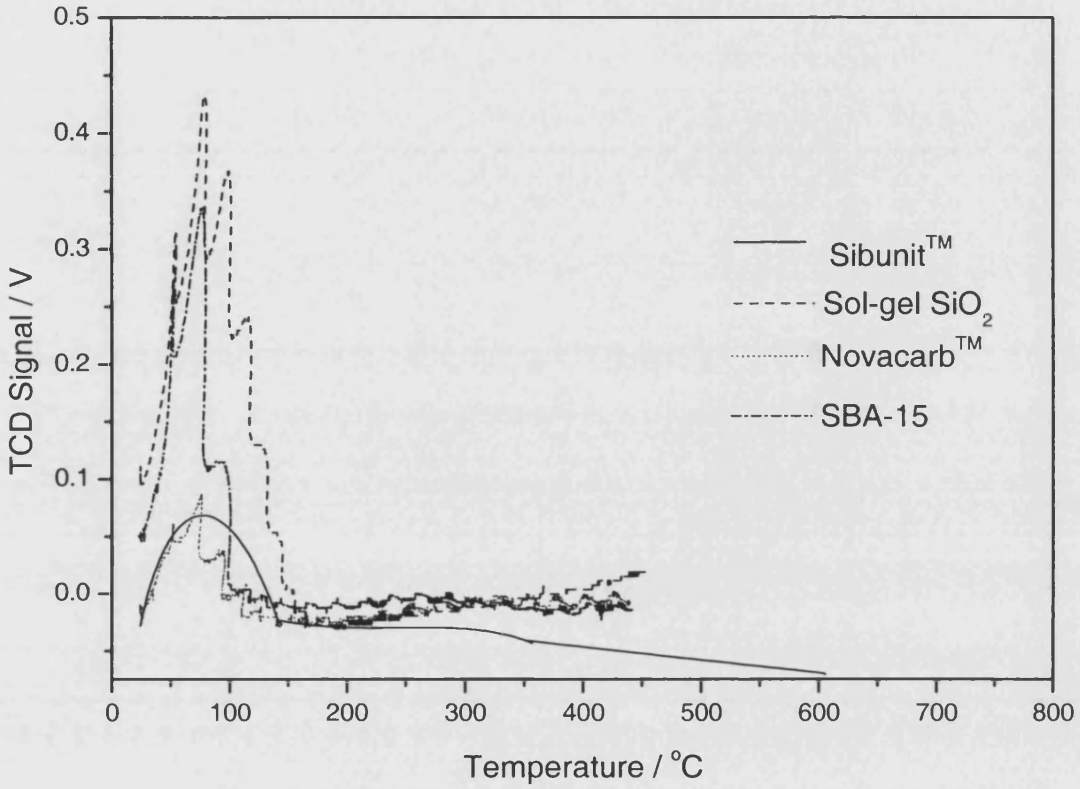

Figure I.IV- 31. TPD analysis of pure supports

The best TPD result was recorded for Mo-HPA impregnated Novacarb™ sample. Figure I.IV-32 shows the change in the TCD signal against temperature. There are three peaks observed and can be clearly seen in the Figure I.IV-32. First peak having a maximum around 150 °C most likely occurs due to desorption of physically adsorbed NH_3 and water vapour. Second peak was registered just below 600 °C and is probably due to the decomposition of Mo-HPA remaining unreacted after the adsorption in the pores. The final peak having a maximum at 760 °C was recorded most probably due to the thermal decomposition of the ammonium salt, $(NH_4)_3PMo_{12}O_{40}$ as NH_3, N_2 and H_2 as explained earlier.

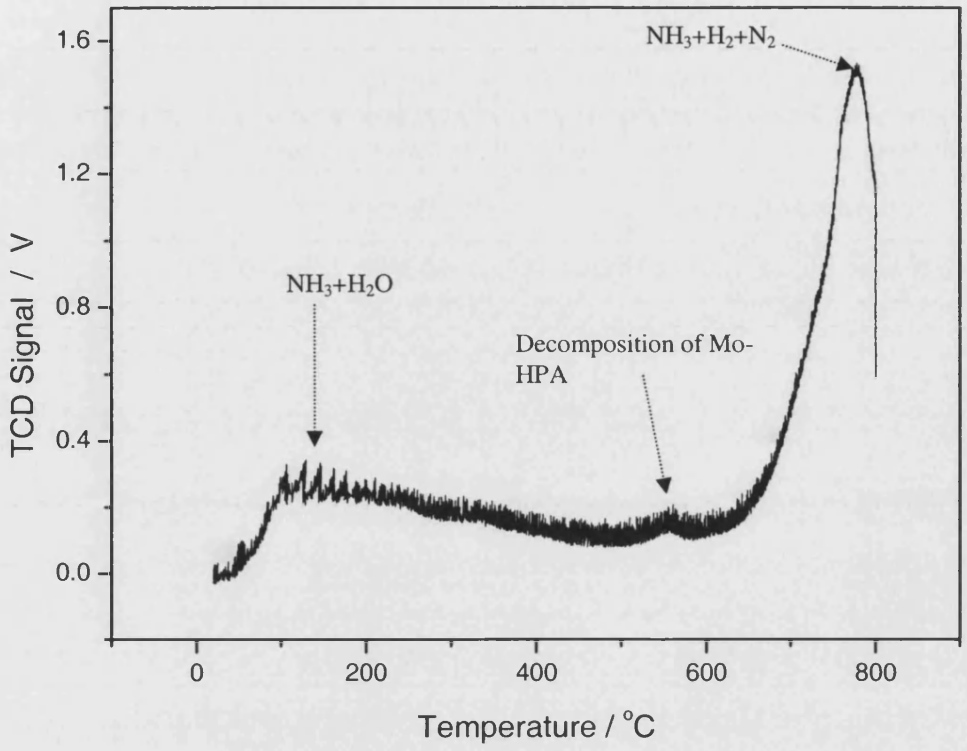

Figure I.IV- 32. TPD diagram of Novacarb™+Mo-HPA

I.V CONCLUSIONS

The aim of this study was to develop novel adsorbents in order to remove basic impurities in gas streams for applications in industrial environments. W-HPA and Mo-HPA were successfully impregnated onto four different mesoporous supports, Novacarb™, Sibunit™, SBA-15 and sol-gel derived amorphous silica, via adsorption from solution. In addition, up to 50 wt% HPA-silica composites were prepared via sol-gel method. The major findings of this study are as follows.

Pure supports were characterised with having both meso and micropores in the structure. Novacarb™ was characterised with the highest BET surface area (522.06 m^2/g) and micro/mesopore volume; Novacarb™ (522.06 m^2/g)>Sol-gel SiO_2 (381.45 m^2/g) >SBA-15 (321.10 m^2/g)>Sibunit™ (286.08 m^2/g). Mean pore diameter of the supports were Novacarb™(174 Å)> SBA-15(62 Å)> Sibunit™ (38 Å)> Sol-gel SiO_2(33 Å).

Highest HPA loading was observed for sol-gel SiO_2, 33w% W-HPA and 35 w% Mo-HPA; Sol-gel SiO_2> Novacarb™(20 w% Mo- and 24 w% W-HPA)>Sibunit™ (19 w% Mo- and 22 w% W-HPA)>SBA-15(16 w% Mo- and 16 w% W-HPA). HPA loading for carbon samples was between 19 and 24%, higher than reported in literature (7-14%). In addition, higher acid loading was observed for pure Novacarb™ than brominated Novacarb™. FT-IR study confirmed that the HPAs retained their structure following the impregnation onto carbon and silica supports.

Pure SBA-15 and sol-gel SiO_2 showed much better performance in ammonia uptake than pure carbons. This is most likely due to their high sorption capacities compared to carbon samples. Moreover, Novacarb™ adsorbs more NH_3 when it is compared to Sibunit™, most probably due to the physical characteristics of the two carbons: higher meso/micro-pore volume results in higher NH_3 uptake. When acid impregnated and composite materials were compared, it was found that although sol-gel SiO_2-W-HPA composites had lower acid loading (0.11 mmol/g) than W-HPA impregnated sol-gel SiO_2 (0.12 mmol/g), this composite showed better performance in ammonia uptake, 2.11 mmol/g vs. 1 mmol/g. Similar result was obtained with the impregnated and

composite SBA-15 samples. This clearly shows that when acid is incorporated into the silica structure, its acidic sites appear to be more accessible. Additionally, higher ammonia uptake was obtained on silica than carbon supports: SBA-15 (0.89 mmol/g)> Sol-gel SiO_2(0.85 mmol/g)> Novacarb™(0.22 mmol/g)> Sibunit™(0.05 mmol/g). Furthermore, although brominated Novacarb™ showed higher ammonia uptake than pure Novacarb™, ammonia uptake performances of brominated and acid loaded samples were not better than acid loaded Novacarb™ samples.

Temperature programmed desorption analysis confirmed that ammonia was both physically and chemically adsorbed onto acid impregnated and composite materials. Finally, regeneration of the Mo-HPA and W-HPA supported on Novacarb™ was carried out by calcination of the samples after NH_3 uptake. FT-IR analysis clearly shows that it is possible to regenerate supported heteropolyacids by following the method proposed.

Overall it was found that 20 w% W-HPA incorporated into SiO_2 is the most promising material for this application amongst all the materials studied in this work.

RECOMMENDATIONS FOR FURTHER STUDY

It is necessary to study the performance of the composites with higher HPA loading to optimise the HPA content in which the properties of both acid and silica units remain intact. The effect of the incorporated acid on the physical structure of the silica however is not known. Porous structure might also have an influence on the ammonia uptake as well as the HPA concentration. It is necessary to perform further characterisation studies to get more information about the porous structure of the acid-silica composites.

HPA-SBA-15 composites also seem promising, however due to the strong interaction between the surfactant heteropolyacid, acid content in the composites is very small. It is necessary to carry out further study to minimise this interaction in order to prepare composites with higher acid uptake. HPA solutions with higher acid content and/or different solvents can be prepared to improve acid impregnation.

TPD experiments have to be carried out for all samples in order to be able to record chemically adsorbed ammonia on each sample. Furthermore, mass spectrometry analysis will have to be coupled with catharometric measurements for quantitative analysis of physically and chemically supported ammonia to deduce the maximum amount of ammonia irreversibly adsorbed by each Keggin unit.

Finally, regeneration process following the method proposed seems to be promising, however, regenerated materials have to be re-tested in ammonia uptake in order to analyse the performance of the regeneration process.

I.VI APPENDICES I

I.VI.1 Appendix: NH_3 Uptake of the Samples

Ammonia uptake of the pure and acid impregnated supports and silica-acid composite materials were measured using custom built apparatus. Experimental procedure and the apparatus were explained in detail. The results obtained for each sample are shown in Figures A1-1.1, A1-1.2, A1-1.3, A1-1.4, A1-1.5, A1-1.6, A1-1.7, A1-1.8, and A1-1.9.

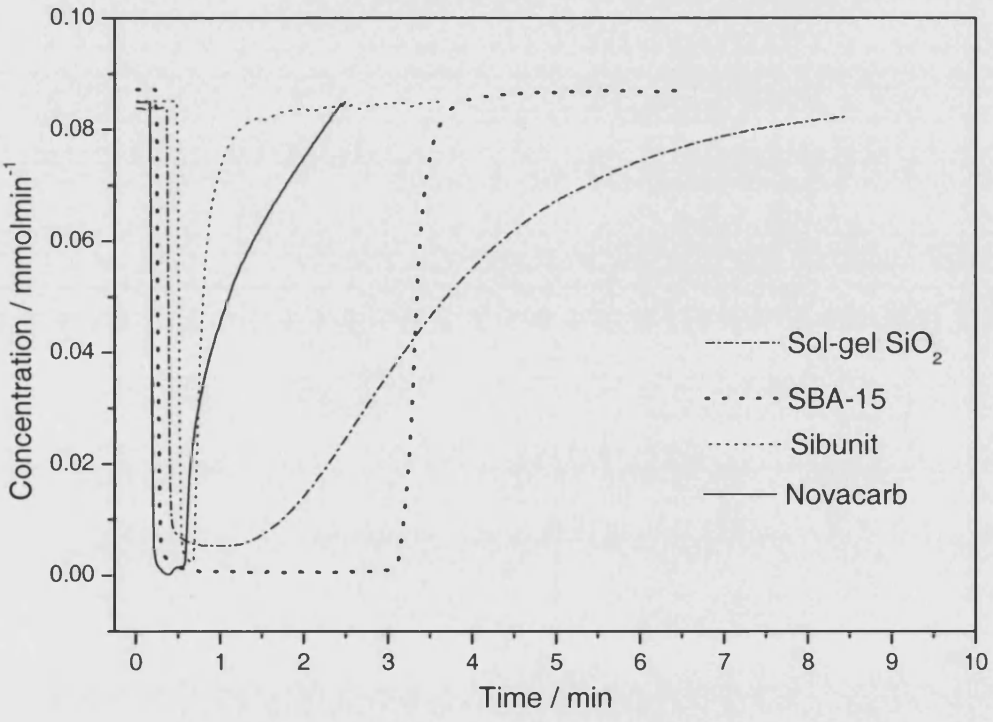

Figure A1-1. 1 NH_3 Uptake Breakthrough curves of the pure supports

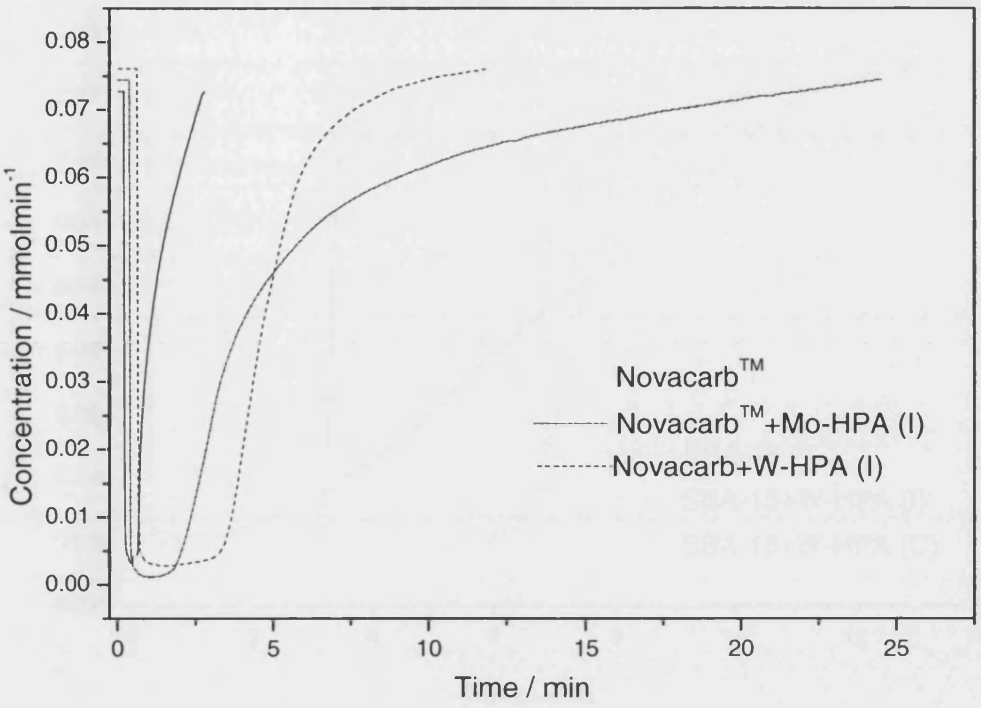

Figure A1-1. 2 Breakthrough Curves of NH_3 Uptake of pure and acid loaded Novacarb™

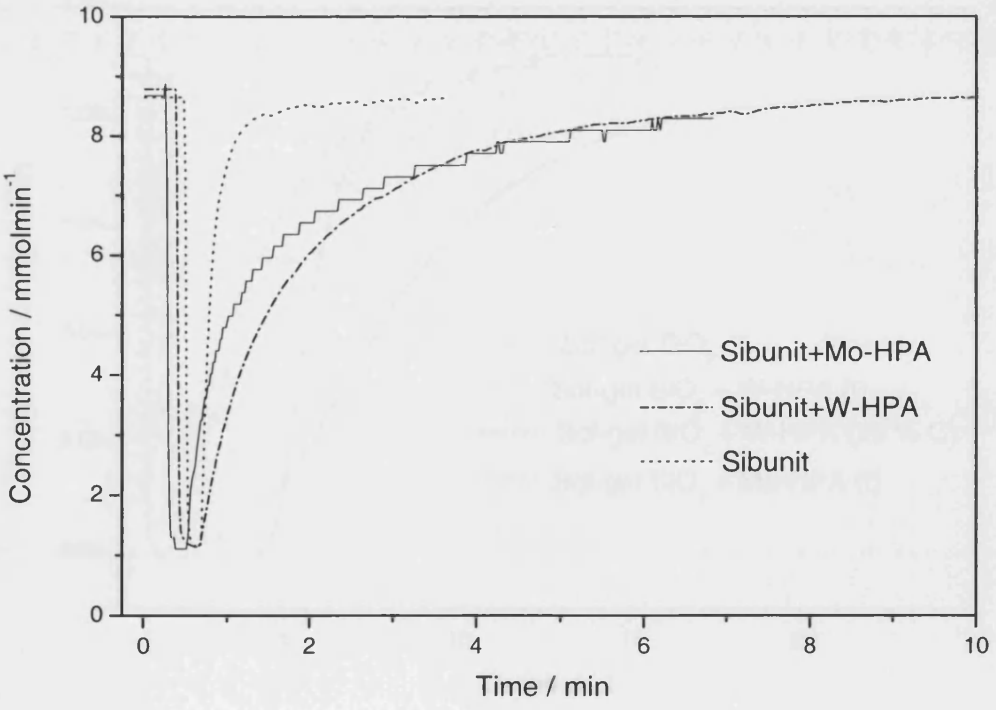

Figure A1-1. 3 NH_3 uptake breakthrough curves of pure and acid loaded Sibunit™

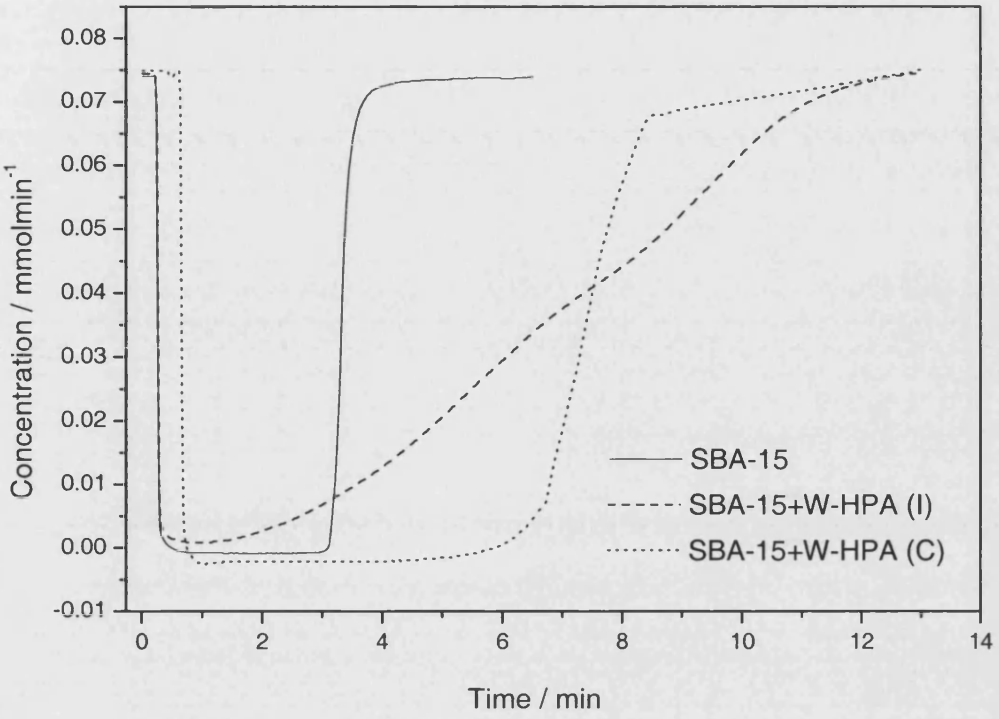

Figure A1-1. 4 NH_3 uptake breakthrough curves of pure and acid loaded SBA-15

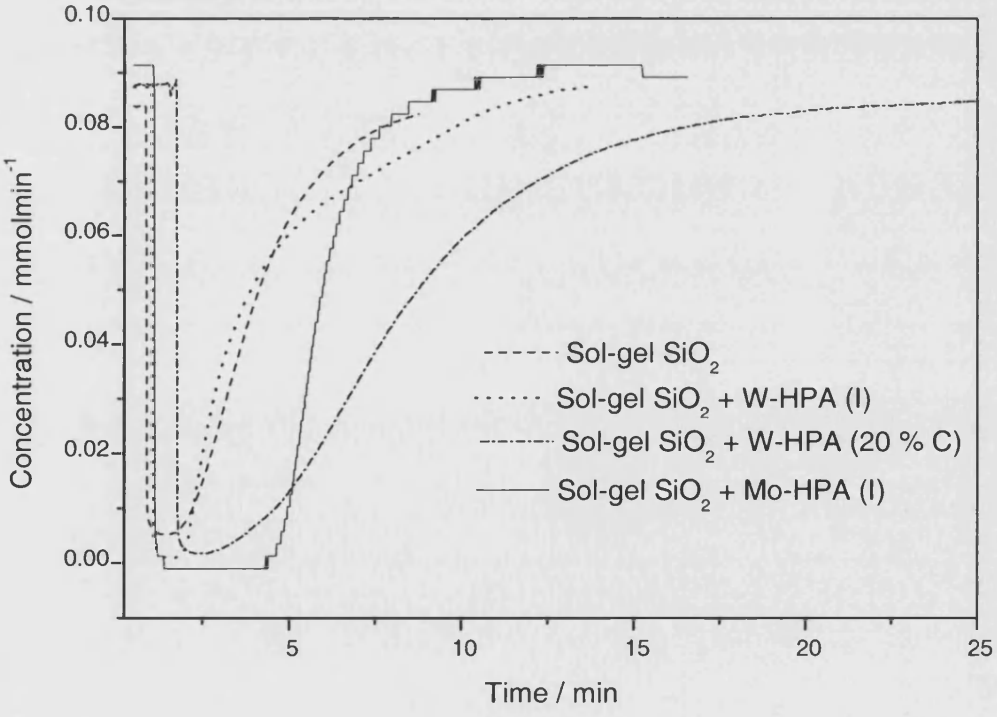

Figure A1-1. 5 NH_3 uptake breakthrough curve for pure and acid loaded sol-gel SiO_2

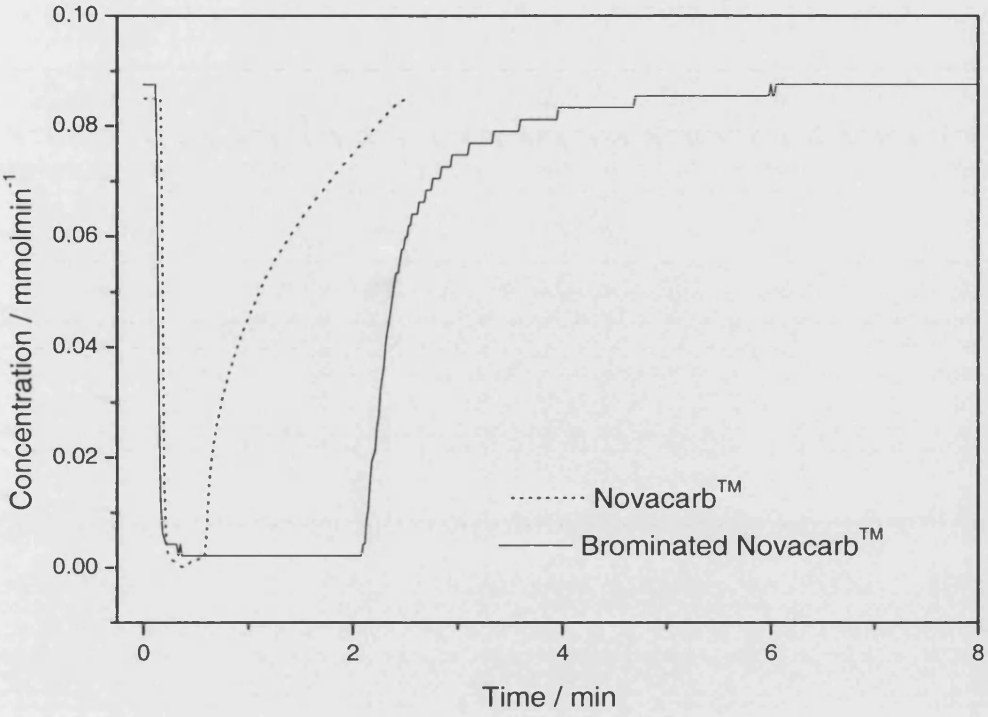

Figure A1-1. 6 Comparison of NH_3 Uptake of Novacarb™ and brominated Novacarb™

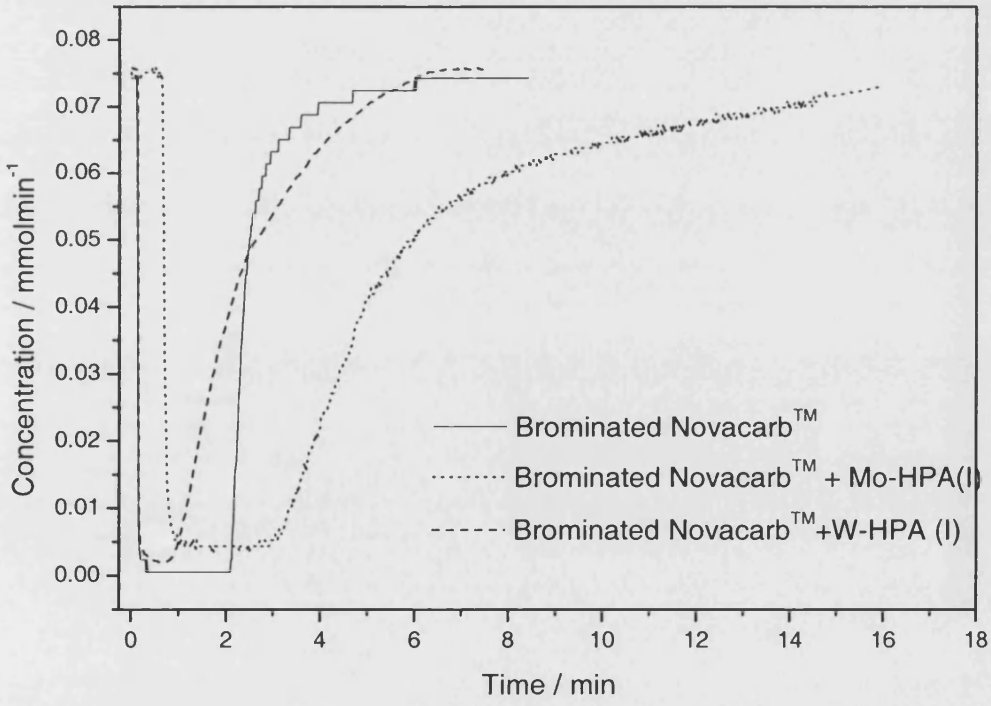

Figure A1-1. 7 NH_3 uptake breakthrough curve of pure and acid loaded brominated Noacarb™

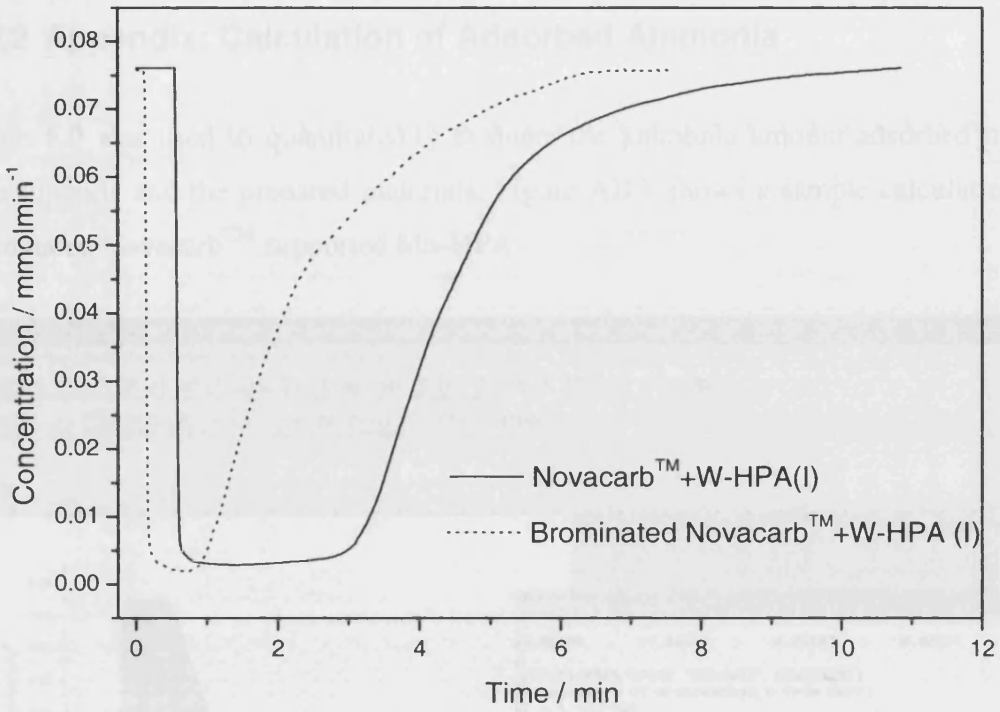

Figure A1-1. 8 Comparison of the NH_3 uptake of W-HPA loaded Novacarb™ and brominated Novacarb™

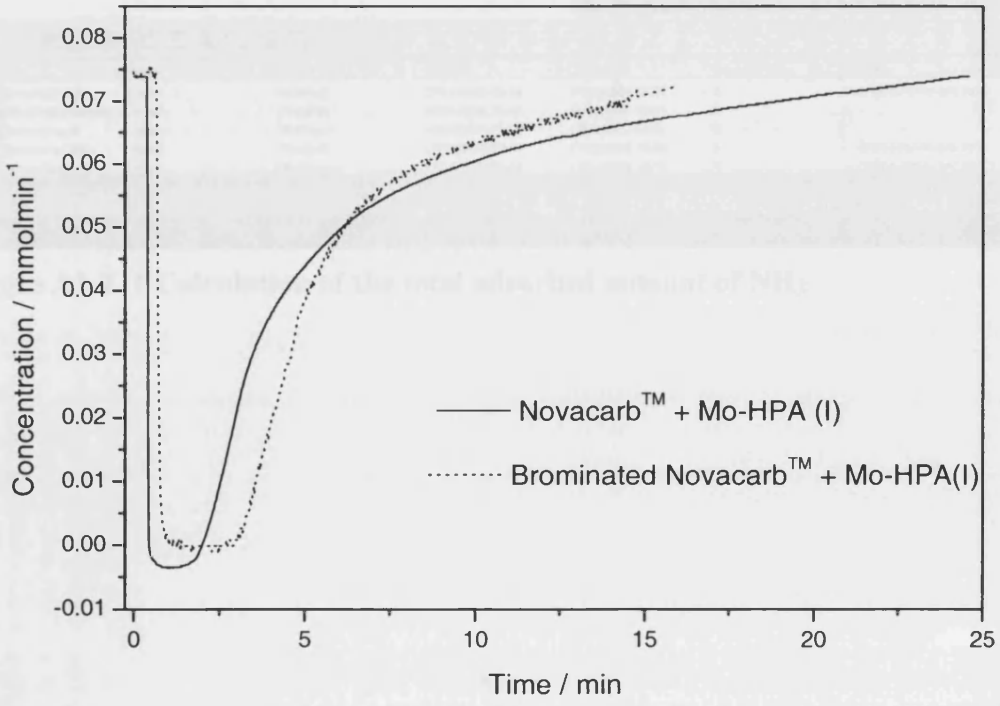

Figure A1-1. 9 Comparison of the NH_3 uptake of Mo-HPA loaded Novacarb™ and brominated Novacarb™

I.VI.2 Appendix: Calculation of Adsorbed Ammonia

Origin 6.0 was used to quantitatively evaluate the ammonia amount adsorbed by the pure supports and the prepared materials. Figure AII.1 shows a sample calculation for brominated Novacarb™ supported Mo-HPA.

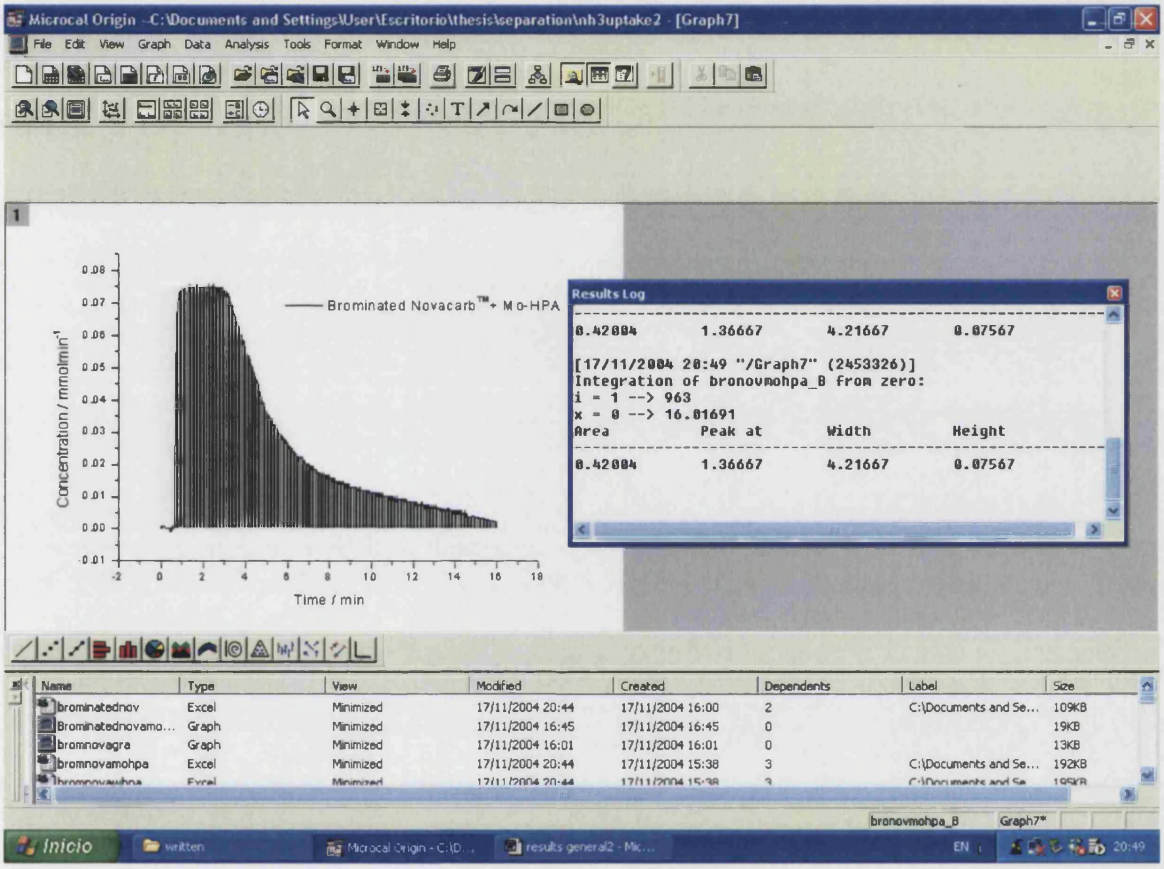

Figure A1-2. 1 Calculation of the total adsorbed amount of NH_3

I.VI.3 APPENDIX: REPEATABILITY

Repeatability of the experiments has been studied by running two experiments under the same conditions. Due to the conditions and unavailability of TCD, it was not possible to repeat all experiments. Samples used for these experiments were W-HPA impregnated Novacarb™ (Exp1) and brominated Novacarb™ (Exp2). In experiment 1, the samples selected were prepared in the same batch in order to obtain same acid loading for both sets of experiments. Experimental conditions were kept unchanged and the results obtained were; 0.94 and 0.98 mmol NH_3/g . That is assumed to be reasonable.

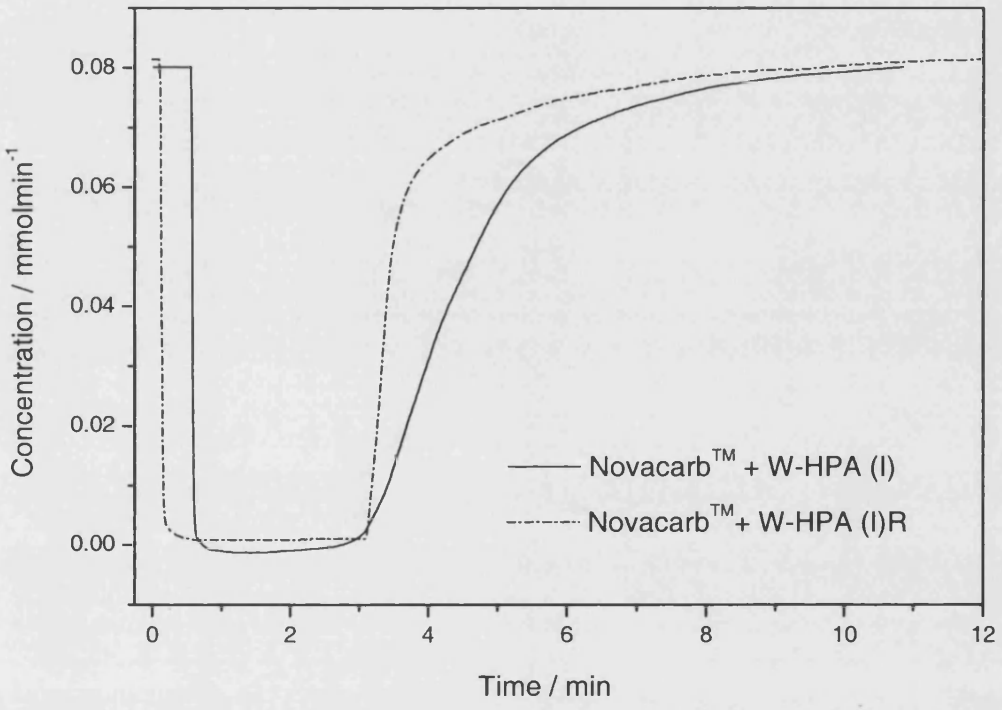

Figure A1-3. 1 Repeat of the ammonia uptake on the W-HPA impregnated Novacarb™.

Similarly, the samples used for experiment 2 were brominated in the same batch. The results obtained were 0.55 and 0.57 mmol NH_3 /g, and again were very reasonable.

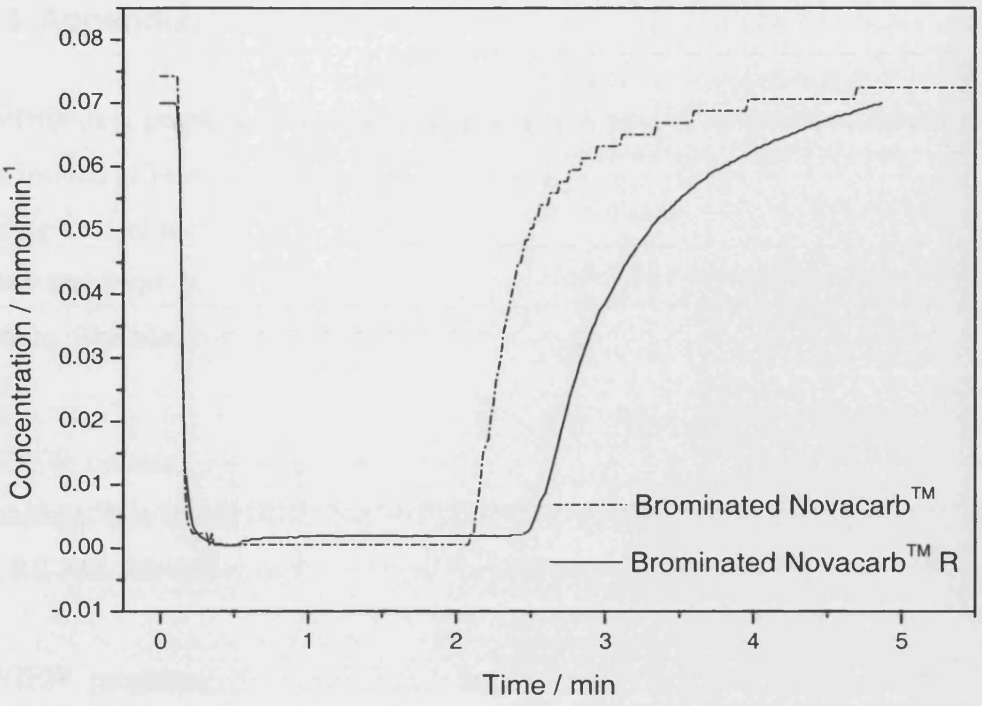

Figure A1-3. 2 Repeat of the ammonia uptake on the brominated Novacarb™

I.VI.4 Appendix: LabVIEW

LabVIEW is a graphical programming language that uses dataflow programming and icons instead of lines of text to create applications. In LabVIEW, a user interface is built by using a set of tools and objects. The user interface is known as the front panel and to control the front panel objects, a code is added using graphical representations of functions. The block diagram contains this code and resembles a flowchart.

LabVIEW contains comprehensive libraries for data collection, analysis, presentation and storage. It is integrated fully for communication with hardware such as GPIB, VXI, PXI, RS-232, RS-485 and plug-in data acquisition devices.

LabVIEW programs are called virtual instruments or VIs, as their appearance and operation imitate physical instruments. Every VI uses functions that manipulate input from the user interface or other sources and display that information or move it to other files or computers.

A VI contains a front panel, a block diagram and an icon and connector pane. Front panel serves as the user interface of the VI. It is built with controls and indicators that are the interactive input and output terminals of the VI, respectively. Knobs, push buttons, dials and other input devices are the controls and they simulate instrument input devices and supply data to the block diagram of the VI. Indicators are graphs, LEDs and other displays. They simulate instrument output devices and display data that the block diagram acquires or generates.

Block diagram contains graphical source code of the VI that defines its functionality. This graphical code is added after the front panel is built up. Front panel objects appear as terminals on the block diagram and every control or indicator on the front panel has a corresponding terminal on the block diagram. Icon and connector pane identifies the VI so that the VI can be used in another VI. A VI in another VI is called a subVI and it corresponds to a subroutine in text-based programming languages. Front panel designed for the two projects are shown in Figures A4.1 and A4.2.

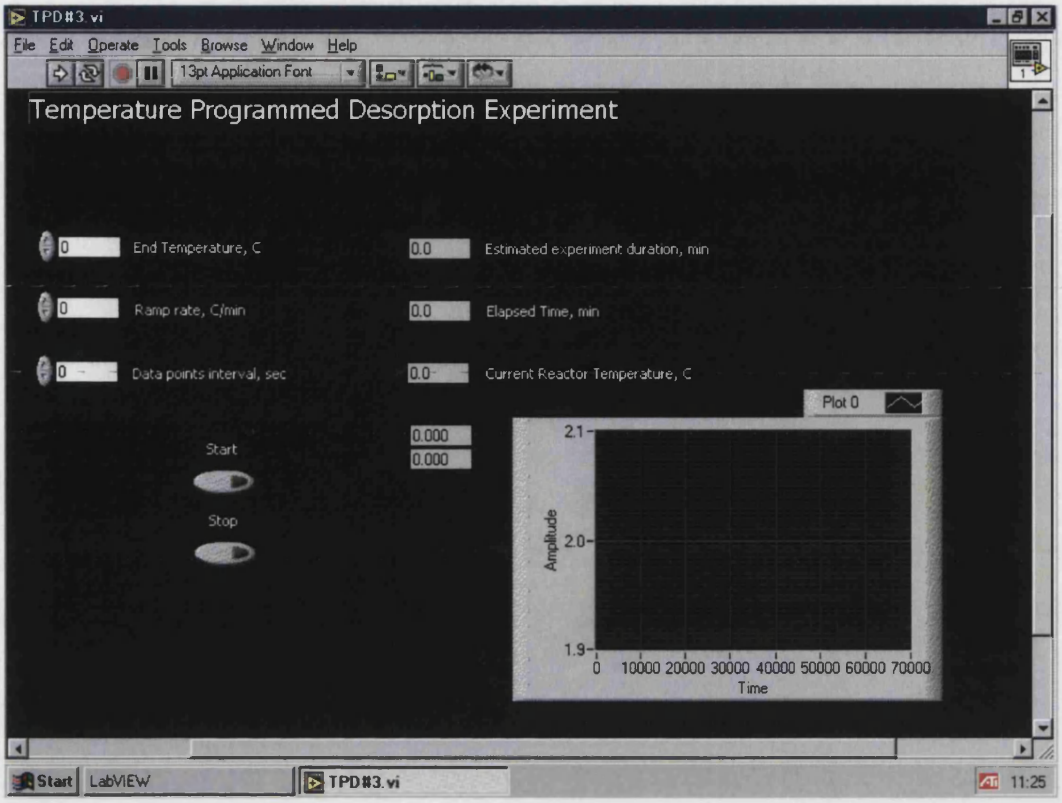

Figure A1-4. 1 Interface used in project I

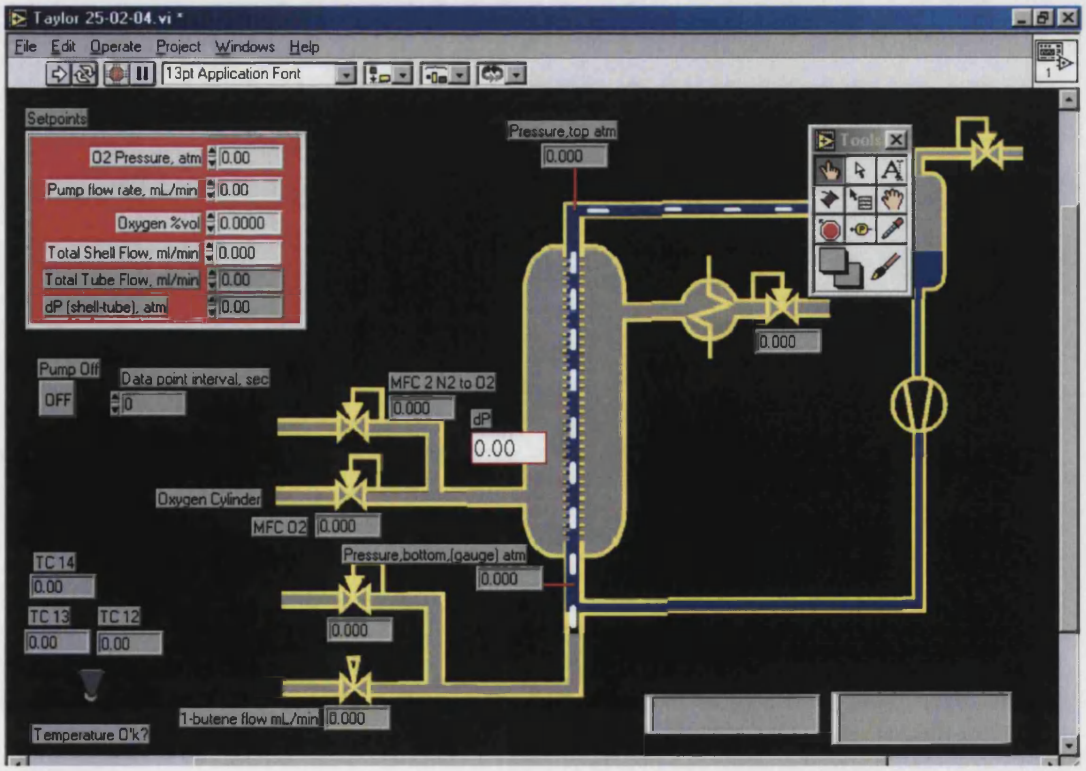

Figure A1-4. 2 Interface used in project II

I.VI.5 Appendix: Preparation and characterisation of chemisorbents based on heteropolyacids supported on synthetic mesoporous carbon and silica

ELSEVIER

Catalysis Today 81 (2003) 611–621

CATALYSIS TODAY

www.elsevier.com/locate/cattod

Preparation and characterisation of chemisorbents based on heteropolyacids supported on synthetic mesoporous carbons and silica

Alexei Lapkin [a,*], Bengü Bozkaya [a], Tim Mays [a], Luisa Borello [b,c], Karen Edler [b], Barry Crittenden [a]

[a] *Department of Chemical Engineering, University of Bath, Bath BA2 7AY, UK*
[b] *Department of Chemistry, University of Bath, Bath BA2 7AY, UK*
[c] *Dipartimento di Scienze dei Materiali ed Ingegneria Chimica, Politecnico di Torino, C.so Duca degli Abruzzi 24, 10129 Turin, Italy*

Abstract

The preparation of chemisorbents based on tungsto- and molybdophosphoric acids supported on two types of synthetic mesoporous carbons and two types of mesoporous silica is described. Strong solid acids with good accessibility to acid sites may potentially be effective adsorbents for the removal of basic molecular impurities, such as amines, from ultrapure manufacturing environments. Prepared materials were characterised by scanning electron microscopy, nitrogen adsorption, Fourier-transform infrared spectroscopy, powder X-ray diffraction, and equilibrium ammonia uptake. Composites of SBA-15 with heteropolyacids were synthesised. It was shown that the inclusion of HPAs into SBA-15 results in the loss of long range order. Adsorbents based on the HPAs impregnated into the supports with the open-pore morphology (Novacarb and SBA-15) were found to be promising materials. A composite of tungstophosphoric acid with sol–gel SiO_2 was found to have the highest ammonia uptake.

Keywords: Heteropolyacids; Clean room; Mesoporous materials; Chemisorption; Synthetic carbons

1. Introduction

The development of solid acid catalysts is an active and very important area of research, underpinning the development of future "green" chemical processes. There is significant need for new catalysts active in such reactions as Friedel–Crafts acylation and alkylation, esterification, and selective oxidation, which would substitute more conventional stoichiometric reactions known to generate large quantities of hazardous waste materials. At the same time porous solid acid materials of very similar physico-chemical and textural properties as solid acid catalysts may also find applications in separation processes.

Removal of molecular impurities from ultrapure manufacturing environments, such as in the manufacture of silicon wafers, is based on the use of acidic and basic chemisorbents [1]. At present, acidic chemisorbents are based on mineral acids, such as phosphoric and sulphuric acids, impregnated into activated carbon and dispersed in a polymer mesh filter. Sorbents based on supported liquid acids have a number of drawbacks. The formation of insoluble salts upon reaction with primary impurities restricts access to the

* Corresponding author. Tel.: +44-1225-383369; fax: +44-1225-386894.
E-mail address: a.lapkin@bath.ac.uk (A. Lapkin).

0920-5861/03/$ – see front matter © 2003 Elsevier B.V. All rights reserved.
doi:10.1016/S0920-5861(03)00159-7

remaining acid, thus decreasing the overall capacity of an adsorption bed. Furthermore, liquid sulphuric and phosphoric acids generate secondary oxide impurities, due to vapour pressure above liquid acids, and require installation of additional downstream filters. Using highly dispersed solid acids could potentially eliminate these drawbacks. The peculiarity of this application is that adsorbents must be efficient at very low concentration of pollutants, whereas high equilibrium capacity is of lesser importance. Therefore, the main focus of the development of such adsorbents should be on the acid strength and good accessibility to the acid sites.

There exist a large number of solid materials exhibiting varying degree of Brönsted acidity, ranging from natural acid-leached clays, amorphous silica–aluminas, meso-structured silicas such as MCM and SBA type materials, zeolites, free and supported heteropolyacids, and sulphated oxides [2]. Amongst these materials heteropolyacids supported onto mesoporous solids seem to be the most promising materials for this application. Heteropolyacids are strong Brönsted acids which already have found a number of commercial applications as catalysts (examples of two commercial applications of heteropolyacid catalysts: (a) direct hydration of propene to propanol; (b) acylation of anisole with acetic anhydride [3]), and are being actively investigated for new catalytic processes (see, e.g. [4]). Their applications as sorbents are much more limited [5]. It was shown in [6] that each Keggin unit of tungstophosphoric acid ($H_3PW_{12}O_{40}$, or W-HPA) is able to adsorb four molecules of ammonia irreversibly, which is higher than the proton content of the acid molecule. Thus, application of heteropolyacids as chemisorbents should ensure high sorbent capacity. However, in order to provide easy accessibility to adsorption sites it is necessary to obtain a highly dispersed acid and preferably use mesoporous supports providing easy pathways for convective and diffusional fluxes.

Preparation of supported heteropolyacids on a variety of support materials is widely reported (see, e.g. [7]). It was shown that the Keggin structure of HPAs is retained upon adsorption onto supports over a broad range of loadings. However, due to the interaction between the acid and the supports, the acidity of heteropolyacids may vary significantly. The acidity of HPAs supported onto carbons is generally lower than that of supported onto silica [7]. Preparation of heteropolyacids supported on a number of mesoporous solids was reported. Thus, it was shown that at loadings up to 23 wt% W-HPA supported onto MCM-41 by impregnation exhibits higher acidity than that of pure acid [8]. However, at higher loadings a significant distortion of the structure of the support and a decrease of acidity were observed. The low thermal stability of MCM-41 may potentially be disadvantageous for application in adsorption processes, as it precludes the use of thermal regeneration methods. Although the filters used in clean-room air purification systems are not regenerated, it is of general interest to develop materials that could be regenerated and re-used. It was shown that following thermal decomposition into β-MoO_3 oxide, the original structure of $H_3PMo_{12}O_{40}$ might be recovered by treatment in an atmosphere of steam [9]. Furthermore, the Keggin structure of tungstophosphoric acid may be regenerated by simple thermal treatment [10]. This may potentially provide a method of regeneration of adsorbents based on heteropolyacids. However, thermal stability and the nature of the supports become important. Compared with MCM-41, sol–gel derived mesoporous silica and SBA-15 are characterised by higher thermal stability. Furthermore, the sol–gel preparation method allows the making of heteropolyacid–silica composites with high acid loading [11].

This paper reports initial results on the preparation and characterisation of heteropolyacids supported on SBA-15, sol–gel derived SiO_2 and two different synthetic mesoporous carbons, to be used for removal of basic molecular impurities (e.g. ammonia and amines) from air in ultrapure manufacturing environments.

2. Experimental

2.1. Support materials

Four different support materials were used in this study: mesoporous phenolic resin derived carbon (Novacarb™), mesoporous synthetic carbon (Sibunit™), mesoporous silica SBA-15 and sol–gel derived silica. Samples of Novacarb™ were kindly provided by MAST Carbon (UK) in the form of microspheres with diameters in the range of 10–45 μm. Detailed information on the preparation and properties

of Novacarb™ can be found in [12]. Brominated Novacarb was prepared by direct contact with bromine gas in a three-neck flask at 673 K over 6 h in an atmosphere of argon to prevent oxidation of carbon. A 35% weight increase was observed following bromination. A sample of mesoporous carbon catalyst support Sibunit™ was kindly provided by the Boreskov Institute of Catalysis (Novosibirsk, Russia). Sibunit was washed in water and ethanol, and dried under vacuum at 473 K for 2–3 h prior to impregnation.

Pure SBA-15 was prepared as described in [13]. In a typical synthesis 2 g of Pluronic (P123) co-polymer was dissolved in a mixture of 52.5 g H_2O and 12 g HCl (36.5 wt.%) at 313 K. 4.28 g of tetraethoxy silane (TEOS) was added dropwise and the resultant mixture was stirred for 24 h. After stirring the mixture was poured into a polypropylene bottle and aged in an oven for 24 h at 363 K. Following ageing the mixture was filtered, washed with deionised water and dried under atmospheric conditions for 48 h. Finally, plain SBA-15 samples were calcined in flowing oxygen. The calcination temperature was increased from ambient to 773 K at 1 K/min and kept at that temperature for 6 h.

Composites of SBA-15 with W-HPA and molybdophosphoric acid ($H_3PMo_{12}O_{40}$), or Mo-HPA, heteropolyacids were synthesised by adding the corresponding acid to a solution of Pluronic co-polymer, water and hydrochloric acid. Mo-HPA (0.3970 g) and W-HPA (0.3065 g) were used to prepare composites containing 0.5 mol% W-HPA and 1 mol% Mo-HPA. The amount of HCl in solution was adjusted to maintain pH $\approx$ 1. The calcination temperature of composite samples was kept below 723 K in order to avoid decomposition of heteropolyacids.

Sol–gel silica and HPA/silica composites were prepared as described in [11]. In a typical synthesis 4.62 g TEOS was dissolved at 353 K in a mixture of 2.753 g of ethylene glycol and 2.67 g of ethanol while stirring. The calculated amount of heteropolyacid, yielding 20 and 50 wt.% composites, was added to the solution. After stirring for 1 h, a mixture of 8 g ethanol, 2 g water and a catalytic amount of acetic acid was added to the solution. The solution was kept at 353 K under stirring until a clear transparent gel was obtained, typically after 3 h. The resulting gel was aged at ambient conditions for 24 h and dried under vacuum at 413 K for 3 h, followed by calcination in flowing oxygen at 723 K for 6 h. The calcination temperature was ramped from ambient to 723 K at 1 K/min.

2.2. Preparation of supported heteropolyacids

W-HPA and Mo-HPA were obtained from Fischer and purified by re-crystallisation prior to impregnation. Supported acids were prepared by adsorption from ethanol–water solutions (1:1 volumetric ratio of demineralised water and 96 wt.% ethanol) as described previously in [14]. Gently stirred samples were equilibrated for 72 h at ambient temperature. The amount of acid adsorbed was evaluated gravimetrically. Sibunit samples were dried in vacuum at 473 K for 2 h following impregnation. Samples of Novacarb, SBA-15 and sol–gel silica were dried in air at 473 K for 2 h. A list of prepared samples and characterisation results is shown in Table 1.

2.3. Materials characterisation

Low temperature nitrogen adsorption experiments were performed using a Micromeritics ASAP-2010 volumetric system. Scanning electron microscopy (SEM) images were obtained using a JEOL 6310 system. Fourier-transform infrared (FT-IR) spectra were recorded using a Bruker Equinox 55 instrument in transmission mode (KBr pellets) and ATR mode (with a Golden Gate™, Specac, cell), using an MCT-A detector and resolution of 4 cm^{-1}. Powder X-ray diffraction (XRD) patterns were measured using a Bruker D8 powder diffractometer with Goebels mirrors.

2.4. Ammonia adsorption experiments

Breakthrough curves of ammonia were recorded using a custom-built setup equipped with a thermal conductivity detector (TCD). U-shaped quartz reactors of 10 and 5 mm ID were used. Sample of 0.3 g were loaded into a reactor with quartz beads and treated in flowing nitrogen at room temperature for approximately 2 h until a stable TCD signal was observed. The breakthrough curve was then recorded. In a typical experiment 2.1 vol.% ammonia in nitrogen and 70 ml/min flow were used. Total equilibrium ammonia uptake was calculated by integration of the breakthrough curves, less the free-volume of the reactor.

Table 1
Characterisation data for the supports and impregnation acids

	Starting solution (g[W]/l)	Starting solution (g[Mo]/l)	HPA loading (wt.%)	S_{BET}[a] (m^2/g)	Mesopore volume[b] (cm^3/g)	Micropore volume[c] (cm^3/g)	Equilibrium NH_3 sorption (mmol/g)
Novacarb	0	–	–	522.1	0.52	0.18	0.22
	–	110	20				1.37
	120	–	24	359.4	0.35	0.12	0.96
Novacarb brominated	0	0	–				0.56
	–	110	19				2.30
	120	–	16				–
Sibunit	0	0	–	286.1	0.23	0.02	0.05
	–	110	19				0.35
	120	–	22	149.1	0.17	0	0.47
SBA-15	0	0	–	321.1	0.38	0.01	0.89
	–	110	16	522.4	0.64	0.05	–
	120	–	16	421.9	0.52	0.04	1.67
SBA-HPA composite	–	–	0.5[d]				
	–	–	1.0[d]				
SiO_2–W-HPA composite	0	0	20				2.11
SiO_2 sol–gel	0	0	–	381.4	0.15	0.03	0.85
	–	110	33				1.29
	120	–	35	240.1	0.10	0.03	1.00

[a] Measured by nitrogen adsorption at 77 K.
[b] Calculated from desorption branch of isotherms using BJH method.
[c] Calculated using *t*-plot method.
[d] Expressed in mol%.

3. Results and discussion

3.1. Novacarb

Amongst the four support materials used, Novacarb shows the highest BET surface area at 522 m^2/g and mesopore volume 0.52 cm^3/g (see Table 1). This comparison is made between the pure support materials: the Mo-HPA impregnated SBA-15 exhibits higher BET surface area and mesopore volume. Novacarb also exhibits appreciable microporosity. This is clearly seen from the relatively high amount adsorbed at low relative pressures on the nitrogen adsorption isotherm (see Fig. 1). The mode of the pore-size distribution in the mesopore range for Novacarb is ca. 17.4 nm (see Fig. 2). The equilibrium loading of HPAs on Novacarb is ca. 20 wt.%. Reduction in the mesopore and micropore volumes after impregnation indicates that some W-HPA molecules are adsorbed in the microporous structure of Novacarb. However, the majority of the acid is located in the mesopores. According to the FT-IR data, the Keggin anion structure of W-HPA is retained upon adsorption on Novacarb (see Fig. 3). The fingerprint bands of the W-HPA Keggin anion at 795, 893, 983 and 1081 cm^{-1} are clearly seen on the spectrum of the supported acid.

The total equilibrium uptake of ammonia on pure Novacarb is relatively high. However, this is likely to be due to physical adsorption in the micropores. The equilibrium uptake of ammonia on the impregnated Novacarb samples corresponds to both reversibly, and irreversibly, adsorbed ammonia. This amount is slightly higher than could be expected from a simple sum of ammonia adsorbed by the support plus the total amount of ammonia adsorbed by the heteropoly-acid. Vedrine and coworkers [6] have estimated that the total, reversible plus irreversible uptake of ammonia by W-HPA is about 7.7 molecules per Keggin anion, which in our case should give approximately 0.86 mmol/g of total uptake. Given that the accuracy

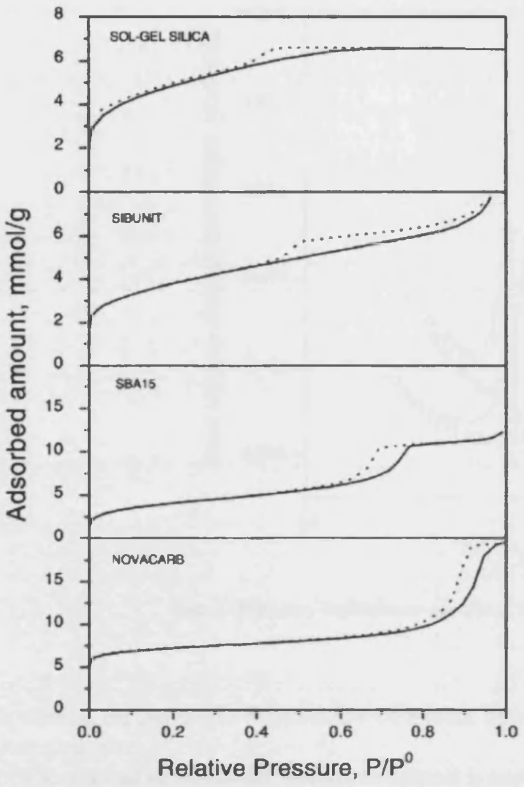

Fig. 1. Nitrogen adsorption–desorption isotherms measured at 77 K.

of gravimetric measurements of HPA loading is quite low, this agreement between the data is very reasonable.

The brominated Novacarb was prepared in order to modify the surface chemistry of carbon. Halogenation of carbon surfaces is used to increase the hydrophobicity of carbon surface, thus altering interaction with polar substances, as well as prevent ageing (oxidation) of carbon surface (see, e.g. [15]). Bromination should result in the formation of fairly labile C–Br bond, and may potentially influence interactions between carbon and heteropolyacids.

The FT-IR spectra of brominated Novacarb shows a band at 1400 cm^{-1}, an increased band at 1709 cm^{-1} and a broad band with a maximum at 1035 cm^{-1}, in comparison to the spectra of the parent Novacarb sample (see Fig. 3). The band at 1577 cm^{-1} present in both samples could be assigned to C=O groups of surface quinine groups [16,17]. An increase in the band at 1709 cm^{-1} (C=O groups of carboxylic acids or lactones) and 1035 cm^{-1} (C–O stretch in ether groups) indicate oxidation of carbon during the bromination reaction. Although reaction of bromination was performed in the atmosphere of argon, some oxygen may have been present in the reaction vessel, resulting in slight oxidation of carbon surface. The band at 1400 cm^{-1} is probably due to symmetrical stretching of $-COO^-$. The band for C–Br stretching could be expected in the frequency range of 600–500 cm^{-1} [18], and could not have been registered in our experiments.

The loading of HPAs on brominated Novacarb is slightly lower than that on the untreated support, indicating that bromination does not have any beneficial effect on the adsorption of heteropolyacids. There is a more significant effect of bromination on the ammonia uptake on both the brominated support and the acid loaded brominated samples. This could be attributed to two factors: (i) an increased acidity of carbon surface, indicated by FT-IR results and (ii) a reaction between ammonia and bromine, resulting in the formation of either NH_4Br or more complex adducts. The available experimental data does not permit to elucidate the true nature of the effect and requires more careful examination of the heats of adsorption and desorption of ammonia.

3.2. Sibunit

Sibunit is a mesoporous carbon support prepared by depositing pyrolytic carbon onto carbon black particulates, followed by controlled gasification of defective pyrolytic carbon, but mainly of carbon black [19]. The resulting open hollow shells are formed into granular particles. Preparation of W-HPA supported onto several Sibunit samples is reported in a recent paper [20]. The Sibunit sample used in this work is characterised by lower BET area, lower mesopore volume and smaller pore diameter, compared to most samples used in [20]. The mode of the pore-size distribution for Sibunit was determined to be 4 nm. The morphology of Sibunit is significantly different from that of Novacarb. Sibunit has virtually zero microporosity. The hysteresis of nitrogen adsorption–desorption on Sibunit shows a long plateau on the desorption branch (see Fig. 1). This type of hysteresis may originate from narrow pore necks, whereas the abrupt nature of

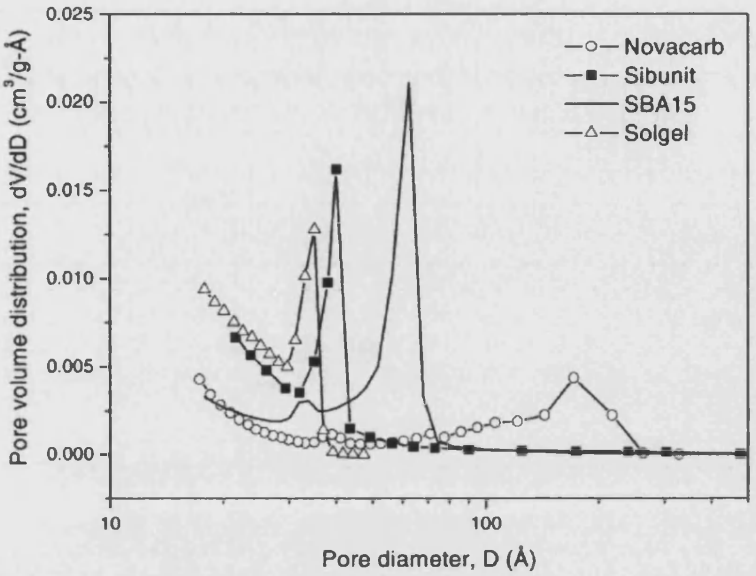

Fig. 2. Pore-size distributions calculated from nitrogen adsorption data using the BJH method.

hysteresis for Novacarb is indicative of a more open-pore structure.

The amount of HPAs adsorbed onto Sibunit is similar to that in the case of Novacarb. The maximum HPA loading found in this work is lower than that in [20]. However, these results cannot be compared directly due to the differences in the solvent and the concentration of the starting HPA solutions used in the two studies. An ethanol–water solution with the maximum concentration of acid ca. 120 g[W]/l was used in this study, whereas Likholobov et al. [20] used a methanol solution and 150 g[W]/l acid concentration.

Pure Sibunit adsorbs very little ammonia. This is due to the absence of microporosity and, possibly, due to lower surface functionality. The total ammonia uptake registered for the HPA loaded Sibunit is also quite low. Using the data of Vedrine and coworkers [6], the total ammonia uptake on samples with this HPA loading could be estimated to be ≈0.5 mmol/g. The low ammonia uptake observed for HPA impregnated Sibunit is possibly due to the strong interaction between HPA molecules and the carbon surface. This is supported by the data that between 12 and 25% of total HPA loading is irreversibly adsorbed onto Sibunit [20].

3.3. SBA-15

Fig. 4 shows the SEM images of synthesised SBA-15 mesoporous silica. The larger magnification image clearly shows hexagonal particles organised into rope-like structures, which are further agglomerated into elongated particles of length of the order of 0.1 μm. Similar structures were reported in earlier papers on SBA-15 [13,21]. The material synthesised in this work is characterised by a BET surface area of 321 m^2/g, which is low compared to literature data. However, the shape of the nitrogen adsorption–desorption hysteresis (see Fig. 1) is characteristic of a narrow pore-size distribution in the mesopore region [22]. The mode of the pore-size distribution was found by the Barrat–Joyner–Halenda (BJH) method to be 6.3 nm and the mesopore volume was determined as 0.38 cm^3/g. The hexagonal structure of synthesised SBA-15 was confirmed by recording the XRD patterns (see Fig. 5). The *d*-spacing of (1 0 0) planes in pure SBA-15 is 9.4 nm.

Apart from pure SBA-15 materials, two composite materials with HPAs were synthesised in an attempt to incorporate HPA anions into the walls of mesoporous silica. At high HPA concentrations in the synthesis

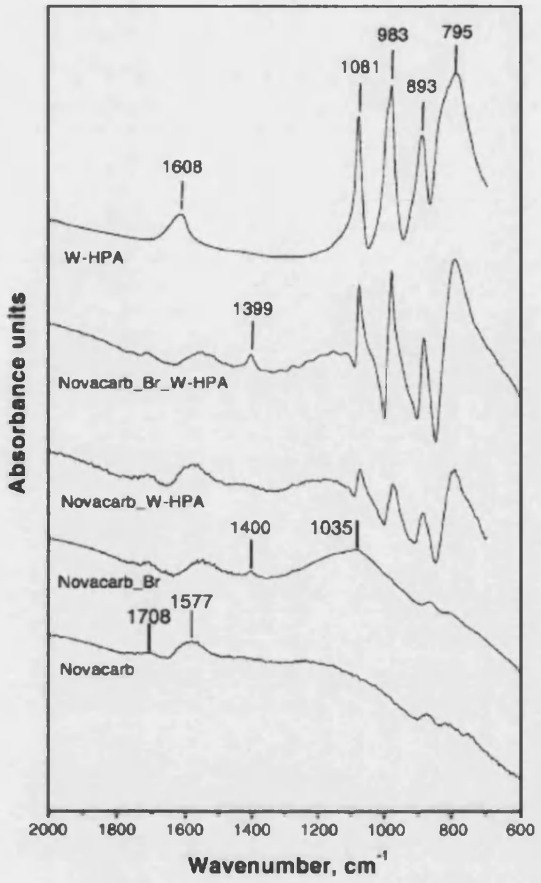

Fig. 3. FT-IR spectra of pure W-HPA, Novacarb, brominated Novacarb and Novacarb impregnated with W-HPA.

solution both acids react with Pluronic surfactant. Therefore, only very small concentrations of HPAs could be used, resulting in 0.5 mol% W-HPA/SBA and 1.0 mol% Mo-HPA/SBA composites. According

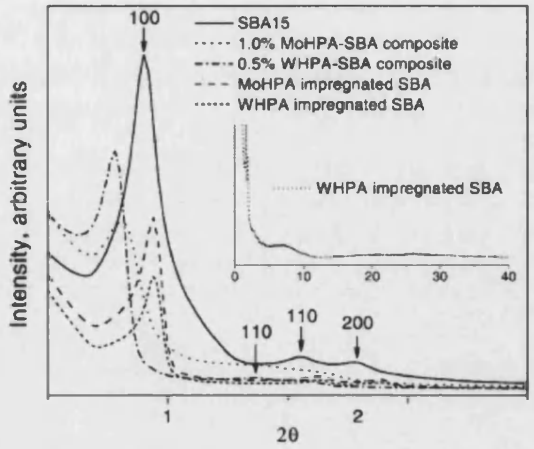

Fig. 5. XRD patterns of SBA-15, 1.0% Mo-HPA/SBA composite, 0.5% W-HPA/SBA composite, Mo-HPA impregnated SBA-15 and W-HPA impregnated SBA-15.

to the XRD patterns for the composite materials, diffraction from (1 0 0) planes is shifted to lower 2θ angles, indicating an increase in d-spacing, possibly due to swelling of the surfactant micelles arising from the strong interaction between the HPAs and surfactant. At the same time the lower intensity diffraction from (1 1 0) and (2 0 0) planes appear as broad peaks, indicating the loss of long range order.

Impregnation of heteropolyacids onto pure SBA-15 resulted in an increase in BET surface area and meso- and micropore volumes, compared to those of pure SBA-15 (see Table 1). The XRD spectra of SBA-15 impregnated with W-HPA and Mo-HPA reveal a shift of the pattern to larger 2θ angles, i.e. a decrease in d-spacings. This is probably due to restructuring of silica during the step of adsorption of HPAs from water–ethanol solution. The XRD spectra showed no

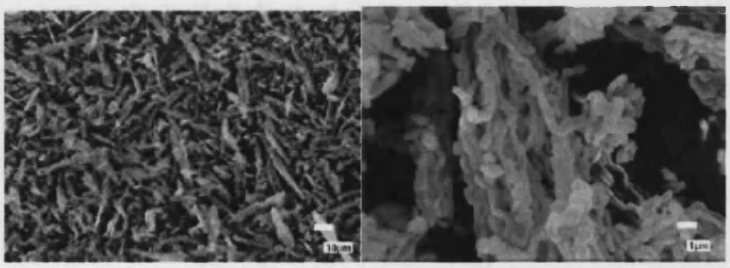

Fig. 4. SEM images of calcined SBA-15 at two magnifications.

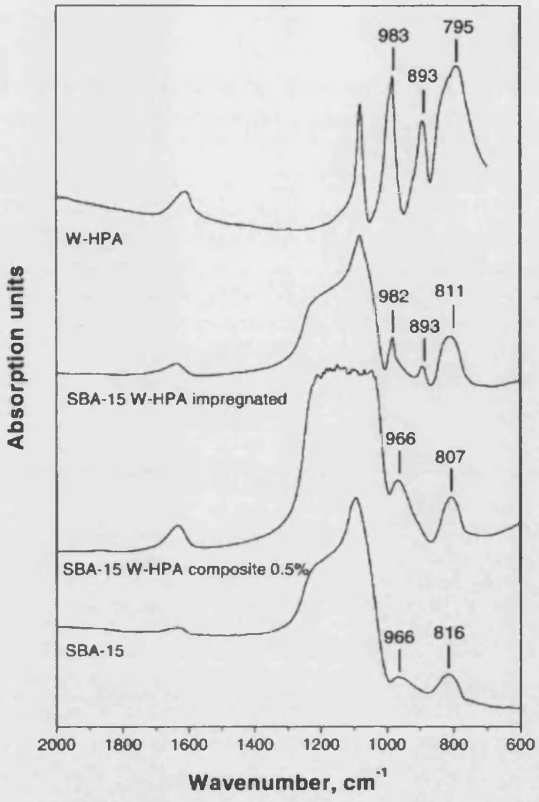

Fig. 6. FT-IR spectra of pure SBA-15, SBA-15 HPA composite and SBA-15 impregnated with W-HPA.

pattern of crystalline HPAs [23] (see inset of Fig. 5), which is probably due to (i) too low a quantity of heteropolyacid for detection, (ii) molecular distribution of heteropolyanions or (iii) too small crystallites of HPA for detection. However, the FT-IR spectrum of the W-HPA impregnated sample (see Fig. 6) clearly shows the fingerprint bands of the Keggin anion, which indicates that the heteropolyacid structure is preserved upon impregnation.

The total equilibrium uptake of ammonia by pure SBA-15 is considerably higher than that of the carbons. This is likely to be due to the acidity of silica itself, as mesopore and micropore volumes of SBA are lower than those for carbon. The total uptake of ammonia by W-HPA impregnated SBA-15 is higher than could be expected from analogous considerations as applied to carbons. However, as was demonstrated in [8], the acidity of the HPA/MCM-41 system depends on acid loading and exhibits maxima at ca. 23 wt.% HPA loading. It is feasible that a similar phenomenon is present in the case of HPA/SBA-15 system and is responsible for the high uptake of ammonia.

3.4. Sol–gel SiO_2

Pure sol–gel SiO_2 was synthesised according to a literature recipe [11]. This material is characterised by a relatively low mesopore volume 0.15 cm^3/g compared to both carbons and SBA-15, but it has a higher micropore volume than SBA-15 and Sibunit. The BET surface area of synthesised sol–gel SiO_2 material was found 381 m^2/g, which is higher than that reported in [11]. Due to the morphology of sol–gel derived materials the adsorption–desorption hysteresis exhibits a long plateau on the desorption branch (see Fig. 1). Similar hysteresis was observed in the case of Sibunit. The morphology of the two materials can probably be described by the spherical pores with narrow opening, which is responsible for long desorption hysteresis.

Similar to the results obtained in [11], impregnation of HPAs results in a decrease in BET surface area. Comparison between the relative changes in the mesopore and micropore volumes of pure support and impregnated support indicates that all the HPA is located within mesopores.

The total equilibrium uptake of ammonia by the pure SiO_2 support is very similar to that of SBA-15 despite the differences in morphology, which indirectly supports our hypothesis that the acidity of silica itself might be responsible for the uptake of ammonia. However, the amount of ammonia uptake by the impregnated samples is considerably lower than that on SBA-15 and similar to the uptake by samples of Novacarb with a much lower HPA loading.

A significantly higher ammonia uptake was measured on the sample of W-HPA/SiO_2 composite containing 20 wt.% acid. This result seems to be in contradiction to the conclusions obtained in [11] that HPA/SiO_2 sol–gel composites have lower acidity compared to the impregnated samples. It was concluded in [11] that after calcination at 723 K the Keggin anion of W-HPA in the composite material is decomposed. However samples containing 20% W-HPA were shown to have catalytic activity in the reaction of 1-butene isomerisation. The FT-IR spectra

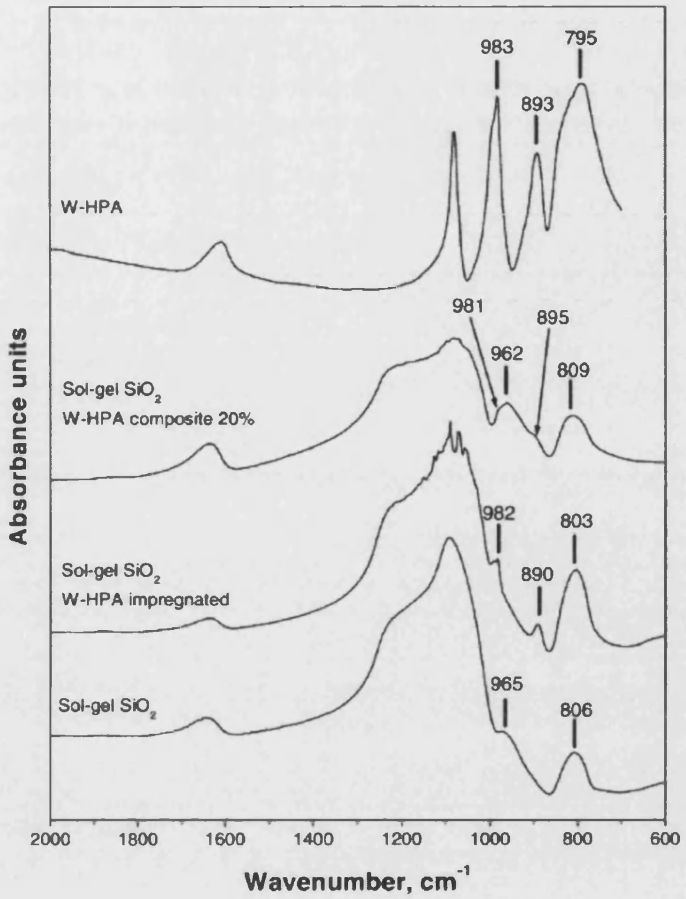

Fig. 7. FT-IR spectra of pure sol–gel derived SiO_2, SiO_2–W-HPA composite and SiO_2 impregnated with W-HPA.

of 20% W-HPA/SiO_2 composite sample does not show clearly resolved W-HPA bands (see Fig. 7). However, weak shoulders at 980 and 895 cm^{-1} are likely to be due to the W-HPA bands at 983 and 893 cm^{-1}, respectively. The bands of heteropolyacids at 1081 and 795 cm^{-1} are masked by stronger absorption of silica at the same wavenumbers. Therefore, the Keggin structure of the acid seems to be at least partially retained. However, at this stage there is no sufficient data to explain why W-HPA/SiO_2 composite material shows such a high ammonia uptake.

It is useful to provide a comparison of the adsorption capacity of materials prepared in this study with that of conventional adsorbents. However, equilibrium uptake, although an important parameter, is not the key function for the specific application in the air purification in clean rooms. Therefore, it would not be possible to make selection of the best material for this specific application based on this information alone.

A recent systematic study of ammonia adsorption on a number of adsorbents [24], aimed at developing adsorbents for a pressure swing adsorption process of separation of ammonia, provides some data for comparison. Thus, in this study the highest ammonia uptake ca. 2.3 mmol/g, at the partial pressure of ca. 2.1 kPa, was measured on the brominated sample of Novacarb impregnated with Mo-HPA acid. At a similar pressure, the highest ammonia uptake ca. 6.7 mmol/g was reported on microporous synthetic zeolite 13X with the mean pore diameter of 0.85 nm

and BET surface area of 430 m^2/g [24]. Ammonia uptake on a mesoporous silica–gel (ca. 1.68 mmol/g) with the mean pore diameter of 10 nm and BET surface area of 238 m^2/g was considerably higher than that on the sol–gel derived silica prepared in this work (0.85 mmol/g).

4. Conclusions

Four different mesoporous supports were impregnated with tungstophosphoric acid $H_3PW_{12}O_{40}$ (W-HPA) and molybdophosphoric acid $Mo_3PW_{12}O_{40}$ (Mo-HPA). Characterisation of the morphology of supports showed that mesoporous synthetic carbon Novacarb™ and template-derived mesoporous silica SBA-15 have relatively narrow pore-size distributions and open porous structures, whereas mesoporous carbon Sibunit™ and sol–gel derived SiO_2 both have bottle-neck type pores.

Between the two mesoporous carbons, the open-pore morphology and larger pore size of Novacarb seem to be beneficial for ammonia uptake. Between the two silicas the impregnated samples show comparable performance in ammonia uptake, although SBA-15 showed slightly higher uptake. It was shown that inclusion of heteropolyacid molecules into the SBA-15 framework results in a significant loss of structure, even at very small concentrations of HPAs. At the same time, the incorporation of HPAs into HPA/SiO_2 composites via the sol–gel technique seems to give a material with the highest total ammonia uptake amongst the materials studied. This phenomenon could not be explained in this study without further characterisation.

Further study is under way to characterise the performance of these materials in the removal of ammonia and amines from air streams at very low concentrations. These results, as well as results on ammonia TPD and regeneration of heteropolyacid based chemisorbents will be presented in a forthcoming paper.

Acknowledgements

This work was funded by the Engineering and Physical Sciences Research Council via grant GR/R18697/01. AL is grateful to Steve Tennison, MAST Carbon, for providing carbon support materials and for many useful discussions.

References

[1] D.A. Kinkead, Air filtering within clean environments, USP 5,607,647 (1997).
[2] (a) A. Coma, Inorganic solid acids and their use in acid-catalysed hydrocarbon reactions, Chem. Rev. 95 (1995) 559–614;
(b) Y. Izumi, K. Urabe, M. Onaka, Zeolite, Clay and Heteropolyacid in Organic Reactions, Kodansha, Tokyo, 1992.
[3] (a) Y. Izumi, Y. Kawasaki, M. Tani, Process for the preparation of alcohols, USP 3,758,615 (1973);
(b) P. Metvier, in: R.A. Sheldon, H. van Bekkum (Eds.), Fine Chemicals Through Heterogeneous Catalysis, Wiley, Weinheim, 2001, p. 161.
[4] J. Kaur, K. Griffin, B. Harrison, I.V. Kozhevnikov, Friedel–Crafts acylation catalysed by heteropolyacids, J. Catal. 208 (2002) 448–455.
[5] D.E. Katsoulis, A survey of applications of polyoxometalates, Chem. Rev. 90 (1998) 359–387.
[6] N. Essayem, R. Frety, G. Goudurier, J.C. Vedrine, Ammonia adsorption–desorption over strong solid acid catalyst $H_3PW_{12}O_{40}$ and its Cs^+ and NH_4^+ salts, J. Chem. Soc., Faraday Trans. 93 (17) (1997) 3243–3248.
[7] L.R. Pizzio, C.V. Caceres, M.N. Blanco, Acid catalysts prepared by impregnation of tungstophosphoric acid solutions on different supports, Appl. Catal. A 167 (1998) 283–294.
[8] A. Ghanbari-Siahkali, A. Philippou, J. Dwyer, M.W. Anderson, The acidity and catalytic activity of heteropolyacid on MCM-41 investigated by MAS NMR, FT-IR and catalytic tests, Appl. Catal. A 192 (2000) 57–69.
[9] C. Rocchiccioli-Deltcheff, A. Aouissi, S. Launay, M. Fournier, Silica-supported 12-molybdophosphoric acid catalysts: influence of the thermal treatments and of the Mo contents on their behaviour, from IR, Raman, X-ray diffraction studies, and catalytic reactivity in the methanol activation, J. Mol. Catal. A 114 (1996) 331–342.
[10] S. Shimizu, H. Ichihashi, K. Nagai, Heteropolyacids and Their Production and Use, USP 4,565,801 (1986).
[11] A. Kukovecz, et al., Synthesis, characterisation and catalytic applications of sol–gel derived silica–phopshotungstic acid composites, Appl. Catal. A 228 (2002) 83–94.
[12] S.R. Tennison, Phenolic resin derived activated carbons, Appl. Catal. A 173 (2) (1998) 289–311.
[13] D. Zhao, et al., Triblock copolymer syntheses of mesoporous silica with periodic 50 to 300 angstrom pores, Science 279 (1998) 548–552.
[14] L.R. Pizzio, C.V. Caceres, M.N. Blanco, Acid catalyst prepared by impregnation of tungstophosphoric acid solutions on different supports, Appl. Catal. A 167 (1998) 283–294.
[15] J.A.F. MacDonald, et al., Chlorine and oxygen on the carbon surface, Carbon 38 (2000) 1825–1830.

[16] A. Pigamo, et al., Effect of oxygen functional groups on synthetic carbons on liquid phase oxidation of cyclohexanone, Carbon 40 (2002) 1267–1278.
[17] J.L. Figueiredo, M.F.R. Pereira, M.M.A. Freitas, J.J.M. Orfao, Modification of the surface chemistry of activated carbons, Carbon 37 (1999) 1379–1389.
[18] L.J. Bellamy, The Infra-red Spectra of Complex Molecules, Chapman & Hall, London, 1975.
[19] V.B. Fenelonov, V.A. Likholobov, A.Yu. Derevyankin, M.S. Mel'gunov, Porous carbon materials prepared from C_1–C_3 hydrocarbons, Catal. Today 42 (1998) 341–345.
[20] M.N. Timofeeva, et al., Adsorption of $H_3PW_{12}O_{40}$ by porous carbon materials, Russ. Chem. Bull. Int. Ed. 51 (2) (2002) 243–248.
[21] M.-C. Chao, H.-P. Lin, H.-S. Sheu, C.-Y. Mou, A study of morphology of mesoporous silica SBA-15, Stud. Surf. Sci. Catal. 141 (2002) 387–394.
[22] M. Kruk, M. Jaroniec, C.H. Ko, R. Ryoo, Characterisation of the porous structure of SBA-15, Chem. Mater. 12 (2000) 1961–1968.
[23] M.J. Verhoef, P.J. Kooyman, J.A. Peters, H. van Bekkum, A study on the stability of MCM-41-supported heteropolyacids under liquid- and gas-phase esterification conditions, Micropor. Mesopor. Mater. 27 (1999) 365–371.
[24] J. Helminen, J. Helenius, E. Paatero, Adsorption equilibria of ammonia gas on inorganic and organic sorbents at 298.15 K, J. Chem. Eng. Data 46 (2001) 391–399.

PARTIAL OXIDATION OF HYDROCARBONS BY MULTIPHASE CATALYTIC MEMBRANE REACTOR USING HETEROPOLYACIDS

List of Figures

List of Tables

II.I INTRODUCTION

Heteropolyanions, $PMo_{12-n}V_nO_{40}^{(3+n)-}$ (HPA) are widely used as co-oxidants in catalytic oxidations of hydrocarbons. The system in which HPAs are used as co-oxidants was discovered by Matveev et al. in the 70s. It is regarded as the most efficient catalyst system in the polyoxometalate series for the oxidation by molecular oxygen.

The Wacker process was the first organometallic catalytic oxidation that contained carbon-metal bonds and mainly used for the production of acetaldehyde from ethylene and oxygen. However, due to the use of high concentrations of chloride, hence high levels of chlorinated side products and the requirement of special construction in the plants due to highly corrosive nature of the solutions, considerable efforts have been expended in the search of an alternative oxidising system which does not require high chloride levels [Davison, 1984]. Matveev et al. (1978) have discovered that vanadium in Keggin phosphomolybdovanadates was a di-oxygen regenerable oxidant. They completely eliminated the use of chloride in the Wacker oxidation. Although the invention of the heteropolyacid solution was an accomplishment, the system did not meet the criteria required by the industrial application, due to very slow olefin and oxygen reaction rates and solution having poor palladium(II) catalyst stability. Grate et al. (1994) developed an improved catalyst system in order to overcome the drawbacks of the Wacker and Matveev's catalyst systems. This system was developed for oxidation of higher olefins to ketones as well as for ethylene oxidation to acetaldehyde. They have prepared a homogeneous catalyst solution containing three key components: palladium(II) catalyst to oxidize olefin to a carbonyl compound, Keggin phosphomolybdovanadates with a general formula of $PMo_{(12-x)}V_xO_{40}^{(3+x)-}$ to provide a dioxygen reversible vanadium(V)/vanadium(IV) redox agent for palladium(0) reoxidation, and chloride at centimolar concentration to maintain stable palladium(II) catalyst activity. Proposed reaction steps for 1-butene oxidation to methyl ethyl ketone are as below:

$C_4H_8 + PdCl_2 + H_2O \rightarrow C_4H_8O + Pd(0) + 2HCl$

$Pd(0) + HPA\text{-}n + 2\,H^+ \rightarrow Pd(II) + H_2(HPA\text{-}n)$

$H_2(HPA\text{-}n) + 1/2O_2 \rightarrow HPA\text{-}n + H_2O$

Many new processes with transition metal catalysts have been developed and many new products have become available as in the last three decades homogeneous catalysis has undergone major growth. Although heterogeneous catalysis is still of much greater economic importance in industrial processes, the share of homogeneous transition metal catalysis in catalytic processes is estimated at 10-15% [Hagen, 1999]. Economic data on homogeneous catalysis is difficult to obtain due to their internal use in a company without this fact being made public and in many cases catalysts are prepared in situ from metal compounds. Examples of homogeneous transition metal catalyzed industrial oxidation processes include: cyclohexane oxidation, production of carboxylic acids (adipic and terephtalic acid), epoxides (propylene oxide, Halcon process), acetaldehyde (Wacker-Hoechst).

In hydrocarbon oxidation processes, due to the danger of explosion via hydrocarbon-air contact, the subject of safety was brought into deep focus by the Flixborough explosion in June 1974 involving a cyclohexane oxidation plant. Following that, many studies focused on the elimination of the risk of explosions. One way of doing that is to avoid direct contact of the oxygen and hydrocarbon and can be achieved by putting a barrier between the two gasses and being able to control the concentrations of the mixtures. In order to achieve this, a hollow fibre membrane contactor was placed in the reactor and oxygen was distributed around it. The distribution of oxygen allows a wider range of operating conditions: by distributing the oxygen feed in the inert membrane reactor it is possible to operate at overall hydrocarbon to oxygen ratios that would be within the explosive region if the same composition was fed at the entrance of a fixed bed reactor.

Membrane contactors offer a number of advantages, such as: no flooding at high flowrates, no unloading at low flowrates, no density difference between fluids is required, high interfacial area. Gas/liquid and liquid/liquid contacting operations are traditionally performed using towers, columns or mixer-settlers. The main challenge usually is to maximise the mass transfer rate by producing as high interfacial area as possible. Membrane contactors typically offer 30 times more area than what is achievable

in gas absorbers and 500 times what is obtainable in liquid/liquid extraction columns [Gabelman & Hwang, 1999]. Furthermore, although columns and other fluid/fluid contactors have been widely used in chemical industry for decades, an important disadvantage is the interdependence of the two fluid phases, which sometimes lead to difficulties, such as creating emulsions, foaming, unloading and flooding. Using a suitable membrane, e.g. hollow fiber or a flat sheet, separate flows of the fluids can be obtained by flowing them on the opposite sides of the membrane.

Chen et al. (1992) claimed that hollow fibers can provide large mass transfer area per unit volume of reactor and reported the results of a study using a membrane reactor for the homogeneous catalytic reaction of direct oxidation of ethylene to acetaldehyde. It was concluded that the large dispersion free gas-liquid interfacial area provided by hollow fiber membranes increases the productivity per catalyst loading to a level considerably higher than that of a comparable bubble column reactor, as long as the membrane does not introduce much excessive mass transfer resistance.

Inert membrane reactors have also been experimentally tested in the concept of lowering partial pressures of oxygen for several reactions of selective oxidation of hydrocarbons [Alfonso et al., 2000]. It has been found that in selective oxidation processes, low partial pressure of oxygen favours the selective oxidation reaction versus the deep oxidation to CO and CO_2.

Additionally, higher gas transfer rates from the hydrocarbon to the liquid catalyst was achieved by creating Taylor flow inside the hollow membrane. Taylor flow is a two phase flow regime in which the liquid slugs are separated by large bubbles that have the length greater than the channel diameter. Recent works on gas-liquid flow have shown that Taylor flow provides very efficient mass transfer from the gas bubble into the liquid phase [Irandoust et al., 1989].

Based on absorption experiments using methane and water, Berčič and Pintar (1997) measured the gas to liquid mass transfer parameter k_La in single capillaries with different diameters and found that the liquid slug lengths influence the mass transport much more than the gas bubble length and they fitted the experimental results to the following empirical correlation:

$$k_L a = 0.111 v^{1.19} / ((1 - \varepsilon_G) UCL)^{0.57}$$

where v is average cell velocity (m/s), ε_G is the gas hold-up and UCL is the unit cell length (m) which is the sum of the liquid slug and the gas bubble lengths. It must be noted that this equation was obtained for the case of methane and water, thus, if a different combination of gas and liquid is used $k_L a$ coefficient must be corrected using the following relation:

$$(k_L a)_{Gas} = (k_L a)_{CH4} \left(\frac{D_{Gas}}{D_{CH_4}} \right)^n$$

where D_{Gas} and D_{CH_4} are the diffusion coefficients for the gas used and methane (m^2/s) and n is the scaling factor and is unity for film theory and 0.5 for penetration theory [Kreutzer et al., 2001; Berčič, 2001].

Development of a system consisting of a hollow fibre contactor for catalytic hydrocarbon oxidation is described in the second part of the thesis. Gas-liquid transfer in Taylor flow regime, characterisation of the carbon membrane used, oxygen transfer through the membrane and oxidation of 1-butene to methyl ethyl ketone as a test reaction were also studied extensively and explained in detail in the following chapters.

II.II PRIOR ART

II.II.1 CATALYTIC OXIDATION OF HYDROCARBONS

Processes involving the oxidation of hydrocarbons in the liquid phase, using air or oxygen, are very important for industrialized economies due to their role in converting petroleum hydrocarbon feedstocks into industrial organic chemicals important for polymer and petro-chemical industries. These products are much more expensive than the parent hydrocarbons and particularly in the case of oxygen containing compounds, a great deal of effort has been expended in attempts to develop processes based on homogeneous gas phase oxidation which will produce such products selectively. However, homogeneous oxidations are unselective and give a complex mixture of potentially valuable products that would require refinery for separation. Hence, efforts have been directed to produce such compounds by catalytic oxidation [Hucknall, 1974].

Early processes for the oxidative transformation of petroleum feedstocks involving vapour phase and liquid phase oxidations began in the 1950s. Systematic studies of the industrially important homogeneous catalysis of oxidation processes also began in 1950s. The Wacker process for the conversion of terminal olefins to carbonyl compounds and the Hock process for the production of phenol from cumene were commercialized during this period. [Suresh et al., 2000].

Catalytic oxidation of hydrocarbons proceeds via the following steps:
-Reaction between the hydrocarbon and the oxide to give products and the reduced catalyst.
-Re-oxidation of the reduced catalyst with gaseous oxygen to restore the catalyst to its original state.

According to this model, the agent responsible for oxidation is oxygen ion of the oxide lattice. Following this theory, Sachtler and De Boer (1965) speculated that the activity and the selectivity of the oxide catalysts towards hydrocarbon oxidation should depend on the strength of the metal-oxygen bond within the catalyst. In other words, strong bonds should produce inactive catalyst, while the weak bonds yield complete combustion of the reactants. Therefore the bonds with intermediate strength should be present in

catalyst for selective oxidation. Simons et al. (1968) attempted to confirm this theory and run sets of experiments that provided good evidence to prove that catalytic activity should increase with decreasing strength of the M-O bond.

Homogeneously Catalyzed Reactions

Many new processes with transition metal catalysts have been developed and many new products have become available as in the last three decades, homogeneous catalysis has undergone major growth. Although heterogeneous catalysis is still of much greater economic importance in industrial processes, the share of homogeneous transition metal catalysis in catalytic processes is estimated as 10-15% [Hagen, 1999]. Economic data on homogeneous catalysis is difficult to obtain due to their internal use in a company without this fact being made public and in many cases catalysts are prepared in situ from metal compounds. Homogeneous transition metal catalyzed reactions are now used in almost all areas of the chemical industry. Figure II.II-1 shows the brief classification of homogeneous transition metal catalyzed reactions.

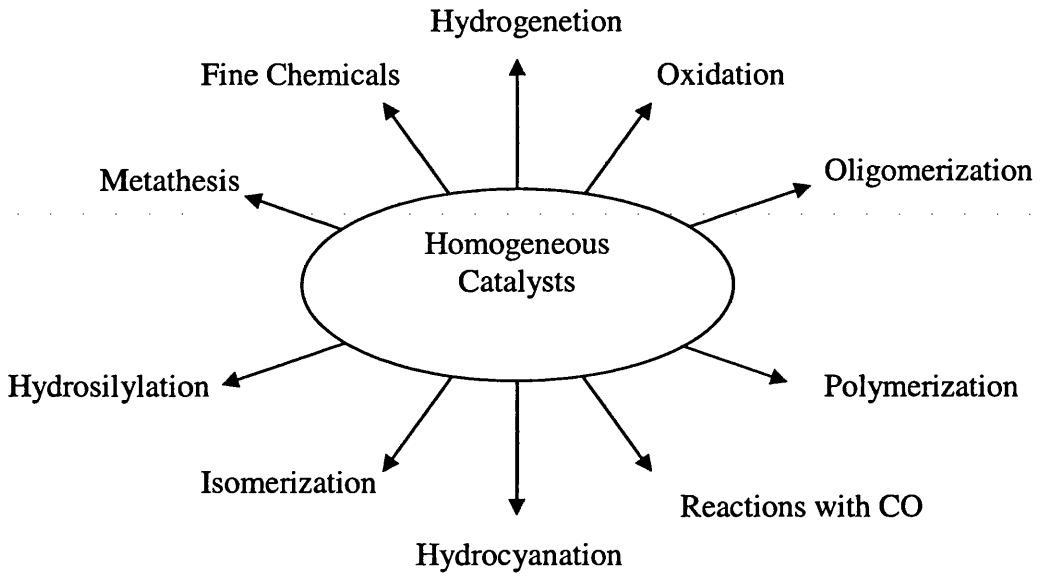

Figure II.II- 1 Industrial homogeneous transition metal catalyzed reactions

The most important industrial application of homogeneous catalysts is the oxidation of hydrocarbons with oxygen or peroxides. Mechanistically, a distinction is made between:

- Homolytic processes: the transition metals react with formation of radicals, and the oxidation or reduction steps are one-electron processes.
- Heterolytic processes: normal two-electron steps of coordination chemistry.

Examples of homogeneous transition metal catalyzed industrial oxidation processes include: cyclohexane oxidation, production of carboxylic acids (adipic and terephtalic acid), epoxides (propylene oxide, Halcon process), acetaldehyde (Wacker-Hoechst).

Homogeneous catalysis also used in the manufacture of low-scale but high-value products such as pharmaceuticals and agrochemicals. Also another rapidly growing area is the sysnthesis of fine chemicals. Production data is listed in Table II.II-1. In addition, Table II.II-2 shows a comparison of homogeneous and heterogenized catalysts in industrial reactions.

Table II.II- 1 Production of chemicals by homogeneous catalysis [Hagen, 1999]

Process	**10^6 t/a**
Oxidation	14.0
Reactions with CO	8.0
Hydrogenation	1.4
Oligomerization	0.8
Hydrocyanation	0.4

TableII.II- 2 Comparison of homogeneous and heterogenized catalysts in industrial reactions [Hagen, 1999]

Reaction	*Homogeneous Catalyst*	*Heterogenized Catalyst*
Hydroformilation of Olefins (oxo synthesis)	Co or Rh complex	Co or Rh complex on polymer or SiO_2 support matrix
Oxidation of Olefins (Wacker Process)	$[PdCl_4]^2$	$PdCl_2$ on support matrix
Carbonylation of methanol to acetic acid	$[Rh(CO)_2I_2]^- + HI$	"$RhCl_3$" on activated carbon or $[RhCl(CO)PR_n]$ on modified polystyrene
Hydrogenation of olefins	$[Rh(PPh_3)_3Cl]$	$[Rh(PPh_3)_nCl]$ on polymer support

Reactors for homogeneously catalyzed reactions with dissolved transition metal complexes are generally the usual two-phase reactors for gas-liquid systems. The standard reactor is the batch or continuous stirred tank. Since the diffusion problems are rarely encountered in homogeneous catalysis, operation is much simpler than in reactors for heterogeneously catalyzed reactions. Catalytic reactors can be classified according to their phase condition. The most important industrial reactor types are two phase reactors for the gas/solid system and three phase reactors for gas/solid/liquid systems [Hagen, 1999].

Safety Issues in Organic Oxidations

In hydrocarbon oxidation processes the danger of explosion via hydrocarbon-air contact is very real. Safety subject was brought into deep focus by the Flixborough explosion of June 1974 involving a cyclohexane oxidation plant. Kletz (1998) discusses this incident together with other major industrial disasters in his book and according to the statistics provided based on an analysis of about 500 incidents, he reveals that of the incidents in storage and blending areas, about 10% was due to the formation of flammable mixtures in the vapour space. In 23% of the cases in which the cause was ascribed as ignition, the source was unknown. In about 1/3 of the cases where the source was unknown, the cause

was autoignition. Hot surfaces, sparks and static electricity were among the other common causes. 7% of the incidents were listed as due to the wrongly selected materials of construction [Suresh, 2000].

The difficulty is that the flammability limits for mixtures of hydrocarbon in air are hardly available under the conditions of temperature and pressure employed in the oxidations. Hence, caution should be taken when the data available for ambient conditions is used. Designs are usually based on very conservative estimates and exhaust oxygen levels below 8% are generally considered safe [Suresh, 2000].

II.II.2 HETEROPOLY COMPOUNDS AS CO-OXIDANTS IN OXIDATION PROCESSES

Heteropolyanions $PMo_{12-n}V_nO_{40}^{(3+n)-}$ (HPA) are widely used as co-oxidants in catalytic oxidations of hydrocarbons. The system in which HPAs are used as co-oxidants was discovered by Matveev et al. in the 70s. It is regarded as the most efficient catalyst system in the polyoxometalate series for the oxidation by molecular oxygen [Grate et al., 1994]. Many polyanions are powerful oxidising agents and undergo multiple reversible one- or two- electron reductions leading to intensely coloured mixed valence species known as heteropoly blues [Pope, 1983].

Catalyst System

The Wacker process was the first organometallic catalytic oxidation that contains carbon-metal bonds, and developed by Smidt et al in 1959 at the Wacker Consortium for Industrial Electrochemistry in Munich. It is mainly used for the production of acetaldehyde from ethylene and oxygen. The process proceeds by homogeneous catalysis on $PdCl_2$. The crucial discovery was the exploitation of this reaction in a catalytic cycle. It had already been known that the solutions of Pd^{II} complexes stoichiometrically to oxidize ethylene to acetaldehyde. A system was developed in which an excess of the oxidising agent Cu^{2+} re-oxidizes the palladium formed in the process before it deposites on the reactor wall. The Cu^{+} formed in the redox process is reoxidized to Cu^{2+} by molecular oxygen. The catalytic cycle for ethylene oxidation is shown in Figure II.II-2.

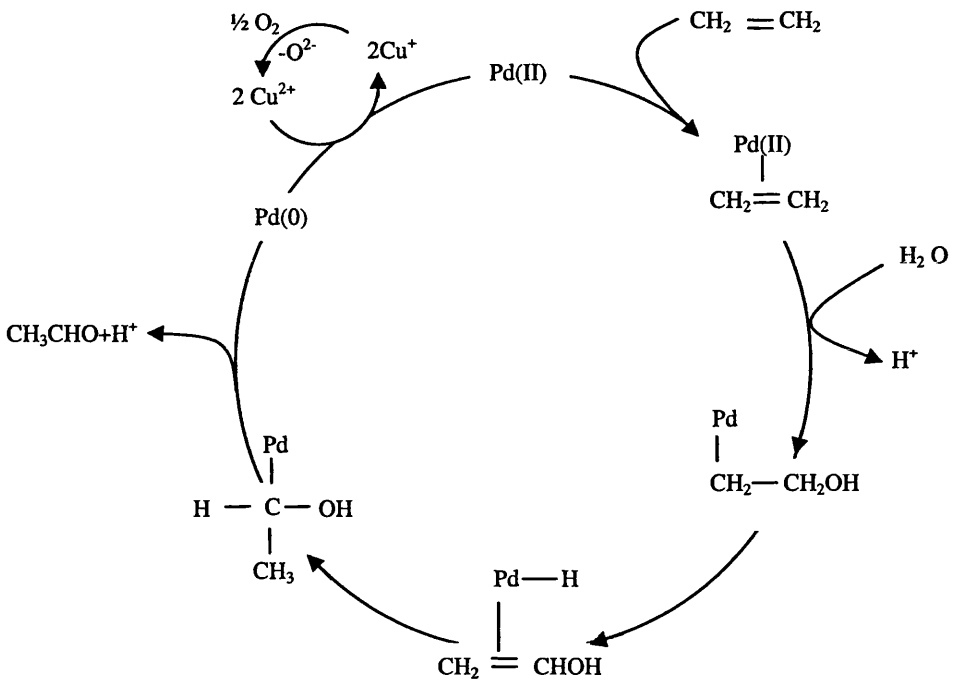

Figure II.II -2 Catalytic cycle for oxidation of ethylene to acetaldehyde in the Wacker process [Hagen, 1999]

A mechanistic study of the Wacker process showed that C-O bond formation occurs, in which the ethylene molecule is not attacked intramolecularly by a coordinated water molecule; instead, a water molecule attacks the double bond. By addition of water coordinated alcohol is formed, and then it is isomerized. The elimination of the product and H^+ gives Pd^0, which is oxidized back to Pd^{2+} by Cu^{2+}/O_2 in excess chloride [Hagen, 1999]. Excess chloride prevents the disproportionation of Cu(I) into Cu(0) and Cu(II), however, in combination with dioxygen, it creates highly corrosive solution which leads to corrosion of the plant and the requirement of the expensive titanium plant. Additionally, formation of chlorinated side products occurs due to the oxychlorinations of acetaldehyde by copper(II)chloride. The amount of chlorinated side products formed increase with the increasing alkene chain length. For ethylene, propylene and n-butenes, percentage of chlorinated side products were 2, 7 and 25, respectively [Matveev et al., 1978]. These side products are difficult to separate from the desired product and difficult to dispose of. Therefore, this process has never been applied to the oxidation of higher alkenes [Stobbe-Kreemers et al., 1997]. This effectively limited the commercial application of the Wacker system for higher olefin oxidation to a few plants for oxidation of propylene to acetone only.

A typical Wacker catalyst solution in the two-stage process is ~10 mM palladium, ~1M copper and ~2 M chloride and the utilized copper(II)-copper(I) redox span is typically ~ 0.3 M, producing ~ 0.15 M acetaldehyde per cycle [Grate et al., 1994].

Considerable efforts have been expended in the search of an alternative oxidising system which does not require high chloride levels. In addition to the elimination of the chlorinated side product formation, lower chlorine concentration would lead to less corrosive solutions and so lower plant costs as a further advantage [Davison, 1984].

Eastman Kodak in 1960s described the use of phosphomolybdic (Mo-HPA) acid and palladium chloride supported on various oxides as catalyst for olefin oxidation and they reported that under such conditions 1-butene was oxidised to methyl ethyl ketone free of impurities. Following that, Matveev et al (1978) noted that the addition of vanadium into palladium chloride-phosphomolybdic acid solution improved the oxidation rate substantially. Furthermore, phosphotungstic (W-HPA) acid has also been used in such oxidation systems [Davison et al., 1984].

Davison et al. (1984) studied palladium sulphate catalyzed oxidation of 1-butene to methyl ethyl ketone using phosphomolybdic (Mo-HPA) and variety of phosphovanadomolybdic acids (MoV-HPA) as reoxidants. They reported that all the oxidants had similar performances in reoxidising the reduced catalyst, however, their ability to be reoxidised themselves by air under the optimum reaction conditions in aqueous acid varied substantially. They also added that Mo-HPA was a good co-oxidant in acidic conditions; however, their ^{31}P NMR study showed that in dilute solutions it was largely dissociated into phosphoric acids. They also found that variety of palladium salts were successful in these reactions, however due to their intention to minimise the chloride content, they carried out most reactions using commercial palladium sulphate. Both V^{V} and Mo^{VI} reoxidise Pd^{0} with about equal efficiency, but the MoV-HPA co-catalysts are themselves more easily reoxidised than formulations without V^{V}. Finally, the mixtures of aqueous MoV-HPA solutions with 6 Vs gave the highest methyl ethyl ketone conversion in Davison's system [Davison et al., 1984].

Grate et al. (1994) developed an improved catalyst system in order to overcome the drawbacks of the Wacker and Matveev's catalyst systems. This system was developed

for oxidation of higher olefins to ketones as well as for ethylene oxidation to acetaldehyde. They have prepared a homogeneous catalyst solution containing three key components: palladium(II) catalyst to oxidize olefin to a carbonyl compound, Keggin phosphomolybdovanadates with a general formula of $PMo_{(12-x)}V_xO_{40}^{(3+x)-}$ to provide a dioxygen reversible vanadium(V)/vanadium(IV) redox agent for palladium(0) reoxidation, and chloride at centimolar concentration to maintain stable palladium(II) catalyst activity. In their system, vanadium(V)/vanadium(IV) redox agent for palladium has replaced the copper(II)/copper(I) redox system in the Wacker process. Additionally, the amount of chloride used was much less than used in the Wacker system. Thus, they managed to eliminate more than 99% of the production of chlorinated organics for acetaldehyde production. Matveev et al. (1978) had already studied this system and their work has been the starting point for the development of Catalytica's system. Matveev et al. (1978) have discovered that vanadium in Keggin phosphomolybdovanadates was a di-oxygen regenerable oxidant and the typical solution contained: aqueous 2 mM $PdSO_4$, 0.2 M phosphomolybdovanadate and sulphuric acid. pH was adjusted to 1 and the palladium concentration was ~1/5 that of the Wacker system. Matveev et al. (1978) report that they have completely eliminated the use of chloride, in order to overcome the production of chlorinated side products and used $PdCl_2$ as precatalyst in some of the recepies. It was also reported by Matveev et al. (1978) that the product yield considerably increased and that was free from chlorinated side products. Table II.II-3 shows the percentage of product yield.

TableII.II- 3 Product yield in the olefin oxidation using Matveev's catalyst system [Matveev et al, 1978]

Olefin	***Ethylene***	***Propylene***	***n-butenes***
Main Product	acetaldehyde	acetone	Methyl ethyl ketone
% Yield of Product	97	95	98

Matveev et al. (1978) also concluded that as the number of vanadium atoms in the polyacid increases, the activity and stability also increase up to six vanadium atoms and further increase in the vanadium content makes the acid thermally less stable. It was also suggested that the molybdophosphate matrix serves two purposes; solubilising high levels of V(V) in acidic aqueous solution, as VO_2^+ has a limited solubility at low pH, and

providing for the rapid oxidation of V(IV) by O_2, since VO_2^+ is oxidised very slowly at low pH [Kozhevnikov et al., 2002].

Although the invention of the heteropolyacid solution was an accomplishment, the system did not meet the criteria required by the industrial application, due to very slow olefin and oxygen reaction rates and solution having poor palladium(II) catalyst stability. Detailed description of catalyst recepies for oxidation of various olefins can be found in the patent [Matveev et al., 1978].

Catalytica's system overcame these shortcomings and demonstrated improved catalyst stability and it also provided oxygen and olefin reaction rates comparable to those obtained with the Wacker catalyst for ethylene oxidation. A typical solution contained aqueous ~ 0.1 mM Pd(II), 5-25 mM Cl^- and ~ 0.30M phosphomolybdovanadic acid partial salt of the general formula $\{Na_yH_{(3+x-y)}PMo_{(12-x)}V_xO_{40}\}$with the average vanadium content of 2-3. Solution had pH<1 and palladium and chloride concentrations are ~1/100th those of the Wacker system. It was observed that the palladium catalyst stability is improved by increasing chloride concentration. The details of the solution preparation and further information can be found in the paper [Grate et al., 1994].

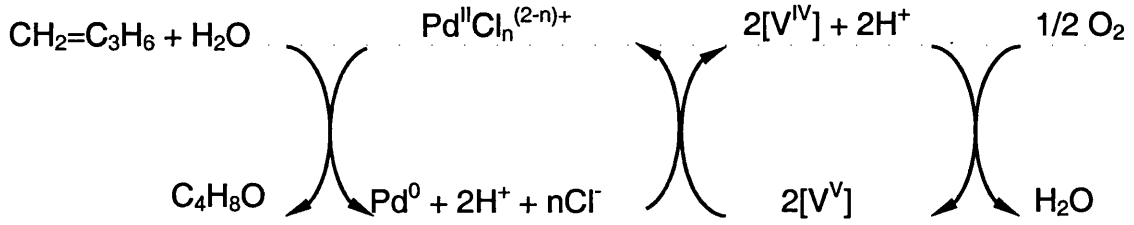

Figure II.II-3 Catalytica's Palladium (II) - Heteropoly Anion $(PMo_9V_3O_{40})^{6-}$ catalyst system for 1-butene oxidation to methylethylketone.

Alternatively, in order to overcome these drawbacks encountered in the homogeneous process, heterogeneous gas phase catalysts have been developed. Scholten et al. (1990) developed a heterogeneous catalyst consisting of Pd(II) deposited on a vanadium pentoxide monolayer, replacing Cu(II)/Cu(I) redox couple, supported on γ-alumina. However, the catalytic activity was almost three orders of magnitude lower than it is in the homogeneous process. Following this, Van der Heide reported that the activity in ethylene oxidation could be improved by over an order of magnitude by replacing γ-

alumina with titania. Stobbe-Kreemers et al. (1997) studied 1-butene oxidation to methyl ethyl ketone in a continuous fixed bed reactor over a titania (anatase) and γ-alumina supported palladium sulphate catalysts, deposited on a vanadium pentoxide monolayer. More than 85% selectivity was achieved and the major side products were acetic acid and acetaldehyde. They also obtained one order of magnitude higher catalytic activity for the titania supported catalyst confirming the report by Van der Heide [Stobbe-Kreemers et al., 1997].

The catalytic cycle in their reaction was:

$Pd^{2+} + C_4H_8 + H_2O \rightarrow Pd\ (0) + C_4H_8O + 2H^+$

$Pd(0) + V_2O_5 + 2H^+ \rightarrow Pd^{2+} + H_2V_2O_5$

$H_2V_2O_5 + ½\ O_2 \rightarrow V_2O_5 + H_2O$ [Stobbe-Kreemers et al., 1997]

In the low-temperature oxidation of 1-butene in the presence of 9:1 SnO_2-MoO_3 and 9:1 Co_3O_4-MoO_3 catalyst, selective production of methyl ethyl ketone has been observed [Hucknall, 1974]. At 135 °C and in the presence of a 9:1 SnO_2-MoO_3 catalyst, a 83.5 % yield of methyl ethyl ketone was obtained from 1-butene at a conversion of 5%. As the temperature increased it has been observed that the yield of methyl ethyl ketone declined to 60.3% and 38.7% at 160 and 180 °C respectively. Co_3O_4-MoO_3catalysts were found slightly less active than the tin-containing compounds. Tin-molybdenum oxide has also been used to convert 1-butene selectively to methyl ethyl ketone [Hucknall, 1974].

Hwang et al (2001) studied electrode assisted phosphomolybdate – mediated oxidation of 1-butene to methyl ethyl ketone. Unlike most of the work that was carried out to develop an alternative catalytic system to replace $CuCl_2$ in the process of reoxidation of Pd(0) molecular oxygen they showed that the oxidation rate of 1-butene can be greatly enhanced by oxidising phosphomolybdate electrochemically rather than by oxygen [Hwang et al., 2001].

II.II.3 KINETICS OF 1-BUTENE OXIDATION

Kozhevnikov et al. (2002) studied the kinetics of one stage oxidation of ethylene, propylene and 1-butene to acetaldehyde, acetone and MEK, respectively using a catalyst system based on aqueous $PdCl_2$-heteropolyanions solutions, similar to that developed by Catalytica.

The composition of the catalyst solution used for measuring the reaction kinetics was 0.05-0.2 mM P(II); [Pc(II)/Cl^-] = 1: 50; 50 mM HPA and the stoichiometric molar oxygen to olefin ratio 1:2 (4 ml/min O_2 and 8 ml/min olefin) in the gas feed. Pd (II) source was $PdCl_2$ and the desired Pd(II)/Cl^- ratio was obtained by the addition of NaCl, by taking into account the amount of chlorine coming from the introduction of $PdCl_2$. Heteropoly anion content was lower than in the Catalytica's system as this amount was found sufficient for the one-stage operation. Experiments were carried out under atmospheric pressure and the temperature range between 20 and 50 °C. The pH of the catalyst solution was adjusted to 1.3 for each temperature by adding NaOH or H_2SO_4. Sodium salt of heteropoly anion $Na_4H_2[PMo_9V_3O_{40}]$ was used. Experimental set-up consisted of a specially designed, double-jacketed cylindrical glass stirred semi-continuous reactor with 125 ml volume. Oxygen and olefin were fed in and removed from the reactor continuously while the product remained in the catalyst solution in the reactor. Temperature was controlled and adjusted with the circulation of water through the jacket placed around the reactor. The gas flows out of the reactor was continuously monitored by a GC and analysed. The rates of olefin and oxygen consumption were calculated from the difference of moles of reactant in and out of the reactor per unit time divided by the volume of the reaction mixture that was 100 ml. The main products were acetaldehyde, acetone and MEK as expected. Small amount of acetic acid was present in addition to the product in the catalyst solution.

During the reaction, catalyst solution that originally has reddish colour turns green, indicating heteropoly acid reduction. Reaction reached steady state after 40-50 minutes with an average degree of heteropoly anion reduction < 0.2 e^- per polyanion. Reaction rates were measured at a time on stream of between 60 and 75 min. In the steady state oxidation of 1-butene at 20 °C, double bond migration occurs and 2-butene was observed

in the flow-out with a 1-butene/2-butene ratio of 5:1 to 10:1. Table II.II-4 shows the kinetic data obtained for 1-butene oxidation [Kozhevnikov et al., 2002].

TableII.II- 4 Kinetics of 1-butene oxidation[a] [Kozhevnikov et al., 2002].

Pd(II) [mM]	*T [°C]*	*Reaction Rate[b] [mmol / L min]*	
		1-butene	*Oxygen*
0.05	30	0.243	0.141
0.10	30	0.475	0.283
0.10[c]	30	0.878	
0.10[c,d]	30	0.929	
0.10	40	0.55	0.32
0.10[c]	40	1.27	
0.10	50	0.622	0.36
0.10[c]	50	1.47	
0.20	30	0.860	0.485

a: Reaction Conditions: 50 mM HPA, $[Pd(II)]/[Cl^-]$ = 1/50 mol/mol, 4 ml/min oxygen, 8 ml/min 1-butene, 1200 – 1500 rpm stirring speed.

b: The rates measured by consumption of olefin and O_2 for a time on stream of 60-75 min.

c: Initial rate for the time on stream of 0-15 min.

d: Reaction in the absence of oxygen.

Reaction steps are as follows:

$$C_4H_8 + PdCl_2 + H_2O \rightarrow C_4H_8O + Pd(0) + 2HCl$$

$$Pd(0) + HPA\text{-}n + 2\,H+ \rightarrow Pd(II) + H_2(HPA\text{-}n)$$

$$H_2(HPA\text{-}n) + 1/2O_2 \rightarrow HPA\text{-}n + H_2O$$

II.II.4 MULTI-FUNCTIONAL REACTORS

Markets for new consumer products, where chemical industry was a major provider, were growing rapidly in the first two decades following the Second World War. The main target was quick development and large scale production. However, the effects of

large scale industrialisation on depletion of scarce natural resources have become apparent since 1980. Besides, consumers have demanded better product quality, also the demands for improvements in health-safety-environment, higher product quality, as well as economic drivers have increased the requirements on process design. That subsequently resulted in the emergence of improved reactors.

In the years to follow, more comprehensive reactor models were made to support debottlenecking and product quality improvement. In addition to the primary function, that is the conversion of compounds into desired product; high volumetric yield, minimum amounts of by-products, minimal consumption of energy and minimal impact on the environment were also important parameters that have to be considered for the design of a reactor. Furthermore, it was better to consider and optimise the process as a whole than isolating the reactor itself from the rest of the process; hence the multifunctional reactors became a logical choice in many cases.

Agar (1999) classified multifunctional reactors according to:

- heat and mass transport processes, e.g. packing in the reactor having function of a catalyst, an adsorbent and a medium for regenerative heat storage.
- supplementary unit operations, e.g. distillation, extraction, absorption, adsorption, pervaporation, crystallisation etc.
- participating phases and mixing modalities in the reactor, i.e. reactive absorption (gas-liquid), reactive adsorption (gas-solid), reactive chromatography (liquid-solid), reactive distillation (gas-liquid-solid) [Agar, 1999].

It is expected that more multi-functional reactors will be developed and operated in the future due to an increased demand for processes that produce no waste, require little energy, low in cost and produce products with better quality. Reactors that combine separation and reaction, mostly unconventional and at laboratory scale, such as chromatographic reactors, catalytic distillation columns, rotating packed beds and membrane reactors have been the subject of many research areas.

Membrane Reactors

Membrane reactor is a special kind of reactor in which the membrane, functioning either as a catalyst or as a barrier, is an integral part of the reactor itself and one of the fastest growing research areas in chemical reaction engineering due to the availability and low cost of materials that can be used as membranes. In recent years, the concept of membrane reactor has been investigated by many researchers and these investigations have made a significant progress in the application of membranes in reaction engineering.

Membrane reactor concept shows various potential benefits, such as increased reaction rate, selectivity and yield for a range of reactions involving the membrane as an extractor, distributor or contactor due to their ability in combining the conversion and separation effect in the same unit [Julbe et al., 2000]. These benefits of using synthetic membranes in reactors have been recognised and membrane bioreactors have been used to carry out enzymatic reactions, where membranes play the role of retaining the relatively large enzyme molecules, while the reactants and products can pass through the membrane freely. The concept of a membrane reactor was later used by many researchers and, conceptually, the advantages of a membrane reactor were extended to homogeneous catalytic reaction systems.

There have been several reviews published, e.g. Tsotsis et al., 1993; Saracco and Specchia, 1994, 1998b; Saracco et al., 1994; Armor 1995; Dalmon, 1997, and almost an entire book is dedicated to inorganic membrane reactors (Hsieh, 1996), as a clear sign of the massive interest of the scientific community in this topic. Figure II.II-4 shows the number of publications published on catalytic membrane reactors per year since 1965. It must also be noted that the membrane reactor research community is not only growing in number but also widening its borders. It has also been reported by Saracco et al. (1999) that the distribution of papers published per application type of catalytic membrane reactors between 1994 and 1997 was as follows: yield enhancement (50 % (1994), 35 % (1997)), selectivity (30 % (1994), 50 % (1997)). These figures clearly show the shift from yield to selectivity enhancement. The most likely reason for this is the fact that partial-oxidations or hydrogenations have a much wider spectrum of industrial

applications than dehydrogenations, and that membrane perm-selectivity is a less urgent need for this kind of applications [Saracco et al., 1999].

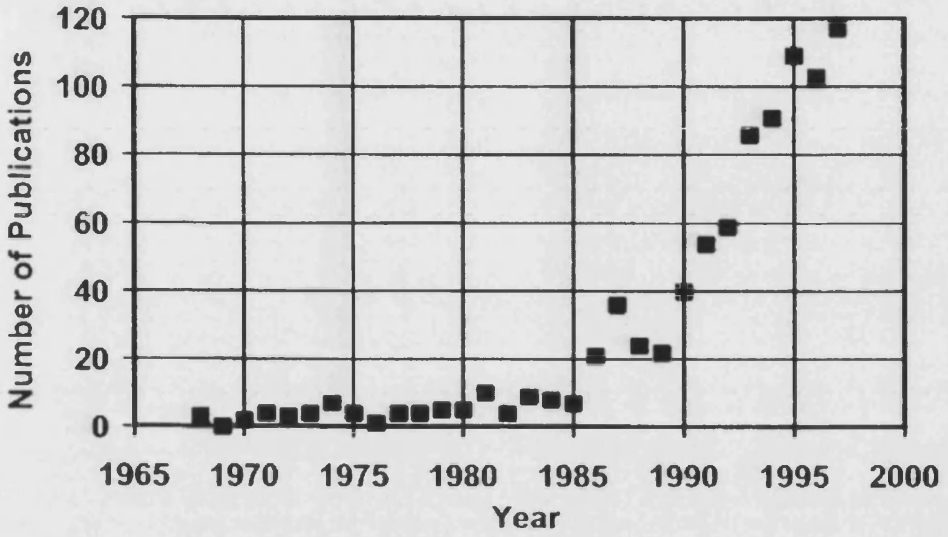

Figure II.II 4 The number of publications published on catalytic membrane reactors per year since 1965 (included in the Chemical Abstracts database) [Saracco et al., 1999].

In addition to the current applications such as yield-enhancement of equilibrium limited reactions and selectivity enhancement, new application opportunities are also emerging. A number of potential applications, membrane reactor with separate feed of reactants, catalytic filters and traps, slurry membrane reactor, etc. have been recently investigated and most of these applications, unlike yield and selectivity enhancement, do not require membrane perm-selectivity to gasses and therefore appear to have more chance to be successful in industrial applications [Saracco et al., 1999].

Membranes have been used in the reactors as either inert material or having catalytic activity. In the case of the inert membrane reactors, membrane is used to add or remove reactants or products in the system. The functions of the inert membrane in the membrane reactor systems can generally be classified into three main groups: acting as an extractor, a distributor or a contactor. It must be noted that this classification is very rough and different systems may exist.

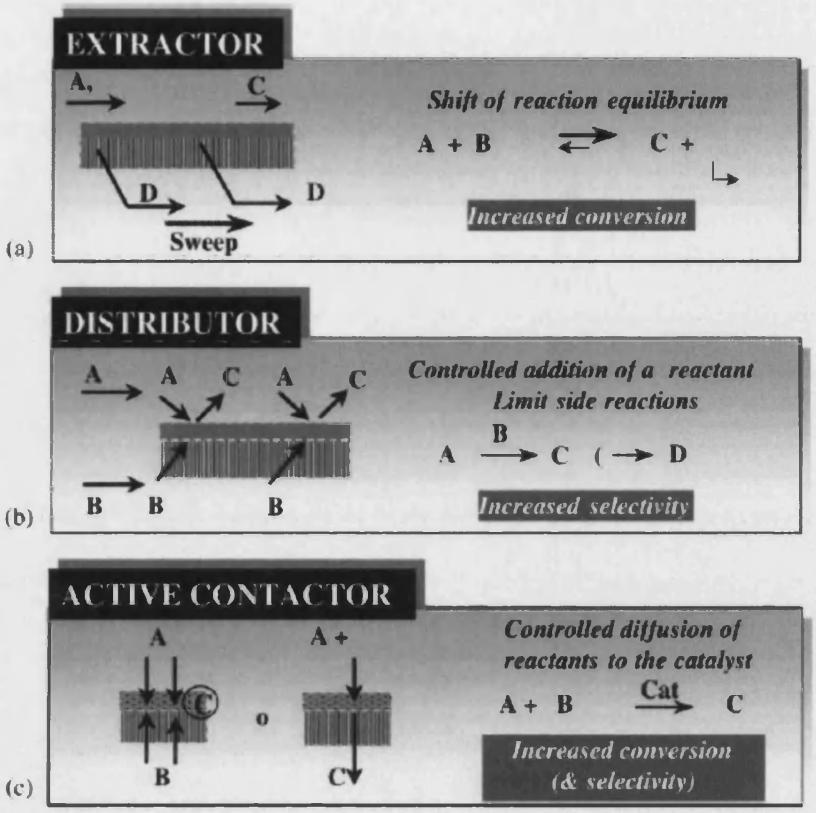

Figure II.II 5 Main functions of an inert membrane in a membrane reactor [Adopted from Julbe et al., 2001]

In catalytic membrane reactors, reaction directly takes place on the membrane. Either the membrane itself has catalytic activity or it is modified by the addition of active materials. Several methods have been developed to incorporate active materials into membranes, such as, chemical vapour deposition, sol-gel techniques, impregnation and ion-exchange. Alternatively, active material can be deposited on the membrane by creating similar porosity and permeability as the membrane itself [Alfonso et al., 2000].

Membranes have been widely used to separate reactant streams when dealing with the heterogeneously catalysed, very fast and exothermic gas phase reactions [Veldsink et al.,1992]. This is done by feeding the reactants to different sides of the membrane, allowing certain amounts to come into contact (Figure II.II-5c). This method is especially useful for fast reaction, as this way they can become mass transfer controlled. Furthermore, due to the separation of reactants, a good control of the system is obtained as the process streams can be varied independently from each other. This is especially important when dealing with processes involving gasses which may form explosive

mixtures at certain concentrations, i.e. hydrocarbon oxidation and combustion reactions [Veldsink et al., 1992 & Alfonso et al., 2000].

Several authors have theoretically studied the possibility of using a catalytic membrane reactor to improve the yield of valuable intermediate products, using the following reaction scheme:

$$A + \nu B \rightarrow \nu_{R1} R \text{ (desired)} \qquad r_1 = k_1 P_A^{n_1} P_B^{n_2}$$

$$A + \nu_{R2} R \rightarrow \nu_P P \text{ (undesired)} \qquad r_2 = k_2 P_A^{m_1} P_R^{m_2}$$

where A is oxygen, B is reactant, P is undesired deep oxidation product, R is desired intermediate and ν, ν_{R1}, ν_{R2} and ν_P are the stoichiometric ratios of reactant, desired intermediate in the first step, second step and product, respectively.

Harold et al. (1993) showed that in the case of $n_1 < m_1$ significant yield improvements can be obtained by using a catalytic membrane reactor with a segregated feed. This scheme is representative of many selective oxidation processes with wide application areas. In the catalytic membrane system, A must be supplied from the support side and reactant B from the active layer side, provided the thickness of the active layer is smaller than the thickness of the membrane. This way diffusion across the inactive support layer results in a lower partial pressure of component A in the active layer, hence increases the selectivity of the desired product. However, only limited success has so far been experimentally achieved by using catalytic membrane reactors [Alfonso et al., 2000]. This concept has also been proposed for inert membrane reactors in which the reduction in the concentration of A is achieved by distributing it to a fixed bed of catalyst. Examples of other partial oxidation reactions include: methane oxidative coupling, oxidative dehydrogenation of ethane, propane and butane [Alfonso et al., 1999; Ramos et al., 2000], oxidation of cyclohexane and n-dodecane at room temperature using polymeric membrane in a catalytic membrane reactor [Langhendries et al., 2000], oxidation of butane to maleic anhydride [Mallada et al., 2000]. Langhendries et al. (1999) have studied selective oxidation of hydrocarbons in a packed bed membrane reactor and they claimed that the efficiency in the membrane reactor was higher than in a classical packed bed reactor [Langhendries et al., 1999].

Stanley and Quinn also stated that many contacting problems associated with conventional phase-transfer catalysis operations can be eliminated by using a membrane reactor due to their accessible interior volume as opposed to the single enclosing surface of a particle or a pellet. The aqueous and organic streams can be contacted across a porous, hydrophobic membrane instead of the mixer/settler sequence of the conventional reactor. Furthermore, because the interfacial area is a fixed specified parameter, the membrane reactor can be operated with a greater flexibility. Since, its mass-transfer properties can be well characterised, membrane contactor can be used to investigate the kinetics of phase-transfer reactions free of the mass transfer complications caused by the dispersed phase [Stanley & Quinn, 1987].

Chen et al. (1992) claimed that hollow fibers can provide large mass transfer area per unit volume of reactor and reported the results of a study using a membrane reactor for the homogeneous catalytic reaction of direct oxidation of ethylene to acetaldehyde. It was concluded that the large dispersion free gas-liquid interfacial area provided by hollow fiber membranes increases the productivity per catalyst loading to a level considerably higher than that of a comparable bubble column reactor, as long as the membrane does not introduce much excessive mass transfer resistance. Additionally, a homogeneous catalytic reaction takes place inside the membrane reactor in a plug-flow configuration and is capable of achieving high conversions without recycle. Yang and Cussler (1986) also demonstrated that the hollow fiber contactor could provide a substantial mass transfer area without significant reduction in the overall mass transfer coefficient [Chen et al., 1992].

Harold et al. (1993) studied the intermediate product yield enhancement with a catalytic inorganic membrane reactor and they observed the confinement of reaction products in the bulk stream on the active layer side, which reduces the downstream separation needs, as an additional benefit of using the membrane reactor [Harold et al., 1993].

Inert membrane reactors have been experimentally tested in the concept of lowering partial pressures of oxygen for several reactions of selective oxidation of hydrocarbons [Alfonso et al., 2000]. It has been found that in selective oxidation processes, low partial pressure of oxygen favours the selective oxidation reaction versus the deep oxidation to CO and CO_2. Additionally, the distribution of oxygen also allows a wider range of

operating conditions: by distributing the oxygen feed in the inert membrane reactor it is possible to operate at overall hydrocarbon to oxygen ratios that would be within the explosive region if the same composition was fed at the entrance of a fixed bed reactor. However, it must be noted that, sometimes the membrane itself or the components used to modify its permeation properties can make an undesirable contribution to the reaction. Therefore, the membranes used in selective oxidation reactions often have to be significantly modified in order to minimise non-selective activity [Coronas & Santamaria, 1999].

Saracco et al (1995) studied hydrocarbon oxidation and have used a membrane reactor due to the possibility to improve the reaction selectivity towards partial oxidation products. Using membrane reactor allows avoiding mixing of reactants, hence avoiding the formation of explosive mixtures and low sensitivity to thermal runaways. Good flexibility and controllability of reaction was shown [Saracco et al., 1995].

Strukul et al. (2000) compared powder catalyst to a membrane supported catalyst system. They have observed that the accumulation of the side products can severely influence the diffusion effects and limit gas/liquid /solid three phase contact which is crucial for both, reaction rate and the selectivity of the reaction. Therefore, both due to the limitation caused by side products and the safety reasons they found using catalyst immobilised onto hollow fibre dialyser reactors would be promising [Strukul et al., 2000].

The first composite membrane catalyst used for combined hydrogen evolution during hydrochloric acid reaction with zinc and hydrogenation by a palladium sponge covering the zinc granules was demonstrated in 1898 by Zelinskii at Moscow University. In 1915, Snelling in the USA patented hydrogen removal through Pt or Pd tubes from a reactor with a granular dehydrogenation catalyst [Gryaznov, 1999]. Pd membrane reactors demonstrated great performances for dehydrogenations, steam reforming reactions etc., where only hydrogen separated from the reaction mixture. However, as Pd is costly and has permeability problems; such as low flux and H_2 brittleness of metals when it comes to industrial applications, Itoh et al. (2000) suggested that carbon membranes gained an interest and become one of the candidates to replace Pd tubes due to their high hydrogen selectivity caused by molecular-sieving effect [Itoh et al., 2000]. Kikuchi was another author who also studied hydrogen production in a membrane reactor and reported that

selective removal of hydrogen in a membrane reactor enables the hydrogen production by steam reforming at lower reaction temperatures than conventional processes. Furthermore, with the reactor consisting of a composite membrane that was prepared by depositing thin palladium layer on a ceramic membrane prepared by electroless-plating method, they obtained 100% selectivity in removal hydrogen from the reaction stream. Tokyo Gas and Mitsubishi Heavy Industries have developed a membrane reformer applicable to the polymer electrolyte fuel cell system. [Kikuchi, 2000].

Membrane reactors have found applications also in green chemistry. Sammels et al. (2000) studied conversion of natural gas to synthesis gas, which is a mixture of CO and H_2 and has important commercial implications, by using a catalytic membrane reactor involving a new class of oxygen anion and electron conducting brownmillerite derived membrane materials. In comparison to commercial methods, this process is exothermic and eliminates the need for a separate oxygen plant, hence decreases the production costs significantly. Additionally, NO_x emissions are eliminated since the membrane only permeates oxygen excluding atmospheric nitrogen [Sammels et al., 2000].

Electro-synthesis has been attracting a great attention to transform organics, such as alcohols, carbohydrates, etc., into more valuable products. Owobi-Andeli et al. (2000) have used a membrane reactor with electrocatalytic activity (with graphite anode and cathode) for the electrochemical transformation of fructose into sorbitol, mannitol and gluconic acid with Pt-Rh catalyst and they combined oxidation and reduction in a paired synthesis [Owobi-Andeli, 2000].

Membrane reactors have been widely used on a laboratory scale, mainly for hydrogenation, dehydrogenation, decomposition and oxidation reactions. It must be noted that some small industrial installations also exist. Table II.II 5 shows examples of possible configurations of porous membrane reactors.

TableII.II- 5 Examples of possible configurations of porous membrane reactors [Coronas & Santamaria, 1999f]

Configuration	Advantages Sought	Type of Membrane
Inert membrane reactor (IMR) Permeation of products	Increased reaction yield by equilibrium displacement	(i)Selective. Thin metallic layers(e.g., Pd or Ag based alloys on ceramic substrates.) (ii)Nonselective. Porous membranes: silica, alumina, titania, glass, etc. (iii)Other: zeolitic membranes
IMR: Permeation of Products plus reaction coupling	As above, although higher yields can be expected due to the thermal/chemical coupling of reactions	As Above
IMR: Distribution of reactants	Increased selectivity through control of the concentration of selected species along the reactor. Increased reactor safety	Meso- or microporous membranes
Catalytic membrane reactor (CMR)-Mobile and active lattice oxygen	Control of the oxygen distribution in the reactor. In principle it is possible to avoid the presence of gas phase oxygen.	(i)Thin layers of Ag-based alloys on top of porous ceramic membranes. (ii)Thin layers of dense oxide on top porous ceramic membranes
CMR-Segregation of reactants on both sides of the membrane	Confinement of reaction to a finite thickness zone inside the membrane. Reactant slip is avoided. Improved safety.	Porous catalytic membranes
Inert/Catalytic composite membrane	Control of the concentration of a reactant by means of mass transfer resistance in the IMR zone.	Composite membranes: inert (diffusion) zone plus catalytically active zone
CMR-Segragation of liquid and gaseous reactants	Improved mass transfer in G-L-S reactions.	Porous catalytic membrane
CMR- Joint permeation of reactants	Improved G-S contact, higher conversions.	Porous catalytic membrane

Membrane Contactors

A membrane contactor can be defined as a device that achieves gas/liquid or liquid/liquid mass transfer without dispersion of one phase within another by passing the fluids on the opposite sides of a porous membrane. Membrane contactors offer a number of advantages, such as: no flooding at high flowrates, no unloading at low flowrates, no density difference between fluids is required, high interfacial area. Gas/liquid and liquid/liquid contacting operations are traditionally performed using towers, columns or mixer-settlers. The main challenge usually is to maximise the mass transfer rate by producing as high interfacial area as possible. Gabelman and Hwang (1999) suggest that the membrane contactors typically offer 30 times more area than what is achievable in gas absorbers and 500 times what is obtainable in liquid/liquid extraction columns [Gabelman & Hwang, 1999]. Furthermore, although columns and other fluid/fluid contactors have been widely used in the chemical industry for decades, an important disadvantage is the interdependence of the two fluid phases, which sometimes lead to difficulties, such as creating emulsions, foaming, unloading and flooding. Using a suitable membrane, e.g. hollow fiber or a flat sheet, separate flows of the fluids can be obtained by flowing them on the opposite sides of the membrane. Hollow fiber membrane modules are widely used membrane phase contactors due to their large surface area per volume, up to 300 $cm^2 cm^{-3}$, and its simple application. Major drawbacks of hollow fibre membranes has been reported and studied by Vladisavljević and Mitrović (2000) as large pressure drop inside the fibers and the shell-side flow maldistribution due to non-uniform fiber packing. They found that the tube-side pressure drop increases linearly with increasing fluid flowrate and that the shell-side pressure drop is much smaller than the tube-side pressure drop, and is proportional to the gas flowrate [Vladisavljević & Mitrović, 2000].

In addition to several advantages, membrane contactors have also some disadvantages. The advantages and disadvantages of using membrane contactors are summarised in Table II.II-6.

TableII.II- 6 The advantages and disadvantages of using membrane contactors

Advantages
The available surface area remains undisturbed at high and low flow rates since the two fluid flows are independent
Emulsion formation does not occur due to nonexistent fluid/fluid dispersion
Unlike traditional contactors, no density difference is required between fluids; membrane contactors can accommodate fluids of identical density and can be operated in any orientation
Scale-up is more straight forward with membrane contactors. Membrane operations usually scale linearly, so that a predictable increase in capacity is achieved simply adding membrane modules.
Modular design allows a membrane plant to operate over a wide range of capacities.
Aseptic operation is possible, a feature which can be advantageous in processes such as fermentation. For example, during fermentation the broth can be circulated through a membrane contactor then back into the fermenter, while a suitable extraction solvent passes through the contactor on the opposite side of the membrane.
Membrane contactors can be used to increase conversion with equilibrium-limited chemical reactions in general by circulating the reactor contents through the contactor against a suitable extraction solvent or stripping gas, the products are removed and reaction equilibrium shifts to the right.
Interfacial area is known and is constant, which allows performance to be predicted more easily than with conventional dispersed phase contactors. On the other hand, interfacial area is quite difficult to determine in dispersive contactors because the bubble or droplet size distribution depends on operating conditions and fluid properties, which is why the mass transfer coefficient and interfacial area are usually lumped together, e.g. k_Ga, k_La, in mass transfer calculations.
Substantially higher efficiency (as measured by the height of a transfer unit or HTU) is achieved with membrane contactors than with dispersive contactors.
Solvent hold-up is low, an attractive feature when using expensive solvents.
Unlike mechanically agitated dispersed phase columns, membrane contactors have no moving parts.

Disadvantages
Membrane introduces another resistance to mass transfer. However, the resistance is not always important and steps can be taken to minimise it.
Membrane contactors are subject to shell side bypassing, which results in a loss in efficiency. Often bypassing is not a problem at laboratory scale, however, becomes an issue upon scale up to larger contactors.
Membranes are subject to fouling, although this tends to be more of a problem with pressure driven devices than with concentration driven ones such as membrane contactors.
Membranes have a limited life, the cost of membrane replacements has to be considered.
The potting, e.g. with epoxy, used to secure the fiber bundle to the tube sheet may be vulnerable to attack by organic solvents
The achievable number of equilibrium stages is limited by pressure drop constraints.

Membrane contactors have been used in a number of liquid/liquid and gas/liquid applications in fermentation, pharmaceuticals, wastewater treatment, chiral separations, semiconductor manufacturing, carbonation of beverages, metal ion extraction, protein extraction, VOC removal from waste gas, and osmotic distillation [Gabelman & Hwang, 1999].

Mavroudi et al. (2003) studied the absorption of CO_2 from a CO_2-N_2 mixture using a commercial hollow fiber membrane contactor and concluded that membrane contactors are significantly more efficient and compact than conventional absorption towers for acid gas removal [Mavroudi et al., 2003].

Hong and Jung (1997) studied selective oxidation of butane to maleic anhydride in a V_2O_5 coated membrane reactor. They have obtained high conversions due to the fact that the product is separated by the membrane, thus shifting chemical equilibrium. Furthermore, since the formation of by-products is suppressed with the use of a membrane between the two reactants, they obtained better selectivity (95%) than the commercially available processes (69%) which are carried out in the fixed bed or fluidized bed reactors [Hong & Jung, 1997].

Superior performances of porous membrane contactors applied to multi-phase heterogeneous catalytic processes have been demonstrated in several studies. Although the specific geometrical area in a contactor is usually lower than in the trickle-bed reactor catalyst particles, because of the liquid distribution pattern and incomplete wetting of particles in the trickle-bed reactors, the actual area of mass transfer maybe comparable for these reactors. Furthermore, a porous contactor may provide complete retention of the liquid catalyst. Vos et al. (1982) have found that the performance of a cross-flow porous contactor is comparable to that of a trickle-bed reactor for three phase nitrobenzoic acid hydrogenation [Vos et al., 1982]. In addition, Wu et al. (2000) have studied the two-phase reaction of n-hexane oxyfunctionalization by hydrogen peroxide in a reactor in which zeolite containing catalytic membranes was used as an interphase contactor [Wu et al., 2000]. Examples of multi-phase reactions where porous contactors have been tested include; hydrogenation of α-methylstyrene and aqueous nitrates, oxidation of n-hexane, cyclohexane and n-dodecane, water remediation technologies by catalytic hydrogenation, H_2O_2 synthesis, natural gas sweetening [Lapkin et al., 2002; Itoh&Haraya, 2000; Centi et al., 2003; Dannström et al., 2000].

Membranes

A membrane can be defined as a selective barrier between two phases. A membrane can be thick or thin natural or synthetic, neutral or charged, its structure can be homogeneous or heterogeneous, transport can be active or passive, being driven by a pressure, concentration or temperature difference.

Membranes can be classified according to different view points in order to obtain a more informative understanding. The first classification is by nature that is the clearest distinction possible, biological or synthetic membranes. These two types of membranes differ completely in structure and functionality. Biological membranes can be subdivided into living and nonliving membranes. Synthetic membranes can be subdivided into organic; polymeric or liquid, and inorganic; ceramic, metal etc., membranes. Another way of classifying membranes is by morphology or structure. Solid synthetic membranes can be classified as either symmetric or asymmetric. Symmetric membranes can be subdivided as cylindrical porous, porous and homogeneous (nonporous) and asymmetric membranes can be subdivided as porous, porous with top layer (integrally skinned) and composite as shown in Figure II.II-6.

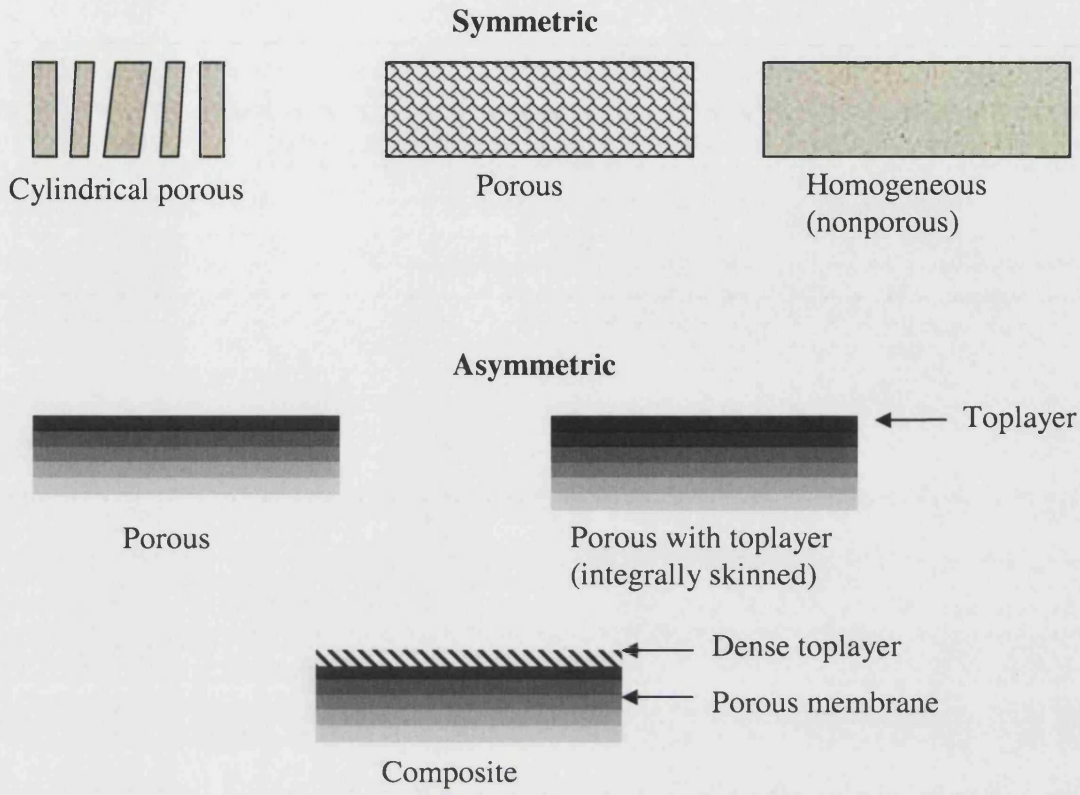

Figure II.II 6 Schematic representation of symmetric and asymmetric membrane cross-sections (Mulder, 1996)

The thicknesses of symmetric membranes, porous or nonporous, range roughly between 10 and 200 μm. The resistance to mass transfer is determined by the total membrane thickness and a decrease in membrane thickness results in an increased permeation rate. Asymmetric membranes consist of a very dense toplayer or skin with a thickness of 0.1 to 0.5 μm supported by a porous sublayer with a thickness between 50 and 150 μm. These membranes combine the high selectivity of a dense membrane with the high permeation rate of a very thin membrane. Differences in membranes and membrane structures are explained in detail in (Mulder, 1996).

Inorganic Membranes

Many industrial catalytic processes involve high temperature and chemically harsh environments and these are the main factors that favour the use of inorganic membrane reactors as most of the inorganic membranes have the ability to withstand severe reaction conditions. Inorganic membranes were industrially developed more than five decades

ago with the aim of separating UF_6 using gas phase diffusion processes. Following that in the 1980s, non-nuclear applications of membranes focused mainly on microfiltration and ultrafiltration processes. Subsequently, the development of the membrane production and control of the porous structure emerged. Again in the 1980s integration of reaction and separation had already been achieved in biochemical reaction engineering using polymeric membranes. Due to reaction temperatures and conditions however, it was not possible to use polymeric membranes in most of the chemical reaction systems. Recently, inorganic membranes attracted more attention for their potential uses in gas and vapour separation and in pervaporation [Kusuki et al., 1997].

Inorganic membranes used in membrane reactors can be:
- Inert or catalytically active
- Dense or porous
- Made from metals, glass, carbon or ceramics
- Uniform in composition or composite
- Homogeneous or asymmetric porous structure
- Supported on porous glass, sintered metal, granular carbon or ceramics such as alumina
- Produced in different shapes; flat discs, tubes, hollow fibers or monoliths [Julbe et al., 2001]

A number of inorganic materials have been found promising for the applications involving elevated temperatures and harsh reaction conditions as a result of the studies carried out. Moreover, some of the inorganic films and membranes composed of carbon, silica or zeolite displayed higher permeability and selectivity than organic membranes [Kusuki et al., 1997].

In order to assure a certain chemical and mechanical stability and for reactions require high temperatures, two types of membranes are mainly considered: inorganic porous membranes and dense metal membranes. Porous membranes are characterised with the permeation of all components through the matrix. Loss of reactants may occur; however, they on the other hand offer high permeability, whereas dense membranes are permeable only to a limited number of components, e.g. H_2, O_2 and posses relatively low permeability. Table II.II-7 shows a classification of inorganic membranes.

TableII.II- 7 Classification of Inorganic Membranes

Type of Membrane	Material	Selectivity	Permeability
Dense	Metallic Solid electrolytes	High (O_2,H_2)	Low to moderate
Porous (oxides, carbon, glass, metal,zeolites)	Macroporous Mesoporous Microporous	Non-Selective Low to moderate Can be very selective	High Moderate to high Moderate
Composite	Glass-metal Ceramic-metal Metal-metal	Can be very selective	Moderate

Carbon Membranes

In the last decade several studies have been focused on the applications of carbon membranes due to their stability at high temperatures and resistance to severe reaction conditions, e.g. corrosive chemicals. Several types of membranes have been prepared and tested. The most commonly used were: sheet, capillary, hollow fibre and composite carbon membranes. Carbon capillary, hollow fibre and tubular composites have found application areas in industry due to their high surface area per unit volume of a reactor, whereas the use of sheets has been limited to laboratory scale applications. Furthermore hollow fibre would be singled out amongst all, as it has the highest area/volume ratio, easier module assembly and the carbonisation of polymer fibres can be carried out as a continuous process. [Itoh&Haraya, 2000].

Carbon membranes are prepared by carbonization or pyrolysis of suitable carbon containing materials such as thermosetting resin, graphite, coal, pitch and plants under inert atmosphere or vacuum. Recently, numerous synthetic precursors, such as polyimide and its derivatives [Kusuki et al.,1997], polyacrylonitrile [Linkov et al.,1994], phenolic resin, polyfurfuryl alcohol, polyvinylidene chloride-acrylate terpolymer, phenol formaldehyde, cellulose and others are also used. Precursor must be selected carefully as different precursors would produce different type of carbon membranes. For example, a thermosetting polymer can withstand high temperatures and it does not liquefy or soften

during any stage of pyrolysis and will not cause any pore holes or cracks after pyrolysis step. Saufi and Ismail (2004) suggest that polymer precursors are preferred for activated carbon production, especially when a carbon with few inorganic impurities is needed.

High performance carbon membrane production is not an easy task as it involves many steps that must be controlled and optimised. The fabrication of carbon membrane in general follows six steps as indicated in Figure II.II-7 [Saufi & Ismail, 2004].

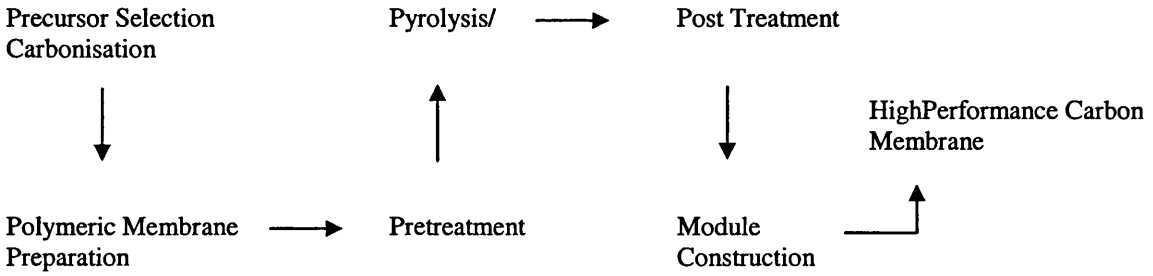

Figure II.II 7 Carbon Membrane Fabrication Process [Saufi & Ismail, 2004].

Sznejer and Sheintuch (2004) studied the application of a carbon membrane reactor for dehydrogenation reactions by operating a membrane reactor at relatively high temperatures (450 and 500 °C), equipped with a molecular sieve carbon membrane, using isobutene dehydrogenation on a chromia alumina catalyst as a model reaction. The system was tested at two types of operating conditions, using either nitrogen as a sweeping gas in counter current flow or using vacuum as a driving force for membrane transport and compared the conversion values with the results obtained from a plug flow reactor operation. The conversions obtained in the vacuum mode show modest gains above the ones obtained in the plug flow reactor; 40% vs. 30% at 500 °C. Sznejer and Sheintuch (2004) also observed that higher conversions were achieved with decreasing feed flowrate. Furthermore, with the use of carbon membranes they have overcome problems, such as membrane mechanical instability, insufficient permeability, permselectivity or simply high cost, created by various inorganic membranes, e.g. ceramic or dense metal, hamper the application of inorganic membranes in the process industry [Sznejer & Sheintuch, 2004].

II.II.5 TAYLOR FLOW

Characteristics

Taylor flow is a two phase flow regime in which the liquid slugs are separated by large bubbles that have the length greater than the channel diameter. The flow was named after British scientist Geoffrey Ingram Taylor (1886–1975).

The application of laminar gas-liquid two phase flow in vertical tubes has a great importance in various research fields and has been the subject of many detailed studies where the flow pattern was an important governing parameter. The flow patterns occurring in two-phase flows mostly depends on the flowrates and properties of the liquid and gas as well as the tube size. The most common flow patterns observed in the tubes are shown in Figure II.II-8 and these are bubble flow, slug flow, Taylor flow and annular flow [Irandoust&Andersson, 1989].

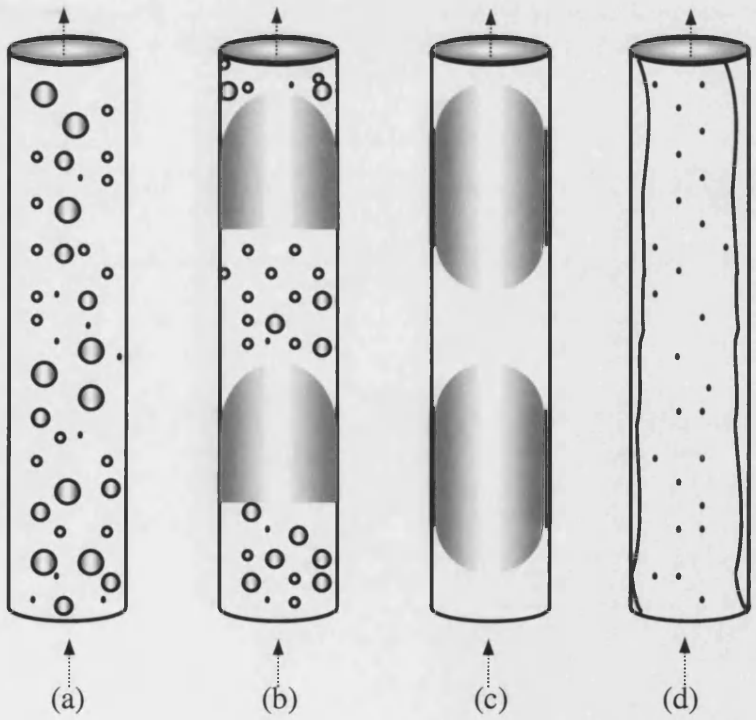

Figure II.II 8 Vertical Flow Patterns (a)Bubble Flow (b) Slug Flow (c) Taylor Flow (d)Annular Flow[Irandoust & Andersson, 1989].

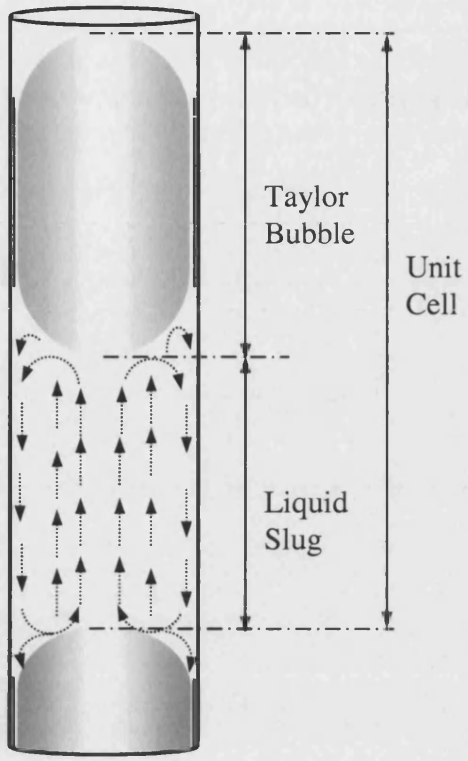

Figure II.II 9 Taylor bubble, liquid slug and the unit cell and the flow pattern in vertical Taylor Flow [Irandoust et al., 1992].

Gas phase is dispersed in the liquid as bubbles much smaller than the tube diameter in the bubble flow pattern. In the case of the slug flow, gas moves in the form of large gas bubbles separated by liquid slugs which also contains small gas bubbles. Annular flow is the flow in which the liquid flows as a wavy film at the tube wall with the gas phase moving in the core.

Taylor flow is a special case of slug flow, where the bullet shaped Taylor bubbles, with a length larger than the channel diameter, are separated by liquid slugs without any gas bubbles in them. In Taylor flow, there is a very thin liquid film between the Taylor bubbles and the channel wall, causing a very low axial dispersion between liquid slugs. Bubbles also prevent the development of parabolic flow in the liquid slugs, and this leads to recirculation of the liquid phase. Hence, the recirculation in the liquid slugs enhances the radial mass transfer considerably. Figure II.II-9 shows the flow pattern occurring in the liquid slugs [Irandoust & Andersson, 1989; Irandoust et al., 1992; Shah et al., 1996]. Shah et al. (1996) claimed that the flow regimes are dominated by the gas flowrate and

have a weak dependency on the liquid flowrates. According to their experimental results and the theory, the diameter of the bubbles becomes smaller as the velocity of the bubbles increases. Furthermore, under the assumption that the length of the bubbles and slugs does not change as they travel inside the capillaries, it follows that both the bubbles and the liquid slugs travel at a velocity equal to the velocity of the bubble [Shah et al., 1996].

Taylor flow can be created over a wide range of liquid and gas flowrates and at sufficient superficial velocities. Some researchers may also argue that the area of the region in which Taylor flow exists on the two phase flow map, increases with decreasing channel diameter. Heiszwolf et al. (1999) derived a rough operating area in which Taylor flow can be expected, that is:

$$u_{s,G} < 1 \ m/s \ \text{ and } \ u_{s,L} < 1 \ m/s$$

where $u_{s,G}$ and $u_{s,L}$ are liquid slug and Taylor bubble superficial velocities. Here it is assumed that velocity of the liquid slugs is equal to the sum of gas and liquid superficial velocities [Heiszwolf et al, 1999; Kreutzer et al., 2001;].

Taylor dispersion is characterized by smooth streamlines and the flow is laminar. This leads to an accurate prediction of the dispersion coefficient. In most natural situations, flow is turbulent and prediction of dispersion coefficient is not possible. In order to obtain Taylor flow, a sharp pulse of solute is injected into a long thin tube filled with solvent flowing in laminar flow. As the solute pulse moves through the tube, it is dispersed. In order to measure the diffusion coefficient, when this pulse comes out of the other end of the tube, its shape is measured with a differential refractometer. It can be operated relatively easily at high temperature and pressure. It has the potential to give results with the accuracy better than 1%. Taylor flow has also been referred to as one of the four best methods of measuring diffusion coefficients [Cussler, 1984].

The concentration profile found in this apparatus is given by equation

$$c_1 = \frac{M}{\pi R_0^2} \frac{e^{-z^2/4Et}}{\sqrt{4\pi Et}}, \qquad (1)$$

where M is the total solute injected, R_0 is the tube radius, and E is a dispersion coefficient given by

$$E = \frac{(v^0 R_0)^2}{48D}, \qquad (2)$$

where v^0 is the average velocity of the flowing solvent. As it can easily be seen from the equations stated above, E varies inversely with D and consequently, a widely spread pulse means a large E and a small D, whereas a very sharp pulse indicates small dispersion and hence fast diffusion [Cussler, 1984].

In many three phase system, the mass transfer rate between the phases is important for efficient design of a reactor. It was claimed by Irandoust et al. (1992) that in the case of two-phase flow, Taylor flow in the monolithic catalyst reactor gives superior mass transfer characteristics [Irandoust et al., 1992]. Additionally, other advantages of the application of the Taylor flow in the monolith channels are low pressure drop, high surface area, uniformity of the distribution of the flow and short diffusion length in the solid catalyst [Irandoust et al., 1992].

Applications

Gas-liquid two-phase flow has great importance in several technical applications, such as two-phase flow through porous media (e.g. oil in sand), boiling in tubes, analytical devices, and monolithic reactors. The previous studies of Irandoust and Andersson have shown that the slug flow gives the best mass-transfer properties in the monolith channels [Irandoust&Andersson, 1989].

In literature, a large number of publications deal with two-phase flow in pipes of diameters $d_c > 0.01m$. These studies are mostly related to characterisation of the type of two phase flow regime and the development of the models for the pressure drop and the liquid hold-up of the two-phase mixture. The flow in channels with small diameters ($d_c < 0.01m$) and capillaries ($d_c < 0.003m$) have not been studied extensively

[Heiszwolf, 1999]. Most of the investigations that were carried out for describing the mass transfer in a two phase flow used pipes with larger diameters than monolith cell diameters [Irandoust et al., 1992]. Analogies between two-phase flow in capillaries and two-phase flow in pipes can easily be found, but these analogies cannot be extended without caution as capillary and molecular forces, which are not important parameters in pipe flow, play a dominant role in the flow inside capillaries. Some of the important differences were listed as:

- Entrance conditions play an important role in capillary flows.
- Capillary forces are important and inertial forces are small or do not exist.
- In capillary bundles, instabilities may develop that would cause variations in flow patterns from one capillary to another [Shah et al., 1996].

Irandoust et al. (1992) have described gas-liquid mass transfer phenomena of upward Taylor flow occurring in a single circular channel of a monolith. Small channel diameters 1.5 and 2.2 mm diameters were studied. The channels used were 0.6 m long glass capillaries. The gas bubble and the liquid slug lengths were varied independently and measured with a photocell attached to the system. The measured lengths of the gas bubbles were between 3.4 and 29.1 mm and the lengths of the liquid slugs varied between 2.9 to 67 mm. Finally the values of average total linear velocity were determined to be between 0.092 to 0.56 m/s. Gas-liquid mass transfer coefficient was determined experimentally using absorption of oxygen from air into three different liquids: water, ethanol and ethylene glycol, processing different properties. Semi-theoretical model and correlation for liquid film thickness and gas-liquid mass transfer coefficient were obtained. These correlations are explained in the following pages in detail. Finally it was concluded that gas-liquid mass transfer in Taylor flow in a capillary is mainly determined by the liquid phase diffusion coefficient and the gas-liquid contact area. The flowrate and the gas bubble and liquid slug lengths have a minor influence. The gas-liquid contact area is affected by the channel diameter and gas hold-up, which makes it possible to calculate the mass transfer coefficient without measurements in the actual system [Irandoust et al., 1992].

Kawakami et al. (1989) studied gas-liquid and gas-solid mass transfer rates in a monolithic reactor with different channel sizes and demonstrated superior mass transfer

properties of the monolithic reactor compared to the packed-bed reactor. Model calculations indicated that the overall effectiveness factor was higher for the co-current up-flow operation compared to co-current downflow operation due to the higher mass transfer rates, most probably caused by the perfect mixing in the liquid phase, in the co-current up-flow operation. Consequently, up-flow operation gave 2-5 times higher k_La values than down-flow operation, this value was also much higher than that obtained in a trickle-bed reactor with the same specific surface as the monolith reactor [Kawakami et al., 1992].

Many studies have been mainly focused on the bubble rise velocity, pressure drop and bubble velocity and little information was obtained about the liquid film thickness for systems where surface tension, inertia and viscous effects are important. Irandoust and Andersson (1989) claimed that the pressure drop is highly correlated to the thickness of the film around the Taylor bubble and measured the film thickness for various liquids in both upward and downward Taylor flow with the tube sizes of interest in monolithic catalysis. Irandoust and Andersson (1989) also calculated the film thickness and bubble size theoretically by numerical solution of the flow and the surface tension equations by considering the surface tension and inertia and viscous effects and concluded that for a given system and at a given flowrate, the liquid film thickness was independent of the length of Taylor bubbles and liquid slug lengths and that the direction of flow had a negligible effect on the measured values of the liquid film thickness. Furthermore, Bretherton (1961) claimed that the liquid film in a vertical tube will be thicker than that in a horizontal tube.

Berčič and Pintar (1997) studied gas-liquid and liquid-solid mass transfer in capillaries under Taylor flow regime. Gas-liquid mass transfer coefficients were determined by measuring the amount of methane dissolved in the water flowing upward through a single glass capillary. It was concluded that the mass transport is mostly determined by the liquid slug length and velocity, that was varied between 0.01 and 0.4 m/s, and the contribution of the mass transferred from the gas bubble to the liquid film has little influence on the overall gas-liquid mass transfer [Berčič and Pintar, 1997].

Heiszwolf et al. (2001) measured gas-liquid mass transfer coefficient (k_La) from oxygen absorption in water for monolith reactor applications. The obtained data was compared

with the model derived by Berčič and Pintar (1997) for the Taylor flow in a single capillary. From this model, Heiszwolf et al. (2001) have predicted the unit cell length for their system and observed that the predicted liquid slug lengths were close to experimentally measured values and hence concluded that the mass transfer models may be used for monolith structures. Furthermore, Heiszwolf et al. (2001) have shown that the liquid slug length may also be estimated from pressure drop measurements and put forward the fact that due to the stationary wall, a circulating flow is induced in a moving liquid slug. This circulation flow refreshes the gas-liquid interface of the gas bubble continuously, leading to a high gas-liquid mass transfer rates. For a given liquid hold-up, Taylor flow with short liquid slugs will have a higher mass transfer rate than flow in which larger liquid slugs occur. This is caused by the increased interfacial area and the more intense mixing for short liquid slugs. Finally Heiszwolf et al. (2001) reported that they obtained k_La values in the range of 0.4-1 s^{-1} which are very high values compared to stirred tank and trickle bed reactors [Heiszwolf et al., 2001].

Kreutzer et al. (2001) studied the mass transfer characteristics of monoliths operated in the Taylor flow regime and investigated the hydrogenation of α-methylstyrene over a palladium catalyst experimentally. Kreutzer et al. (2001) were also amongst the researchers who used the empirical correlation derived by Berčič and Pintar and pointed out that this correlation is not a function of the bubble length or the channel diameter.

Theoretical Correlations

Andersson and Irandoust carried out the most important work concerning the fundamentals of liquid-solid and gas-liquid mass transfer in capillaries. Derived correlations for the prediction of mass transfer coefficients were used in most of the works dealing with the modelling of systems with gas-liquid-solid reactions taking place in monoliths. They have carried out series of experiments in single capillaries in which they have measured the absorption of oxygen from air into three different liquids, water, ethanol and ethylene glycol, and developed a semi-theoretical model for correlating the mass transfer coefficients. They have assumed that the gas bubbles were cylindrical with hemi-spherical top and bottom menisci surfaces and that they were separated by liquid slugs well. It was further assumed that the mass transfer occurred partly from the hemi-spherical ends and partly from the cylindrical lateral surface of the bubble. They have

also shown that the spherical ends of the Taylor bubbles can be treated as rigid spheres. Taking into account the assumptions made, they derived a semi-theoretical correlation as follows:

$$k_L a = 4[\delta(d_t - \delta)U_{av} y_m + DShd_B]/[d_t^2(L_l + L_g)], \qquad (3)$$

The first term accounts for the mass transfer into liquid film between the gas bubble and the wall and the second term refers the mass transferred through spherical ends of liquid slugs δ is the liquid film thickness and given by the empirical relationship below[Irandoust & Andersson, 1989b]:

$$\delta = 0.18 d_t \{1 - \exp[-3.1(\mu v/\sigma)^{0.54}]\}, \qquad (4)$$

where v is the average cell velocity (m/s), μ is the liquid viscosity (kg/m/s) and finally σ is the surface tension (N/m).

U_{av} is the average total velocity in the liquid film over a cross section of the film and is given by the equation;

$$U_{av} = (\rho g \delta^2 / 3\mu) + v, \qquad (5)$$

y_m is the mixed cup concentration of the solute in the liquid film, being in contact with the cylindrical part of the Taylor bubble and is equal to:

$$y_m = \frac{c_m - c_0}{c^* - c_0}, \qquad (6)$$

where c_m is the mixed cup solute concentration, c_0 is the initial solute concentration and finally c^* is the saturation concentration (all in mol/m^3). Sh is the Sherwood number and depends on the Reynolds number, d_t is the tube diameter (m), D is the liquid phase diffusion coefficient (m^2/s), d_B is Taylor bubble diameter (m), L_l and L_g are the liquid

slug and the Taylor bubbles lengths (m) respectively. Detailed explanation and the list of assumptions can be found in Irandoust et al. (1992).

Based on absorption experiments using methane and water, Berčič and Pintar (1997) measured the gas to liquid mass transfer parameter $k_L a$ in single capillaries with different diameters and found out that the liquid slug lengths influence the mass transport much more than the gas bubble length and they fitted the experimental results to the following empirical correlation:

$$k_L a = 0.111 v^{1.19} / ((1-\varepsilon_G) UCL)^{0.57}, \qquad (7)$$

where v is average cell velocity (m/s), ε_G is the gas hold-up and UCL is the unit cell length (m) which is the sum of the liquid slug and the gas bubble lengths. It must be noted that this equation was obtained for the case of methane and water, thus, if a different combination of gas and liquid is used $k_L a$ coefficient must be corrected using the following relation:

$$(k_L a)_{Gas} = (k_L a)_{CH4} \left(\frac{D_{Gas}}{D_{CH_4}} \right)^n , \qquad (8)$$

where D_{Gas} and D_{CH_4} are the diffusion coefficients for the gas used and methane(m^2/s) and n is the scaling factor and is unity for film theory and 0.5 for penetration theory [Kreutzer et al., 2001; Berčič, 2001].

II.III EXPERIMENTAL

II.III.1 GAS PHASE MASS TRANSFER MEASUREMENTS IN A SINGLE CAPILLARY

Experimental Apparatus

The apparatus was designed and constructed to perform experiments to obtain gas-liquid mass transfer coefficients for the tube side of the system. Straight glass capillaries with a 1.5 mm internal diameter and various lengths between 10 cm to 120 cm were used to conduct experiments at ambient temperature and atmospheric pressure. 1-butene and water were fed from the lower vertical port and the side port respectively and the glass capillary was connected to the free upper vertical port of the T-connector. 1-butene was fed to the system prior to water feeding in order to prevent water leaking in the gas line due to the gravitational effect. 1-butene flowrate was adjusted with a needle valve and the flowrate was measured with a bubble flowmeter which was connected to the exit line of the gas-liquid separator. A schematic diagram of the system is shown in Figure II.III-1.

A Micropump™ centrifugal pump was used for pumping water through the system. A two-neck glass flask with 200 mL volume was used as a phase separator. Water was collected in the separator, while 1-butene was directed to the local extraction line through the bubble flowmeter. A 1m long Tygon tube was used to connect bubble flowmeter and the ventilation in order to prevent air entering the system.

In order to enable sample collection, a ¼ " stainless steel tee connector was placed on the line between the glass capillary and the separator. A silicon septum was tightly placed in the free port of the tee connector allowing the sample collection with a liquid GC syringe.

A VARIAN CP-3800 model gas chromatograph was used to measure the amount of dissolved 1-butene in water. Calibration of the GC and the parameters selected for the analysis are tabulated in the Appendix II.VI.2.

Tygon™ was used as connecting tubing in the whole system in order to prevent 1-butene diffusing through the lines. Connecting tubing in the system was kept as short as possible to limit mass transfer to the glass capillary only.

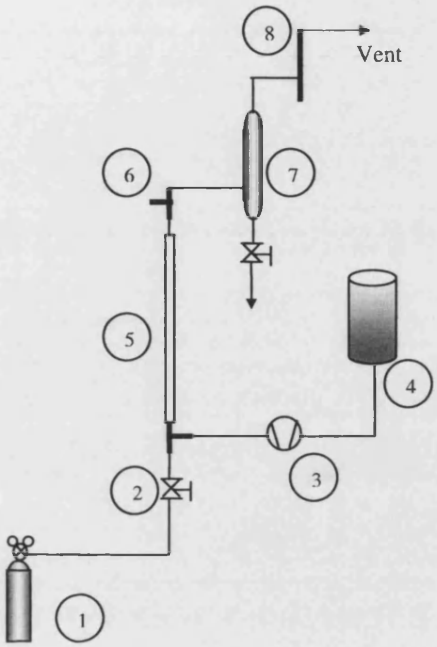

1 : 1-butene Cylinder
2 : Needle Valve
3 : Gear Pump
4 : Water Reservoir
5 : Glass Capillary
6 : Sample Collection
7 : Phase Separator
8 : Bubble Flowmeter

Figure II.III- 1 Experimental set-up for gas-liquid mass transfer measurements

Experimental Procedure

Experiments were performed by measuring the amount of 1-butene dissolved in water, flowing upward through a single glass capillary in the form of a segmented gas-liquid "Taylor" flow. This data was used to evaluate experimental mass transfer coefficients.

Once gas flowrate was set, water was introduced into the system. Water flowrate was measured gravimetrically as follows: tubing connected to the upper end of the glass capillary was disconnected and the flow coming out of the capillary was collected in a flask that was placed on a balance for a certain time interval. After the collection, tubing was reconnected tightly in order to prevent degassing of the liquid phase during the

experiments. Gas and liquid flowrates were varied between 4-15 ml/min and 3.5-14 ml/min, respectively.

Once the gas and the liquid flowrates were adjusted and the Taylor flow was clearly observed in the glass capillary, 1μL samples were collected with a syringe and injected into GC to measure the amount of 1-butene dissolved in water.

In order to eliminate the effect of the connecting tubing and the connectors on the mass transfer, each experiment was repeated in the absence of the reactor and this data was used for the calculations.

Figure II.III- 2 Experimental set-up of the gas-liquid mass transfer studies

This system was also used to obtain the equilibrium concentration of 1-butene in water at atmospheric pressure and ambient temperature by re-circulating water in the system.

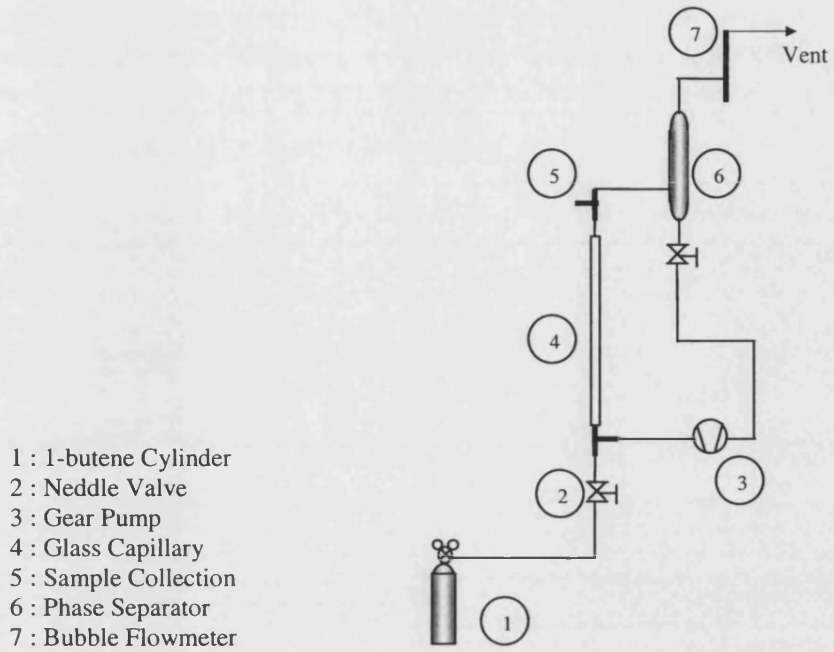

Figure II.III- 3 Experimental set-up for obtaining equilibrium 1-butene concentration.

Bubble Length Measurements

Photographic technique, using digital camera Nicon Coolpix 5700, was employed to record the Taylor bubble and liquid slug lengths during the experiments. In order to decrease the light loss due to scattering, red light was used as a light source. Short shutter speed (2000 frame per second) was used to ensure faithful representation of bubble and liquid slug shape. Ten pictures were taken for each experimental set and measurements were averaged. Each glass capillary that was used for gas-liquid mass transfer measurements was marked as shown in Figure II.III-4. By using the marked length it was possible to estimate the actual length of the Taylor bubble and the liquid slugs.

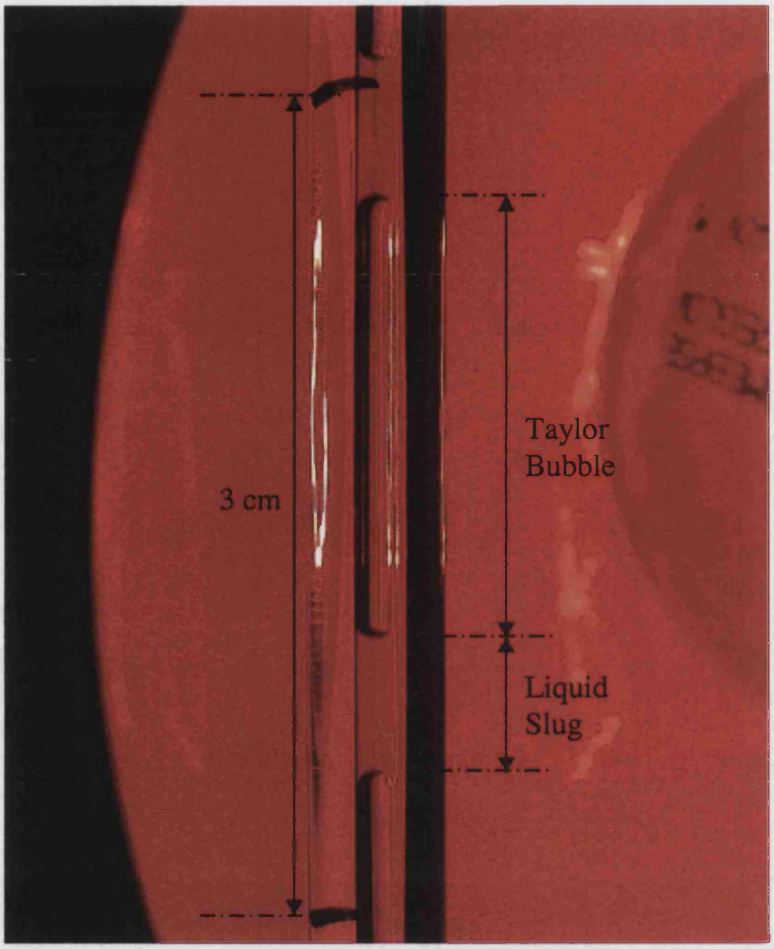

Figure II.III- 4 Single glass capillary used for gas-liquid mass transfer and Taylor bubble-liquid slug length measurements

II.III.2 PREPARATION & CHARACTERISATION OF THE CARBON TUBES

Synthetic carbon tubular membranes and membrane precursors were supplied by Mast Carbons Ltd. (UK). Carbon membranes were characterised using low temperature nitrogen adsorption, mercury porosimetry, scanning electron microscopy and nitrogen permeation techniques.

Preparation

In order to prepare membrane tubes, partially cured Novolak phenolic resin particles were milled to a mean particle size of 10 μm using classifying jet mill. This powder was then made into a dough using water, methyl cellulose as a viscosity modifier and

polyethylene oxide as a lubricant. The prepared dough was extruded using a small ram extruder mounted in an Instron machine, and a specially constructed die.

The extruded precursor tubes were dried in air, followed by curing at 523 K in air for 6 hours (increasing the temperature from ambient to 523 K at a rate of 1 K/min). Curing process was followed by carbonisation of the tubes in the flow of nitrogen at 1073 K for 8 hours. Temperature was increased from ambient to 1073 K at a rate of 5 K/min.

During the curing and carbonisation processes, precursor tubes were placed in stainless steel tubes of diameter ¼" in order to retain their original shape and avoid bending. Stainless steel tubes were connected to the air or nitrogen flow accordingly and placed in a temperature controlled tubular furnace. Carbonised membranes were than washed with ethanol and water and dried in vacuum at 373 K for 24 hours.

Characterisation

Scanning Electron Microscopy

The images shown in Figure II.III-5 and II.III-6 were taken using JOEL 6310 (JOEL UK Ltd.) model scanning electron microscope at 15 kV. Samples were immobilised on an aluminium tray with 1.5 cm diameter and coated with gold prior to the measurements.

By using the first picture the thickness of the membrane was precisely measured as 0.575 mm. Figure II.III-6 shows the cross-section of the membrane and has a higher magnification. It can clearly be seen that large pores having up to 10 μm diameter exist in the membrane structure.

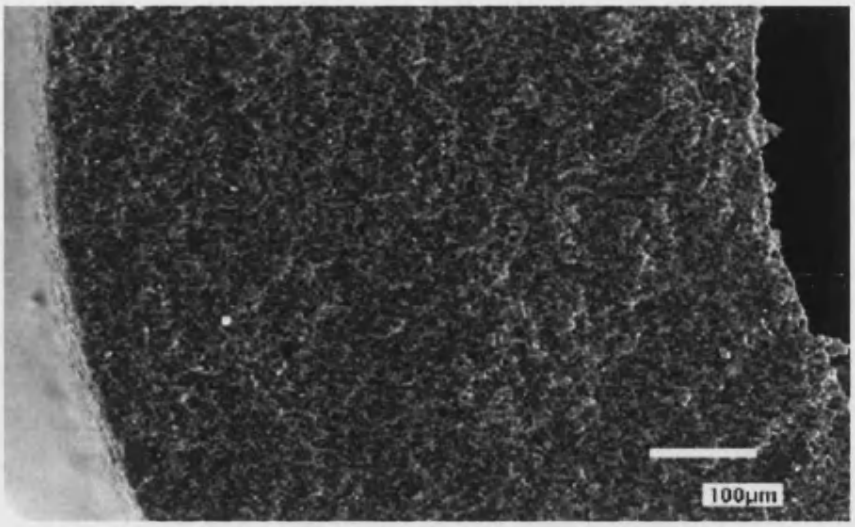

Figure II.III- 5 SEM Image of the carbon membrane (1)

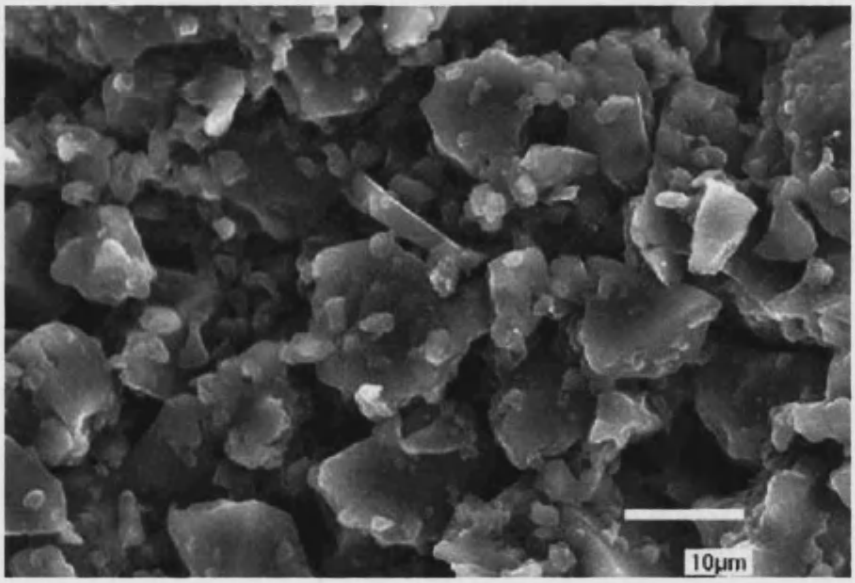

Figure II.III- 6 SEM Image of the carbon membrane

Mercury Porosimetry

Porosity and mean pore radius of the carbon tubes were measured using mercury porosimeter, Micromeritics AUTOPORE II. The sample amount used was 0.2 gr and the measurements were performed at ambient temperature.

The result obtained is shown in Figure II.III-7. From the mercury porosimetry measurements, porosity and mean pore radius were obtained 41.29 % and 0.39 µm, respectively. Porosity value corresponds reasonably well to the theoretical value for

random packing of spheres (ca. 39 %). A slightly larger level of porosity could be due to non-monodisperse size distribution of precursor particles and non-spherical shape, due to jet-milling process. The latter is seen in the SEM image taken at higher magnification (see Figure II.III-6).

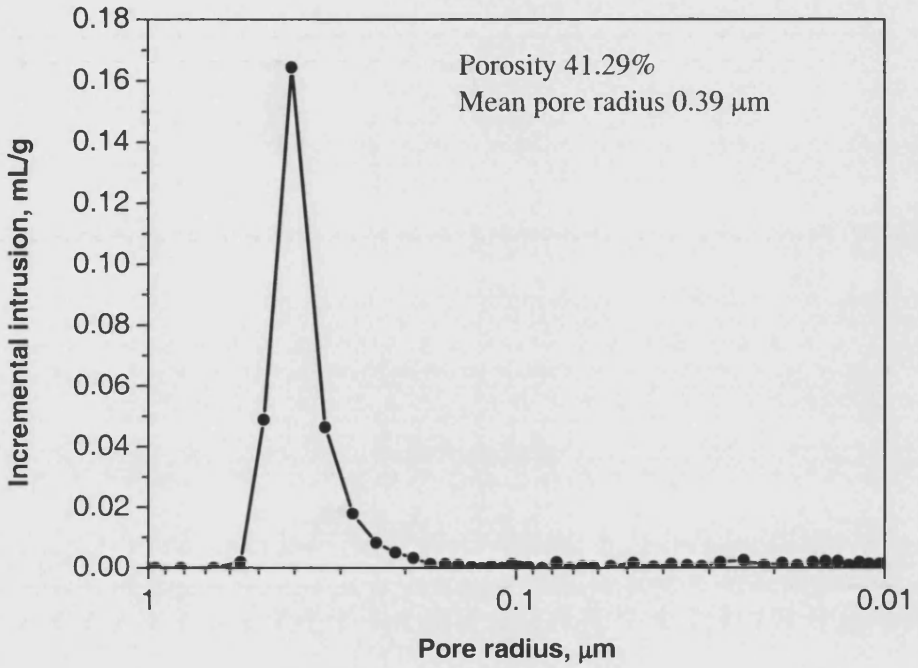

Figure II.III- 7 Mercury Porosimetry results of carbon tubes

Low Temperature Nitrogen Adsorption

Low temperature nitrogen adsorption experiments were performed at -196 °C using ASAP-2010 instrument (Micromeritics). Samples were treated under vacuum at 200 °C for 12 hours prior to the measurements. The isotherm obtained is shown in Figure II.III-8. High nitrogen uptake at low relative pressures indicates the presence of micropores and in addition to that the histerysis observed between the relative pressures of 0.6 and 1 shows that mesopores also exist in the structure. However, the small size of hysteresis and the relatively long plateau between 0.1-0.95 p/p_0 suggests that the material largely consists of micropores, and macroporosity was determined by SEM and Hg porosimetry. Microporosity in this type of carbon can be controlled by the activation/carbonisation process [Tennison, 1998]. BET surface area, cumulative pore volume and BJH average pore diameter were obtained as 1029 m^2/g, 0.47 cm^3/g and 0.22 nm, respectively.

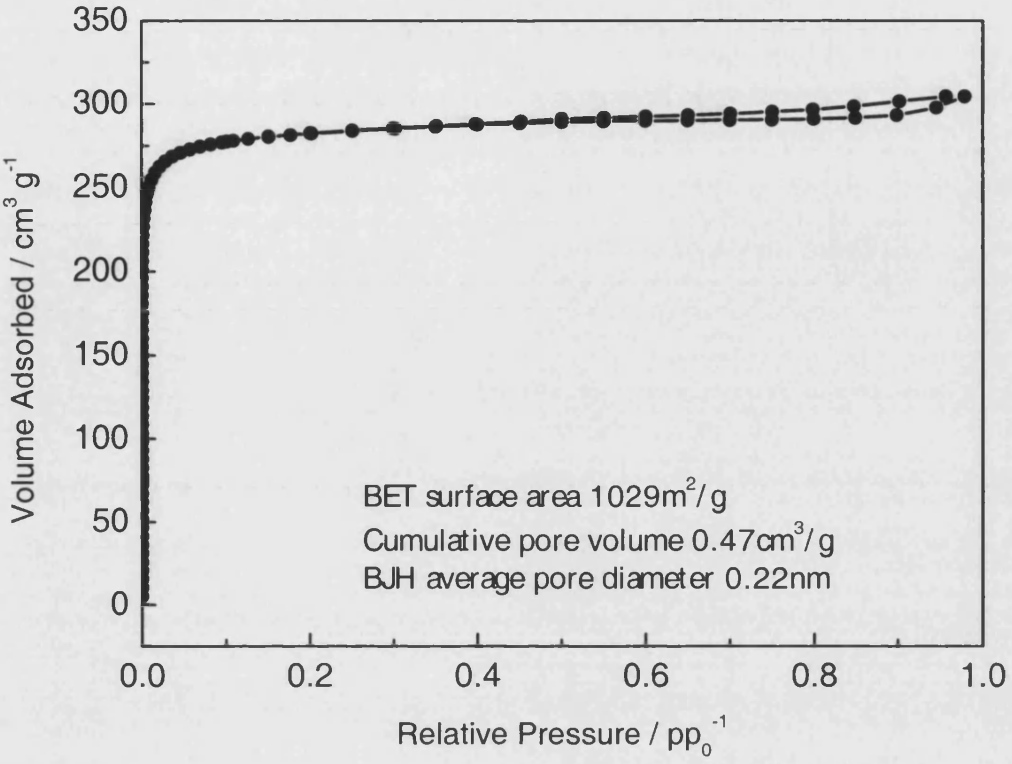

Figure II.III- 8 Nitrogen Adsorption Isotherm of carbon membrane

Nitrogen Permeation Experiments

Information about the particle size and the porosity of the membrane was also obtained by measuring the gas permeation of the membrane.

Carbon tube was placed in a stainless steel shell as shown in Figure II.III-9 and one side of the membrane was sealed with epoxy resin. Nitrogen was flown from the open end of the tube and created pressure in the tube. As the flowrate of the nitrogen was increased, the difference in the pressure in the tube and the shell side was measured with a pressure meter. Flowrate of the nitrogen permeating through the membrane was measured using a bubble flowmeter. Recorded pressure difference against the nitrogen flow and the superficial velocity of the gas is shown in Table AII.3.1. Figure II.III.10 also illustrates the nitrogen permeability of the carbon membrane. Superficial velocity was obtained from the equation below;

$$v_o = \frac{Q}{A}, \qquad (9)$$

where, Q is the volumetric flowrate(m^3/sec) and A is the effective area(m^2), which is equal to 2□rL in our case.

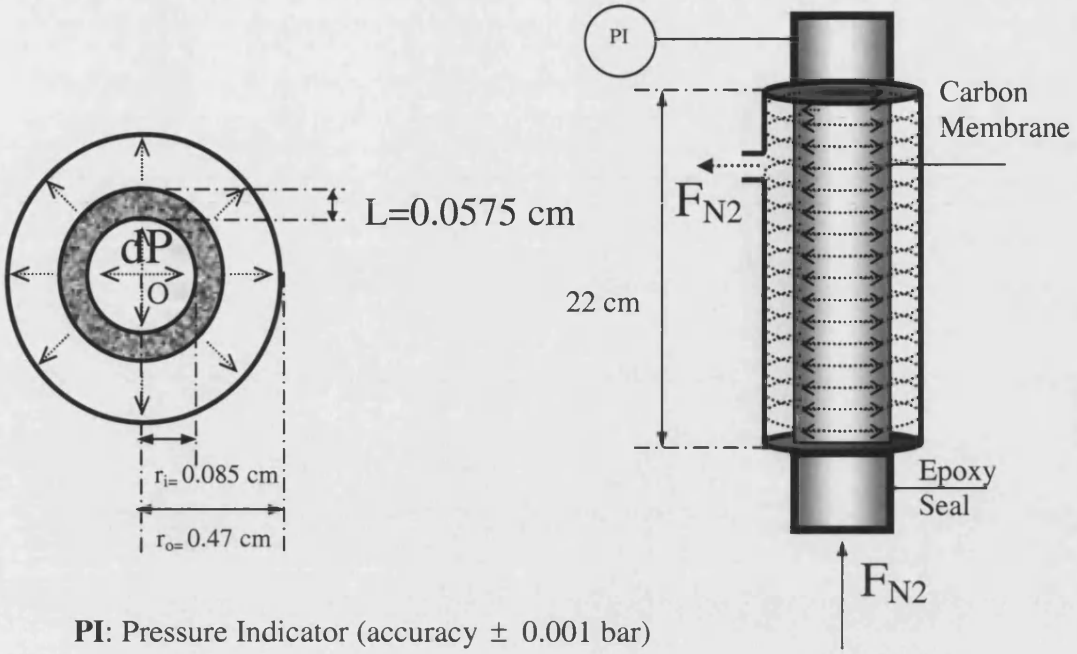

Figure II.III- 9 Experimental set-up of the permeation experiments

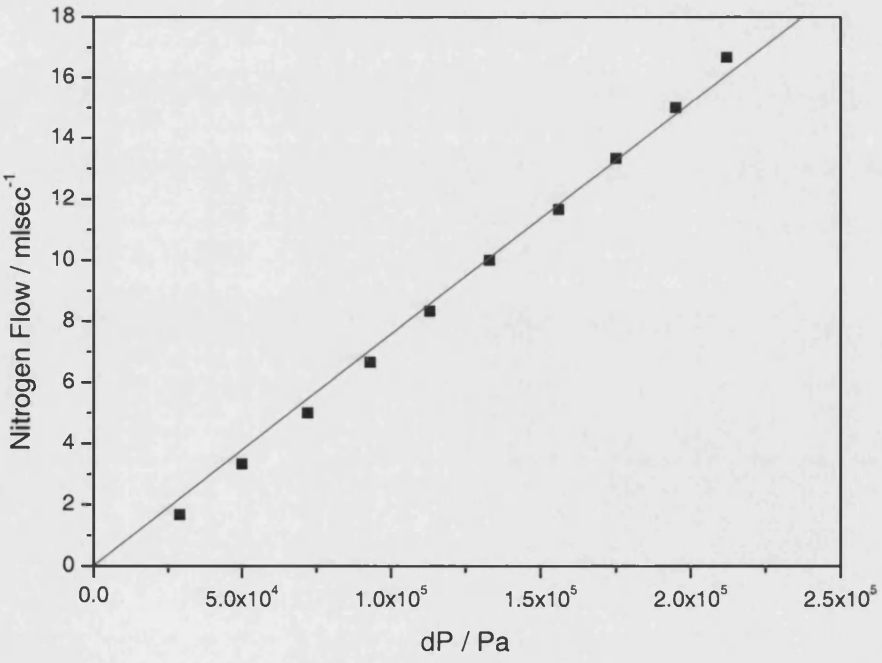

Figure II.III- 10 Nitrogen permeability of the porous carbon membrane

Data obtained from the permeation measurements was fited to the empirical Blake-Kozeny equation:

$$v_o = \frac{(P_o - P_L)}{L} \frac{D_p^2}{150\mu} \frac{\varepsilon^3}{(1-\varepsilon)^2}, \qquad (10)$$

where, v_o is the superficial velocity of the gas, μ is the viscosity of the gas (0.180×10^{-4} Pas), ε is the porosity of the medium, (P_o-P_L)is the pressure difference between the two sides of the porous medium D_p is the particle size in the porous medium(m) and L is the thickness of the porous medium(m).

The membrane itself is assumed as a packed column due to its structure that is made of approximately spherical particles and the Blake-Kozeny equation for our system was evaluated as follows.

For laminar flow in circular tubes of radius R the linear velocity is,

$$v = \frac{(P_o - P_L)R^2}{8\mu L}, \qquad (11)$$

In addition, if the carbon membrane is assumed as a packed bed with hydraulic radius R_h, the average flow velocity then becomes,

$$v = \frac{(P_o - P_L)R_h^2}{2\mu L}, \qquad (12)$$

Hydraulic radius may be expressed in terms of void fraction ε and wetted surface area per unit volume as:

$$R_h = \frac{\text{Cross} - \text{section available for flow}}{\text{wetted perimeter}} \qquad (13)$$

$$R_h = \frac{\text{Volume available for flow}}{\text{total wetted surface}} \qquad (14)$$

$$R_h = \frac{\left(\frac{\text{volume of voids}}{\text{volume of bed}}\right)}{\left(\frac{\text{wetted surface}}{\text{volume of bed}}\right)} = \frac{\varepsilon}{a} \qquad (15)$$

a is expressed as:

$$a = a_v(1-\varepsilon), \qquad (16)$$

where, a_v is the specific surface area and equals to the ratio of total particle surface to the total volume of the particles. Mean particle diameter and the superficial velocity are defined as:

$$D_p = \frac{6}{a_v} \qquad v_o = v\varepsilon, \qquad (17)$$

If all these definitions are combined with the modified Hagen-Poiseuille formula:

$$v_o = \frac{(P_o - P_L)R_h^2}{2\mu L}\varepsilon$$

$$= \frac{(P_o - P_L)\varepsilon^3}{2\mu L a^2}$$

$$= \frac{(P_o - P_L)\varepsilon^3}{2\mu L a_v^2 (1-\varepsilon)^2}$$

$$= \frac{(P_o - P_L)D_p^2}{2\times 36\mu L}\frac{\varepsilon^3}{(1-\varepsilon)^2}$$

$$= \frac{(P_o - P_L)}{L}\frac{D_p^2}{2\times 36\mu}\frac{\varepsilon^3}{(1-\varepsilon)^2} \qquad (18)$$

Experimental measurements indicate that the theoretical formula can be improved if the 2 in denominator is changed to a value between 4 & 5. The value selected to replace 2 is 25/6. Then the equation becomes Blake-Kozeny equation:

$$v_o = \frac{(P_o - P_L)}{L}\frac{D_p^2}{150\mu}\frac{\varepsilon^3}{(1-\varepsilon)^2}, \qquad (19)$$

This equation can be used for porous materials with void fractions less than 0.5 and is valid only in the laminar flow region given by $(D_p G_o / \mu)(1-\varepsilon)^{-1}<10$, where $G_o=\rho v_o$ [Bird et al., 2002].

In order to check this constraint, $(D_p G_o / \mu)(1-\varepsilon)^{-1}$ was calculated using D_p and ε data already reported in the literature. These are $D_p \leq 10\mu m$ and $\varepsilon \approx 40$ % [Tennison, 1998]. When these values were used $(D_p G_o / \mu)(1-\varepsilon)^{-1}$ was calculated as 1.647. As the flow is laminar, data obtained was fited to the Blake-Kozeny equation. Porosity and the particle diameter were obtained as 35.3% and 1.3 μm, respectively. These data are in good agreement with the data published in the literature [Tennison, 1998] and the data obtained from mercury porosimetry measurements.

II.III.3 OXYGEN TRANSFER THROUGH THE MEMBRANE

Experimental

Several experiments were carried out at 30 °C to obtain the optimum flow rate of oxygen-nitrogen mixture and the Henry's constant which will be used to calculate the required oxygen composition in the shell side of the reactor for a desired oxygen concentration in the tube side for hydrocarbon oxidation experiments.

Experimental Apparatus and Method

The apparatus used for oxygen transfer measurements was similar to that used for hydrocarbon oxidation experiments, consisting of nitrogen and oxygen mass flow controllers, a centrifugal pump for liquid circulation, a carbon membrane reactor, a dissolved oxygen meter, a plastic 50 ml container, in which the probe was placed, magnetic stirrer to obtain 0.3 m/sec liquid movement that was required for an accurate measurement of the DO meter and a bubble flowmeter. Oxygen and nitrogen were mixed before entering the reactor's shell side and the flowrates were adjusted using mass flow controllers. Total flow rate of the gas in the shell was varied between 400 and 500 ml/min. The oxygen and nitrogen mixture entered at the bottom of the reactor, flowed around the tube in upwards direction and left the top of the reactor to the ventilation as shown in Figure II.III-11.

Tube flow consisted of water and nitrogen. Nitrogen flow was controlled and adjusted by a mass flow controller. Additionally nitrogen flow rate was measured using a bubble flowmeter that was connected to the gas exhaust line of the system assuming that oxygen was dissolved in water and that it did not mix with the nitrogen bubble. Since the flowrates were selected according to the hydrodynamic studies of Taylor flow, it was also assumed that Taylor flow regime was obtained on the tube side.

In order to create similar conditions to hydrocarbon oxidation experiments, a set of experiments was carried out using heteropoly acid solution firstly. However, the acid solution went through the glass filter of the DO meter's probe, mixed with the electrode solution and gave unreliable results. Therefore, given that the heteropoly acid solution is

aqueaous, the results obtained from the measurements with water were used for the calculations.

There was no hydrocarbon present in the whole system during these measurements. Tube gas flowrate was varied between 5 and 10 ml/min. while the liquid flowrate was kept constant at ca. 15 ml/min.

Figure II.III-11 shows the small part of the reactor, tube and the shell flows. Part of the oxygen transfers through the membrane and dissolves in water.

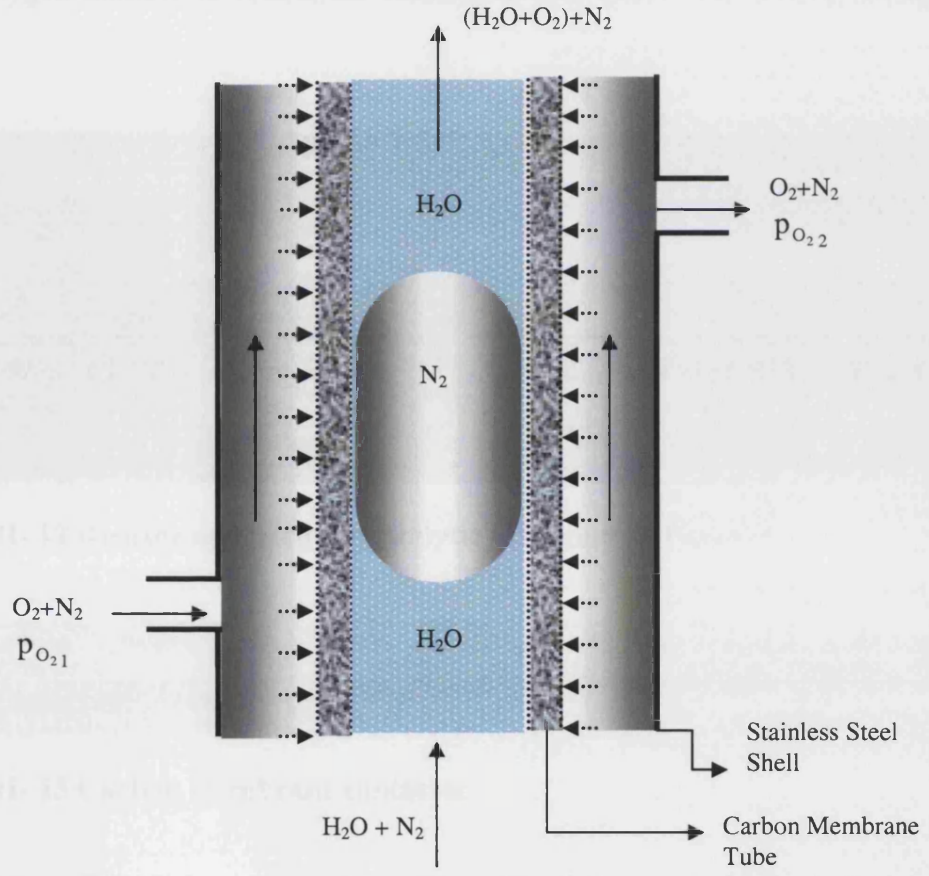

Figure II.III- 11 Oxygen transfer through the membrane

II.III.4 PARTIAL OXIDATION OF 1-BUTENE

Experimental Apparatus

The apparatus was designed and constructed to perform catalytic hydrocarbon oxidation experiments. A custom built tubular reactor was used to conduct experiments at various temperatures and pressures listed in Appendix II.4. A stainless steel tube with 3/8" diameter and two tee pieces were used as a shell around the carbon membrane contactor as shown in Figure II.III-12. Figure II.III-13 shows the carbon membrane contactor placed in the stainless steel shell. Tee pieces were used as an inlet and an outlet for the nitrogen+oxygen mixture to enable the continuous flow around the carbon membrane contactor.

Figure II.III- 12 Reactor operated for catalytic oxidation of 1-butene

Figure II.III- 13 Carbon membrane contactor

Three Bronkhorst™ mass flow controllers were used to set and control oxygen and two nitrogen flows, through the tube and shell sides. Two pressure controllers, automatic (Bronkhorst™) and manual were used to regulate the pressure of the system. A pressure transducer was placed in the tube side of the reactor outlet in order to observe the pressure in the system and adjust the transmembrane pressure accordingly. A Micropump™ gear pump was employed for the circulation of the catalyst solution in the system. The reactor and the PTFE tubing between the gear pump and the reactor were

heated in order to obtain constant temperature during the experiments. Any change in the temperature was observed by means of the thermocouple placed in the tube side of the reactor.

A custom built separator was used as a reservoir for the catalyst solution as well as used as a gas-liquid separator during the experiments. A 1/16" valve was placed on the exit line of the separator in order to collect samples to analyse with a VARIAN CP-3800 model gas chromatograph. An IKA™ magnetic stirrer was placed under the separator and the catalyst solution was mixed during the experiments in order to obtain a homogeneous mixture. ¼" PTFE tubing was used as connecting tubing throughout the system. A condenser was placed at the gas outlet of the separator in order to condense MEK that might have been stripped by the feed gas. Water was used as a coolant and was pumped by a rotary pump.

Gas and liquid flowrates were set via computer using LabView 6 software. A brief description about LabView 6 is given in Appendix I.4.

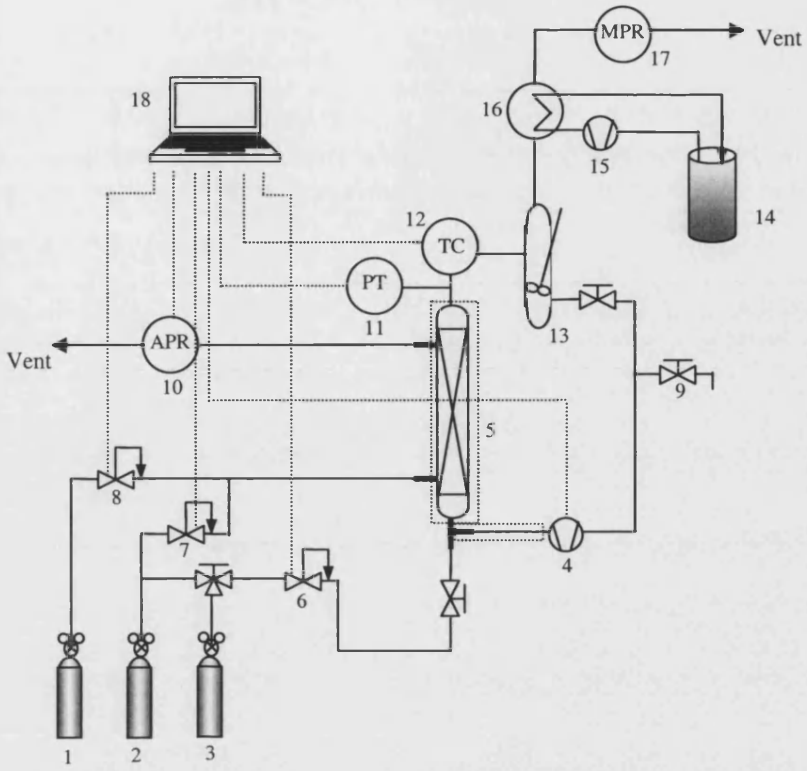

1 : O_2 Cylinder
2 : N_2 Cylinder
3 : N_2+C_4H_8 Cylinder
4 : Gear Pump
5 : Reactor
6 : N_2 Mass Flow Controller
7 : N_2 Mass Flow Controller
8 : O_2 Mass Flow Controller
9 : Sample Collection Valve
10 : Automatic Pressure Regulator
11 : Pressure Transducer
12 : Thermocouple
13 : Phase Separator
14 : Cold Water Reservoir
15 : Rotary Pump
16 : Condenser
17 : Manual Pressure Regulator
18 : Computer

Figure II.III- 14 Experimental set-up for catalytic hydrocarbon oxidation experiments

Experimental Procedure

Catalytic experiments were carried out to observe performance of the Taylor flow membrane reactor. The selected test reaction was 1-butene oxidation to methyl-ethyl-ketone (MEK). Experimental apparatus was described earlier in detail and the schematic diagram is shown in Figure II.III-14.

Initially, the liquid reservoir in the system was loaded with 100 ml aqueous HPA-Pd(II) catalyst solution. Pressures of the tube and the shell sides of the system were then increased to the desired level with pure nitrogen flow and adjusted by means of a manual pressure regulator and an automatic pressure controller, respectively. The control and the

adjustment of the pressures in the tube and the shell sides enabled the adjustment of the trans-membrane pressure. Circulation of liquid phase was started after total pressure reached set point. Consequently, a stable Taylor flow in the reactor was created as well as the carbon membrane was sufficiently wetted, prior to the introduction of the feed gas and the consequent reaction. Flowrates of the liquid and gas streams were selected according to the data obtained from the experiments conducted to evaluate mass transfer coefficients.

Reaction started following the introduction of the feed gas in the system by switching from pure nitrogen flow to the 1-butene-nitrogen mixture. Oxygen was introduced in the shell side and mixed with nitrogen flow. The volumetric ratio of oxygen was 80%. In order to maintain the pressure in the shell side and obtain continuous oxygen source, gas flowrate in the shell was kept constant at 400 ml/min. Feed gas mixture was prepared by filling a 4.6 L stainless steel gas cylinder with 1-butene and nitrogen and its concentration was measured by GC. 1-butene feed concentration varied between 8.35 mmol/L and 40.8 mmol/L for various experiments. Gas flowrate in the tube varied between 4ml/min and 10 ml/min, whereas flowrate of the catalyst solution was kept constant at 14 ml/min. A Gas Chromatograph was used to measure the product MEK concentration at 5-15 min time intervals. HPA-Catalyst solution samples were collected in the 10 ml glass vials by means of a sampling valve located at the exit of the separator and analysed immediately after collection.

Experiments were conducted at various temperatures (30-50 °C), pressures (1-6 bar), trans-membrane pressures (0.15-2 bar), catalyst concentrations (0-2 mM) and HPA concentrations (25-50 mM).

Preparation of the HPA- $PdCl_2$ Solution

The catalytic system consisted of an aqueous solution of heteropoly anion $[PMo_9VO_{40}]^{6-}$ [HPA] and $PdCl_2$. HPA solution was prepared by mixing 5.999 g (0.05 mol) NaH_2PO_4 (Aldrich), 64.773 g (0.45 mol) MoO_3 (BDH) and 18.289 g (0.15 mol) $NaVO_3$ (Aldrich) in a flask and dissolved into 600 ml of deionised water by stirring at 353 K for 3 hours. Significant colour change from orange to dark red was observed during the mixing. After cooling down, the dark red solution was diluted up to 1 litre and 2 litres to obtain 0.05 M

and 0.025 M solution respectively. The pH of this solution at 30 °C was between 1.5 and 1.6. The pH was then adjusted to 1.3 by adding concentrated H_2SO_4 solution.

The concentration of Pd[II] in the solution was varied between 0 and 2 mM. The ratio of Pd^{2+} to Cl^- concentrations was 1:50. The amount of Cl was adjusted according to the concentration of Pd^{2+} in the aqueous HPA solution and the required amount of chlorine to achieve this ratio was supplied by the addition of NaCl. For example, 1mM Pd[II] (0.01773 gr $PdCl_2$) was mixed with 48 mM NaCl (0.2805 gr) and 2mM Pd[II] (0.03564 ± 0.0001 gr $PdCl_2$) was mixed with 46 mM NaCl (0.26688 ± 0.001 gr), considering that the chlorine was also introduced with $PdCl_2$.

II.IV RESULTS AND DISCUSSION

II.IV.1 TAYLOR BUBBLE AND LIQUID SLUG LENGTHS

The lengths of Taylor bubble (TBL), liquid slug (LSL) and the unit cell (UCL) were measured for each gas-liquid mass transfer experiment with various gas and liquid flowrates. Unit cell is defined as gas bubble with a single liquid slug: UCL = TBL + LSL.

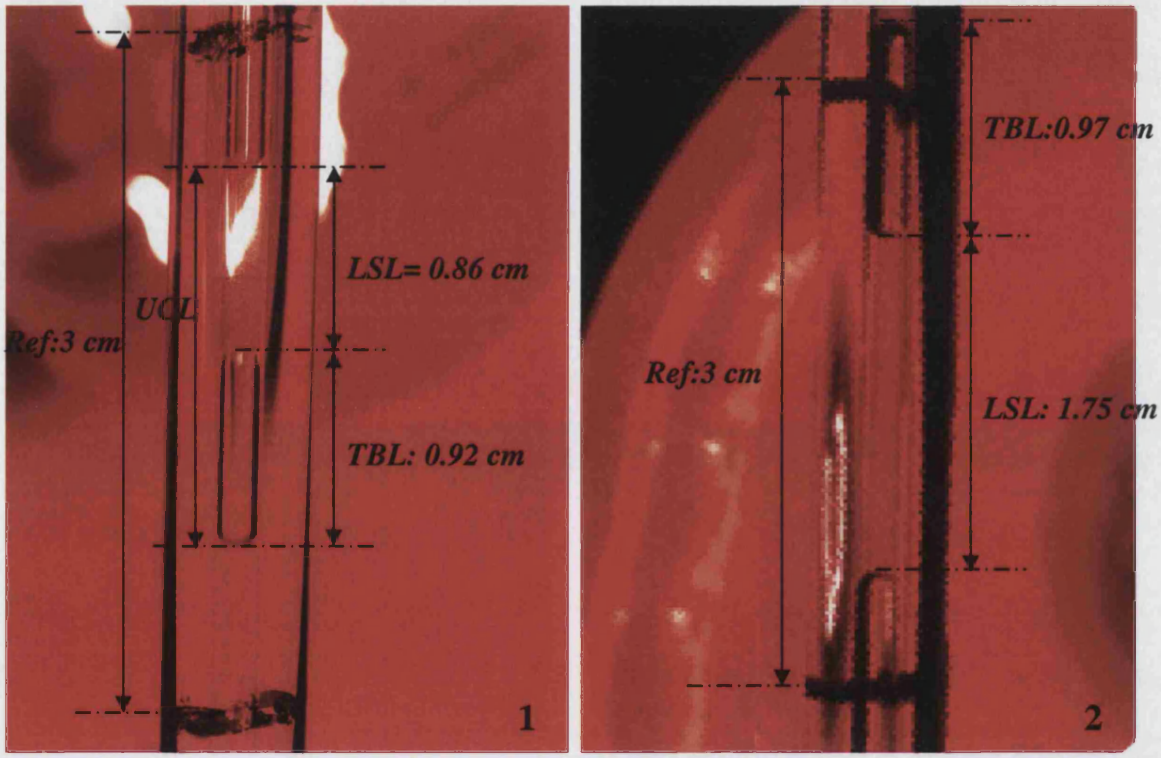

Figure II.IV- 2 Samples of images of Taylor flow [Capillary : 20 cm, H_2O=14 ml/min and C_4H_8=10(1) and 6(2) ml/min]

The change either in the gas or liquid flows induced changes in the lengths of the gas bubble and the liquid slug. Figure II.IV-1 shows two pictures that were taken during one of the experiments, in which a 20 cm long capillary was used. It can be observed that as the gas flow rate decreased liquid slug length increased significantly. The data obtained from the measurements is tabulated in tables in Appendix II.1. TBL, LSL and UCL data was also tabulated with experimentally and theoretically evaluated k_La data in Table II.IV-3.

Initially experiments were carried out using low liquid flowrates. However, at low liquid flowrates a significant experimental scatter was observed in the TBL and LSL. Then, the liquid flowrate was increased to 14 ml/min, which resulted in an appreciable decrease in the experimental error.

Figure II.IV-2 shows the effect of the gas flowrate at constant liquid flowrate on the Taylor bubble and the liquid slug lengths. It can clearly be seen that as the gas flowrate increases liquid slug length decreases while the Taylor bubble length increases. It can also be seen that the effect of the change in the gas flowrate on liquid slug lengths are greater than its effect on the Taylor bubble length.

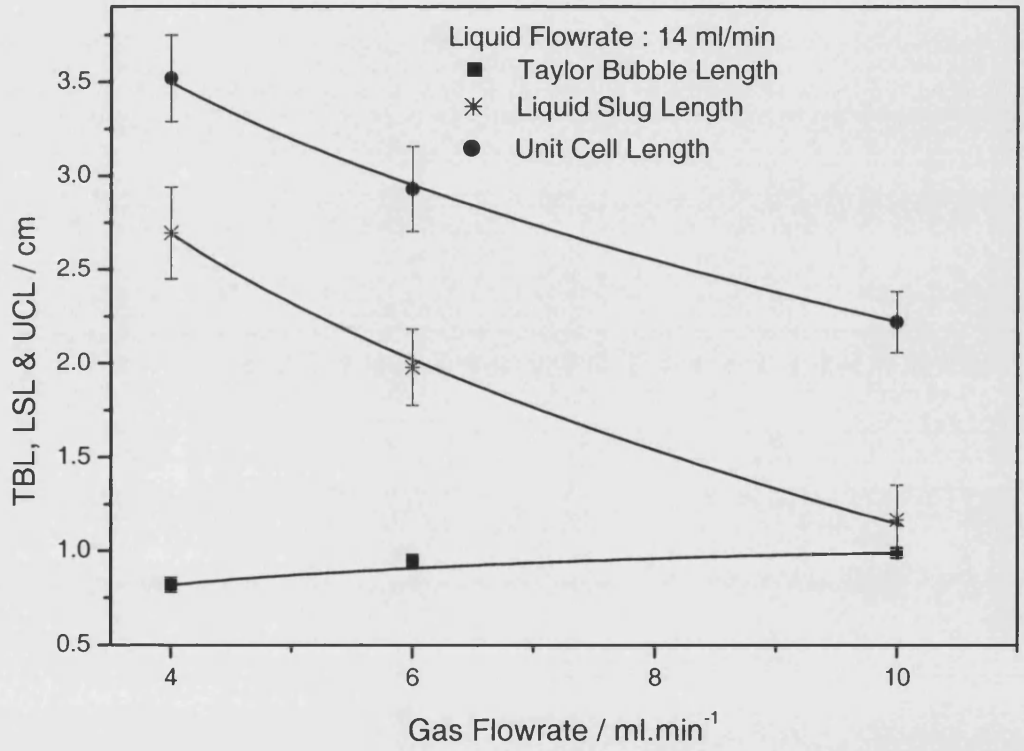

Figure II.IV- 3 Effect of gas flowrate on TBL, LSL and UCL at constant liquid flowrate.

In addition, according to the measurements carried out at constant gas flowrate and different liquid flowrates longer liquid slugs were observed at higher liquid flow rates.

Table II.IV- 1 Effect of change in liquid flowrate on TBL and LSL at constant gas flowrate (6 ml/min).

Liquid Flowrate (ml/min)	*TBL (cm)*	*LSL (cm)*	*UCL (cm)*
3.5	1.3 ± 0.4	0.65 ± 0.1	1.9 ± 0.5
13.9	0.96 ± 0.05	2 ± 0.2	2.9 ± 0.3

Table II.IV- 2 Effect of change in liquid flowrate on TBL and LSL at constant gas flowrate (15 ml/min).

Liquid Flowrate (ml/min)	*TBL (cm)*	*LSL (cm)*	*UCL (cm)*
3.6	5 ± 1	0.4 ± 0.1	7 ± 1
5.6	4.3 ±1	0.9 ± 0.1	6.3 ± 1

II.IV.2 EVALUATION OF THE EXPERIMENTAL GAS-LIQUID MASS TRANSFER COEFFICIENT

Mass transfer rate is determined by the product of the mass transfer coefficient (k_L) and the interfacial area per unit volume (a). Experimental techniques have been developed to measure both the overall mass transfer coefficient k_La and the interfacial area. Only overall coefficient (k_La) will be considered in our system, as the experimental techniques will not give satisfactory data for interfacial area.

The concentration of 1-butene in water increases as the gas-liquid flows upwards in the capillary due to the effect of the mass transfer from the gas bubble into the liquid until the liquid is saturated. If we select a control volume as shown in Figure II.IV-5, from the entrance to the exit of the reactor, mass conservation equation is given by:

$$\frac{dC}{dz} = \frac{k_L a}{\dot{V}}(C^* - C), \qquad (20)$$

where, $\frac{dC}{dz}$ is the change in the concentration along the capillary, k_L is the mass transfer coefficient, a is the specific interfacial area, $\dot{V}$ is the superficial velocity of liquid (m/s),

C^* is the saturation concentration of 1-butene in water and C is the concentration of 1-butene at z=L.

In order to obtain the total amount of gas transferred from the Taylor bubble into water the equation 20 was integrated between L=0 and L=L. It was also assumed that 1-butene concentration in water was initially equal to 0.

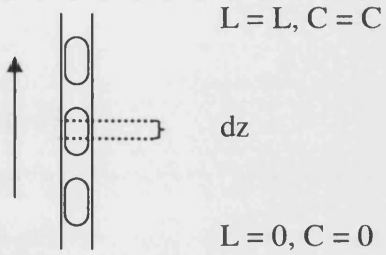

Figure II.IV- 4 Control volume of the gas-liquid mass transfer calculations

Superficial velocity of the liquid is also equal to $\dot{V} = \frac{\dot{V}_L}{A_{cs}}$ and when the equation is rewritten replacing the superficial velocity with volumetric liquid flowrate ($\dot{V}_L$) and the crosssectional area (A_{cs}), it becomes:

$$\frac{dC}{dz} = \frac{k_L a}{\dot{V}_L} A_{cs}(C^* - C), \qquad (21)$$

which can be rearranged as:

$$\frac{dC_1}{(C^* - C)} = \frac{k_L a}{\dot{V}_L} A_{cs} dz, \qquad (22)$$

and integrated:

$$\int_0^C \frac{dC}{(C^* - C)} = \int_0^L \frac{k_L a}{\dot{V}_L} A_{cs} dz, \qquad (23)$$

left side of the equation is integrated between 0 to C:

$$\int_0^C \frac{dC}{(C^* - C)} = \int_0^C -\ln(C^* - C) = -\ln(C^* - C) + \ln(C^* - 0) = \ln\frac{C^*}{C^* - C}, \qquad (24)$$

Right side of the equation 24 is integrated between 0 to L:

$$\int_0^L \frac{k_L a}{\dot{V}_L} A_{cs} dz = \int_0^L \frac{k_L a}{\dot{V}_L} A_{cs} z = \frac{k_L a}{\dot{V}_L} A_{cs} L, \qquad (25)$$

Thus, the equation below was obtained:

$$\frac{k_L a}{\dot{V}_L} A_{cs} L = \ln\frac{C^*}{C^* - C}, \qquad (26)$$

Therefore, mass transfer coefficient is equal to:

$$k_L a = \ln\frac{C^*}{C^* - C}\frac{\dot{V}_L}{A_{cs} L}, \qquad (27)$$

In order to eliminate the effect of the connecting tubing and the connectors, experiments were repeated in the absence of the reactor and this data is included in the equation as follows. It was assumed that the initial concentration was equal to the effect of the connecting parts, that is $C_1 = C_c^{out} - C_c^{in}$ and the final concentration was equal to the effect of the reactor including the connecting parts, $C_2 = C_r^{out} - C_r^{in}$. Therefore, integrating this equation between these two points, C_1 and C_2 gives the mass transfer in the reactor only. Since:

$$\int_{C_1}^{C_2} -\ln(C^* - C) = -\ln(C^* - C_2) + \ln(C^* - C_1) = \ln\frac{C^* - C_1}{(C^* - C_2)} = \ln\frac{(C^* - C_c^{out} + C_c^{in})}{(C^* - C_r^{out} + C_r^{in})}, \qquad (28)$$

and, C_c^{in} and C_r^{in} are equal to 0, the final equation becomes:

$$k_L a = \ln \frac{C^* - C_c^{out}}{C^* - C_r^{out}} \frac{\dot{V}_L}{A_{cs} L}, \qquad (29)$$

The equation above was used for the experimental k_La calculations. k_La coefficients were also calculated using empirical correlation reported by Berčič and Pintar (1997):

$$k_L a = p_1 v^{p_2} / ((1 - \varepsilon_G) UCL)^{p_3}, \qquad (30)$$

where, v is the average cell velocity (m/sec), ε_G is gas hold-up, UCL is the unit cell length (m), and finally p_1,p_2 and p_3 are the constants having the value 0.111, 1.19, 0.57, respectively [Berčič and Pintar, 1997]. p_1-p_3 fitting parameters were obtained for methane [Berčič and Pintar, 1997]. In order to obtain k_La for any other gas, the following equation is used [Berčič and Pintar, 1997].

$$(k_L a)_{Gas} = (k_L a)_{CH_4} \left(\frac{D_{Gas}}{D_{CH_4}} \right)^n, \qquad (31)$$

where, $(k_La)_{CH_4}$ is k_La of 1-butene calculated using the theoretical equation based on methane solubility in water, D_{CH_4} is the diffusivity constant of methane and D_{Gas} is the diffusivity constant of 1-butene. Diffusivity of 1-butene in water was calculated using Wilke-Chang correlation as follows:

$$D_{GL} = \frac{7.4 \times 10^{-8} T \sqrt{\psi_L \times Mw_L}}{\mu_L u_G^{0.6}}, \qquad (32)$$

where, T is temperature (K), ψ is an associate parameter for water and is 2.26, Mw is the molecular weight of water (g/mol), μ_L is the viscosity of water (cp) and u_G is the specific volume of gas (cm^3/mol). According to this correlation $D_{C_4H_8-H_2O}$ was found as, 0.95 x 10^{-5} cm^2/sec. According to Cussler [Cussler, 1984] diffusivity of methane in water is 1.49 x 10^{-5} cm^2/sec. When we put this data in the correlation,

$$(k_L a)_{C_4H_8} = (k_L a)_{CH_4} \left(\frac{0.95 \times 10^{-5}}{1.49 \times 10^{-5}} \right)^{0.5} \qquad (33)$$

we obtain,

$$(k_L a)_{Gas} = 0.798(k_L a)_{CH4} \quad (34)$$

The $k_L a$ data obtained experimentally and from the theoretical correlation is tabulated for various flow sets in Table II.IV-3.

Table II.IV- 3 Experimental and theoretical $k_L a$ data

H_2O (ml/min)	C_4H_8 (ml/min)	Velocity (m/s)	TBL (cm)	LSL (cm)	UCL (cm)	Experimental $k_L a$ (sec^{-1})	Theoretical $k_L a$ (sec^{-1})
Capillary Length: 100 cm							
14	10	0.226	1	2.05	3.05	0.066	0.150
14	10	0.226	1.05	1.5	2.55	0.070	0.166
14	6	0.188	0.97	2.13	3.1	0.073	0.108
14	6	0.188	0.88	2.1	2.98	0.074	0.110
14	4	0.169	0.86	2.9	3.76	0.036	0.080
14	4	0.169	0.84	2.84	3.68	0.037	0.081
5.6	15	0.194	1.68	0.64	2.32	0.045	0.226
5.6	15	0.194	1.8	0.61	2.41	0.051	0.221
Capillary Length: 80 cm							
14	10	0.226	1.12	1.69	2.81	0.078	0.157
14	10	0.226	1.09	1.67	2.76	0.087	0.159
14	6	0.188	1.03	2.26	3.29	0.076	0.104
14	6	0.188	0.94	2.01	2.95	0.068	0.111
14	4	0.169	0.96	3.51	4.47	0.049	0.073
14	4	0.169	0.88	3.21	4.09	0.049	0.076
5.6	15	0.194	1.71	0.65	2.36	0.044	0.224
5.6	15	0.194	1.94	0.64	2.58	0.046	0.213
Capillary Length: 60 cm							
14	10	0.226	1.26	1.7	2.96	0.076	0.153
14	10	0.226	1.19	1.46	2.65	0.075	0.163
14	6	0.188	1.12	1.41	2.53	0.070	0.121
14	6	0.188	1.12	1.41	2.53	0.070	0.121
14	4	0.169	0.9	3.24	4.14	0.052	0.076
14	4	0.169	0.9	2.9	3.8	0.037	0.080
Capillary Length: 20 cm							
14	10	0.226	0.95	1.08	2.03	0.166	0.189
14	10	0.226	1.03	1.25	2.28	0.154	0.177
14	6	0.188	0.89	2.03	2.92	0.112	0.112
14	6	0.188	1	1.93	2.93	0.106	0.111
14	4	0.169	0.85	2.97	3.82	0.063	0.080
14	4	0.169	0.79	2.42	3.21	0.055	0.088
5.6	15	0.194	1.91	0.71	2.62	0.061	0.211
5.6	15	0.194	1.91	0.7	2.61	0.043	0.211

Equilibrium Solubility of 1-butene

Equilibrium concentration of 1-butene in water was measured at atmospheric pressure and 18 °C. According to the first order exponential fit of the data obtained, it was observed that after ca. 200 min the solution reached equilibrium, and the concentration was evaluated as 0.01075 mol/L (see Figure II.IV-4). This data was used for the calculations of experimental gas-liquid mass transfer coefficient in the tube side.

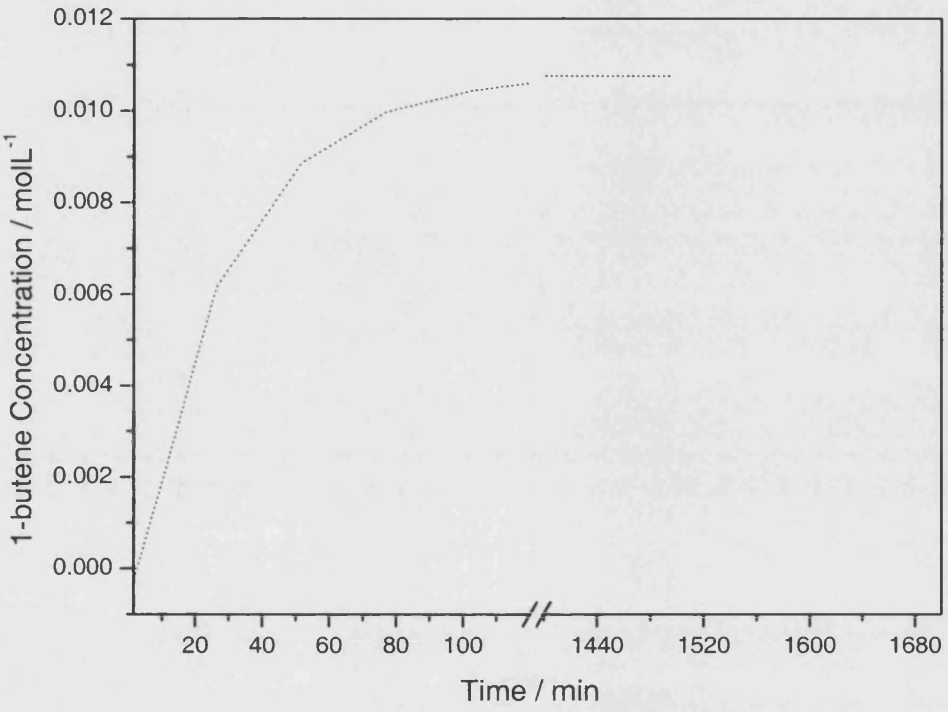

Figure II.IV- 5 Equilibrium solubility of 1-butene

The solubility data found in the literature is 0.004 mol/L at 25 °C [Gallant and Yaws, 1992]. This data is lower than the value that was obtained in this study. This is most probably due to the temperature difference or the calibration of the GC.

Factors Effecting k_La

The effects of TBL-LSL-UCL and velocity of the total flow on the experimentally and theoretically evaluated k_La were investigated. Figure II.IV-5 shows the effect of the velocity and it can easily be seen that the velocity plays an important role. As the velocity increases k_La increases linearly. Berčič and Pintar (1997) also observed this

effect, reflected in the derived empirical correlation (Eqn. 30). Using equation 30, theoretical values of k_La were also calculated and the data are shown in Figure II.IV-5. There are two points at each velocity showing the repeat of the experiment.

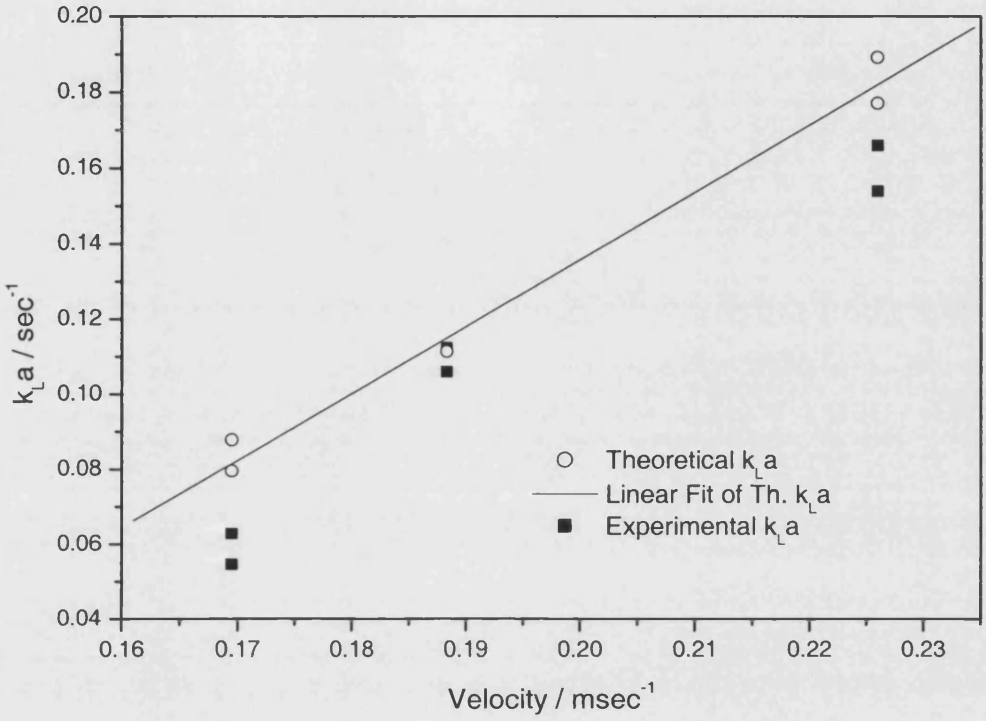

Figure II.IV- 6 Effect of velocity on k_La

In order to calculate theoretical k_La values shown in Figure II.IV-6, experimentally measured unit cell lengths were used. Since UCL measurements were repeated, both values obtained were used for the calculation of the theoretical k_La values and pointed on Figure II.IV-6.

It was observed that the k_La decreases significantly with an increase in LSL at constant TBL. Figure II.IV-6 shows the data obtained with the 20 cm capillary. By lowering the water flowrate and increasing the gas flowrate it is possible to obtain longer TBL and shorter LSL as it is shown in Table II.IV-4 from the data obtained for 5.6 ml/min water flowrate and 15 ml/min gas flowrate. However, experimental k_La obtained for this set of flowrates is considerably lower than it is for the rest of the experimental sets. When the system was carefully studied it was seen that the amount of mass transfer occurring in the connecting lines is much greater for this condition than for others. Table II.IV-4 shows

the experimental data collected from the measurements carried out in the absence of the reactor, marked as "bare".

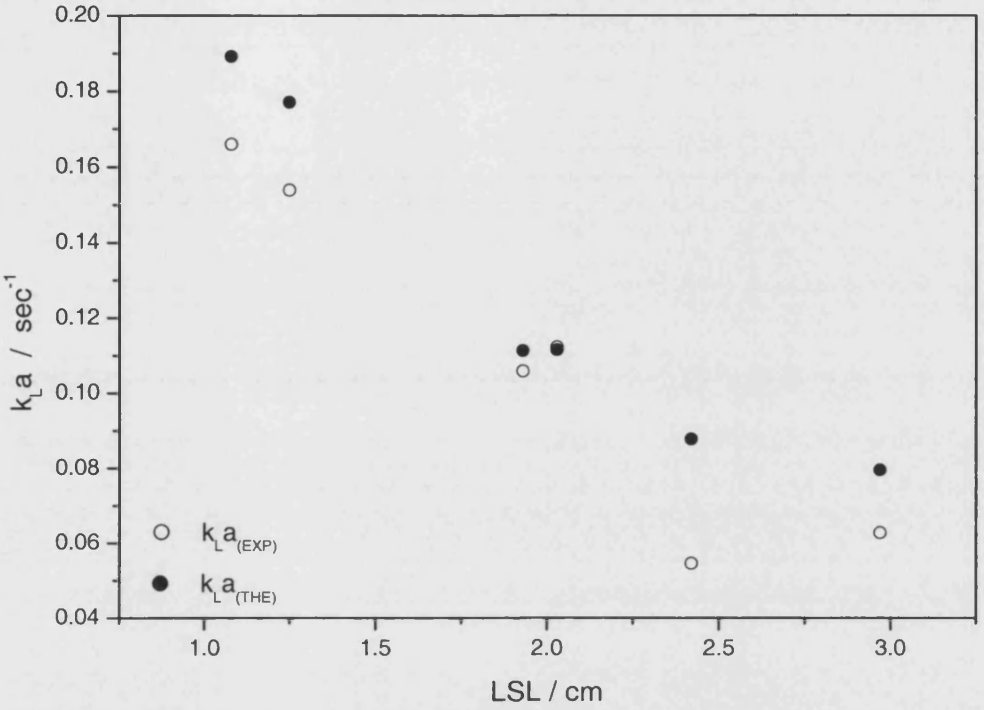

Figure II.IV- 7 Effect of LSL at constant TBL

Table II.IV- 4 Effect of connecting pieces on the mass transfer

H_2O (ml/min)	C_4H_8 (ml/min)	Concentration Full Out mol/m^3	Concentration Bare Out mol/m^3	Experimental k_La (sec^{-1})
14	10	5.190	1.547	0.066
14	10	5.339	1.547	0.070
14	6	5.233	1.1475	0.073
14	6	5.261	1.1475	0.074
14	4	3.226	0.8915	0.036
14	4	3.328	0.8915	0.037
5.6	15	7.508	3.1925	0.045
5.6	15	7.851	3.1925	0.051

This finding clearly shows that the external effects, e.g. connecting lines, on the mass transfer should be carefully studied.

II.IV.3 OXYGEN TRANSFER THROUGH THE MEMBRANE

In order to obtain the required amount of oxygen dissolved in the liquid phase in the tube side of the reactor, where the reaction takes place, one should have a good knowledge of the effect of the concentration and the flow of oxygen in the reactor. Hence, oxygen transfer through the carbon membrane was studied, at 400 and 500 ml/min total shell flowrate with different partial oxygen pressures, various tube gas flow rates between 10 and 5 ml/min, and a constant liquid flowrate in the tube side at ca. 15 ml/min.

The effects of the change in total shell flowrate, partial pressure of oxygen and the liquid flowrate in the tube side can clearly be seen in the figures below. Figure II.IV-7 shows the increase in the oxygen concentration in water and eventually equilibrates. It can be seen that it is a very rapid process.

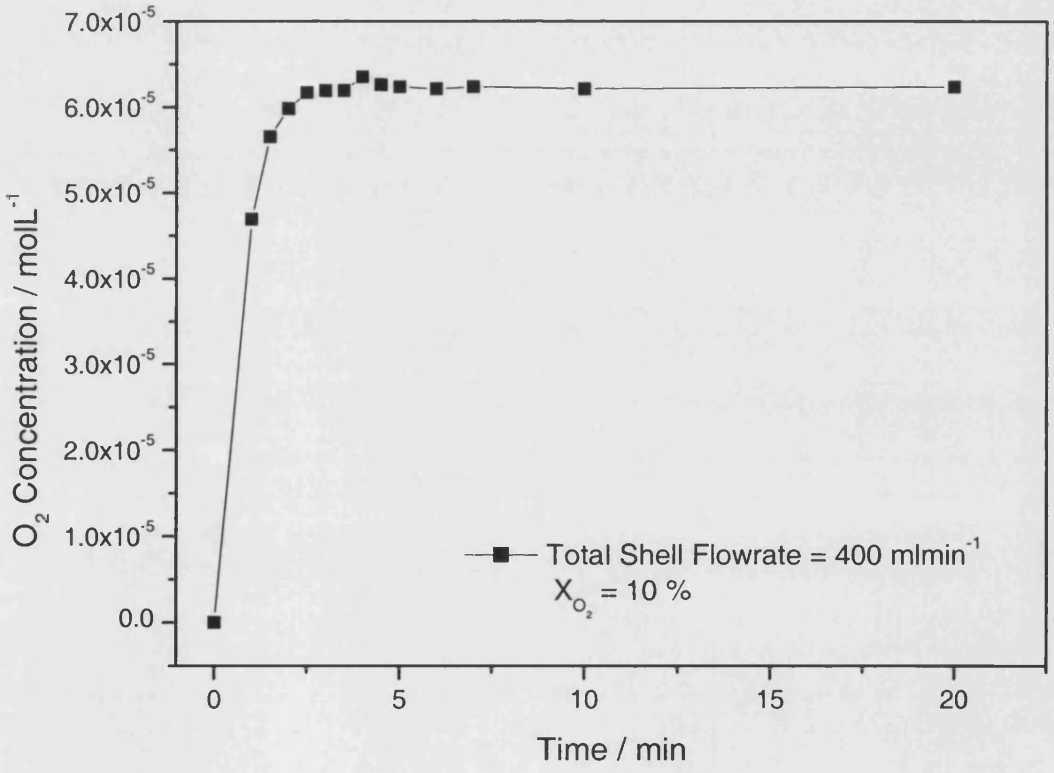

Figure II.IV- 8 Increase in the oxygen concentration in water (Tube Gas Flowrate: 10 ml/min)

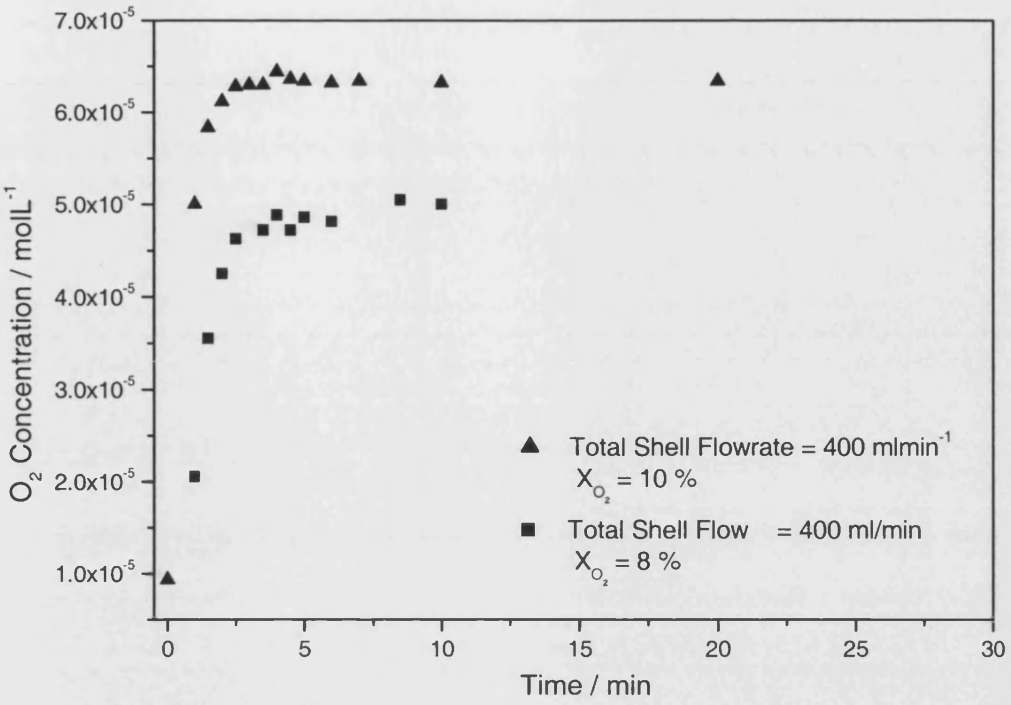

Figure II.IV- 9 The effect of the oxygen concentration, tube gas flowrate is 10 ml/min.

As the partial pressure of oxygen in the shell flow increases, the solubility of oxygen in the tube side liquid increases as it is expected according to the Henry's Law. Henry's Law is explained at the end of this section. Figures II.IV-8 and II.IV-11 demonstrate this effect clearly. It has also been observed that the higher tube gas flowrate gives lower oxygen concentration, similarly due to the lower oxygen partial pressure. Increasing nitrogen flowrate in the tube will increase the total pressure in the system, resulting in the decrease of the oxygen partial pressure and lower solubility of oxygen.

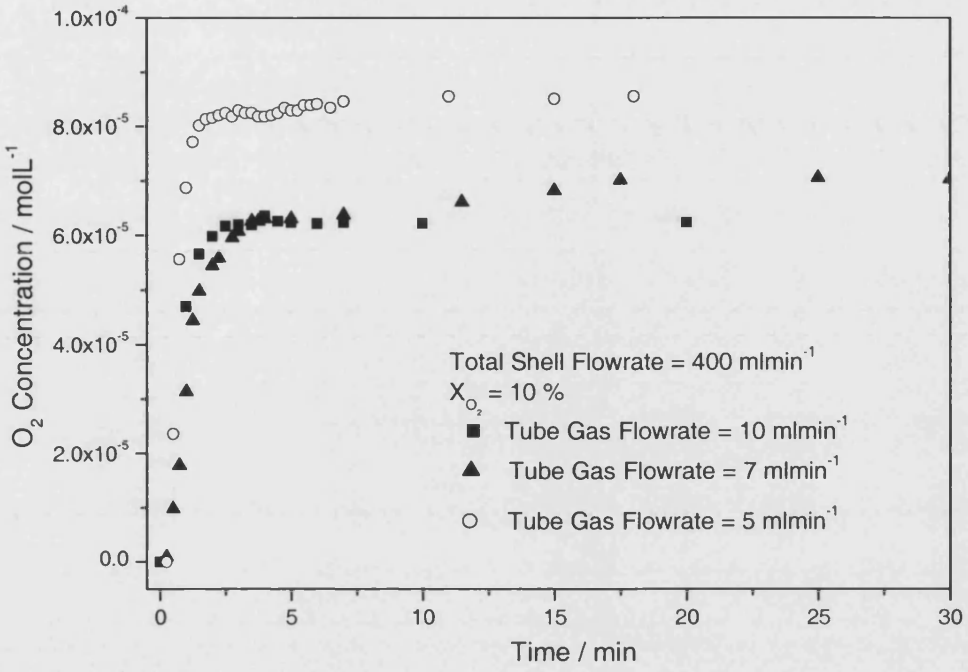

Figure II.IV- 10 The effect of the tube gas flowrate, partial pressure of oxygen is 0.1 in the shell flow

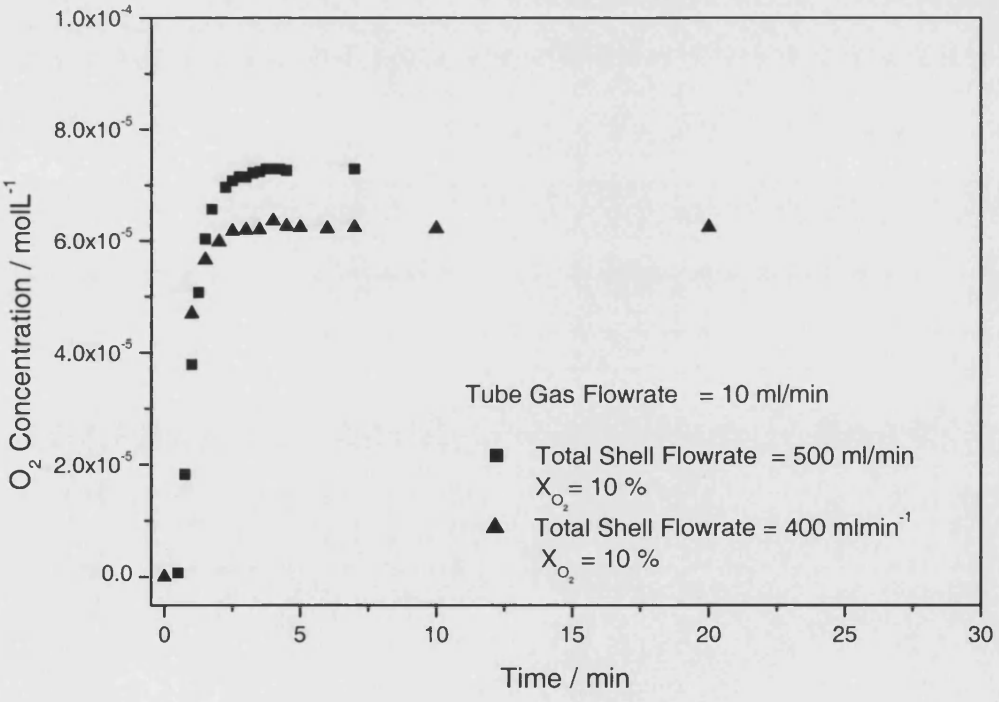

Figure II.IV- 11 The effect of the total shell flowrate on the solubility of oxygen

Figure II.IV-10 shows the effect of the total shell flowrate on the solubility of oxygen in the tube side liquid.

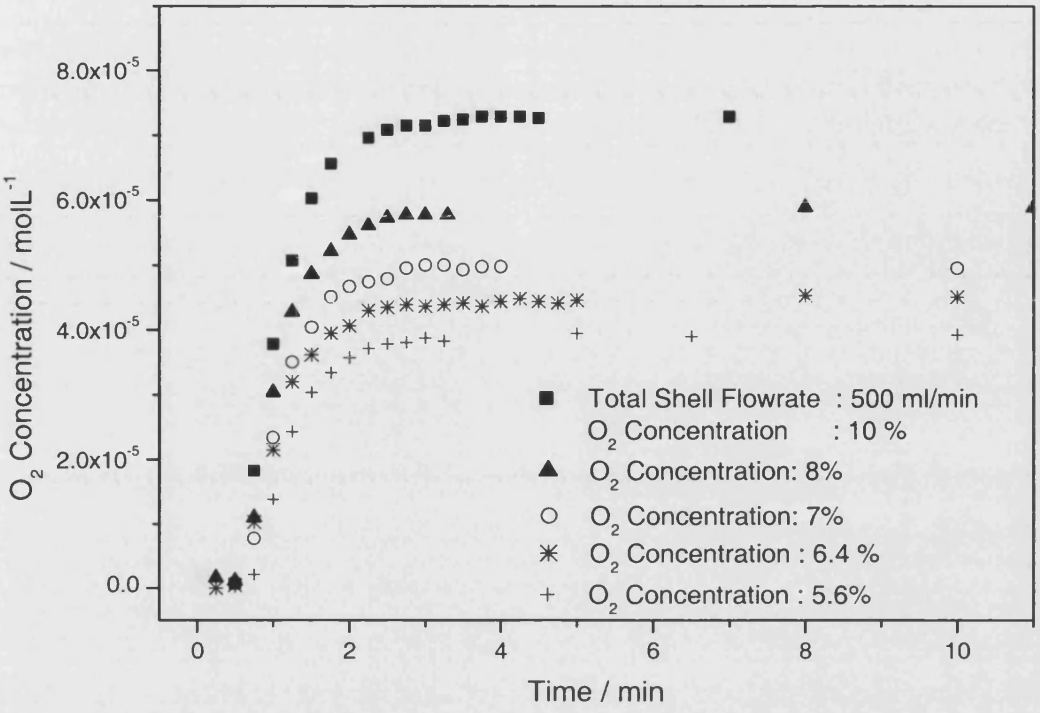

Figure II.IV- 12 The effect of the oxygen concentration in the shell flow on the solubility of oxygen, tube gas flowrate is 10 ml/min

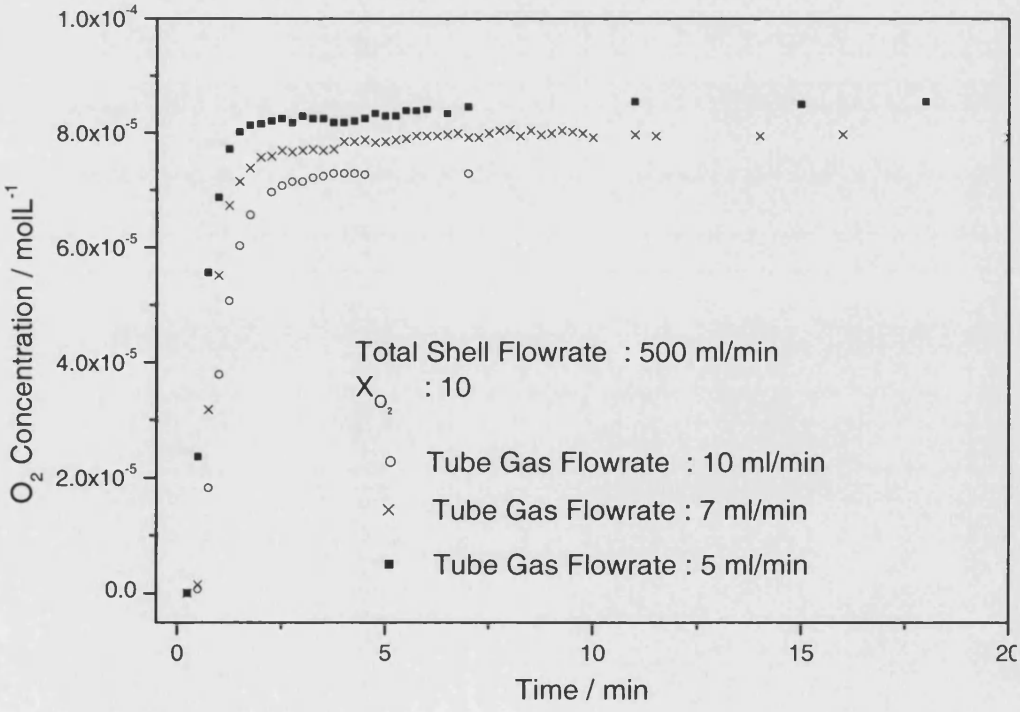

Figure II.IV- 13 The effect of the tube gas flowrate on the oxygen solubility

Henry's law

Henry's law describes the relation between solubility and the partial pressure of a gas. Solubility is the amount of particular solute that can dissolve in a given amount of a particular solvent. In order to improve the solubility of gasses in water, the magnitude of their negative entropies of solution must be decreased. One way to accomplish that is to make the gas above the solvent more ordered by increasing the pressure of the gas. William Henry discovered this property of the gasses and reported the relation as follows:

$$C = kp \qquad (35)$$

where, C is the concentration of the dissolved gas (mol/L), p is the partial pressure of the gas (atm) and k is the Henry's constant (mol/Latm). This equation has been used for estimation of the oxygen solubility in the liquid phase in the tube as follows. Solubility of oxygen in water against various partial pressures of oxygen was drawn in a figure. Figures II.IV-13 and II.IV-14 show these data for 400 and 500 ml/min total shell flowrates, respectively. These slopes of the lines in Figures II.IV-13 and II.IV-14 give the constants of the Henry's Law equation and they are 0.00062 and 0.00072 $molL^{-1}atm^{-1}$ for 400 and 500 ml/min respectively.

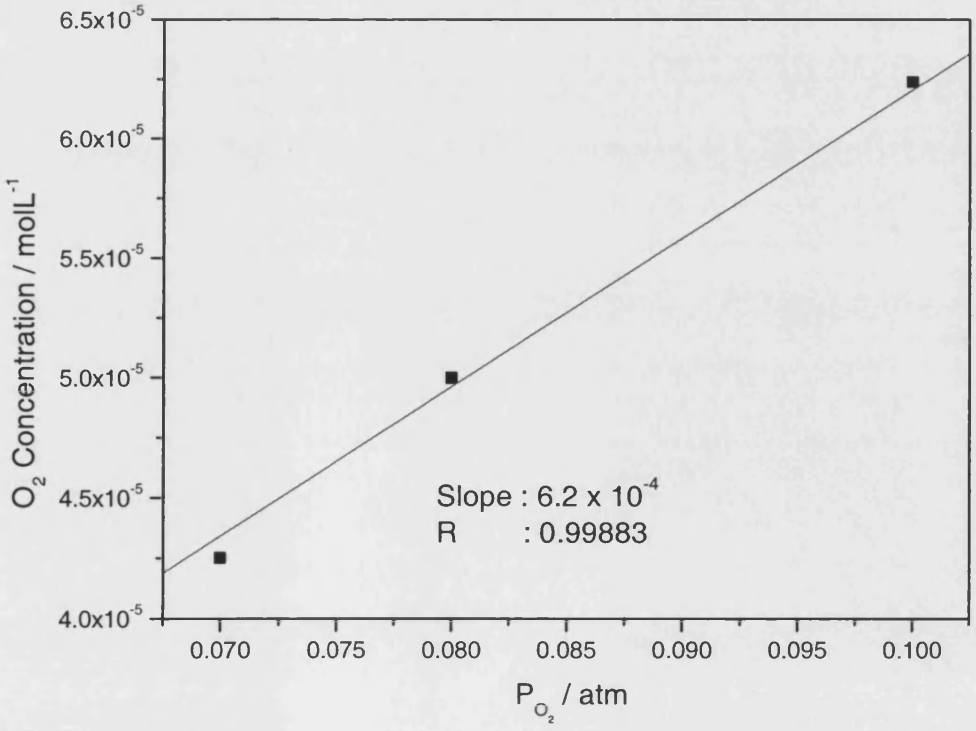

Figure II.IV- 14 Solubility of Oxygen, total shell flow: 400 ml/min

These coefficients were used to calculate required oxygen pressure in the shell flow for the hydrocarbon oxidation experiments.

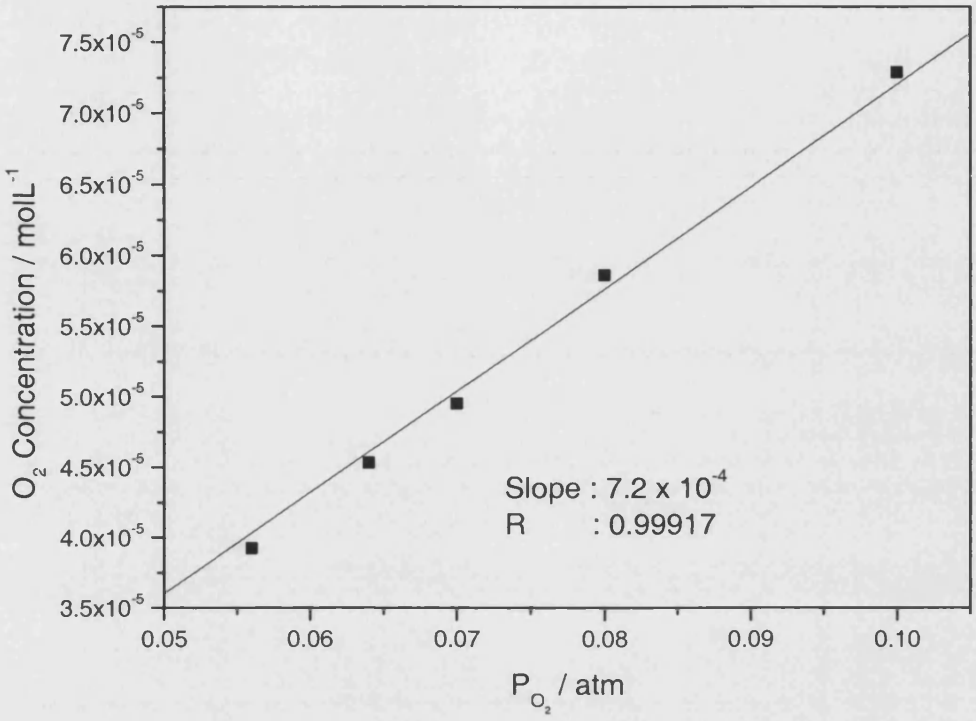

Figure II.IV- 15 Solubility of oxygen, total shell flow: 500 ml/min.

Oxygen concentration in the reactor was adjusted according to the estimated 1-butene amount in the catalyst solution so that the stoichiometric ratio of oxygen to olefin in the catalyst solution 1:2 is achieved. Henry's constant obtained from 1-butene solubility measurement is 0.0107475 mol/Lbar. Using this value, 1-butene concentration in the catalyst solution was calculated for a known 1-butene partial pressure and this value was confirmed with an experiment by switching the feed gas off and consuming the total feed gas present in the catalyst solution. Using nitrogen – 1-butene gas mixture with 0.35 bar 1-butene pressure, the amounts of 1-butene dissolved in the solution calculated with Henry's constant and experimentally were 3.8 mmol/L and 3 mmol/L, respectively. That proves that the Henry's constant obtained had a reasonable value.

The 1-butene concentration in the feed gas mixture was adjusted to 10 %. Therefore the concentration of 1-butene in the catalyst solution at 1 bar system pressure was predicted as 1.07475 mmol/L. When the pressure inside the tube was 1 bar, pressure in the shell

side was 1.15 bar. When the partial pressure of oxygen was set to 0.92 bar in the shell side, according to the Henry's Law (k_{O_2} = 0.62 mmol/Lbar) dissolved oxygen amount in the catalyst solution was, 0.57 mmol/L. The stoichiometric ratio of oxygen to olefin in the catalyst solution therefore 1:2 was achieved with 400 ml/min O_2+N_2 flowrate and 80% O_2 concentration.Solubility of oxygen in this study, 19.57 mg/L, was found higher than the data reported in literature, 9.09 mg/L, most probably due to a systematical error made during the experiments.

II.IV.4 CATALYTIC OXIDATION OF 1-BUTENE TO MEK

Catalytic oxidation of 1-butene was performed as a test reaction in order to observe the performance of the Taylor flow membrane reactor. Various parameters were studied and reaction rates were obtained accordingly. These parameters were:

- Catalyst concentration
- Temperature
- Total pressure
- Feed gas concentration
- Feed gas flowrate
- HPA concentration
- Oxygen Pressure and trans-membrane pressure

The analysis of gas-liquid oxidation reactors requires separation of mass transfer and reaction kinetics effects and is a difficult issue as the coupling between mass transfer and chemical reaction needs to be considered also. The behaviour of such reactors is dominated by the relative rates of mass transfer and chemical reaction. The location of the reaction and the impact of operating variables on the reaction are also dictated by these rates. Although kinetics are usually determined under conditions of reaction, i.e. same temperature and pressure, difficulties arise in prediction of mass-transfer rates as they were measured at ambient conditions and oxidation reactions are usually carried out at higher temperatures and pressures. It is not clear that extrapolation of the data obtained at ambient conditions to higher temperature and pressure is a valid exercise. Therefore, we will use the obtained data to optimise the process conditions.

Calculation of the Reaction Rates

The system is fed with the fresh 1-butene-nitrogen mixture continuously and the liquid catalyst solution is recycled in the system. Figure II.IV-15 shows a simple diagram of a batch-recycle reactor with a liquid reservoir that is very similar to our system. Reaction rates were calculated assuming a differential-reactor operation in the system, in which the reaction constant is nearly constant throughout the reactor.

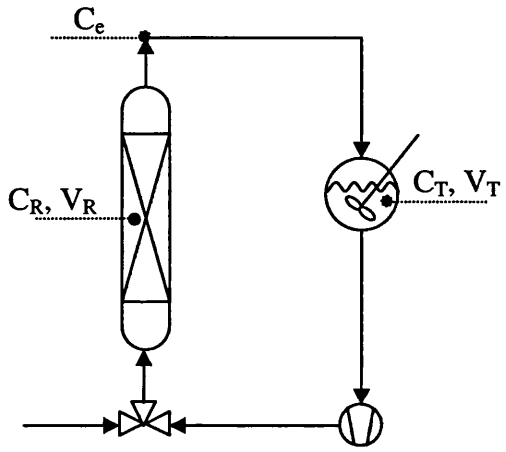

Figure II.IV- 16 Schematic diagram of batch recycle reactor

Firstly a mass balance is written around the entire system of reactor and reservoir in Figure II.IV-15. It is assumed that the volume of the connecting lines, valves and the pump is negligible and that the reaction only occurs in the reactor. The rate of production of MEK is equal to $\int_0^{V_R} r_{MEK} dV_R$. Both the volumes of the reactor V_R and the reservoir V_T will have a contribution to the accumulation term. These volumes will be assumed to be constant and the content of the reservoir well mixed. Hence, the total accumulation of MEK can be expressed as;

$$\left\{\begin{array}{l}\text{Rate of MEK into}\\ \text{volume element}\end{array}\right\} - \left\{\begin{array}{l}\text{Rate of MEK out}\\ \text{of volume element}\end{array}\right\} + \left\{\begin{array}{l}\text{Rate of production}\\ \text{of MEK within the}\\ \text{volume element}\end{array}\right\} = \left\{\begin{array}{l}\text{Rate of accumulation of}\\ \text{MEK within the volume}\\ \text{element}\end{array}\right\}$$

Since rate of MEK into volume element and rate of MEK out of volume element are equal to zero. The equation is rewritten as;

$$\left\{\begin{matrix}\text{Rate of production}\\ \text{of MEK within the}\\ \text{volume element}\end{matrix}\right\} = \left\{\begin{matrix}\text{Rate of accumulation of}\\ \text{MEK within the volume}\\ \text{element}\end{matrix}\right\}$$

That is equal to the rate of production of MEK in the reactor and the reservoir. The equation can be written as below;

$$\int_0^{V_R} r_{MEK} dV_R = V_R \frac{dC_R}{dt} + V_T \frac{dC_T}{dt} \qquad (36)$$

It was also assumed that the concentration also doesn't change significantly in the system after leaving the reactor; hence, $C_R \approx C_T$. So, the equation becomes;

$$rV_R = (V_R + V_T)\frac{dC_T}{dt} \qquad (37)$$

$$r = \frac{(V_R + V_T)}{V_R}\frac{dC_T}{dt} \qquad (38)$$

The equation above was used to calculate the overall reaction rate. Furthermore, the change in the concentration of MEK per pass, that is C_T, was calculated as follows. Mass balance around the reactor for MEK is written as below:

$$QC_T - QC_e + \int_0^{V_R} r dV_R = V_R \frac{dC_R}{dt} \qquad (39)$$

As, $\int_0^{V_R} r_{MEK} dV_R = V_R \frac{dC_R}{dt} + V_T \frac{dC_T}{dt}$ the equation above can be rewritten as,

$$QC_T - QC_e + V_R \frac{dC_R}{dt} + V_T \frac{dC_T}{dt} = V_R \frac{dC_R}{dt} \qquad (40)$$

$$Q(C_T - C_e) = -V_T \frac{dC_T}{dt} \qquad (41)$$

$$C_T - C_e = -\frac{V_T}{Q}\frac{dC_T}{dt} \qquad (42)$$

$$C_e - C_T = \frac{V_T}{Q}\frac{dC_T}{dt} \qquad (43)$$

Since,

$$r = \frac{(V_R + V_T)}{V_R}\frac{dC_T}{dt} \qquad (44)$$

and therefore,

$$\frac{dC_T}{dt} = r\left(\frac{V_R}{V_R + V_T}\right) \qquad (45)$$

$$C_e - C_T = \frac{V_T}{Q} r\left(\frac{V_R}{V_R + V_T}\right) \qquad (46)$$

Effect of Catalyst Concentration

Pd^{2+} concentration was varied between 0 and 2 mmol/L. Temperature, pressure and HPA concentration were kept constant at 30 °C, 3.5 atm and 50 mmol/L, respectively. Flowrate of the nitrogen-1-butene mixture was 10 ml/min, while the liquid flowrate was adjusted to 14 ml/min on the tube side.

Table II.IV-5 shows the change in the reaction rate against the change in Pd^{2+} concentration. The experiment was repeated keeping all the parameters constant. However, for repeated experiments, the difference between the feed gas concentrations was unavoidable. Feed gas concentration of experiment 34 was 50 % higher than experiment 33 and it made a significant difference. On the other hand, experiment 14 and 16 that were carried out under same conditions and had similar feed gas concentrations gave very similar reaction rate values.

Theoretically, rate of reaction must be equal to zero if there is no catalyst present in the system. However, in the absence of palladium the observed reaction rate was 9.57 mmol/Lmin. This is most probably due to the amount of palladium deposited in the system during the previous experiments.

Table II.IV- 5 Effect of the catalyst concentration on the reaction rate

No of Experiment	*Pd^{2+} (mmol/L)*	*Feed Gas Concentration (mmol/L)*	*Reaction Rate (mmol/Lmin)*
29	0	18.5	9.57
33	1	12.3	21.53
34	1	18	37.13
14	2	10.2	24.44
16	2	10.3	22.31

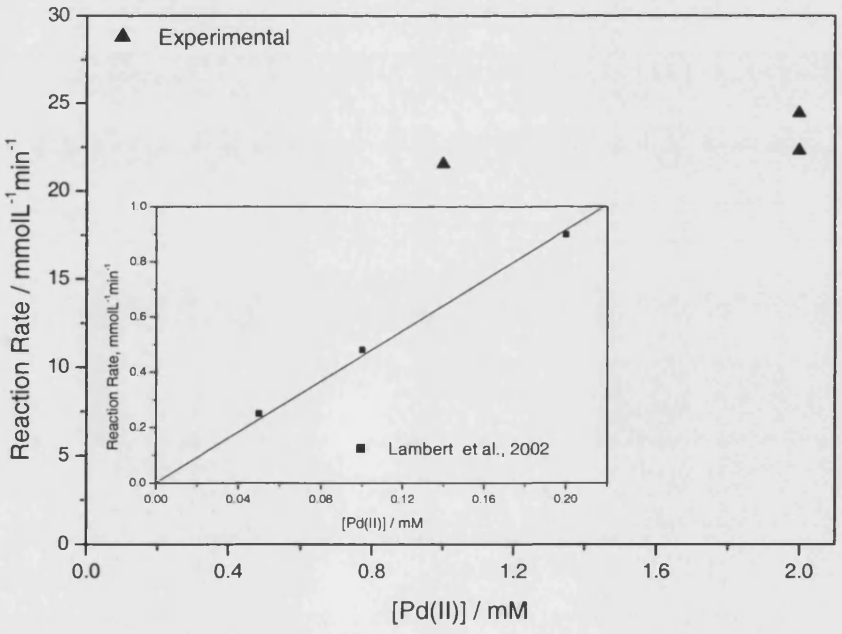

Figure II.IV- 17 The effect of the catalyst concentration on the reaction rate.

Lambert et al. (2002) studied the kinetics of 1-butene oxidation to MEK using same catalyst system and showed that the reaction rate increases linearly with increasing Pd(II) concentration, between the concentrations of 0 and 0.2 mmol. It is expected that the reaction rate will further increase with the increased catalyst concentration. However, Lambert et al. also observed that the oxidation of 1-butene follows a complex course with a monotonous decrease of the reaction rate as the conversion of V(V) to V(IV) completes. They explain this behaviour by the isomerisation of 1-butene to less reactive 2-butene and by the formation of relatively strong π-allyl Pd (II) complexes which could decrease catalyst activity in 1-butene oxidation. In this work, reaction was studied at higher Pd(II) concentrations in order to obtain higher reaction rates. The reaction rate data obtained from the experiments carried out with 1 and 2 mM Pd(II) and similar feed gas concentration is shown in Figure II.IV-18. According to earlier kinetic study of one-stage 1-butene oxidation carried out by Lambert et al., it is expected that the reaction rate would double as the catalyst concentration is doubled. However, it is not straight forward, due to different feed gas concentrations, and possibility of isomerisation of 1-butene and formation of π-allyl Pd (II) complexes. Additionally, this could also indicate that the system was mass transfer limited and the reaction rate strongly depend on the solubility of the feed gas, 1-butene.

Temperature Effect

Temperature was varied between 30 and 50 °C, while all other parameters were kept constant. Table II.IV.6 shows the experimental conditions and the reaction rates evaluated for each experiment.

Table II.IV- 6 Effect of temperature on the reaction rate.

No of Experiment	*Temperature (°C)*	*Feed Gas Conc. (mmol/L)*	*Reaction Rate (mmol/Lmin)*
14	30	10.2	24.44
16	30	10.3	22.31
42	40	8.78	12.82
43	40	9.31	11.91
40	50	9.13	14.44
41	50	8.85	13.18

Figure II.IV-17 shows the effect of the temperature on the reaction rate. It is suggested by Arrhenius Law that the reaction proceeds faster at higher temperatures.Additionally, Lambert et al. observed that as the temperature increases, reaction rate increases under kinetic control in one-stage 1-butene oxidation [Lambert et al., 2002]. However, solubility hence the concentration of the feed gas in the catalyst solution is also a function of temperature. In the majority of cases, gas solubility decreases with an increase in the temperature. Thus, an increase in the temperature results both in the decrease in the solubility of 1-butene and increase in the reaction rate.

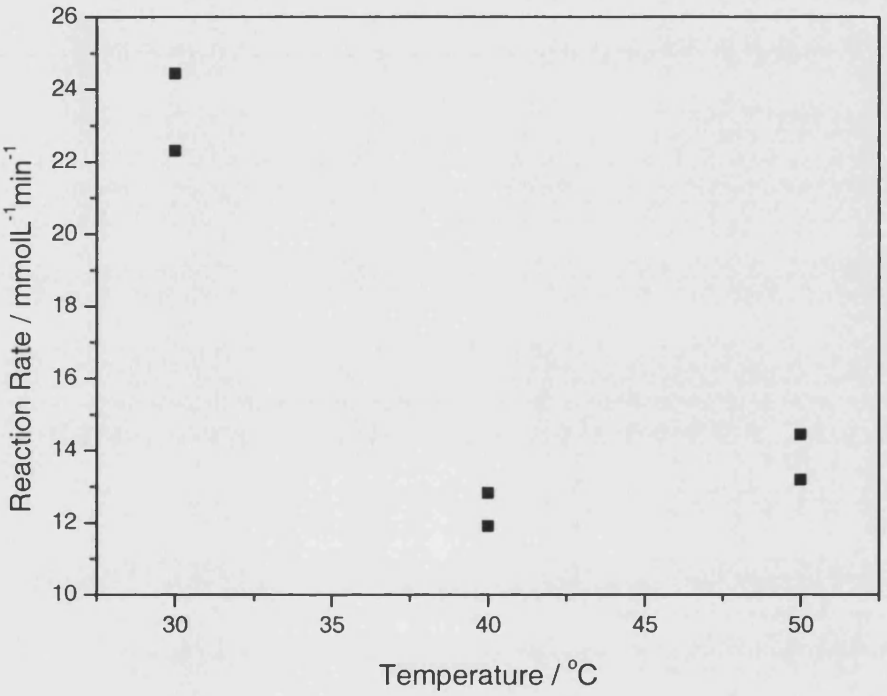

Figure II.IV- 18 Effect of the temperature on the reaction rate

However, overall, due to the decrease in the reaction rate it is clearly shown that the solubility has a dominant effect and indicates that the system is mass transfer limited confirming the independence of the reaction rate on the Pd (II) concentration.

Effect of Total Pressure

Pressure of the system was varied between 1 bar and 6 bar, while all other parameters were constant. Reaction rates obtained are tabulated in Table II.IV-7.

Table II.IV- 7 Reaction rates obtained at various pressures

No of Experiment	*Pressure (bar)*	*Feed Gas Conc. at 1bar (mmol/L)*	*Reaction Rate (mmol/Lmin)*
27	1	24.6	95.82
14	3.5	10.2	24.44
16	3.5	10.3	22.31
21	6	12.3	69.29
25	6	10.6	43.08

Feed gas flowrate was similar in experiments 14, 16 and 25. Therefore, these experiments were compared to study the effect of pressure.

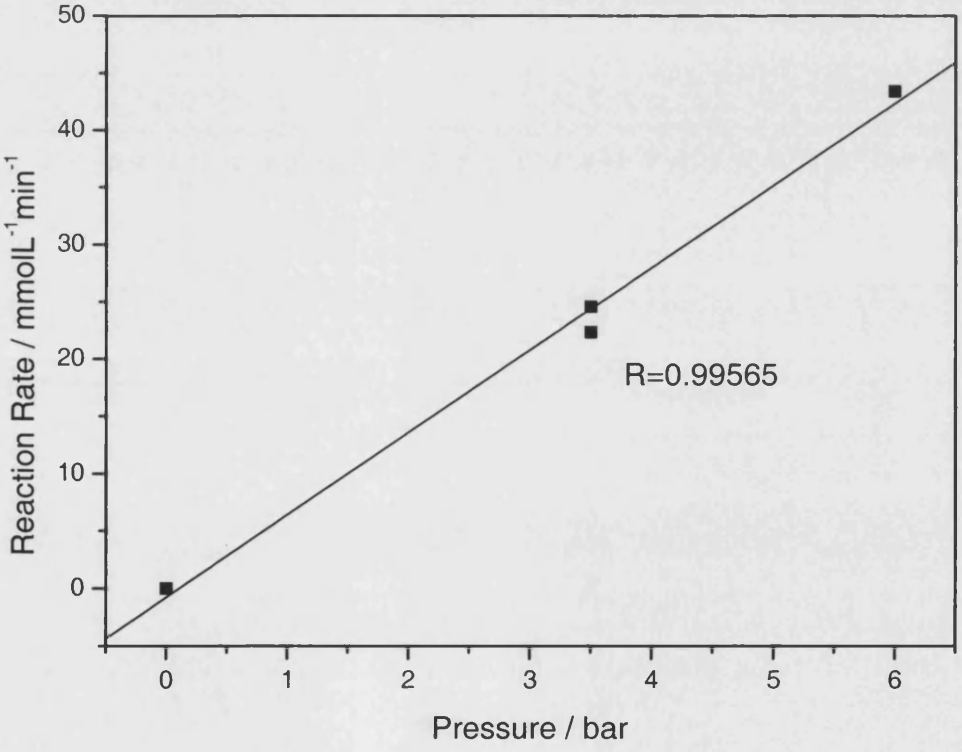

Figure II.IV- 19 Effect of the pressure on reaction rate

According to Henry's Law, as the partial pressure of the gas increased, the solubility in the solvent also increases. Feed gas concentration was measured at 1 atm. 10.3 mmol. According to universal gas law, that is equal to 0.25 L C_4H_8 / 1 L of mixture and that is

also equal to 0.25 bar C_4H_8 partial pressure at 1 bar. As the gas concentration is constant, when the pressure is 3.5 and 6 atm, partial pressure of 1-butene will be 0.875 and 1.5 bar, respectively. Increase in the partial pressure will linearly increase the solubility of feed gas and hence the reaction rate. Figure II.IV-20 clearly shows that there is a linear relation between the pressure and the reaction rate in our system.

Feed Gas Concentration Effect

Feed concentration is directly related to the partial pressure of the feed gas, hence the reaction rate. Table II.IV-8 shows the results obtained from the experiments run at 1 and 6 bar total pressure.

Table II.IV- 8 Effect of feed gas concentration on reaction rate

No of Experiment	*Total Pressure (bar)*	*Partial Pressure (bar)*	*Feed Gas Conc. (mmol/L)*	*Reaction Rate (mmol/Lmin)*
47	1	1	30.1	56.37
36	1	0.4	17.1	8.682
21	6	1.5	12.3	69.29
25	6	1.3	10.6	43.083

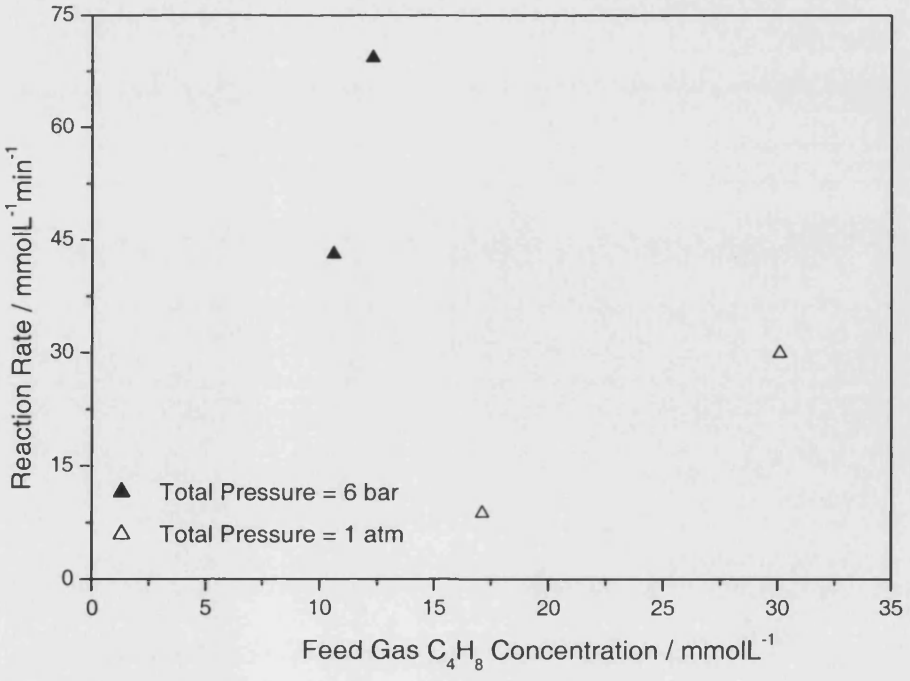

Figure II.IV- 20 Effect of the feed gas 1-butene concentration

Higher system pressure allows higher partial pressure of 1-butene. Therefore, if the feed concentration and the total system pressure are increased simultaneously, higher reaction rates will be achieved.

Two additional experiments were run to observe the effect of 1-butene concentration in the solution. In these experiments 1-butene-nitrogen flow was switched to pure nitrogen after 1 hr and the experiment was carried out in the absence of 1-butene for 1 hr (see Figure II.IV-20). Following that 1-butene flow was reintroduced in to the system. 1-butene that already existed in the system was consumed in the next 20 min, MEK production was then stopped at the 80th minute indicating the complete consumption of 1-butene. When 1-butene was re-introduced in to the system at the 120th minute, it was observed that MEK production started at 140th min of the experiment. Besides, 20 minutes delay in the production of MEK was also observed in the first 20 min of the experiments. It is clear that the reaction is limited in the first 20 minutes due to the resistance in the mass transfer of 1-butene.

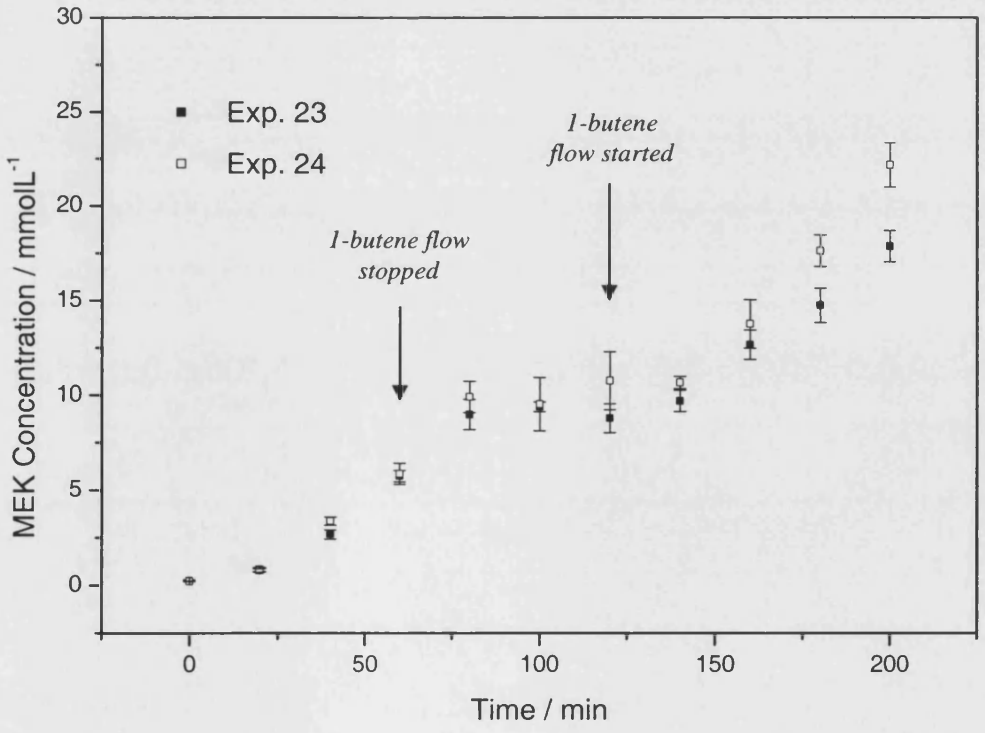

Figure II.IV- 21 Reaction in the absence of the 1-butene flow

Effect of the Feed Gas Flowrate in the Tube Side

Gas and the liquid flowrates used in the tube side were selected according to the results obtained from the gas-liquid mass transfer measurements that were performed in the glass capillaries. Selected gas-liquid flowrates; 10 ml/min 1-butene and 14 ml/min water, gave the highest gas-liquid mass transfer coefficients using a glass capillary of 20 cm.

Table II.IV- 9 Reaction rates observed at various tube gas flowrates.

No of Experiment	*Tube Gas Flow (ml/min)*	*Feed Gas Conc. (mmol/L)*	*Reaction Rate (mmol/Lmin)*
14	10	10.2	24.43
16	10	10.3	22.31
38	6	8.58	5.4
39	6	8.93	6.31
17	4	11.7	9.93
18	4	9.68	8.09

It was observed from the gas-liquid mass transfer measurements that as the gas flowrate decreases mass transfer also decreases. However we have observed that the reaction rate measured in the experiment with 4ml/min tube side gas flowrate is slightly higher than that measured with 6 ml/min tube side gas flowrate. This is most probably caused by the difference between 1-butene concentrations in the feed gas. Feed gas concentrations of the experiments are tabulated in Table II.IV-9.

HPA Concentration

Table II.IV-10 shows the results obtained from the experiments performed at two different HPA contents. 1-butene concentrations in the feed gas for experiments 44 and 50 are almost equal. When these two experiments are compared it can easily be seen that the reaction rate is almost double as the HPA concentration is doubled.

Table II.IV- 10 Effect of HPA concentration on the reaction rate

No of Experiment	*HPA Conc. (mmol/ml)*	*Feed Gas Conc. (mmol/L)*	*Reaction Rate (mmol/Lmin)*
30	25	18.65	34.26
44	25	8.35	11.55
15	50	8.36	21.15

From the experiments that were run in the absence of oxygen, the change in the colour of the HPAs solution indicating HPA reduction was clearly observed as shown in Figure II.IV-21.

Figure II.IV- 22 Reduction of HPA in the catalyst solution

Oxygen Concentration and Trans-membrane Pressure

In order to observe whether the reduced HPA solution was re-oxidised by molecular oxygen and predicted reaction mechanism was working, 1-butene oxidation reaction was performed in the absence of oxygen.

Figure II.IV-23 shows the data obtained from experiments 46 and 47 that were performed with 50 and 25 mM HPA catalyst solution, respectively. In both experiments MEK concentration gradually increased and eventually reached a plateau. Oxygen was introduced at this point, however no further increase was observed as seen in Figures II.IV-23. It is probably due to reduced Pd depositing on the surface of the system. Once

palladium was reduced it must be re-oxidised immediately. Deposition of palladium was also observed visibly in the system. Connecting tubing used was transparent PTFE tubing. At the end of the reaction tubing was coated with palladium as seen in Figure II.IV-22. Therefore, after the reduction of palladium, introduction of oxygen showed no effect on the MEK production.

Figure II.IV- 23 Palladium deposited on the PTFE tubing

These two experiments have also allowed us to study redox reaction taking place in the HPA via V^{V} and V^{IV}. Each HPA molecule contains 3 V^{V}, for example in 25 mM HPA solution, there is 75 mM V^{V}. In order to re-oxidise 1 mM Pd (0) 2 mM V^{V} is required. Therefore, 100 % reduction of V^{V} into V^{IV} would re-oxidise 37.5 mM Pd (0). That is also stoichometrically equal to the production of 37.5 mM MEK (Figure II.IV-23). When the initial Pd (II) concentration that is 2 mM is added to this amount, total MEK production is equal to 39.5 mM in the solution. Considering that the equilibrium solubility of 1-butene is higher than this amount. However, only ca. 65% of V^{V} has undergone the redox reaction in our system. This is most probably caused by the increase in the pH of the solution.

In addition, 1-butene accummulation as well as an increase in MEK concentration in the solution during the reaction was recorded in both experiment 46 and 47 as shown in Figure II.IV-23.

It can be clearly seen that in exp 47 reaction stops at around 105^{th} minute of the experiment and that point corresponds the start point of the accumulation of 1-butene. Partial pressure of 1-butene in the feed was 1.12 bar. As 1-butene concentration in the

catalyst solution was much higher than the solubility of 1-butene in water, the solubility of 1-butene in the reaction system was re-measured. Figure II.IV-24 shows the data obtained from the solubility of 1-butene measurements in water in the reaction system. It must be noted that very small amount of MEK was also recorded in water. Higher solubility could be due to the low pH of the solution. Solubility of 1-butene in this experiment was actually measured in water, however, it is possible that the acid that was deposited on the surface of the carbon membrane and the connecting tubing would dissolve in water hence increase the solubility.

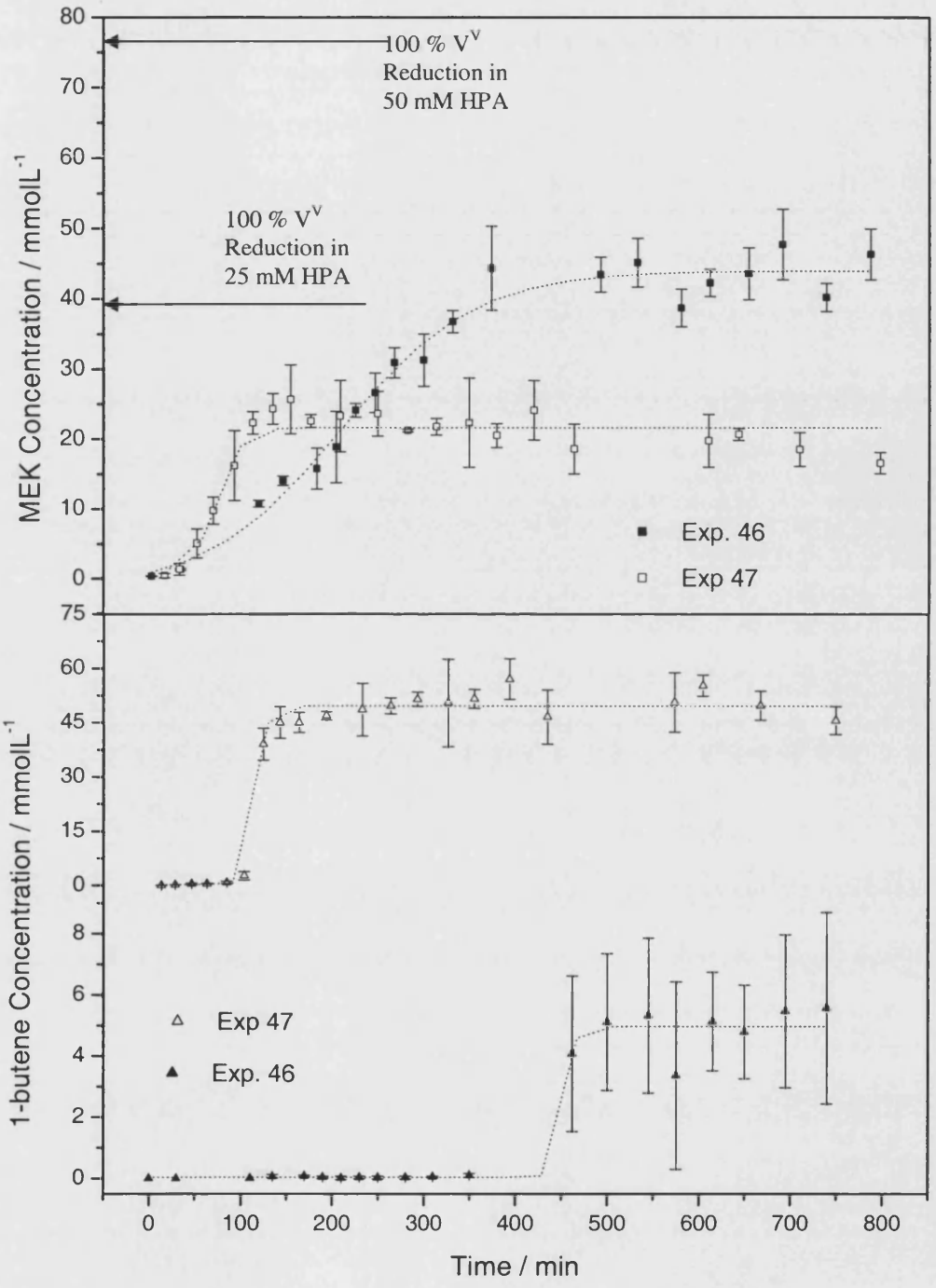

Figure II.IV- 24 Total reduction of HPA solution

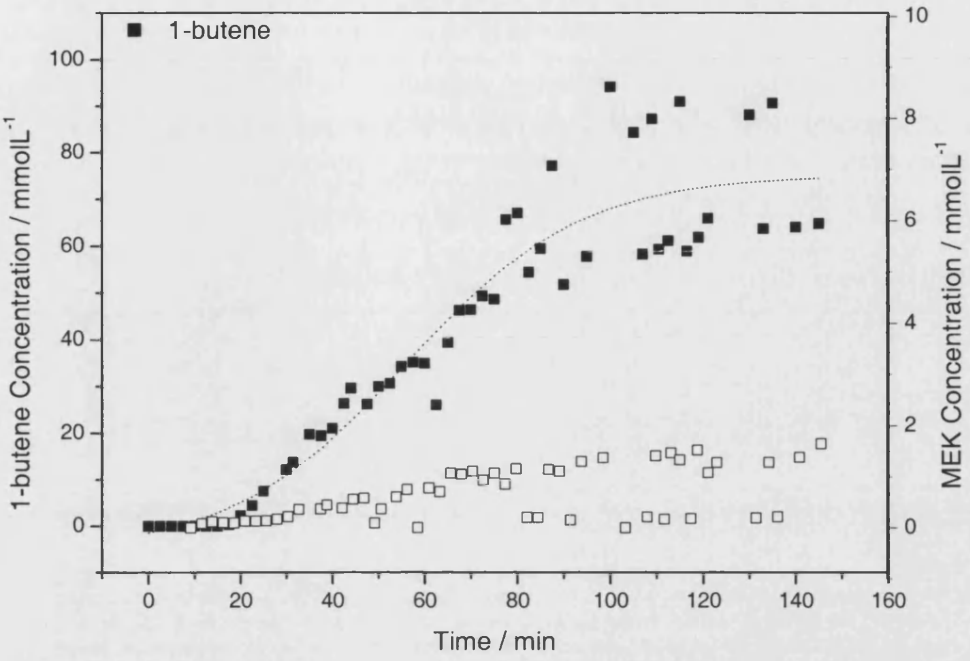

Figure II.IV- 25 Solubility of 1-butene in the reaction system

Due to the low reaction temperatures (30-50 °C) re-oxidation of HPA by molecular oxygen was not possible. It was reported by Grate et al. that for re-oxidation of the reduced HPA, temperature should be ca. 120 °C. Experiments were run also at various transmembrane pressure in the range of 0.15 and 2, in order to observe the change in the maximum amount of MEK production, hence the effect of oxygen in the re-oxidation of HPAs. However, as the transmembrane pressure was increased, maximum MEK production was still ca. 40 mM, that is equal to what was obtained from the experiments in the absence of oxygen, see Table II.IV-1.

Table I.IV- 1 MEK production at various trans-membrane pressures

No of Experiment	*Feed Gas Conc. (mmol/L)*	*Trans-membrane Pressure (bar)*	*MEK Conc. (mmol/L)*
19	10.3	0.75	40
20	11.4	0.75	45
28	11.2	2	42
46[a]	13.23	0.15	45

a: In the absence of oxygen

II.V CONCLUSIONS

The aim of this study was to investigate the feasibility of the system designed for one stage catalytic hydrocarbon oxidation purposes. Heteropolyacids were used as co-oxidants and 1-butene oxidation to methyl ethyl ketone was selected as a test reaction.

Several experiments were performed to optimise the conditions of gas liquid mass transfer in the tube side of the reactor to obtain high gas-liquid mass transfer rates. Mass transfer coefficients obtained were in the range of 0.0057 and 0.166 s^{-1}, similar to those reported in the literature. Highest rate was obtained with 20 cm long capillary with d_i=1.5 mm, 10 and 14 ml/min gas and liquid flowrates, respectively. Theoretical gas-liquid mass transfer coefficients were also calculated from the data collected from these experiments using empirical correlations proposed in the literature. Theoretical coefficients were slightly higher than experimental coefficients due to the assumption of perfect mixing in the capillaries. It was observed that the mass transfer coefficient is directly proportional to the velocity of the total flow and inversely proportional to the liquid slug lengths.

Oxygen transfer through the porous carbon membrane contactor has been studied by performing several experiments. It was necessary to optimise the flowrate and the composition of oxygen in order to supply required amount for the oxidation experiments. Selected total shell flowrate for oxidation experiments was 400 ml/min with 80 v% oxygen flow.

Effects of pressure, temperature, catalyst concentration, feed gas flowrate, HPA concentration, oxygen concentration and trans-membrane pressure were carefully studied by varying a single parameter for each experiment. Main results of these experiments are as follows:

- Maximum reaction rate obtained was 95.82 mmol/Lmin at catalyst concentration 2mM, gas flowrate in the tube side 10 ml/min, liquid flowrate in the tube side 14 ml/min, pressure 1 bar, 1-butene flowrate/tube flowrate 1, temperature 30 °C, HPA concentration 50 mM, total shell flowrate 400 ml/min, oxygen flow/total shell flow 80 v%, trans-membrane pressure 0.15 bar.

- Solubility of the feed gas in the catalyst solution has the highest impact on the reaction rate.
- Catalyst concentration was increased from 1mM to 2mM, however, very small change in the reaction rate was observed as the system was mass transfer limited.
- 65 % of the V^V content of the HPA solution undergoes the redox reaction. Change in the colour, from red to dark green clearly indicates the reduction of the HPA solution.
- Re-oxidation of the HPA was unsuccessful due to low reaction temperatures.

RECOMMENDATIONS FOR FURTHER STUDY

Chemistry of the HPA solution has to be modified in order for the HPA to be re-oxidised with molecular oxygen at lower temperatures. It is necessary to obtain deeper knowledge about the catalyst system.

It is difficult to handle carbon membrane as it is very brittle. Teflon membrane could be an alternative to carbon membrane due to its mechanical stability, resistance to heteropolyacids and flexible structure.

II.VI APPENDICES

II.VI.1 APPENDIX. TBL,LSL and UCL Lengths for Various Gas-Liquid Flowrates

Taylor bubble, liquid slug and unit cell lengths were measured at various gas-liquid flowrates using photographic method and the data obtained were tabulated in Tables AII.1 1- AII.1 6.

Table AII.1 1 Results obtained from photographic measurements of TBL, LSL and UCL for H_2O : 3.6 ml/min - C_4H_8 : 15 ml/min flow set.

H_2O : 3.6 ml/min - C_4H_8 : 15 ml/min									
Capillary Length (cm)	*TBL (cm)*	*ε (+ %)*	*ε (- %)*	*LSL (cm)*	*ε (+ %)*	*ε (- %)*	*UCL (cm)*	*ε (+ %)*	*ε (- %)*
10	2.7	12.22	16.30	0.55	34.55	20.00	3.27	10.09	16.51
10	3.3	24.24	21.21	0.7	14.29	14.29	4	17.50	15.00
20	2.2	36.36	26.82	0.6	16.67	16.67	2.8	28.57	20.36
20	2.5	12.00	14.80	0.47	34.04	36.17	2.97	5.05	4.71
30	1.8	21.11	10.00	0.56	23.21	16.07	2.37	15.19	5.49
30	2.24	33.93	19.64	0.59	10.17	15.25	2.84	23.24	13.03
40	2.07	9.18	5.31	0.59	6.78	5.08	2.65	6.79	4.91
40	2.4	8.33	15.83	0.51	9.80	17.65	2.91	8.93	15.81

Table AII.1 2 Results obtained from photographic measurements of TBL, LSL and UCL for H_2O : 3.5 ml/min - C_4H_8 : 6 ml/min flow set.

H_2O : 3.5 ml/min - C_4H_8 : 6 ml/min									
Capillary Length (cm)	*TBL (cm)*	*ε (+ %)*	*ε (- %)*	*LSL (cm)*	*ε (+ %)*	*ε (- %)*	*UCL (cm)*	*ε (+ %)*	*ε (- %)*
10	0.92	3.26	2.17	0.5	60.00	20.00	1.5	16.67	13.33
10	1.8	10.56	15.56	1.4	16.43	20.00	3.2	12.81	7.50
20	1.58	22.15	22.78	0.7	2.86	4.29	2.28	16.23	17.11
20	0.9	23.33	13.33	0.58	17.24	13.79	1.49	8.05	6.71
30	1.44	9.72	10.42	0.68	20.59	27.94	2.1	14.29	12.86
30	1.3	25.38	23.85	0.62	20.97	19.35	1.93	16.58	15.03
40	1.5	24.67	19.33	0.65	29.23	20.00	2.15	26.05	14.88
40	1.41	13.48	4.26	0.83	3.61	2.41	2.26	4.42	3.54

Table AII.1 3 Results obtained from photographic measurements of TBL, LSL and UCL for H_2O : 5.6 ml/min - C_4H_8 : 15 ml/min flow set.

H_2O : 5.6 ml/min - C_4H_8 : 15 ml/min									
Capillary Length (cm)	*TBL (cm)*	*ε (+ %)*	*ε (- %)*	*LSL (cm)*	*ε (+ %)*	*ε (- %)*	*UCL (cm)*	*ε (+ %)*	*ε (- %)*
10	1.84	16.30	18.48	0.79	25.32	1.14	2.63	19.01	27.76
10	1.93	29.53	32.64	0.65	23.08	38.46	2.58	27.91	34.11
20	1.91	14.66	7.85	0.71	39.44	18.31	2.63	21.29	10.27
20	1.91	30.89	42.93	0.7	10.00	2.86	2.6	22.31	30.38
30	1.6	17.50	8.75	0.73	28.77	17.81	2.34	20.51	11.54
30	2.1	33.33	31.90	0.83	20.48	33.73	2.92	13.01	18.84
40	1.67	15.57	19.16	0.57	36.84	24.56	2.23	13.00	16.14
40	1.82	8.79	9.34	0.59	3.39	3.39	2.41	7.47	7.88
80	1.71	90.06	35.67	0.65	32.31	53.85	2.62	46.95	46.56
80	1.94	33.51	41.24	0.64	35.94	21.88	2.58	21.71	31.40
100	1.68	31.55	35.12	0.64	34.38	32.81	2.32	15.52	27.16
100	1.8	19.44	20.56	0.61	27.87	36.07	2.41	12.86	13.28
120	1.54	6.49	7.14	0.71	21.13	14.08	2.25	8.89	8.89
120	1.81	9.94	14.36	0.72	15.28	18.06	2.53	13.44	13.44

Table AII.1 4 Results obtained from photographic measurements of TBL, LSL and UCL for H_2O : 14 ml/min - C_4H_8 : 10 ml/min flow set.

H_2O : 14 ml/min - C_4H_8 : 10 ml/min									
Capillary Length (cm)	*TBL (cm)*	*ε (+ %)*	*ε (- %)*	*LSL (cm)*	*ε (+ %)*	*ε (- %)*	*UCL (cm)*	*ε (+ %)*	*ε (- %)*
20	0.95	3.16	3.16	1.08	21.30	18.52	2.16	8.33	8.80
20	1.03	0.97	2.91	1.25	14.40	11.20	2.28	5.70	6.58
60	1.26	7.94	7.14	1.7	3.53	3.53	2.95	1.36	4.41
60	1.19	6.72	14.29	1.46	15.75	6.85	2.65	2.26	4.53
80	1.12	12.50	7.14	1.69	18.34	17.16	2.81	10.32	11.03
80	1.09	5.50	3.67	1.67	2.40	16.77	2.64	6.06	5.30
100	1	5.00	4.00	2.05	17.07	15.61	3.05	10.16	11.48
100	1.05	10.48	7.62	1.5	18.00	10.00	2.55	14.90	7.84
120	0.95	6.32	7.37	1.27	29.13	26.77	2.23	18.39	13.90
120	0.91	6.59	10.99	1.5	23.33	15.33	2.41	17.01	10.79

Table AII.1 5 Results obtained from photographic measurements of TBL, LSL and UCL for H_2O : 14 ml/min - C_4H_8 :6 ml/min flow set.

H_2O : 14 ml/min - C_4H_8: 6 ml/min									
Capillary Length (cm)	*TBL (cm)*	*ε (+ %)*	*ε (- %)*	*LSL (cm)*	*ε (+ %)*	*ε (- %)*	*UCL (cm)*	*ε (+ %)*	*ε (- %)*
20	0.89	3.37	6.74	2.03	12.32	7.39	2.93	9.56	7.51
20	1	2.00	4.00	1.93	10.36	10.88	2.93	7.51	6.48
60	1.12	13.39	12.50	1.41	18.44	10.64	2.54	5.51	3.94
80	1.03	1.94	3.88	2.26	12.39	11.06	3.3	7.88	7.27
80	0.94	4.26	7.45	2.01	22.39	10.45	2.95	18.98	7.46
100	0.97	4.12	3.09	2.13	5.63	7.51	3.1	3.55	6.13
100	0.88	1.14	2.27	2.1	14.29	11.43	2.98	10.07	7.72
120	0.8	2.50	5.00	2.95	13.90	14.24	3.75	9.87	10.67
120	0.72	5.56	2.78	2.58	13.95	11.63	3.3	9.70	10.91

Table AII.1 6 Results obtained from photographic measurements of TBL, LSL and UCL for H_2O : 14 ml/min - C_4H_8 : 4 ml/min flow set.

H_2O : 14 ml/min - C_4H_8: 4 ml/min									
Capillary Length (cm)	*TBL (cm)*	*ε (+ %)*	*ε (- %)*	*LSL (cm)*	*ε (+ %)*	*ε (- %)*	*UCL (cm)*	*ε (+ %)*	*ε (- %)*
20	0.85	4.71	4.71	2.97	8.08	11.45	3.83	5.74	8.36
20	0.79	5.06	3.80	2.42	8.26	8.26	3.21	5.30	6.54
60	0.9	11.11	7.78	3.24	13.27	9.26	4.14	12.80	9.18
60	0.9	5.56	7.78	2.9	7.59	8.28	3.79	6.07	5.28
80	0.96	6.25	6.25	3.51	12.54	10.83	4.47	14.54	8.28
80	0.88	6.82	6.82	3.21	21.50	7.79	4.09	17.36	4.65
100	0.86	4.65	5.81	2.9	7.93	6.90	3.49	7.16	7.74
100	0.84	3.57	3.57	2.84	12.32	11.97	3.68	9.51	10.05
120	0.72	6.94	6.94	3.01	10.63	16.28	3.73	9.92	13.94
120	0.81	4.94	7.41	3.02	16.23	17.55	3.83	7.83	15.40

II.VI.2 APPENDIX GC Calibration

Varian CP3800 gas chromatograph equipped with a FID detector and a capillary column Econo-Cap Ec-Wax (Alltech), 15 m. was used for verification of the MEK concentration during the experiments.

GC was calibrated for 1-butene solubility measurements and the calibration line was obtained by injecting volumes between 0.05 and 0.2 ml of 0.1 %1-butene+ balance helium mixture at ambient pressure and temperature. Ideal gas behaviour was assumed in order to calculate the concentration of 1-butene.

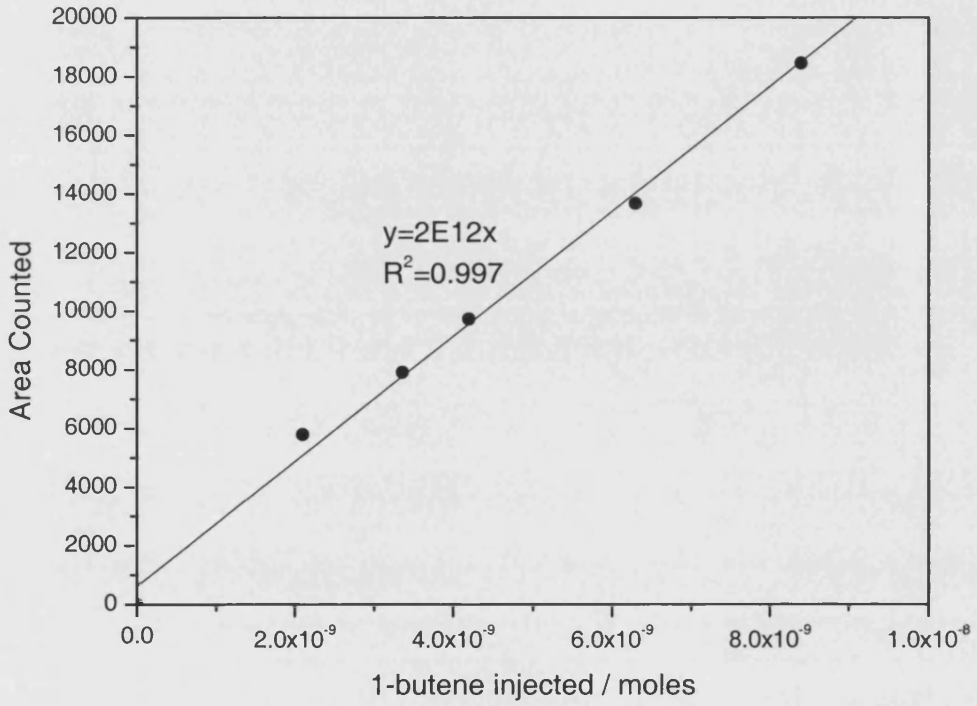

Figure AII.2 1 1-butene calibration data

GC was also calibrated for MEK by syringe injection of aqueous MEK solution. Solutions with various MEK concentrations between 2 and 10 mmol/L were used to obtain calibration line (see figure AII.2 2).

In some of the experiments two main peaks were observed and it was found that the second main peak belongs to 1-butene. Hence, the GC was once more calibrated for 1-butene using pure 1-butene in gas phase.

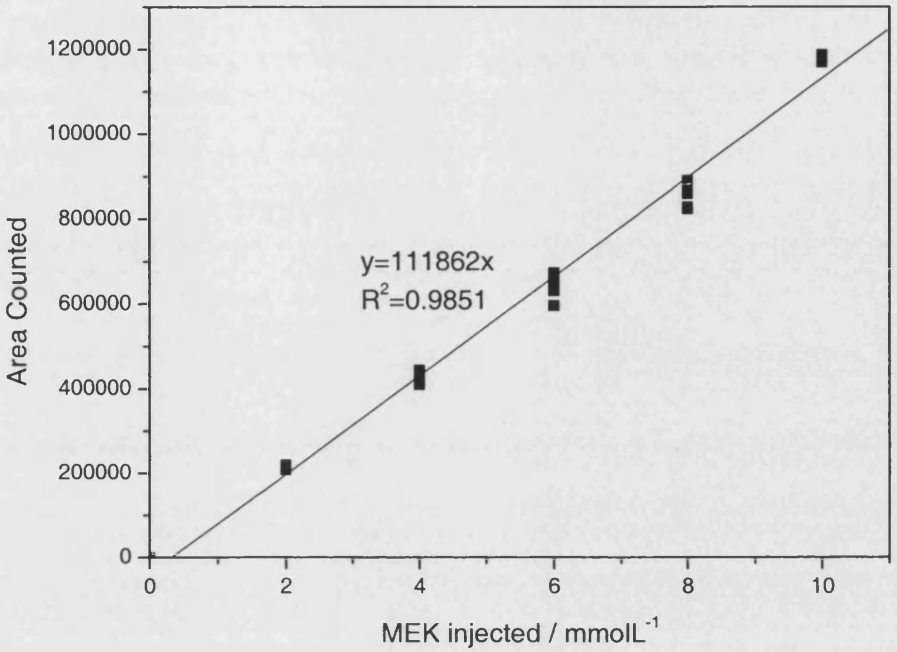

Figure AII.2 2 MEK calibration data

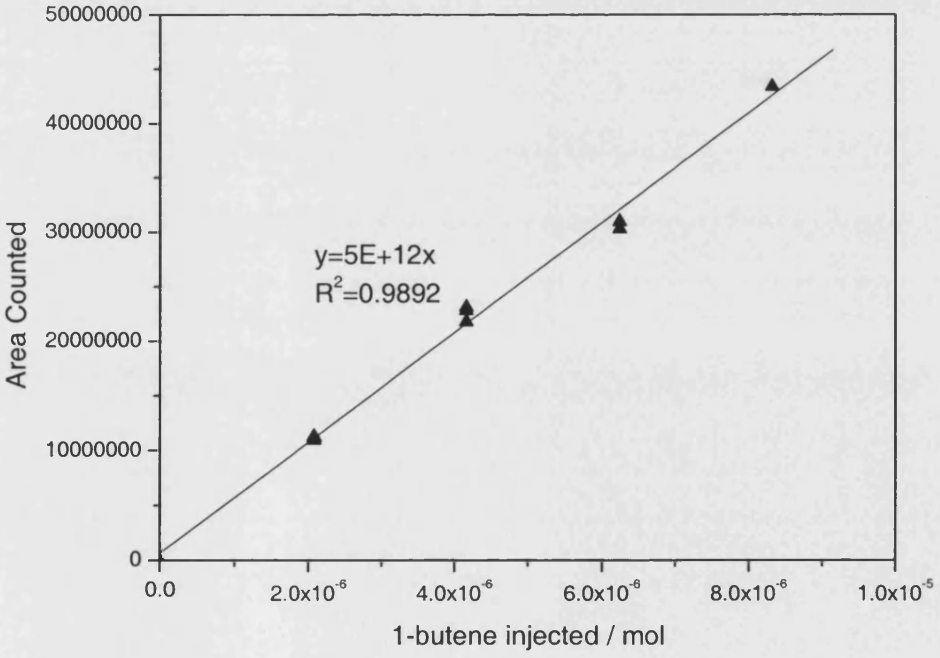

Figure AII.2 3 Second 1-butene calibration

II.VI.3 APPENDIX Nitrogen Permeation

Nitrogen permeation data obtained from the membrane characterisation experiments are tabulated in Table II.3 1.

Table AII.3 1 Data obtained from nitrogen permeation experiments.

Nitrogen Flow, Q (ml/sec)	*dP (Pa)*	*Vo (m/sec)*
1.667	16200	1.42E-03
2.500	24200	2.13E-03
3.333	31700	2.84E-03
4.167	39000	3.55E-03
5.000	46300	4.26E-03
5.833	53100	4.97E-03
6.667	60000	5.68E-03
7.500	66200	6.39E-03
8.333	72900	7.10E-03
9.167	79200	7.81E-03
10.000	85200	8.52E-03
10.833	91200	9.22E-03
11.667	97000	9.93E-03
12.500	102700	1.06E-02
13.333	108400	1.14E-02
14.167	113900	1.21E-02
15.000	119300	1.28E-02
15.833	124600	1.35E-02
16.667	130000	1.42E-02

APPENDIX Experimental Conditions for Hydrocarbon Oxidation

Experimental conditions are tabulated in Table AII.4 1

Table AII.4 1. Experimental Conditions

Experiment Number	*Feed Concentration (mmol/L)*	*Temperature (°C)*	*Pressure (bar)*	*Tube-Gas Flowrate (ml/min)*	*Trans-membrane Pressure (bar)*	*Oxygen Ratio (%)*	*Catalyst Concentration (mmol/L)*	*HPA Concentration (mmol/L)*
12	40.8	30	3.5	4	0.15	80	2	50
14	10.2	30	3.5	10	0.15	80	2	50
15	8.36	30	3.5	10	0.15	80	2	50
16	10.3	30	3.5	10	0.15	80	2	50
17	11.7	30	3.5	4	0.15	80	2	50
18	9.68	30	3.5	4	0.15	80	2	50
19	10.3	30	3.5	10	0.75	80	2	50
20	11.4	30	3.5	10	0.75	80	2	50
21	12.3	30	5	10	0.15	80	2	50
23	10.8	30	3.5	10	0.15	80	2	50
24	14	30	3.5	10	0.15	80	2	50
25	10.6	30	5	10	0.15	80	2	50
26	12.9	30	3.5	10	0.15	0	2	50
27	24.6	30	1	10	0.15	80	2	50
28	11.2	30	3.5	10	2	80	2	50
29	18.5	30	3.5	10	0.15	80	0	50

Experiment Number	*Feed Concentration (mmol/L)*	*Temperature (°C)*	*Pressure (bar)*	*Tube-Gas Flowrate (ml/min)*	*Trans-membrane Pressure (bar)*	*Oxygen Ratio (%)*	*Catalyst Concentration (mmol/L)*	*HPA Concentration (mmol/L)*
30	18.65	30	3.5	10	0.15	80	2	25
32	14	30	3.5	10	0.15	0	2	50
33	12.3	30	3.5	10	0.15	80	1	50
34	18	30	3.5	10	0.15	80	1	50
36	17.1	30	1	10	0.15	80	2	50
37	18.1	30	1	10	0.15	80	2	50
38	8.58	30	3.5	6	0.15	80	2	50
39	8.93	30	3.5	6	0.15	80	2	50
40	9.13	50	3.5	10	0.15	80	2	50
41	8.85	50	3.5	10	0.15	80	2	50
42	8.78	40	3.5	10	0.15	80	2	50
43	9.31	40	3.5	10	0.15	80	2	50
44	8.35	30	3.5	10	0.15	80	2	25
46	13.23	30	3.5	10	0.15	0	2	50
47	30.1	30	1	10	0.15	0	2	25

REFERENCES

D.W. Agar, Multifunctional reactors: Old preconceptions and new dimensions, Chemical Engineering Science, 54 (1999) 1299-1305.

M.J. Alfonso, A. Julbe, D. Farrusseng, M. Menéndez, J. Santamaría, Oxidative dehydrogenation of propane on V/Al_2O_3 catalytic membranes. Chemical Engineering Science, 54 (1999) 1265-1272.

M.J. Alfonso, M. Menéndez, J. Santamaría, Vanadium based catalytic membrane reactors for the oxidative dehydrogenation of propane, Catalysis Today, 56 (2000) 247-252.

G. Berčič, Influence of operating conditions on the observed reaction rate in the single channel monolith reactor, Catalysis Today, 69 (2001) 147-152.

G. Berčič, A. Pintar, The role of gas bubbles and liquid slug lengths on mass transport in the Taylor flow through capillaries, Chemical Engineering Science, 52 (21/22) (1997) 3709-3719.

R.B. Bird, W.E. Stewart, E.N. Lightfoot, " Transport Phenomena", Wiley, 2002.

G. Centi, R. Dittmeyer, S. Perathoner, M. Reif, Tubular inorganic catalytic membrane reactors, Catalysis Today, 79-80 (2003) 139-149.

S. Chen, H. Fan, Y. Kao, A membrane reactor with two dispersion-free interfaces for homogeneous catalytic reactions, The Chemical Engineering Journal, 49 (1992) 35-43.

A. Concellón, P. Vázquez, M. Blanco, C. Cáceres, Molybdophosphoric acid adsorption on titania from ethanol-water solutions, Journal of Colloid and Interface Science, 204 (1998) 256-267.

A. Corma, Inorganic solid acids and their use in acid catalyzed hydrocarbon reactions, Chemical Reviews, 95 (1995) 559-614.

J. Coronas, J. Santamaría, Catalytic reactors based on porous ceramic membranes, Catalysis Today, 51 (1999) 377-389.

E.L. Cussler, "Diffusion Mass Transfer in Fluid Systems", Cambridge University Press, 1984, (USA).

H. Dannström, D.B. Stuksrud, H. Svendsen, Membrane gas/liquid contactors for natural gas sweetening, Gas Processors Association, UK.

S.F. Davison, B.E. Mann, P.T. Maitlis, Phosphomolybdic acid as a reoxidant in the palladium (II)-catalysed oxidation of but-1-ene to butan-2-one, J. Chem. Soc. Dalton Trans., (1984) 1223-1228.

R. De Vos, V. Hatziantoniou, N.-H. Schöön, The cross flow catalyst reactor. Chemical Engineering Science, 37 (1982) 1719-1726.

J.A. Dias, J.P. Osegovic, R.S. Drago, The solid acidity of 12-tungstophosphoric acid, Journal of Catalysis, 183 (1999) 83-90.

N. Essayem, R. Frety, G. Coudurier, J.C. Vedrine, Ammoniaadsorption-desorption over the strong solid acid catalyst $H_3PW_{12}O_{40}$ and its Cs^+ and NH_4^+ salts, J. Chem. Soc., Faraday Trans., 93 (17) (1997) 3243-3248.

D. Farrusseng, A. Julbe, C. Guizard, The first redox switchable ceramic membrane, J. Am. Chem. Soc., 122 (2000) 12592-12593.

D. Farrusseng, A. Julbe, C. Guizard, Evaluation of porous ceramic membranes as O_2 distributors for the partial oxidation of alkanes in inert membrane reactors, Separation and Purification Technology 25 (2001) 137-149.

V.B. Fenelonov, V.A. Likholobov, A.Yu. Derevyankin, M.S. Mel'gunov, Porous carbon materials prepared from C_1–C_3 hydrocarbons, Catalysis Today, 42 (1998) 341-345.

J.L. Figueiredo, M.F.R. Pereira, M.M.A. Freitas, J.J.M. Orfao, Modification of the surface chemistry of activated carbons, Carbon, 37 (1999) 1379-1389.

A. Gabelman, S. Hwang, Hollow fiber membrane contactors, Journal of Membrane Science, 159 (1999) 61-106.

A. Galarneau, D. Desplantier-Giscard, F. Di Renzo, F. Fajula, Thermal and mechanical stability of micelle templated silica supports for catalysis, Catalysis Today, 68 (2001) 191-200.

R.W. Gallant, C.L. Yaws, "Physical Properties of Hydrocarbons", 2nd Ed., Gulf, (1992).

J.H.Grate, D.R. Hamm, S. Mahajan, Palladium and phosphomolybdovanadate catalyzed olefin oxidation to carbonyls "Polyoxometalates" (M.T. Pope and A.A. Müller, Eds), Kluwer Academic, Dordrecht (1994) 281-305.

S.J. Gregg, K.S.W. Sing, "Adsorption, surface area and porosity", Academic Press, London, 2nd Ed. (1982).

V. Gryaznov, Membrane catalysis, Catalysis Today, 51 (1999) 391-395.

J. Hagen, "Industrial Catalysis- A Practical Approach". Wiley-VCH (1999).

M.P. Harold, C. Lee, Intermediate product yield enhancement with a catalytic inorganic membrane, Chemical Engineering Science, 52 (1997) 1923-1939.

Y. He, F. Li, P. Wang, Z. Du, Preparation and characterization of a solid superacid heteropoly acid, Symposium on solid superacids, American Chemical Society, Las Vegas, NV, (1997) 722-725.

J.J. Heiszwolf, E. Crezee, L.B. Engelvaart, F. Kapteijn, J.A. Moulijn, Hydrodynamics of cocurrent two-phase flow in monoliths, Brite Eurom Project, (1999).

J.J. Heiszwolf, M. Kreutzer, M.G. van den Eijnden, F. Kapteijn, J.A. Moulijn, Gas-liquid mass transfer of aqueous Taylor flow in monoliths, Catalysis Today, 69 (2001), 51-55.

H.W. Hillhouse, M.T. Tuominen. Modelling and thermoelectric transport properties of nanowires embedded in oriented microporous and mesoporous films. Microporous and Mesoporous Materials, 47 (2001), 39-50.

S.I. Hong, J.H. Jung, Characteristics of a V_2O_5 coated membrane reactor for the selective oxidation of 1-butene, Applied Catalysis A: General, 156 (1997) 239-252.

W. Hua, Y. Yue, Z. Gao, Acidity enhancement of SBA mesoporous molecular sieve by modification with SO_4^{2-}/ZrO_2, Journal of Molecular Catalysis A: Chemical, 170 (2001) 195-202.

D.J. Hucknall, "Selective Oxidation of Hydrocarbons", Academic Press Inc. (London) Ltd., 1974.

D.Y. Hwang, S.Y. Ha, S. Kim, Electrode-asisted Wacker process, Bull. Korean Chem. Soc., 22 (2001) 441-442.

S. Irandoust, B. Andersson, Liquid film in taylor flow through a capillary, Ind. Eng. Chem. Res., 28 (1989), 1684-1688.

S. Irandoust, S. Ertlé, B. Andersson, Gas-liquid mass transfer in Taylor flow through a capillary,, The Canadian Journal of Chemical Engineering, 70 (1992) 115-119.

N. Itoh, K. Haraya, A carbon membrane reactor, Catalysis Today, 56 (2000)103-111.

Y. Izumi, R. Hasebe, K. Urabe, Catalysis by heterogeneous supported heteropoly acid, Journal of Catalysis, 84 (1983) 402-409.

Y.P. Jeannin, The nomenclature of polyoxometalates: How to connect a name and a structure, Chem. Rev., 98 (1998) 51-76.

A. Julbe, D. Farrusseng, C. Guizard, Porous ceramic membranes for catalytic reactors, Journal of Membrane Science, 181 (2001) 3-20.

K. Kawakami, K. Kawasaki, F. Shiraishi, K. Kusunoki, Performance of a honeycomb monolith bioreactor in a gas-liquid-solid three-phase system, Ind. Eng. Chem. Res., 28 (1989) 394-400.

E. Kikuchi, Membrane reactor application to hydrogen production, Catalysis Today, 56 (2000) 97-101.

D.A. Kinkead, Air filtering within clean environments, United States Patent 5,607,647, (1997).

Y. Konishi, K. Sakata, M. Misono, Y. Yoneda, Catalysis by heteropoly compounds, Journal of Catalysis, 77 (1982) 169-179.

I.V. Kozhevnikov, A. Sinnema, R.J.J. Jansen, K. Pamin, H. van Bekkum, New acid catalyst comprising heteropoly acid on a mesoporous molecular sieve MCM-41, Catalysis Letters, 30 (1995) 241-252.

I.V. Kozhevnikov. Catalysis by heteropoly acids and multicomponent polyoxometalates in liquid-phase reactions. Chemical Review, 98 (1998) 171-198.

M.T. Kreutzer, P. Du, J. J. Heiszwolf, F. Kapteijn, J.A. Moulijn, Mass transfer characteristics of three-phase monolith reactors, Chemical Engineering Science, 56 (2001) 6015-6023.

Á. Kukovecz, Zs. Balogi, Z. Kónya, M. Toba, P. Lentz, S.-I. Niwa, F. Mizukami, Á Molnár, J.B. Nagy, I. Kiricsi, Synthesis, characterization and catalytic applications of sol-gel derived silica-phosphotungstic acid composites, Applied Catalysis A: General, 228 (2002) 83-94.

Y. Kusuki, H. Shimazaki, N. Tanihara, S. Nakanishi, T. Yoshinaga, Gas permeation properties and characterization of asymmetric carbon membranes prepared bypyrolyzing asymmetric polyimide hollow fiber membrane, Journal of Membrane Science, 134 (1997) 245-253.

A. Lambert, E.G. Derouane, I.V. Kozhevnikov, Kinetics of one-stage Wacker-type oxidation of C_2-C_4 olefins catalysed by an aqueous $PdCl_2$-heteropoly-anion system, Journal of Catalysis, 211(2002) 445-450.

G. Langhendries, G.V. Baron, P.A. Jacobs, Selective and efficient hydrocarbon oxidation in a packed bed membrane reactor, Chemical Engineering Science, 54 (1999) 1467-1472.

G. Langhendries, G.V. Baron, I.F.J. Vankelecom, R.F. Parton, P.A. Jacobs, Selective hydrocarbon oxidation using a liquid phase catalytic membrane reactor, Catalysis Today, 56 (2000) 131-135.

A.A. Lapkin, S.R. Tennison, W.J. Thomas, Aporous carbon membrane reactor for the homogeneous catalytic hydration of propene, Chemical Engineering Science, 57 (2002) 2357-2369.

U. Lavrenčič Štangar, N. Grošelj, B. Orel, A. Schmitz, Ph Colomban, Proton conducting sol-gel hybrids containing heteropoly acids, Solid State Ionics, 145 (2001) 109-118.

T. López, R. Gómez, J.G. Hernández, E. López-Salinas, X. Bokhimi, A. Morales, J.L. Boldú, E. Muñoz, O. Novaro, Acidity of tungtophosphoric acid-zirconia catalysts prepared by the sol-gel method, Langmuir, 15 (1999) 5820-5824.

Z. Luan, J.Y. Bae, L. Kevan, Photoionisation of N-alkylphenothiazines in titanosilicate mesoporous TiSBA-15 molecular sieves. Microporous and Mesoporous Materials, 48 (2001) 189-194.

J.A.F. MacDonald, M.J.B. Evans, S. Liang, S.E. Meech, P.R. Norman, L. Pears. Chlorine and oxygen on the carbon surface, Carbon, 38 (2000) 1825-1830.

J.D. Mackenzie, Present and future directionsin sol-gel science and technology, Sol-gel Science and Technology (E.J.A. Pope, S.Sakka, L.C. Klein eds.), The American Ceramic Society, (1995) 25-31.

R. Mallada, M. Menéndez, J. Santamaría, Use of membrane reactors for the oxidation of butane to maleic anhydride under high butane concentrations, Catalysis Today, 56 (2000) 191-197

K.I. Matveev, Catalyst for liquid phase oxidation of olefinsand a method of preparing same, UK Patent 1 508 331, (1978).

M. Mavroudi, S.P. Kaldis, G.P. Sakellaropoulos, Reduction of CO_2 emissions by a membrane contacting process, Fuel, 82 (2003)2153-2159.

R.L. McCormick, S.K. Boonrueng, A.M. Herring, In situ IR and temperature programmed desorption-mass spectrometry study of NO absorption and decomposition by silica supported 12-tungstophosporic acid, Catalysis Today, 42 (1998) 145-157.

N. Mizuno, M. Misono, Heterogeneous Catalysis, Chem. Rev., 98 (1998), 199-217.

Á. Molnár, C. Keresszegi, B. Török, Heteropoly acids immobilized into a silica matrix: characterization and chatalitic applications, Applied Catalysis A: General, 189 (1999) 217-224.

J.A. Moulijn, Chemical Engineering Science, 54 (1999) 1297.

S. Mukai, T. Sugiyama, H. Tamon, Immobilization of heteropoly acids in the network structure of carbon gels, Applied Catalysis A: General, 256 (2003) 99-105.

M. Mulder, "Basic Principles of Membrane Technology", 2nd Ed., Kluwer Academic Publishers, 1996.

K. Na, T. Okuhara, M. Misono, Catalysis by heteropoly compounds, Journal of Catalysis, 170 (1997) 96-107.

J.W. Niemantsverdriet. Spectroscopy in Catalysis, 2ndEd., Wiley-VCH, 10-11, Germany (2000).

K. Nowińska, R. Fórmaniak, W. Kaleta, A. Waclaw, Heteropoly compounds incorporated into mesoporous material structure, Applied Catalysis A: General, 256 (2003) 115-123.

T. Ohmi, Ultra clean processing, Microelectronic Engineering, 10 (1991) 163-176.

T. Okuhara, Microporous heteropoly compounds and their shape selective catalysis, Applied Catalysis A: General, 256 (2003) 213-224.

Y. Owobi-Andely, K. Fiaty, P. Laurent, C. Bardot, Use of electrocatalytic membrane reactor for synthesis of sorbitol, Catalysis Today, 56 (2000) 173-178.

M.T. Pope, Heteropoly and Isopoly oxometalates, 3rd Ed., Springer-Verlag, 1983 (Berlin).

L.R. Pizzio, C.V. Cáceres, M.N. Blanco, Adsorption of tungstophosphoric or tungstosilicic acids from ethanol-water solutions on carbon, Journal of Colloid and Interface Science, 190 (1997) 318-326.

L.R.Pizzio, C.V. Cáceres, M.N. Blanco, Acid catalysts prepared by impregnation of tungstophosphoric acid solutions on different supports, Applied Catalysis A: General, 167 (1998) 283-294.

R. Ramos, M. Menendez, J. Santamaria, Oxidative dehydrogenation of propane in an inert membrane reactor.

C. Rocchiccioli-Deltcheff, A. Aouissi, M. M. Bettahar, S. Launay, M. Fournier, Catalysis by 12-molybdophosphates, Journal of Catalysis, 164 (1996) 16-27.

C. Rocchiccioli-Deltcheff, A. Aouissi, S. Launay, M. Fournier, Silica supported 12-molybdophosphoric acid catalysts, Journal of Molecular Catalysis A: Chemical, 114 (1996) 331-342.

A.F. Sammells, M. Schwartz, R.A. Mackay, T.F. Barton, D.R. Peterson, Catalytic membrane reactors for spontaneous synthesis gas production, Catalysis Today, 56 (2000) 325-328.

G. Saracco, J.W. Veldsink, G.F. Versteeg, W.P.M. Van Swaaij, Catalytic combustion of propane in a membrane reactor with separate feed of reactants, Chemical Engineering Science, 50 (1995) 2005-2015.

S.M. Saufi, A.F. Ismail, Fabrication of carbon membranes for gas separation-a review, Carbon, 42 (2004) 241-259.

T. Schroth, New HEPA/ULPA filters for clean room technology, Filtration & Separation, March (1996) 245-249.

Y.T. Shah, M.A. Abraham, R.L. Cerro, Oxidation of phenol in a three phase monolithic froth reactor, Three Phase Sparged Reactors (K.D.P. Nigam, A. Schumpe, eds.), (1996) 423-460.

S. Shimizu, H. Ichihashi, K. Nagai, Heteropoly-acids and their production and use, United States Patent 4,565,801 (1986).

S. Soled, S. Miseo, G. McVicker, W.E. Gates, A. Gutierrez, J. Paes, Preparation and catalytic properties of supported heteropolyacid salts, The Chemical Engineering Journal, 64 (1996) 247-254.

B.W.L. Southward, J.S. Vaughan, C.T. O'Connor, Infrared and thermal analysis studies of heteropoly acids, Journal of Catalysis, 153 (1995) 293-303.

T.J. Stanley, J.A. Quinn, Phase transfer catalysis in a membrane reactor, Chemical Engineering Science, 42 (1987) 2313-2324.

A.W. Stobbe-Kreemers, M. Makkee, J.J.F. Scholten, The performance of titania supported Wacker catalysts in the oxidation of 1-butene, Applied Catalysis A: General, 156 (1997) 2219-238.

G. Strukul, R. Gavagnin, F. Pinna, E. Modaferri, S. Perathoner, G. Centi, M. Marella, M. Tomaselli, Use of palladium based catalysts in the hydrogenation of nitrates in drinking water: from powders to membranes, Catalysis Today, 55 (2000) 139-149.

A.K. Suresh, M.M. Sharma, T. Sridhar, Engineering aspects of industrial liquid phase air oxidation of hydrocarbons, Ind. Eng. Chem. Res., 39 (2000) 3958-3997.

S.R. Tennison, Phenolic-resin-derived activated carbons, Applied Catalysis A: General, 173 (1998) 289-311.

M.N. Timofeeva, M.M. Matrosova, T.V. Reshetenko, L.B. Avdeeva, A.A. Budneva, A.B. Ayupov, E.A. Paukshtis, A.L. Chuvilin, A.V. Volodin, V.A. Likholobov, Filamentous carbons as a support for heteropoly acid, Journal of Molecular Catalysis A: Chemical, 211 (2004) 131-137.

M.N. Timofeeva, M.M. Matrosova, T.V. Reshetenko, L.B. Avdeeva, E.A. Paukshtis, A.A. Budneva, A.L. Chuvilin, V.A. Likholobov, Adsorption of $H_3PW_{12}O_{40}$ by porous carbon materials, Russian Chemical Bulletin, Int. Ed., 51 (2) (2002) 243-248.

J.S. Vaughan, C.T. O'Connor, J.C.Q. Fletcher, High-Pressure Oligomerization of Propene over Heteropoly Acids. Journal of Catalysis, 147 (1994) 441-454.

J.W. Veldinsk, R.M.J. van Damme, G.F. Versteeg, W.P.M. van Swaaij, A catalytically active membrane reactor for fast, exothermic, heterogeneously catalysed reactions, Chemical Engineering Science, 47 (1992) 2939-2944.

G.T. Vladisavljević, M.V. Mitrović, Pressure drops and hydraulic resistances in a three phase hollow fiber membrane contactor with frame elements, Chemical Engineering and Processing, 40 (2001) 3-11.

Y. Wang, M. Noguchi, Y. Takahashi, Y. Ohtsuko, Synthesis of SBA-15 with different pore sizes and the utilization as supports of high loading of cobalt catalysts, Catalysis Today, 68 (2001) 3-9.

L. Washmon-Kriel, V.L. Jimenez, K.J. Balkus Jr., Cytochrome c immobilization into mesoporous molecular sieves, Journal of Molecular Catalysis B: Enzymatic, 10 (2000) 453-469.

T.E. Wood, H. Dislich, An abbreviated history of sol-gel technology, Sol-Gel Science and Technology (E.J.A. Pope, S.Sakka, L.C. Klein eds.), The American Ceramic Society (1995) 3-23.

S. Wu, J. Gallot, M. Bousmina, C. Bouchard, S. Kaliaguine, Zeolite containing catalytic membranes as interphase contactors, Catalysis Today, 56 (2000) 113-129.

H.H.P. Yiu, P.A. Wright, N.P. Botting, Enzyme immobilization using SBA-15 mesoporous molecular sieves with functionalized surfaces, Journal of Molecular Catalysis B: Enzymatic, 15 (2001) 81-92.

D. Zhao, J. Feng, Q. Huo, N. Melosh, G.H. Fredrickson, B.F. Chmelka, Triblock copolymer syntheses of mesoporous silica with periodic 50 to 300 angstrom pores, Science, 279 (1998) 548-552.